ULTRAFAST ELECTRON-OPTICAL VISIBLE / X-RAY-SENSITIVITY STREAK AND FRAMING CAMERAS

David R. Walker

A Thesis Submitted for the Degree of PhD
at the
University of St Andrews

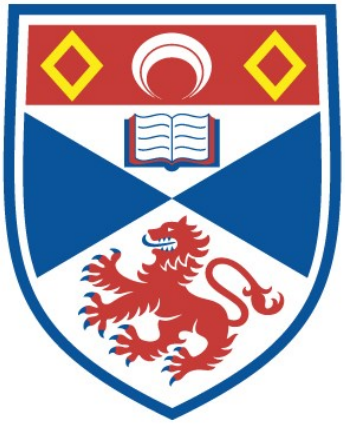

1990

ULTRAFAST ELECTRON-OPTICAL VISIBLE / X-RAY - SENSITIVITY STREAK AND FRAMING CAMERAS.

A Thesis presented by David R Walker (BSc. Hons) to the University of St Andrews in application for the degree of Doctor of Philosophy.

Department of Physics and Astronomy
North Haugh
St. Andrews University
Fife KY16 9SS.

(1989)

Declaration

I David R Walker hereby certify that this thesis has been composed by myself, that it is a record of my own work, and that it has not been accepted in partial or complete fulfilment of any other degree or professional qualification.

I was admitted to the Faculty of Science of the University of St Andrews under Ordinance General No. 12 on 1/9/82 and as a candidate for the degree of Ph.D. on 1/9/87.

D Walker

14th September 1989

Certificate

I hereby certify that the candidate has fulfilled the conditions of the Resolution and Regulations appropriate to the Degree of Ph.D.

Prof. W Sibbett

14th September 1989

Copyright

Abbreviations

ICHSP International Conference on High Speed Photography.

ICHSPP International Conference on High Speed Photography and Photonics.

SPIE Society of Photo-Instrumentation Engineers.

AWE Atomic Weapons Establishment.

Abstract

In this thesis the development of ultrafast electron-optical streak and framing cameras having radiation sensitivities ranging from the visible to soft X-ray are discussed. A framing camera incorporating a vacuum demountable image tube with ultraviolet / soft X-ray sensitivity has been demonstrated to be capable of providing multiple, temporally separated, two-dimensional images with picosecond image exposure times under various operating conditions. Experimental evidence has been presented to show that this camera system can provide up to four high quality temporally separated images with an exposure time of 230 ps (FWHM) and inter-frame times of ~1ns under UV illumination. In the two-frame operation with soft X-ray illumination (generated using a laser produced plasma) image exposure times of as short as 100 ps (FWHM) and inter-frame times of 400 ps have been achieved. The dynamic spatial resolution of the camera has been shown to be ~8 lp/mm and ~5 lp/mm for the UV and soft X-ray sensitive devices respectively.

A visible-sensitivity electron-optical single-shot streak camera possessing a novel travelling-wave deflection structure has been experimentally evaluated using a mode-locked cw ring dye laser. The limiting temporal resolution for this has been measured to be 300 fs and the merits of the travelling-wave deflection structure have been discussed. The implementation of this type of deflector geometry has also been demonstrated in conjunction with the vacuum demountable framing camera system.

Computer aided design techniques have been utilised to further optimise the electron-optical framing tube configuration, and modifications have been proposed to enable shorter frame periods to be obtained while maintaining the dynamic spatial resolution. Results from preliminary evaluations of this design using a vacuum demountable UV-sensitive system are included.

A novel streak camera design has also been proposed in which very high electrostatic photocathode extraction fields (up to 12 kV/mm) may be employed without danger of structural damage arising from electrostatic breakdown. This has been achieved by the removal of the usual mesh electrode placed in close proximity to the photocathode. Preliminary evaluations of a vacuum demountable UV-sensitive version of this camera geometry have been achieved which demonstrate a static spatial resolution of 80 lp/mm (when referred to the photocathode).

CONTENTS

Chapter 1

Electron-Optical Streak And Framing Cameras

1.1 Introduction

The generation of picosecond (10^{-12} seconds) and femtosecond (10^{-15} seconds) optical pulses directly using laser mode-locking techniques [1,2] or indirectly via optical pulse compression [3, 4, 5] is becoming routine in the field of ultrashort pulse generation. Such techniques allow the generation of optical pulses whose wavelengths vary from >1.5 μm (colour centre [6] and semiconductor diode lasers [7]) to ~100nm (excimer [8] and frequency-doubled, quadrupled laser systems eg. Nd:YAG) and so diagnostic instrumentation is required to cover this spectral range. Recently, considerable interest has been shown in the Ultra-Violet (UV) and soft X-ray self-emissions from laser produced plasmas which are created by the illumination of targets with short (100ps to 1ns) pulsed ultra-intense (in excess of ~10^{11} W/cm^2) laser radiation. Thus the requirement for one and two dimensional picosecond and femtosecond linear response diagnostics has now been extended to radiation wavelengths of ~4 Angstroms ($4x10^{-10}$m).

Historically optical temporal information was available from rotating mirror or drum [9] type streak cameras. These systems imaged a slit of light onto photographic film via a rotating mirror or drum assembly which was rotated at high speed. The temporal resolution of such a system is limited by the angular velocity at which the mirror could be rotated before centrifugal forces cause mirror disintegration, and the optical moment arm that could be conveniently accommodated. The temporal resolution of such a system is typically >1ns [9], they are inherently difficult to operate, and not easily adapted for use in different environments (such as vacuum chambers).

The electron-optical streak cameras offer many advantages over the mechanical counterparts and so has now been almost universally adopted where high temporal resolution is required. Suitable photocathode materials may be used to cover the entire spectrum from infrared to X-ray, they are reasonably small compact devices and demonstrate temporal resolutions that are superior to other linear measurement

techniques. However, despite intensive research by many workers the temporal resolution of even the state-of-the-art electron optical streak cameras is ~300fs. If greater temporal resolution is required the only techniques currently available are based on nonlinear optics and examples include two-photon fluorescence [10] and most commonly second harmonic generation autocorrelation [11]. These techniques do not unambiguously provide data for the optical pulse shape, but if bandwidth-limited features can be confirmed then the temporal profile may be inferred from consideration of the bandwidth and intensity and/or interferemetric autocorrelations [12]. Ongoing experimental and theoretical work being undertaken involving intensity and interferemetric cross-correlation techniques should provide more useful details of pulse shape. These techniques are usually restricted to the visible or near infrared spectral region because of the difficulty in finding suitable second harmonic generation materials. Photodetectors now have been demonstrated to have a frequency bandwidth of ~110GHz [13] with inferred rise-times of ~4.5ps, but oscilloscopes are limited to ~50ps rise-time for real-time single-shot operation and ~25ps for the sampling of repetitive events.

1.2 Streak Cameras

The electron-optical streak camera then offers the unique ability of measuring optical phenomena down to sub-picosecond resolution directly, and is also capable of doing so with several 'channels' simultaneously (eg. time domain spectroscopy [14]). The modern streak camera consists of five main components; the photocathode, mesh electrode, focussing geometry, deflection structure, field-free drift region, and the phosphor screen. While all camera structures consist of these components, their position or structure varies greatly. The design favoured by most workers is shown as figure 1.1 and employs an electrostatic electron-optical lens structure.

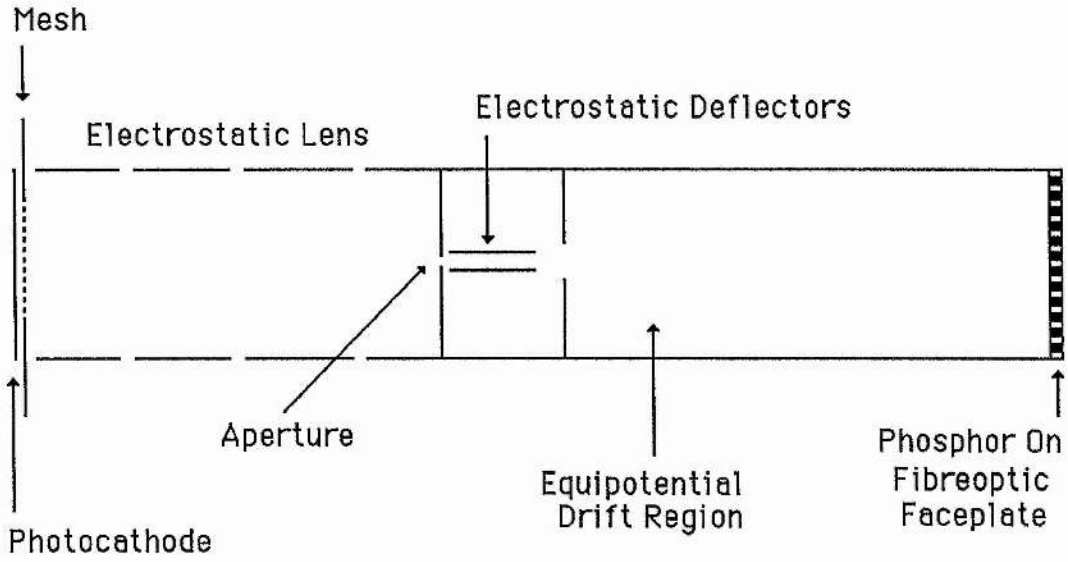

Figure 1.1. Structure of the electrostatically focussed Photochron IV type streak camera.

In operation, the desired optical signal is imaged via a narrow (typically 10 or 20μm wide) slit onto the photocathode. The electrons liberated from this photocathode are rapidly accelerated by the mesh electrode to ~5 or 10keV. The inverting electrostatic lens structure images the photoelectrons onto the phosphor screen which forms a reproduction of the input image. Near the 'crossover' point of the electron trajectories a deflection structure is situated which allows the electron beam to be rapidly swept or 'streaked' across the phosphor screen, and so converting the resultant image into a recording of the temporal behaviour of the light intensity reaching the photocathode.

Other systems have employed magnetic focussing [15], pre-focussing deflection [16] and proximity focussing [17] and cylindrical electron-optical lenses [18]. While many workers have proposed that these different techniques are superior in one way or another, little experimental evidence has been published to date of any system demonstrating superior temporal resolution to that of the above 'standard' design. The electron-optical streak camera may be operated in one of two distinct modes which are generally referred to as 'single-shot' and 'synchroscan' operations.

1.2.1 Single Shot Operation

In single-shot operation (typically used for pulsed lasers or phenomena in which only a low repetition rate is achievable) the electrostatic deflection structure is driven by a rapidly changing linear voltage ramp, such as that produced by a laser activated spark gap [19], high frequency valve [20], krytron [21], photoconductive switch [22] or avalanche transistor circuit [23]. The synchronisation of the activation (or triggering) of the ramp generator must be such that the photoelectron packet released by the incident optical pulse illuminating the photocathode falls on the phosphor screen while being streaked by the deflection structure. While this presents no particular problems at low to moderate streak speeds due to the 'large' time window available (several tens of nanoseconds, 10^{-9} s), high streak speeds (in which the electron beam is swept across the phosphor screen at rates approaching the speed of light) required to achieve optimal temporal resolution offer a usable 'window' of only ~100ps. In order to ensure a recording on every shot therefore, the triggering of the deflection circuit should provide very low shot-to-shot temporal variation (called 'trigger jitter') with respect to the incoming optical pulse. Because of this, avalanche transistor circuits (typically demonstrating a trigger jitter of 50ps) and photoconductive switches (whose jitter has been shown to be as low as 2ps [24]) are now almost exclusively employed for high temporal resolution single-shot streak cameras. While photoconductive switches (capable of switching many kilovolts in tens of picoseconds) have shown to be an effective solution to many of the problems associated with deflection ramp generation, they do require moderate energy optical trigger pulses (>200 μJ delivered in several picoseconds [24, 25]) in order to be fully utilised, and their operation has been found to be alignment-sensitive and inconvenient. Avalanche transistor circuits while slower and having a larger trigger jitter have the advantage that they may be triggered with low optical energies (~nJ) and offer flexibility due to the ability of operation in conjunction with electrical transmission line type delays.

1.2.1.1 Temporal Resolution

The temporal resolution of a streak camera may be thought to be a function of the achievable spatial resolution and streak speed achievable at the phosphor screen.

Simplistically it might be imagined that if a static spatial resolution of x μm and a streak speed of v μm/second was achievable then a limiting temporal resolution of x/v seconds would attainable, but this is rarely the case in practice for reasons outlined below.

1.2.1.2 Space Charge Effects

Streak cameras suffer from a number of limiting effects (some of which are intensity dependent) which reduce their temporal resolution and usable dynamic range. Theoretical considerations indicate that that the liberation of photoelectrons excited from a suitable photocathode occurs within ~10fs [59] and so electron 'lagging' does not occur. At high irradiance (required to achieve sufficient electrons at the phosphor screen to record with a single shot streak camera) the electron current demand from the photocathode leads to voltage dropped across the cathode material due to its finite resistance (typically 50 to 150 Ohms per square with modern fabrication techniques). These voltage perturbations lead to space charge effects causing image distortion [26] and so low resistance photocathodes should be employed. Modern photocathode fabrication techniques allow a very thin photo-active layer to be deposited upon a highly conductive substrate. The photocathode window is typically quartz or silica which is overlaid with a very fine (photolithographically generated) mesh with a period of ~1 μm. This maintains the cathode at a constant potential over the active area and thus greatly reduces space charge effects at the cathode surface.

At high photocurrents the Coulomb repulsion of the electrons also becomes considerable [29] and leads to the electron packet (which may have spatial dimensions of only a few micrometers) becoming distorted in space. This is an accumulative effect between the photoelectron emission from the photocathode and the entrance to the deflection structure. A small change in length (along the image tube axis) of the liberated photoelectron packet will result in transit time differences to the deflection structure and so will be deflected to different regions on the phosphor screen. This leads to a measured pulse broadening which is intensity dependent and so degrades the performance of the single-shot streak camera appreciably.

1.2.1.3 Photoelectron Energy Spread

The photoelectrons are emitted at different velocities and energies (characterised by the secondary electron emission energy spread of the cathode) from the same point on the cathode and so follow different paths through the electron-optical lens. When streaked in the deflection structure, the different initial velocities of these electrons result in a temporal separation due to the temporal difference accumulated between them in transit between the photocathode and deflectors. Also, the photoelectrons must be accelerated away from the photocathode to minimise the space charge that arises in its close proximity [27,28]. This deficiency which increases with increasing optical stimulation causes image distortion in both spatial and temporal domains. These problems can be alleviated by introducing an accelerating electric field perpendicular to the photocathode surface, thus accelerating the electrons to high energies quickly. The temporal resolution degradation of a streak camera within the photocathode-mesh region is a function of electron emission energy spread and electrostatic extraction field. Given that an emitted photoelectron may have a statistical energy emission distribution in any direction, it is possible to analytically calculate the temporal resolution degradation within this region. When using the following definitions; d, cathode-mesh separation, V, cathode-mesh potential difference, m, electron rest mass, x, axial electron position, e, electronic charge, t, time ($t = 0$ at $x = 0$), v_0, initial electron emission velocity in the x direction, it may be shown that (neglecting space charge effects) the electron transit time T between the photocathode and mesh electrode is given by

$$T = \frac{\sqrt{v_0^{\,2} + \frac{2eV}{m}} - v_0}{\frac{eV}{md}} \qquad (1.1)$$

where

$$v_0 = \sqrt{\frac{2eE_0}{m}} \qquad (1.2)$$

and E_0 is the initial electron emission energy. It is clear that to minimise the electron transit time spread (ΔT) in this region, V should be maximised and d minimised for a given E_0. In fact it may be seen that ΔT is proportional to $d / V^{1/2}$ within this region. The temporal resolution of the entire camera may be estimated using the Gaussian response approximation and as such, evaluated using quadrature summation of the individual temporal responses. This Gaussian approximation technique has now been superseded by advanced computer simulations which allow a more accurate analysis of electron-optical systems and these are briefly discussed in chapter 9.

1.2.1.4 Dynamic Range

Intensity-dependent effects lead to a loss of camera 'dynamic range' which is defined as the ratio between the maximum input light intensity which causes a measured pulse broadening of 20% to the minimum intensity required to faithfully record the pulse. In order to alleviate many of these intensity-dependent effects, an image intensifier is coupled to the output of the phosphor screen of single-shot streak cameras so that the input light intensity to the camera may be reduced. In the limit single photoelectrons may actually be recorded, but a sufficient number of photoelectrons must be recorded so that adequate signal-to-noise ratios may be achieved.

1.2.1.5 Image Intensification

Image intensifiers have had considerable development and evaluation over the years (principally for military applications) and may be divided into two main categories, ie. those with and without microchannel plates. The output of the camera phosphor screen is coupled to the input photocathode either by lens or fibre-optic faceplate and the image intensifier type often dictates which method is adopted.

Both electrostatic and magnetic electron-optical focusing configurations have been employed within intensifiers. Both of these systems rely on the photoelectrons emitted from the photocathode being accelerated to considerable energies (> 5 KeV) before impinging upon a photoemissive phosphor screen. The gain of these systems is

therefore intrinsically low (typically ~50, restricted by the phosphor efficiency) and so these units are often cascaded together, resulting in a total system gain of ~10^6 for a four stage device. The spatial resolution of these devices is a property of the electron-optical focussing system employed. Electrostatic proximity-focussing is the simplest technique, but positive feedback often results from ion migration from the output phosphor screen to the photocathode, causing impact ionisation. This results in considerable noise when cascaded units are employed. Electron-optical focussed devices, either electrostatic or magnetic do not suffer from the positive feedback effects to such an extent and so are intrinsically less noisy, while the spatial resolution is often high (typically 80 lp/mm). These cascaded devices are heavy and bulky however and often require water cooling and high current demands (for the electromagnets) in the case of the magnetically focussed devices. Another problem associated with these cascaded devices is the large potential difference between the input photocathode and output phosphor screen, requiring lens coupling to any other systems for safety reasons.

For the reasons outlined above, smaller, lighter and more convenient systems have been developed in the form of microchannel plate (MCP) [32] intensifiers. These comprise a proximity or electrostatically focussed geometry where the photoelectrons are imaged onto the MCP and the output of the MCP is proximity focussed onto a phosphor screen. The MCP is constructed from a high quality insulator and has small diameter holes (or 'channels') through it, packed together as close as possible. Within these channels a material with a high secondary electron emission coefficient is deposited, and so an electron entering one of these channels causes avalanche ionisation, and hence intensification. Gains of 10^6 are readily available from these MCP image intensifier devices and may be easily adjusted by altering the potential difference between the input and output of the plate without affecting the spatial resolution. The device is compact, easy to operate and may be fibre-optically coupled at the input and output due to the modest voltages (~5kV) usually employed. The spatial resolution of the device is principally limited by the channel diameter and separation which is typically 10μm and 15μm respectively yielding a spatial resolution in excess of 20 lp/mm. Loss of device resolution due to proximity focussing is slight due to the

fabrication techniques developed which enable elements to be placed <1 mm apart while maintaining a high voltage hold-off capability. The total device spatial resolution (usually ~20 lp/mm) is sufficient for most applications although recently it has become evident that, when operated at high gains the spatial resolution may be seriously degraded (chapter 8.4). Indeed, this image degradation has been so severe on occasions that gross image intensity modulation has been experienced when an MCP intensifier was operated in conjunction with a single-shot streak camera. It is believed that these effects may be caused by contamination within the image intensifier and this problem will require careful consideration in future.

1.2.1.6 Dynamic Slit Curvature

Another problem related to single-shot camera operating at high streak speeds is dynamic slit curvature [21]. This effect results from the fact that photoelectrons emitted from points away from the camera axis must travel a greater distance to the electron-optical crossover then those emitted from a point at the centre of the photocathode. This causes a difference in photoelectron transit time between the photocathode and the deflector structure and thus a different spatial position when deflected. This results in the streaked image slit becoming curved, and while this does not degrade the temporal resolution provided care is taken in analysis of the results, it does provide difficulties when a number of optical channels are positioned along the input slit. In this case the dynamic slit curvature must be accurately known so that the relative temporal synchronisation between the channels can be achieved.

When fast streak speeds are employed as in single shot streak cameras, dynamic fringing fields associated with the electrostatic deflection system lead to image defocussing in the streak direction causing a loss in temporal resolution. This effect is described in more detail in chapters 3.7.1 and 7.

1.2.2 Synchroscan Operation

Synchroscan operation of a streak camera [21] is achieved by driving the electrostatic deflection plates with a sinusoidal voltage which is in phase with a periodic luminous event. Providing only the central portion of a sinusoidal deflection voltage is

employed then the achieved streak linearity is better then 5% over a limited region (0.1 of the deflection period) of the waveform as indicated in figure 1.2. For this reason it is essential that sufficient deflection voltages are generated to maintain streak linearity over the required deflection region and this is discussed in further detail elsewhere (chapter 6).

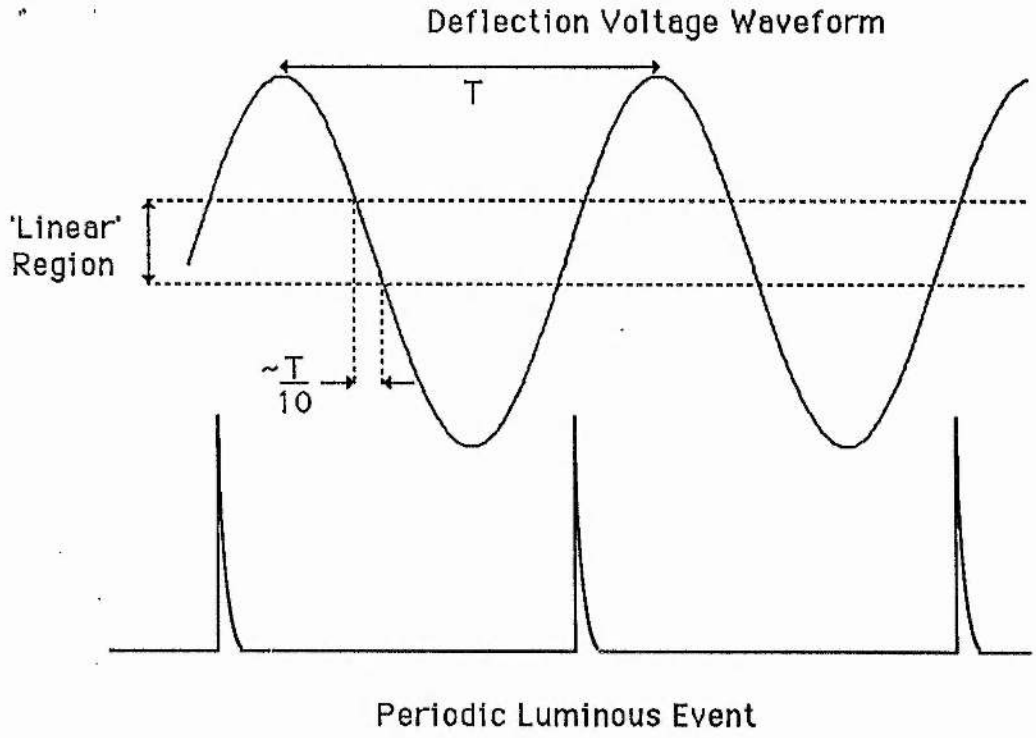

Figure 1.2. Synchronisation of the deflection waveform with the luminous event.

1.2.2.1 Deflection Waveform

The sinusoidal deflection waveform is usually derived from the output of the continuously operating mode-locked laser oscillator whose output or related phenomena is to be measured. Typical mode-locked laser repetition rates are between 50 MHz and 150 MHz so that, when their output is monitored with a fast photodetector, the fundamental (principal) harmonic output will be at the laser repetition rate. This fact may be used to directly generate the deflection waveform which may actually be selected as any one of the harmonics of the laser repetition output. This technique is shown schematically as figure 1.3.

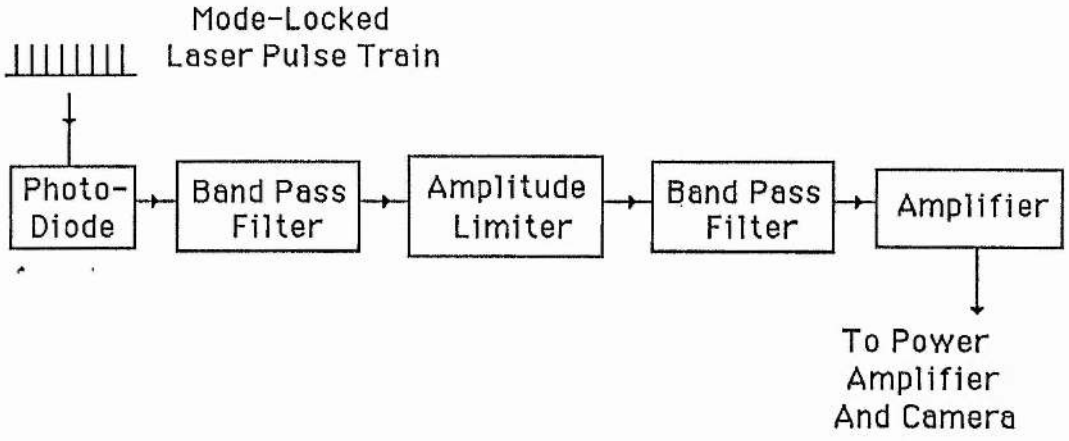

Figure 1.3. A 'passive' reference generation technique.

In this system the filter removes all the unwanted harmonics of the photodiode output, and the limiter removes most of the signal amplitude modulation which results from any intensity variations present in the laser output (see section 6.5.2). This technique is described as being 'passive' in that no active elements are used in the generation of the resultant output. An alternative technique relies on an unstable oscillator being repeatedly triggered and is therefore described as'active'. Figure 1.4 shows the stages involved in this system which is somewhat more complicated than the one above.

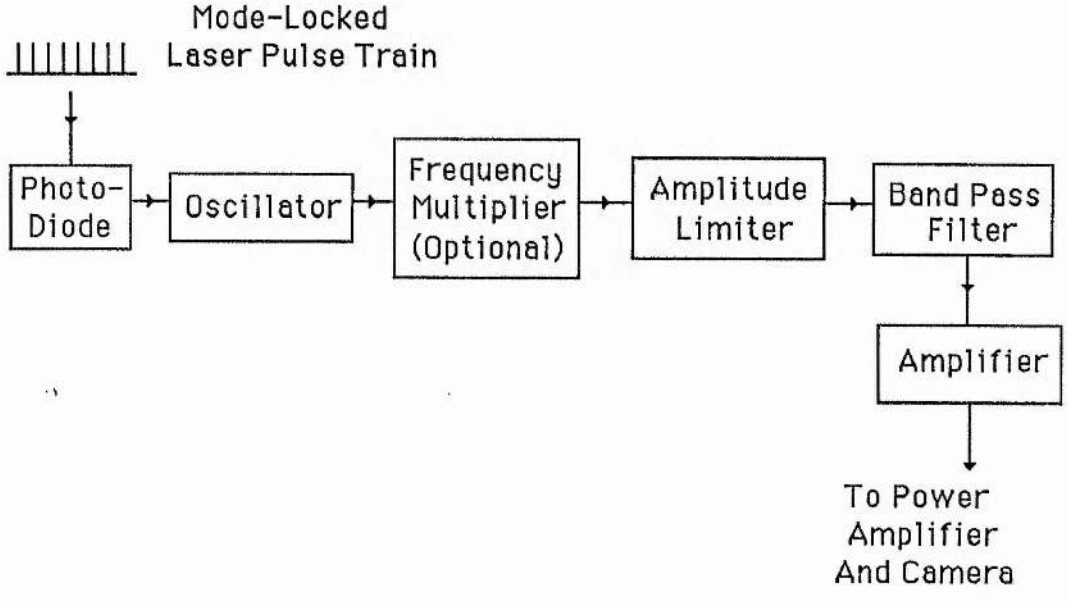

Figure 1.4. An 'active' synchroscan technique.

The unstable oscillator (typically a tunnel-diode configuration [31]) is designed in such

a way as to oscillate for a few periods when triggered. The frequency of oscillation of this device may be altered to be at an exact harmonic of the laser oscillator output so that the diode output repeatedly triggers the device into oscillation. In this way the oscillator is 'nudged' into phase by the photo-diode output and the oscillations are maintained. Further filtering and limiting improve the spectral purity of this reference signal.

Both techniques employ a radio frequency (r.f.) resonant circuit (chapter 6) to generate large deflection voltages for moderate r.f. power levels to the deflectors of the camera.

The synchroscan technique offers some advantages over single-shot operation and these are (i) synchronisation between the deflection waveform and optical signal is ensured (to within the laser repetition period) as the two are 'phase-locked', (ii) the improvement of signal-to-noise due to the integration of many streak images on the phosphor screen and (iii) the reduction of space charge and Coulomb repulsion effects within the streak camera due to the lower optical peak powers and hence lower peak photocurrents that need be employed. Applications for this system are numerous [30] mainly due to the ability of detecting very weak optical signals and so considerable effort is being spent trying to improve temporal and spatial performance characteristics.

Problems also arise in respect to the synchroscan technique. For instance, the phase matching required between the incident optical pulses and the r.f. drive voltage is rather exacting due to the need for image overwriting on the phosphor screen. Amplitude modulation causes slight variations in writing speed at the output and may only be tolerated to some extent due to the 'over-scanning' employed (although the limiter reduces this considerably), but phase noise on either the r.f. voltage or the laser output leads to streak smearing and can be extremely detrimental [31]. To this end, work is being undertaken to reduce this undesired modulation to further improve the performance of the synchroscan streak camera because it is believed that the resolution is considerably limited by these effects rather then the inherent design of the image tube. This has been shown to be the case with the Photochron IV camera where the best reported single shot resolution was 700fs while the best synchroscan result was recently reported to be 900fs.

1.3 Read-Out Devices

Image capture of the image produced on the phosphor screen of either the image intensifier or the camera may be achieved using photographic film, Polaroid film, one or two dimensional charge coupled-device (CCD) systems or optical multichannel analysers (OMA) employing a linear array of optical sensors. Where data from a single-shot camera is required, the dynamic range of the read-out device need not be particularly high (several hundred is usually sufficient) as the dynamic range of the streak or framing camera is often low for reasons previously above. On the other hand, synchroscan cameras offer high dynamic ranges of >1000 and so the read-out device should have a dynamic range greater than this. In all cases the signal-to-noise ratio and spatial resolution should be higher than that of the output of the image intensifier or camera in order that as little image degradation as possible occurs . Most electronic read-out systems suffer from either poor spatial resolution (typically 20μm diameter detector size) or small field of view (due to the large image demagnification required) which can make them difficult to use with a single-shot camera, but they still represent useful data acquisition systems for synchroscan type cameras where the camera output image is 'effectivly stationary' with time allowing 'real time' analysis.

1.4 Laser-Induced Plasma Reactions and Framing Cameras

1.4.1 Introduction

With the invention and development of high power pulsed lasers it became reasonable to assume that, under favourable conditions, nuclear fusion reactions [33] could be initiated by laser irradiation of small quantities of low atomic number (typically deuterium and tritium) material. Providing the energy transport efficiency between the laser radiation and the processes leading to nuclear fusion were controllable it was, and still is believed that sufficient energy could be released (if the 'Lawson criteria' is met [34]) to demonstrate commercial viability in the generation of energy. The most attractive features of controlled fusion reactions as a source of energy is the availability of fuel, which is virtually limitless, and by using isotope separation techniques it

should be possible to use the fusion reactor neutron flux to burn up harmful waste by converting long lived isotopes into short lived variants. It is easy to see then why such immense effort is being put into fusion generators as they should provide an inexhaustible amount of energy safely.

It is worth pointing out at this stage that work is also being undertaken into fusion using magnetic containment techniques, which in some ways is more attractive and is certainly more advanced at present. However the projected cost of these units is much higher then that of the laser inertial confinement fusion (ICF) systems and there are still many problems to overcome, so it is sensible to proceed with both techniques.

It is not within the scope of this thesis to present detailed information on laser-induced fusion reactions or laser plasma interactions but it is realised that the continuing development of the Ultra-Violet (UV) / X-ray sensitive Picoframe type, ultra-high speed two dimensional framing camera into the soft X-ray spectral region demands some understanding of the basic processes involved in X-ray emission. It is planned that the camera system will eventually be used to obtain temporally resolved two dimensional pictures of the expanding plasma created by intense laser illumination of deuterium-tritium filled micro-balloon targets.

While nuclear fusion is hopefully the end result of much of the work being undertaken in laser irradiated target experiments, the X-ray emission of the plasma caused by laser radiation is the principle topic of the following sections as the analysis of this radiation is of prime importance in the understanding and implementation of laser initiated fusion reactions.

1.4.2 Plasma Generation

It is well understood that the generation of photons may be caused by electron energy transitions within an atom or by Bremsstrahlung [35] emission. This effect is caused by any charged particle (eg. an electron) being accelerated rapidly causing high flux density photon emission and is most easily seen in electron bombardment experiments, where different electron-electron collisions result in a broadband photon emission spectra. Conversely, inverse Bremsstrahlung [37] occurs when an electron in binary collision with an ion absorbs a photon.

It is likely that after ionisation of the laser irradiated target occurs due to the leading part of the laser pulse, that the initial resultant energy absorption would be mainly due to inverse Bremsstrahlung. Linear absorption at laser power densities of ~10^{12} W/cm^2 at wavelengths of ~1μm predicted theoretically has now been confirmed by experimental results and so a reasonable understanding of the transport dynamics has now been achieved. At the higher laser energy densities required to initiate fusion reactions due to heating and compression effects, non-linear processes were predicted and that electromagnetic and electrostatic effects would become important with relativistic effects predominating at power densities of 10^{18} W/cm^2. These predicted results have not yet been conclusively proven experimentally and a great deal of work is still required in order to do so.

As previously mentioned, when laser energy is incident upon a solid surface with power densities of 10^{11} to 10^{12} W/cm^2 or more a plasma is formed near the surface. The exact details of this initial plasma generation have not been extracted from experimental work to date, but it is believed that multi-photon absorption plays a predominant role. Inverse Bremsstrahlung causes initial plasma heating and serves to increase the plasma density until resonant effects predominate. At these optical field intensities, free or weakly bound electrons will be accelerated significantly by the intense optical electric field. Under the influence of such intense optical fields, the free electrons may acquire sufficient energy to ionise neutral atoms or molecules at or near the solid surface over the time span of a few optical cycles (~10 femtoseconds for 1μm radiation). The resulting cascade ionisation rapidly increases the free electron density near the surface which, in turn, increases the rate of absorption. The plasma development in front of a laser irradiated slab target may then be described according to steps shown in figure 1.4.

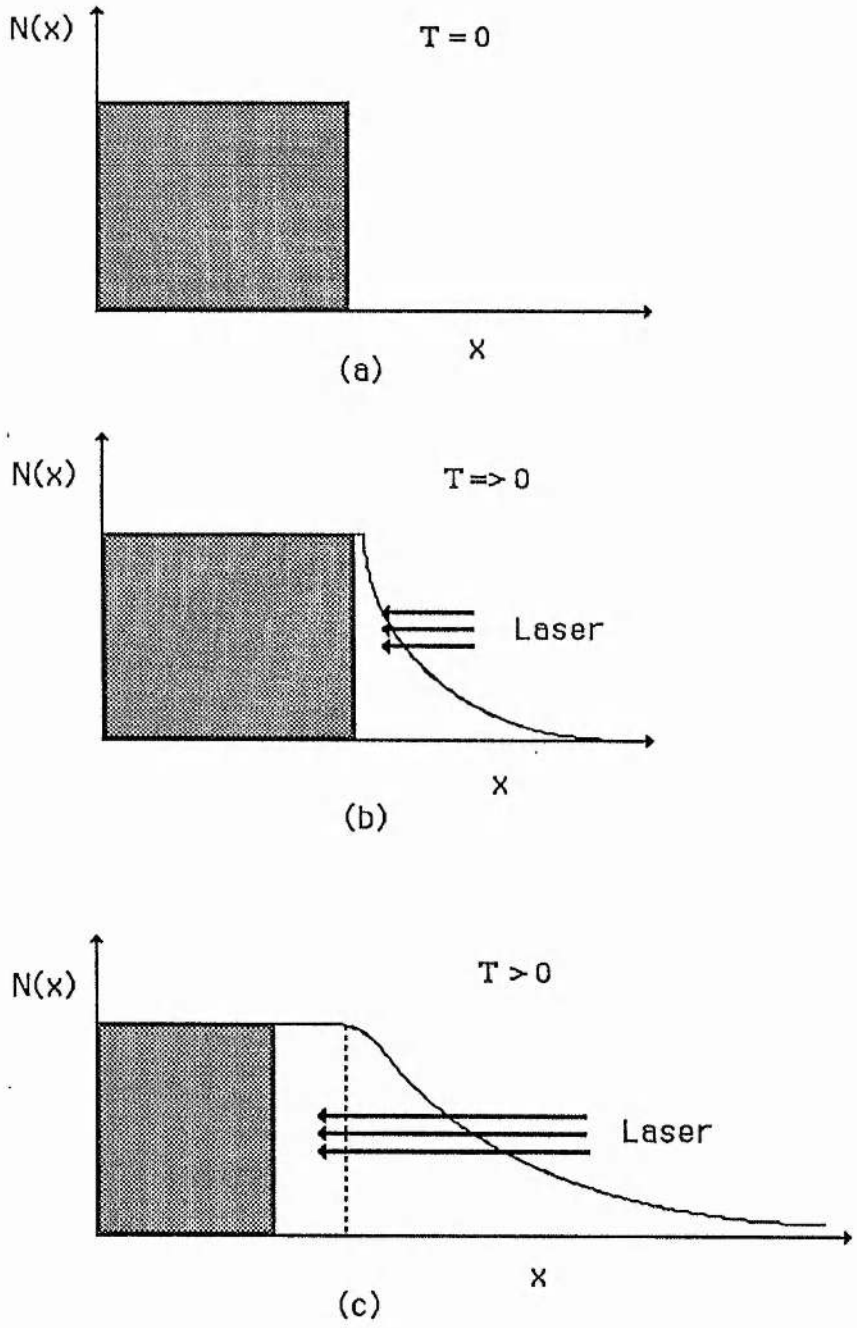

Figure 1.4. Evolution of a laser produced plasma with respect to electron density and spatial dimensions.

Figure 1.4, (a) shows the electron number density distribution for a target before laser irradiàtion. Figure 1.4, (b) shows the initiation of the plasma due to the laser radiation and the resulting particle density fall-off with distance from the target surface. Figure 1.4, (c) indicates the plasma density distribution which has developed, which may become approximately stable (although not fixed in space) depending upon the time

scale of the laser irradiation.

1.4.2.1 Plasma Oscillations

The electrons within the plasma can execute oscillations under the plasma electrostatic forces. The frequency of the oscillation is proportional to the square root of the particle density [38]. This implies that the plasma oscillation frequencies will be typically in the region of 5×10^{14} Hz for the plasmas involved in these thesis studies.

1.4.2.2 Critical Density

Where the electron density reaches a level (called the 'critical' density) such that the electrons oscillate at the same frequency as the applied optical field, incident laser energy is stored within the medium via resonant absorption. This absorption process may be up to 40% efficient under favourable conditions.The damping of these oscillations excites many processes, including (i) particle heating, (ii) fast particle excitation, (iii) back scattered radiation at the laser wavelength and various harmonics and (iv) radiation of X-rays.

The balance of energy among the various plasma processes depends on many factors such as laser intensity and target composition. The time-scale of the laser irradiation is also important although short time scale irradiation may not optimise the total X-ray production by the plasma, it is most likely to avoid significant ion heating. This is due to the fact that almost all of the energy is initially coupled into the electrons, which then transfer in energy by collisional processes, in the same way as normal thermal conduction. Thus, at the outer extremities of the plasma the massive ions will be highly energetic with a typical ion expansion energy of 10keV or more.

1.4.2.3 Superthermal Electrons

Superthermal electrons [36] result in these ultra-intense optical fields due to the very high acceleration they experience by the intense electrostatic fields. These superthermal electrons and associated ions may be accelerated to considerable energies, resulting in considerable emission of hard X-rays.

1.4.2.4 Plasma Density and Temperature

Ignoring a few details, the plasma electron temperature and density profiles at some instant during a short laser pulse irradiation have features such as those illustrated in figure 1.5, a more detailed version of which may be found in [37]. As shown in figure 1.5 the average plasma temperature may typically reach or exceed 1keV and so much of the electromagnetic radiation emission results in the XUV and soft X-ray spectral range.

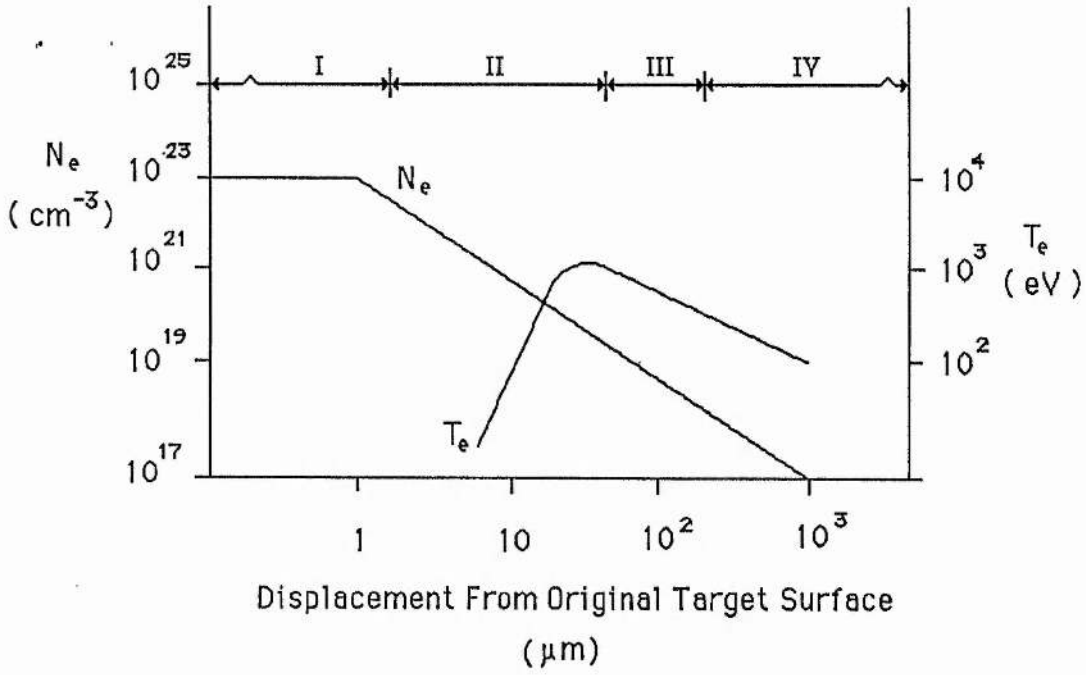

Figure 1.5. Simplified diagram of the typical plasma temperature and density with respect to the spatial dimensions.

There are four major regions of interest indicated on this diagram which are described below.

Region I, represents solid target material which is not heated significantly during the short laser pulse. Electrons may be free or bound depending upon target material. Region II, showing steeply decreasing electron density and rapidly increasing electron temperatures. This region forms the plasma where thermal conductivity keeps the temperature high through the outer zone of region II. Region III is the low density and high temperature region called the 'coronal' region. Only weak absorption of the laser

energy occurs here but the primary loss mechanism is due to expansion which is not effective on very short time scales and so the associated temperature tends to be high in this region. In Region IV free expansion of particles will occur when the target is situated within a vacuum. Negligible absorption of the laser energy occurs in this region due to the low density and so collisions are infrequent consequently the thermal velocities of the particles near the outer edge of the corona (III) become directed velocities of expansion in region IV and thus the kinetic temperature is reduced in this region.

1.4.3 X-Ray Self Emission

Once the plasma is established in a few optical cycles, x-ray emission occurs due to many processes, some of which are briefly outlined below.

1.4.3.1 Recombination

Direct recombination and relaxation processes which depends upon the degree of initial ionisation of the targets and their structure. The radiation process may lead to a complicated emission spectrum due to the possibility of high and low energy electrons relaxing into similar energy levels causing a 'continuous' spectra with some finite maximum and minimum photon energy. Predominant features such as M to N level transitions for gold (1.6keV to 2.9keV) irradiated with ~1 Joule (in 100ps FWHM) of 532nm radiation are however clearly evident as shown in figure 1.6.

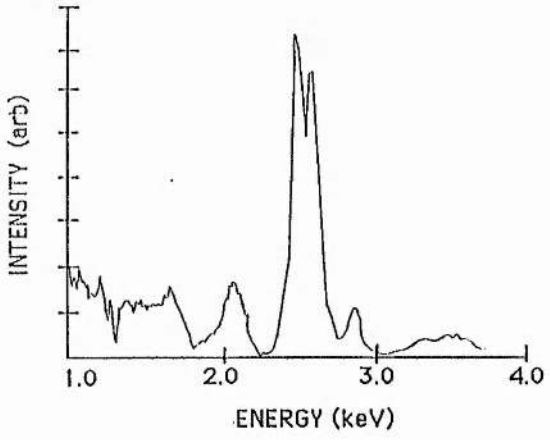

Figure 1.6. Time integrated spectrum of a laser produced plasma. The target was a gold foil and the laser radiation wavelength was 532nm.

This recombination process usually predominates in regions III and IV. Any observed emission spectrum is further complicated by absorption which may occur within the plasma corona because of the existence of large variations in electron densities and temperatures.

1.4.3.2 Bremsstrahlung

Bremsstrahlung emission may occur and this will be predominant within the high density, high temperature regions eg. III and IV. This effect is dependent upon the laser pulse duration, as if sufficiently short, the plasma will collapse before sufficient particle collisions may occur to produce a noticeable emission.

As previously mentioned, the plasma oscillates due to the electrostatic components of the intense optical fields and the collisionless damping of these oscillations ('Landau' damping or 'wave breaking' [37]) may result in X-ray production due to Bremsstrahlung. Also emission of the laser fundamental frequency and subsequent harmonics may result when a sufficient (critical) plasma density is reached.

1.4.3.3 Secondary Photo-excitation

Photons emitted from the above processes may of course reach the target surface (region I) and thus cause photo-ionisation and hence further emission would result. In this way it is feasible to imagine high energy X-rays being absorbed to produce lower energy photons, on recombination for example.

1.4.4 Relevent Plasma Diagnostics

It may be seen from the above brief outline of X-ray generation of laser produced plasmas that they may be used as an intense picosecond point X-ray source[38, 58], whose dimensions are approximately equal to the laser focal spot diameter. Much information regarding the plasma may be deduced from this X-ray emission spectrum and spatial emission distribution from within the plasma itself. Typical measurements taken include (i) time-integrated and time-resolved [39] X-ray spectra using an X-ray diffraction spectrometer and X-ray-sensitive streak camera respectively or (ii)

time-integrated [39] and time-resolved two-dimensional images of the plasma typically using pinhole cameras or grazing incidence microscopes in conjunction with X-ray-sensitive film or X-ray-sensitive electron-optical framing cameras.

1.5 Framing Cameras

Time integrated and resolved one and two dimensional measurements of the plasma allow the characterisation of the plasma with a reasonable degree of accuracy, but accurate data is often difficult to obtain. While time-resolved spectroscopy may be achieved with modern X-ray-sensitive streak cameras[40, 41], great difficulty has been experienced in the development of X-ray-sensitive framing cameras, capable of obtaining multiple images or 'frames' of the plasma within a single laser shot. Due to the velocity of the expanding plasma (typically 10^7 cm/s), frame exposure times of ~100ps are desired to prevent image motion blur and dynamic spatial resolutions of 10 lp/mm are required to image the small plasmas successfully. 'Direct' techniques have been attempted in the visible electromagnetic spectrum by gating the photon flux using accousto-optic and electro-optic devices, but suitable crystals cannot be found at present for the XUV to soft X-ray spectral range (~10nm to 1.3 Angstroms). 'Intrusive" techniques involving short 'flash' illumination have been developed, and the simplest device often used is flash X-ray back illumination of the plasma [eg. 42, 43]. This technique is useful but suffers from the fact that only one image may be recorded along the one viewing axis per laser shot and so analysis of the images becomes difficult, and multiple back-lighters are required to image more then one temporally resolved image.

1.5.1 Holography

Attempts have also been made at obtaining two dimensional images of the plasma density rather then the self X-ray emission from the plasma. Recently holographic [44] techniques utilising laser probe beams have allowed four temporally separated images of a laser plasma showing the plasma density to be recorded with a temporal resolution of ~20ps and a spatial resolution of ~1μm. Unfortunately this system is extremely complicated and image reconstruction is a lengthy process. Shadow Schlieren interferometry [45] has also been successfully used but again this technique is rather

involved with intricate optical components, and like the holographic technique, does not allow multiple frames to be recorded along the same viewing axis.

1.5.2 Electron-Optical Framing Cameras

Alternative (non intrusive) techniques have almost exclusively been electron-optical in nature and of these systems two main classifications may be defined as the 'proximity-focused type' and the 'electron-lens focused type'.

1.5.2.1 Gated Intensifiers

The proximity-focused camera design was initially based upon the X-ray-sensitive, proximity or magnetically focussed [46,47] image intensifiers which were gated on for short periods. Many problems were encountered with this device such as poor shutter contrast and direct excitation of the phosphor screen by the X-rays transmitted through the photocathode. Variants on the multi-channel plate (MCP) proximity focused image intensifier[48, 49, 50, 51], gated on for very short periods allow good shutter contrast and X-ray attenuation so reducing the background noise recorded. The minimum frame exposure time of these devices is limited by the electron transit time spread through the MCP which has been experimentally shown to be ~150ps [48]. These devices have been developed by a great number of workers and so will not be discussed in detail, although it is worth noting that that multiple frames may only be recorded from different viewing angles at present due to the extreme practical difficulty in arranging suitable mirror / beam-splitter arrangements in the soft X-ray spectral region.

1.5.2.2 'Electron Beam' Cameras

The 'electron beam focussed' type of electron-optic imaging camera is based around an image tube (similar to a streak camera) comprising of a photocathode, electron lens, electrostatic deflectors and a phosphor screen. Four different systems of operation of these devices has been attempted, but the point in common with all of the systems is that they are able to provide multiple frames along the same viewing axis and are suitable for use in a broad spectral range from infrared to X-ray (dictated by the

cathode used).

1.5.2.2.1 Gated Cathode

In one mode of operation the camera cathode is gated [52, 53] repetitively and the subsequent electron-optical images spatially separated at the phosphor screen by suitable deflection waveforms being applied to the electrostatic deflection plates. This technique has so far produced only relatively long frame exposure times (the shortest reported is ~400 ps FWHM) and only moderate spatial resolution (<= 5lp/mm at these frame exposure times) with visible light due to the problems associated in gating the cathode sufficiently fast.

1.5.2.2.2 Staircase Deflection

In another mode, the imaging electron beam is deflected very rapidly between points on the phosphor screen [54] using travelling-wave deflectors (see chapter 7) with a 'staircase' shaped voltage waveform. This technique resulted in image formation at the electron beam stationary positions, and provided the inter-frame deflection speed was sufficiently fast, very few photons were recorded in the 'smeared' deflection region. This system was tested on an X-ray source and although four frames could be generated poor spatial resolution (<4 lp/mm) was achieved. Another problem associated with this technique was that the frame and inter-frame times were not independent. The inter-frame time had to be less than the frame time by a factor of ~3 in order to achieve reasonable resolution, which meant that at the desired 100ps exposure times the deflection signal risetime would have to be ~33ps, which is too short for most practical purposes.

1.5.2.2.3 Image Dissection

Another mode of operation attempted with this image tube type was the 'image dissection' technique [55]. This system relied on sweeping the pre-focussed photoelectron image (using electrostatic deflection pates) perpendicular to a small slit electrode placed at the image plane of an electrostatic lens. The resultant 'segments' transmitted by the slit were reconstructed to reform the image at the phosphor screen by

the use a further set of electrostatic deflection plates and electron-optical lens. This system produced three frames (using a three slit electrode) with visible incident light, each frame having a spatial resolution of ~5 lp/mm and a frame exposure, inter-frame times of ~250 ps and 400 ps respectively.The main problem with this technique was that the resultant camera electrodes (comprising of two separate electron-optical lenses and two sets of deflection electrodes) were difficult to manufacture accurately and was complicated to operate. Another aspect of this camera design was that the image produced on the phosphor screen was not 'exposed' all at once but in sections, and so the image formed was not truly time resolved. This situation becomes worse as the image size is increased with this mode of operation.

1.5.2.2.4 'Shutter' Camera

The final mode of operation attempted with this electron beam focused image tube is the 'shutter' operation [56, 57]. This technique is similar to that employed by Kalibijan et. al. [55] previously mentioned but instead of placing a slit electrode at the image plane of the electron-optical lens, a small aperture (or apertures) is positioned at the electron beam crossover or waist. The image forming electron beam is then swept rapidly across this aperture to provide a short temporal burst to be transmitted. A further set of electrostatic deflectors is included within the image tube to remove the transverse electron velocity imparted by the first set of deflectors. Full details of the operation of this camera design will be presented in chapter 2 and it suffices here to mention some of the advantages associated with this system.These are (i) multiple frames may be achieved by scanning the image forming electron beam across the aperture many times, using multiple aperture schemes, or a combination of the two techniques, (ii) the frame exposure time is adjustable by varying the speed at which the electron beam is scanned across the aperture and the whole frame is 'exposed' at once, (ii) high dynamic spatial resolution should be possible with this scheme although this will be defined to a large degree by the electrostatic lensing system and (iv) all the frames generated are along the same line of sight.

The development of an UV and X-ray-sensitive vacuum demountable 'shutter' type of framing camera allocated the name 'Picoframe', is the subject matter for much

of the thesis content that follows.

References for Chapter 1

1 S De Silvestri, P Laporta, O Svelto

IEEE Journal of Quantum Electronics, QE-20 (5), 533, 1984

2 E B Treacy

IEEE Journal of Quantum Electronics, QE-5 (9), 454, 1969

3 R N Thursten, J P Heritage, A M Wiener, W J Tomlinson

IEEE Journal of Quantum Electronics, QE-22 (5), 682, 1986

4 B Zysset, W Hodel, P Beaud, H P Weber

Optics Letters, 11 (3), 156, 1986

5 A M Johnson, W M Simpson

Opics Letters 8 (11), 554, 1983

6 N Langford, K Smith, W Sibbett

Optics Comm., 64 (3), 272, 1987

7 D Burns, D W Crust, J T K Chang, W Sibbett

Electronics Letters, 24 (23), 1439, 1988

8 W Margulis

Ph D Thesis, University of London, 1981

9 J S Courtney - Pratt

Proc. Advances in High Speed Photography 10, 12, 59, 1972 and Advances in High Speed Photography JSMPTE, 82, 167, 1973

10 H E Rowe, T Li

IEEE J Quant. Elect., QE-6, 49, 1970

11 C V Shank, R L Fork, R Yen, R H Stolen, W J Tomlinson

Applied Physics Letters, 40, 761, 1982

12 J C M Diels, J J Fontain, I C Mcmicheal, F Simoni

Applied Optics, 24 (9), 1270, 1985

13 D G Parker, P G Say, S M Hansom, W Sibbett

Electronics Letters, 23, 527, 1987

14 C Kalpouzos, G A Kenney-Wallace, P M Kroger, E Quitevis, S C Wallace

'Picosecond Phenomena III', Springer Verlag series in Chemical Physics, 23, New

York, Editor Eisenthal, 221, 1982

15 K Kinoshita, M Ito, Y Suzuki

Rev. Sci. Instrum., 58 (6), 1977

16 K Kinoshita, M Ito, M Suyama

Proc. 18th ICHSPP (Xian), SPIE 1032, 441, 1988

17 A J Lieber, R F Benjamin, H D Sutphin, C B Webb

Nucl. Inst. Meth., 127, 87, 1975

18 H Niu, V P Degtyareva, V N Platonov, A M Prokhorov, M A Schelev

Proc. 18th ICHSPP (Xian), SPIE 1032, 79, 1988

19 B Liddy

Ph D Thesis, The Queens University of Belfast, 1971

20 Hadlands Photonics Ltd., Newhouse Labs., Newhouse Rd., Bovingdon, England

21 W Sibbett

Ph D Thesis, The Queens University of Belfast, 1973

22 D H Auston

Applied Physics Letters, 26, 101, 1975

23 M C Jackson, R D Long, D Lee, N J Freeman

Laser and Particle Beams, 4 (1), 145, 1986

24 G Mourou, W H Knox, S Williamson

'Picosecond Optoelectronic Devices', Editor Chi Lee, Chaper 4, 73, 1984

25 W Knox, G Mourou, S Letzring

Proc. 15th ICHSPP (San Diago), SPIE 348, 308, 1982

26 R Kalibjan, G G Paterson

Proc. 15th ICHSPP (San Diago), SPIE 348, 195, 1982

27 S Majumdar

Proc. 12th ICHSPP, SPIE 97, 24, 1976

28 R Kalibjan

Proc. 13th ICHSPP , SPIE 189, 452, 1978

29 H Niu, W Sibbett

Rev. Sci. Instrum., 52 (12), 1830, 1981

30 W Sibbett

Proc. 15th ICHSPP (San Diego), SPIE 348, 15, 1982

31 A Finch, Y Liu, W E Sleat, W Sibbett, G Chen

Proc. 18th ICHSPP (Xian), SPIE 1032, 97, 1988

32 S F Bryant

Ph D Thesis, University of London, 1978

33 J Nuckolls, L Wood, A Thiesen, G Zimmerman

Nature, 239, 139, 1972

34 J D Lawson

Proc. Physics Soc. London, B70, 6, 1957

35 eg. 'Physics of The Atom' 3rd Edition

Addison-Wesley Publishing Company

36 S K Goel, P D Gupta, D D Bhawalker

Rev. Sci. Instrum., 50 (9),1157, 1979

37 M H Key

Phil. Trans. R. Soc. London, A298, 141,1980

38 eg. J M Forsyth, T C Bristow, B Yackobi, A Haur

'Laser Induced Fusion and X-ray Studies', Editors S F Jacobs, M O Scully, M Sargent III, C D Catrell III, Addison Wesley Publishing Company Inc., 581, 1976

39 S A Letzring, R S Marjoribanks, M C Richardson, D M Villeneuve

Proc. 15th ICHSPP (San Diego), SPIE 348, 325, 1982

40 eg C F Conaghy, L W Coleman

Applied Physics Letters, 25 (5), 268, 1974

41 P A Jaanimagi, D K Bradley, J Duff, G G Gregory, M C Richardson

Rev. Sci. Instrum., 59 (8), 1854, 1988

42 C Yamanaka, N Miyanaga, K Imasaki, Y Kitayawa, Y Kato, M Nakatsuka, T Mochiruiki, T Yamanaka

Proc. 15th ICHSPP (San Diego), SPIE 348, 783, 1982

43 R R Whitlock, S P Obenschain, J Grun, J A Stamper, B V Sweeney

Proc.15th ICHSPP (San Diego), SPIE 348, 789, 1982

44 G E Busch, C L Shephard, L D Siebert, J A Tarvin

Rev. Sci. Instrum., 56 (6), 879, 1985

45 A G M Maaswinkel, R Sigel, H Baumhacker, G Brederlow

Rev. Sci. Instrum., 55 (1), 48, 1984

46 eg Eschard

Proc.7th ICHSP, 1968

47 S Majumdar

Proc. 16th ICHSPP (Strasbourg), SPIE 491, 913, 1984

48 B K F Young, R E Stewart, G Woodworth

Rev. Sci. Instrum., 57 (11), 2729, 1986

49 N Fleurot, J P Gex, M Rostaing, R Saneuf

Proc. 15th ICHSPP (San Diego), SPIE 348, 772, 1982

50 M J Eckart, R L Hanks, J D Killkenny, R Pasha, J D Wiedwald

Rev. Sci. Instrum., 57 1(8), 2046, 1986

51 A S Lundy, A E Iverson

Proc.15th ICHSPP (San Diego), SPIE 348, 178, 1982

52 A E Huston

Proc.15th ICHSPP (San Diego), SPIE 348, 251, 1982

53 V V Ludikov, A M Prokhorov, V K Chevokin

Advances in Electronics and Electron Physics 74, 268, 1988

54 N Finn, T A Hall, E McGoldrick

Applied Physics Letters 46 (8), 731, 1985

55 R Kalibjian, S W Thomas

Rev. Sci. Instrum., 54 (12),1626, 1983

56 S A Varga, T S V'yugina, M I Krutik, V B Lebedev, G G Feldman, N V Chernyshev

Proc. 16th ICHSPP (Strasbourg), SPIE 491, 247, 1984

57 M R Baggs, R T Eagles, W Margulis, W Sibbett, W E Sleat

Advances in Electronics and Electron Physics, 64B, 627, 1985

58 H C Gerritsen, H Van Brug, F Bijkerk, M J van der Wiel

Journal of Applied Physics, 59 (7), 2337, 1986

59 E K Zavoisky, S D Franchenko

Applied Optics, 4 (1), 1155, 1965

Chapter 2

UV-Sensitive Picoframe I Camera

In Single and Double Frame Modes of Operation

2.1 Introduction

The Picoframe type framing camera consists of a cathode, mesh electrode, electrostatic lens, deflection regions and phosphor screen. A schematic of the Picoframe I (with a single framing aperture) is shown in figure 2.1

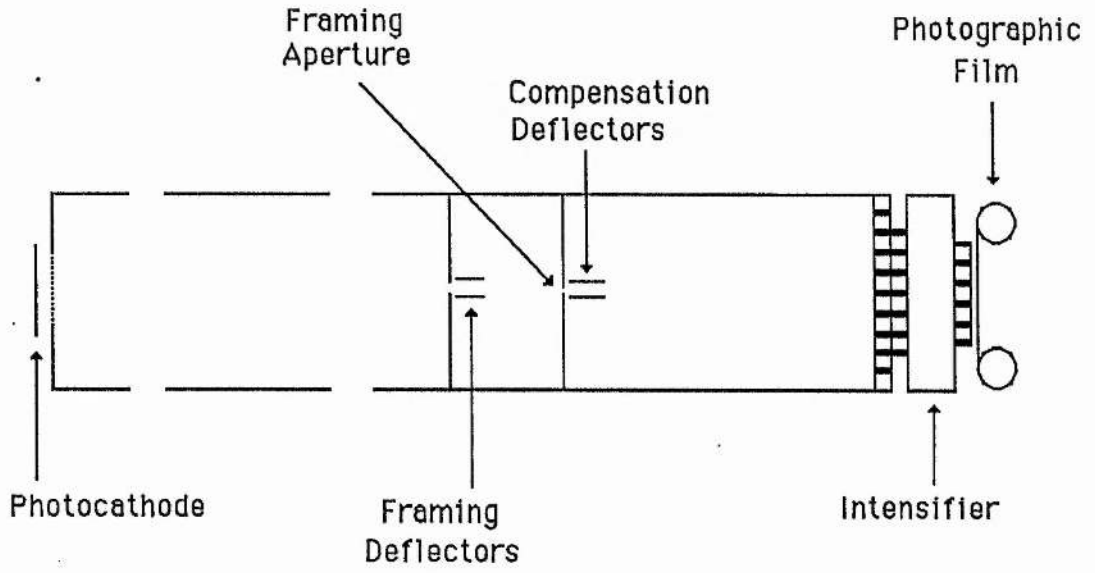

Figure 2.1.Schematic diagram of the Picoframe I framing camera.

2.2 Operation of the Picoframe I

In operation, the photons imaged onto a suitable photocathode cause electron emission. These electrons are emitted from the cathode with varying energy and direction and so must be collimated and focussed to faithfully reproduce the incident photon image. The mesh electrode is positioned in close proximity to the cathode and is positively biased with respect to the cathode, so that the photoelectrons can be accelerated within this high field region. While some electrons are absorbed by the mesh (typically 70% transmission) others will continue into the electrostatic lens

region. The three cylindrical electrodes employed were biased at -10kV, -12.8kV and 0V (from left to right in figure 2.1) with the photocathode maintained at -15kV to produce the equivalent of two spherical lenses for the photoelectrons. Full details of the electrostatic lens may be found elsewhere [1]. The electrons are then focussed to a small diameter crossover by the lens system. The anode aperture (maintained at ground potential) is positioned before the electron crossover to enable a set of electrostatic deflectors (called the framing deflectors) to be inserted. These allow the electron beam to be rapidly swept across the second (framing) aperture by applying a linear, time-varying voltage to cause a short temporal transmission of photoelectrons into the drift region ahead of the phosphor screen. In this region a further set of electrostatic deflectors (compensation) are positioned and a suitable time- varying voltage applied to remove the transverse velocity imparted to the electrons by the framing deflectors [1, 2]. Providing this compensation can be achieved to suitable accuracy a so-called framed image with short temporal exposure will be formed without smear on the phosphor screen.

2.3 UV and X-ray Two-Dimensional Imaging

While it has been shown that good spatial resolution and reasonable frame times may be obtained from the Picoframe I camera designs and potentially good performance from the twin aperture Picoframe II system with a visible light sensitive photocathode, the diagnostic would be much more useful in the UV / x-ray spectrum [3]. In laser irradiated deuterium-tritium filled microballoon experiments spectral and temporal information may be obtained from crystal spectrometers and streak cameras, but at present the most successful system available for obtaining two-dimensional images of the imploding microballoon and the associated expanding plasma density is by using backlighting and x-ray-sensitive film. The system adopted relies on a short (typically 100ps) laser pulse being focused onto an x-ray emitting substance (usually a carbon fibre) with sufficient energy (~20 joules) to provide a point source of x-rays. An x-ray-sensitive film is then positioned opposite the microballoon target so that a 'shadowgraph' of the plasma is recorded, rather then the plasma self emission. Two main problems exist with this system, (i) finding a suitable backlighter for a particular

target (the target plasma must become opaque to the backlighting emission for any information to be obtained) and (ii) only one image may be recorded from one viewpoint per shot. Multiple images may be formed using separate backlighters and film but the data collected are very difficult to interpret due to the different perspective of each of the images.

The main reason for investigating the UV/x-ray spectrum self-emission of the laser produced plasma is that the plasma temperature, density and and evolution may all be deduced from the origin and energy of the (typically x-ray) photons emitted. Thus details of the plasma may be obtained from a sequence of these two-dimensional frames. Another consideration is that the incident laser radiation is very often visible (frequency-doubled Nd:YAG, Nd:Glass laser radiation ,~530nm) which is so intense that difficulties are experienced in suitable filtering within the visible spectrum.

2.4 The UV / X-ray-Sensitive Picoframe I Design

With these problems in mind it was believed that the Picoframe framing camera design could be employed. Initially it was realised that the higher secondary electron emission energy spread of a UV or x-ray-sensitive photocathodes (some 4eV as compared to 0.3eV for standard multi-alkali cathode) would cause problems due to the fact that the electron trajectory paths would stray much further from the electron-optical lens axis causing increased spatial and temporal distortion [4]. It was also pointed out that the electron beam crossover would have a larger diameter which would understandably cause problems at the anode aperture due to a reduction in electron transmission. Similarly, the deflection plate structure and framing aperture may all be regions of interest in the evaluation of an improved electron optical lens for the x-ray framing camera. A new design, slightly modified from the visible version was proposed [4] to overcome some of these problems. This design involved a doubling of the cathode-mesh separation and the applied potential difference, a small reduction in length of the last electrostatic lens cylinder to alter the crossover position and a reduction of the anode aperture-to-framing aperture separation. Although these modifications were implemented the performance of the camera was not improved to any appreciable degree; the frame time was increased by ~70%, the magnification was

increased from -1.4 for the visible camera to -1.9 and the spatial resolution was only marginally improved. The problem is that the secondary electron energy spread increase from ~0.3eV from a typical S20 photocathode to ~4eV for a typical x-ray-sensitive gold photocathode is so large that drastic redesign would have to be undertaken to substantially improve the performance.

2.5 Construction of the Electron-Optical Lens

The camera geometry adopted was similar to that of the visible-sealed off version which had been previously assessed [1]. The only modification made was to increase the anode aperture to 4mm in order to maintain the usable cathode area while this ensured that the electron beam could not impinge on the framing deflectors whose separation was maintained. In fact it has been found that the usable cathode area for the demountable camera is quite large (6 mm by 6 mm). The camera electrostatic lens electrodes were constructed out of aluminium and supported on four machinable glass ceramic rails to provide electrical insulation. The cathode plate was mounted using ceramic spacers and nylon bolts to the first cylindrical electrode. The mesh employed was identical to that of the sealed-off tube (60 cells per mm). With a cathode-mesh separation of 2.5mm and potential difference of 5kV the extraction field was very low (20 kV/cm) compared to that of streak tubes and so the camera could be operated at a vacuum of 4×10^{-5} Torr without any incidence of electrostatic breakdown. The entire lensing section was placed in an aluminium cylinder of 20cm diameter.

The electron-optical magnification of the constructed demountable UV / x-ray-sensitive framing camera was measured to be -1.4 with a static limiting resolution of 20lp/mm referred to the input cathode. The drift region was simply constructed in interchangeable aluminium segments while the anode aperture and framing slot (rather then aperture) were machined into 1.6mm thick steel plates which were screw mounted within the sections. The deflection plates were constructed out of 0.5mm thick, flat copper sheet cut and bent into shape and then polished. The demountable Picoframe I camera posed no difficulties in mounting the plates which were fixed directly onto the 50Ω 'BNC' bulkhead sockets which were mounted through the drift tube wall. This

system offered good mechanical stability while introducing very little parasitic reactance. The plate separation was easily altered and the 11mm long by 11mm wide framing plates were separated by 4.4mm (measured using slip gauges). Similarly, the 14.8mm long 7.8mm wide compensation plates were separated by 4.2mm in order to maintain equal dc sensitivity and capacitance.

2.5.1 The Vacuum System

The entire system was evacuated using a turbo-pump (type Pfeiffer Duo 1.5A), a Vac-valve was used to isolate the camera at night so that the camera was maintained under vacuum as much as possible to extend cathode life and prevent contamination of the internal components. The Vac-valve also had the effect of aperturing the input radiation slightly (valve internal diameter was ~2cm) which improved the signal-to-noise ratio by reducing the amount of light internally reflected within the aluminium vacuum T-piece. A diagram of the complete demountable framing camera system employed as indicated in figure 2.2

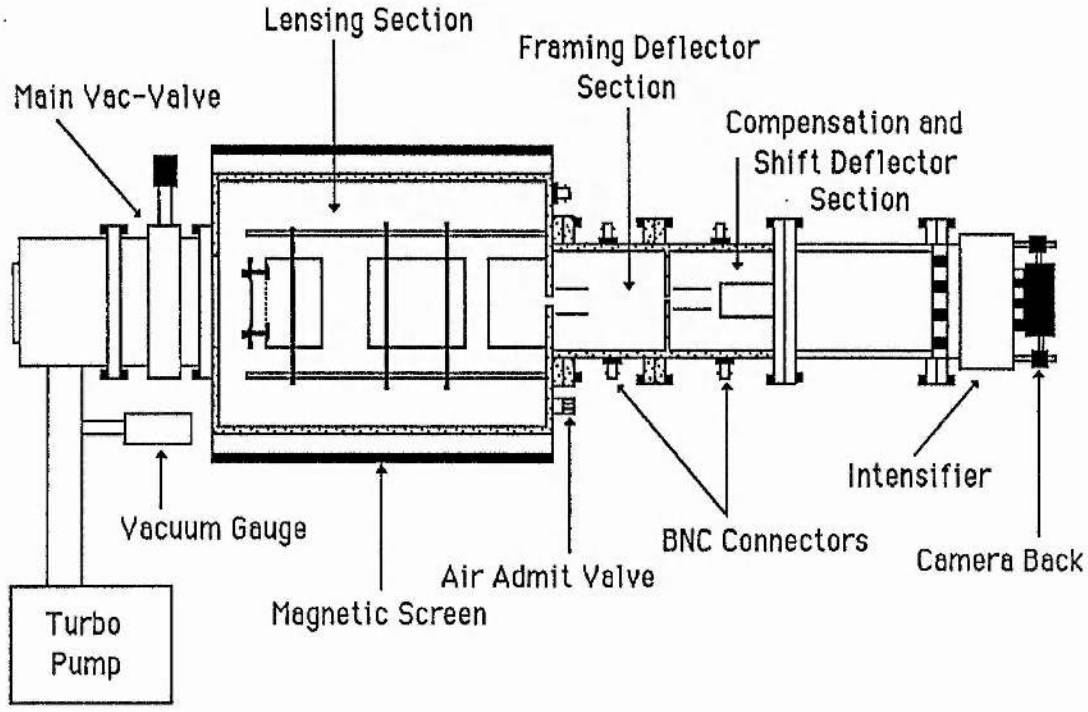

Figure 2.2.Diagram of the vacuum demountable Picoframe I UV-sensitive camera.

2.5.2 Environmental Isolation of the Electron-Optical Lens

Initially spurious magnetic fields associated with power supplies and other equipment in close proximity to the demountable camera caused electron beam deflection to such an extent that the beam was being partially intersected by the anode and framing apertures. This problem was remedied by placing a ferrous (iron) shield around the lensing section of the system. One unfounded concern was that the metal sleeve surrounding the lensing section would provide electrostatic boundary conditions which were not compatible to those initially modelled. This did not seem to be the case as the system focussed at the correct voltages and provided a static resolution comparable to that modelled for a gold UV-sensitive photocathode.

2.6 The Spatial Resolution Test Chart

The test chart employed for all of the UV-sensitive experiments on the framing camera was a negative chromium 1951 USAF resolution test chart deposited on a 1.0 inch diameter 0.5mm thick fused silica substrate. This chart was adopted due to it having both horizontal and vertical resolution elements with the higher resolution being towards the centre of the chart. A magnified reproduction of the chart is shown in figure 2.3

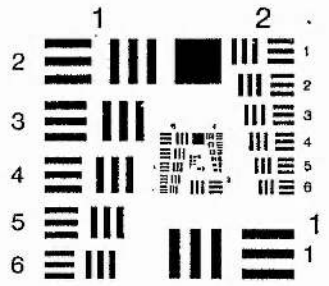

Figure 2.3. Reproduction of the USAF resolution test chart.

2.6.1 UV Photocathodes

A 10nm gold photoemissive layer was then evaporated onto the chromium test chart to form the UV-sensitive photocathode [5]. Initially aluminium photocathodes were used but although these exhibited a higher quantum efficiency when first evaporated, ion migration [6] rapidly reduced their efficiency to an unusable level, while the gold photocathodes maintained their sensitivity for two or three weeks if maintained under vacuum.

2.7 Image Recording

The phosphor screen employed was a green P20 type deposited onto a fibre-optic faceplate of 49mm diameter. A layer of aluminium ~10nm thick was evaporated on the back of the phosphor to improve the emission efficiency, aid the conductivity of the electrons and to reduce the amount of straight through UV excitation of the phosphor. In order to reduce space-charge effects due to large photocurrent densities required to image events on a short time scale a microchannel plate (MCP) image intensifier (Mullard type XX1330A possessing a magnification of -2/3) with fibre-optic couplers on input and output windows was intimately coupled to the fibre-optic faceplate of the phosphor screen. The MCP was gated on for 200μs to reduce the noise integration on the photographic film. The complete system (image tube plus intensifier) exhibited a limiting static spatial resolution of 14 lp/mm with respect to the input photocathode when illuminated with 266nm laser radiation. Events were recorded either on Polaroid film or Ilford HP5 sheet film (push processed to 1600 ASA) held in contact with the intensifier faceplate.

2.8 Compensation Voltage Deflection Waveform Requirements

In order to achieve the dynamic spatial resolution of 10 lp/mm (referred to the photocathode) the electron trajectories must be compensated to better then 70μm at the phosphor. With a dc sensitivity of ~2.5cm/kv for both sets of deflectors to the phosphor, this implies a compensation of better then 2.8 volts over the entire frame duration. As the voltages required to deflect the electron beam sufficiently fast are of the order of 3kV, the amount of error allowed in matching the voltage gradient to both sets

of deflectors is ~0.1%. The framing and compensation deflectors are designed to be nominally equal deflection sensitivities but the dc deflection sensitivity for a set of parallel plates is given by equation 2.1.

$$S = \frac{1(\frac{1}{2} + L)}{2 V_a d} \qquad (2.1)$$

where the relevant parameters are as defined in chapter 7.1. It is easily deduced that the positional requirement placed upon the deflectors is far beyond any reasonable limit, if the desired dynamic resolution is to be achieved when using identical voltage gradients. It is therefore essential that the voltage ramp gradient be adjustable over a suitable range in order that the correct compensation may be achieved. Trimming capacitors were initially used to alter the rate of change of voltage on the deflection electrodes to counteract any slight differences in sensitivity between the framing and compensation deflection plates [7]. However, it became apparent that this technique was not particularly effective with the new deflection geometry as only poor compensation could be obtained. Two possible reasons for this observation are, (i) the inability to position the trimmer capacitors very close to the deflection plates due to the connectors used and (ii) the more inductive nature of the deflection plate geometry feed throughs.

2.8.1 The Resistive Divider Network

It became clear that some alternative technique was required and so the resistive divider chain, shown schematically in figure 2.4 was adopted.

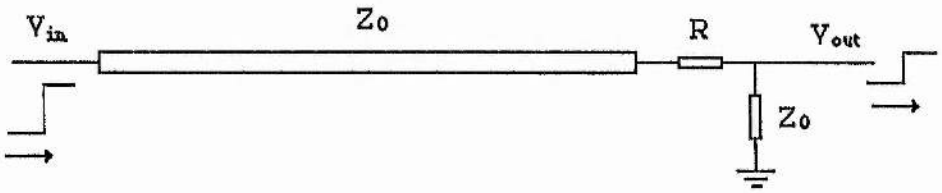

Figure 2.4. The resistive divider network.

The reflection coefficient r of a signal propagating within a transmission line of

characteristic impedance Z_0 incident upon a resistor of value R is given by equation 2.2

$$r = \frac{R' - Z_o}{R' + Z_o} \qquad \text{where } R' = R + Z_o \qquad (2.2)$$

If the resistor has the value of zero ohms then it is clear that the signal will propagate down the line with no reflections. If the resistor is 50Ω then any signal incident upon the discontinuity will 'see' two 50Ω resistors in series forming a 100Ω network. The reflection coefficient is then given by equation 2.3

$$r = \frac{100 - 50}{100 + 50} = \frac{1}{3} \qquad (2.3)$$

The signal transmitted T is then given by equation 2.4 where V is the input 'step' voltage.

$$T = V (1 - r) \qquad (2.4)$$

The transmitted signal may thus be continuously 'attenuated' from zero to up to a third if a 50Ω variable resistor is employed. It is possible in this way to change the effective rate of change of voltage applied to the deflection plates. In practice a 100Ω carbon track variable resistor is put in parallel with a 100Ω carbon resistor which is then mounted within a small r.f. screening box with 'BNC' connections on either end. This technique allowed good voltage gradient variation and good compensation was thereby achieved.

2.9 Single Frame Evaluation of the UV-Sensitive Picoframe I Camera

Initial testing of the camera was aimed at reproducing the results reported with the single aperture, sealed-off image tube that has visible sensitivity [7]. Before any

experiments using x-rays could be considered the camera first had to be characterised with UV illumination.

2.9.1 The UV Laser Source

The test source used was a (Lumonics*) mode-locked, Q-switched, frequency-quadrupled Nd:YAG laser with single pulse selector and a one stage single-pass amplifier. The system provided up to 2mJ of energy in a single pulse of 266nm radiation in ~60ps FWHM with a repetition rate of 4Hz. Figure 2.5 shows an oscillogram (oscilloscope employed was a Tektronix type 7104, <400ps rise-time) of the Q-switched and mode-locked pulse train with rejected pulse (due to the insertion of a quarter wave plate during laser set up only). The diode employed was a BPX 65 PIN diode.

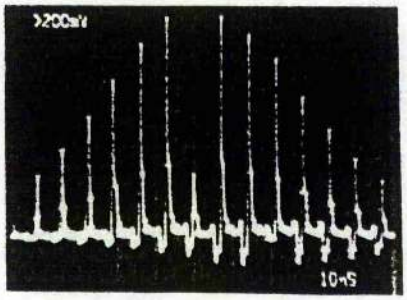

Figure 2.5 showing the Q-switched and mode-locked laser output with single pulse 'selected'.

2.9.2 The Sweep Circuits

Generation of the fast voltage ramps was achieved with the use of avalanche transistor circuits developed at AWE [8] which are based around the National Semiconductor 2N3700 transistor type. The circuit consists of two chains of avalanche transistors which are triggered simultaneously to provide complementary positive and negative-going outputs switching 3kV each. In this way proper symmetrical deflection was achieved. The ramp generators have a measured rise-time of 1.5ns into a 50Ω resistive load and a measured trigger jitter of ± 20ps when triggered with a suitable fast rise-time step voltage with an amplitude exceeding 30V, which is usually provided by a

(*Lumonics, Cosford Lane, Swift Valley, Rugby)

cheap (typically BPX 65) silicon PIN photodiode reverse biased at ~120V. If it is ensured that the photodiode is completely saturated by the optical pulse then the system jitter is defined by the avalanche circuit jitter alone. They exhibit an intrinsic delay of ~10ns between the trigger input and the start of the ramp so that in all experiments a suitable optical delay must be introduced in order that the camera is timed correctly for the single optical pulse. Each set of deflection plates must be fed by the output of an independent avalanche circuit as it has been found that excessive load placed upon the transistors causes increased rise-times and even damage to the transistors themselves.

With a photoelectron accelerating voltage of 15kV the avalanche circuits provided a streak speed of 1.8×10^9 cm/s at the framing aperture plate, hence giving a frame time of ~100ps (FWHM) given that the framing aperture has a diameter of 1.8mm.

2.9.3 The Experimental Set Up

The experimental arrangement is shown below in figure 2.6.

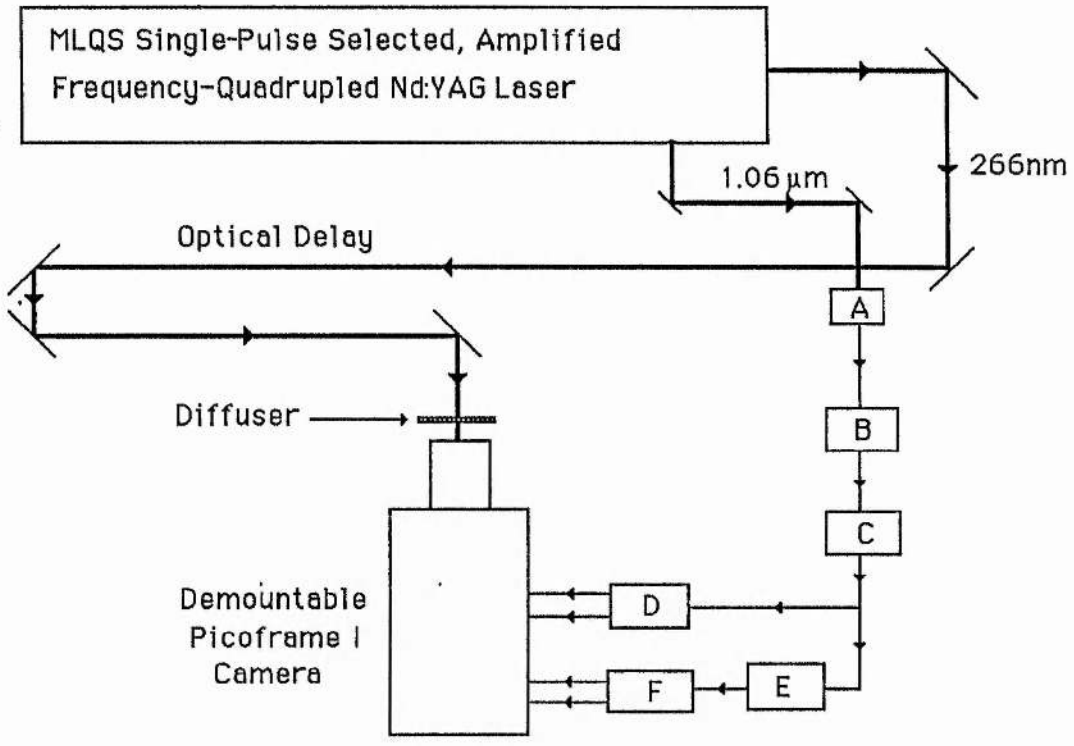

Figure 2.6. Key to diagram :- A trigger photodiode, B,E transmission line type delay (Tektronix, continuously variable from 0 to 1ns), C transmission line type delay (Hamamatsu C1097, adjustable in 250ps steps from 0 to 64ns), D, F avalanche transistor circuits.

A reproduction of a typical frame achieved is displayed in figure 2.7.

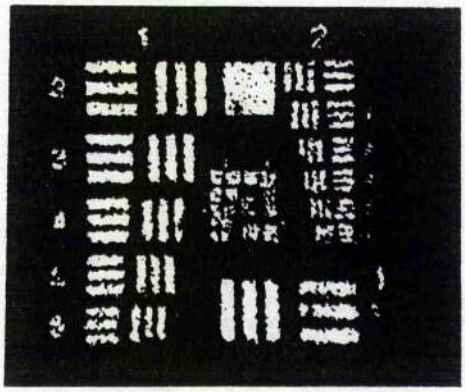

Figure 2.7. Reproduction of a typical frame achieved with the UV-sensitive Picoframe I.

The dynamic spatial resolution was optimised by the careful adjustment of the electrical delays image tube focusing potentials and resistive trimmers.The spatial resolution of the recorded frame is not less than 8 lp/mm with respect to the photocathode. This resolution was only achieved when the intensifier gain was reduced to moderate levels (~100) and the input illumination increased until correct film exposure was achieved. The reasons for this will be discussed at the end of the chapter.

2.9.4 Evaluation of the Frame Exposure Time

In previous experiments on the sealed-off, visible-sensitivity framing camera it was relatively easy to deduce the frame open time with the use of an ultrashort pulse laser [7]. The generation of ultrashort optical pulses in the UV with sufficient energy to excite the gold photocathode is at present problematical so it was necessary to adopt an alternative temporal calibration scheme based upon the Tektronix sampling system [9]. In order to implement this system it is only necessary to alter the overall electrical (or optical) delay in such a way that the timing of the camera is swept from being mistimed by some positive amount, through the correct timing to a negative amount. By placing a suitable photodiode in contact with the faceplate of the MCP intensifier and replacing the USAF test chart masked photocathode with an unmasked version, it is then possible to evaluate the relative light output from the camera system. In this way (and averaging over typically five shots per delay setting) it is possible to derive the camera temporal

transmission function with respect to the relative delay introduced. Thus the frame open time may be deduced (deconvolution of the exciting 60ps FWHM laser pulse is necessary to obtain the true instrumental response). The frame-times presented in this thesis are the full width half maximum (FWHM) of the MCP intensifier output unless otherwise stated. In this way it was deduced that the frame open time of the UV-sensitive, single-aperture Picoframe I camera was 100ps FWHM and the temporal transmission function is shown as figure 2.8.

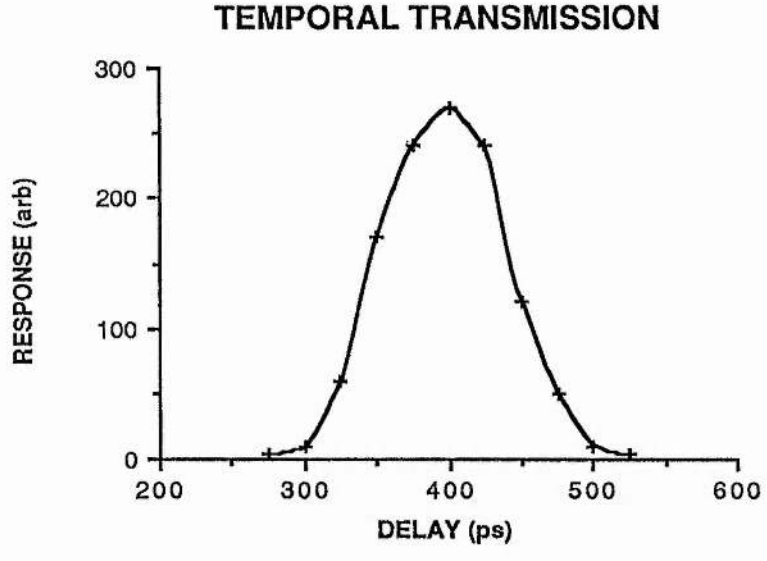

Figure 2.8 showing the temporal transmission function of the UV-sensitive Picoframe I.

2.10 Double-Frame Operation Of Picoframe I Camera

When operating the Picoframe I camera in a double-frame mode, the image-forming photoelectrons must be swept across the framing aperture twice. In order to achieve this it is necessary to generate triangular pulses of kilovolt amplitude. Various pulse forming techniques are available, such as the Blumlein networks and their associated family, but these systems rely on signals propagating along the outer braid of the transmission line. This leads to ambiguity in the ground potential and practical difficulties in connection to the deflection plates due to the short cable lengths required to give the desired pulse width of ~2ns.

2.10.1 The Pulse Forming Network

The chosen pulse-forming network (PFN) consists of two equal length transmission line stubs of characteristic impedance of 50Ω intersecting a 50Ω transmission line [10]. The length of the stubs which had a dc short circuit at one end defined the pulse width whose duration was equal to the round-trip time of the stubs. Providing the stub length is arranged to produce pulse widths of the same duration as the rise-time of the ramp input voltage then a triangular voltage output is achieved with a peak amplitude one half of that of the input. The PFN's are often constructed out of semi-rigid coaxial cable to maintain frequency response and mechanical rigidity, although it has been found during the course of this work that they may be constructed out of standard coaxial cables and 'BNC' connectors with no adverse effects at the frequency response required to produce 1.5ns rise-time waveforms. The PFN's were previously employed in the operation of the visible-sensitivity Picoframe I camera [11] with considerable success, but it was noted that the second frame was always the poorer of the two and had a shorter exposure duration. It was therefore felt that the falling edge of the triangular waveform was faster then the rising edge. This was attributed to the capacitors employed in the system, required due to the dc shorts employed in the PFN's.

2.10.2 Controlling the Fall Time of the Voltage Waveform

In order to reduce the gradient of this falling edge, the dc short on one of the stubs was replaced with a small low inductance variable resistor. Computer simulation of the entire system (shown schematically in figure 2.9) was undertaken using a comprehensive software package (SPICE2 which was written at University of California, Berkeley, Ca 94720) which assumes ideal (lossless) transmission lines. The diodes (type Mullard BY127) used on the inputs are to suppress the inverse polarity reflections which have been found [12] to damage the avalanche transistors.

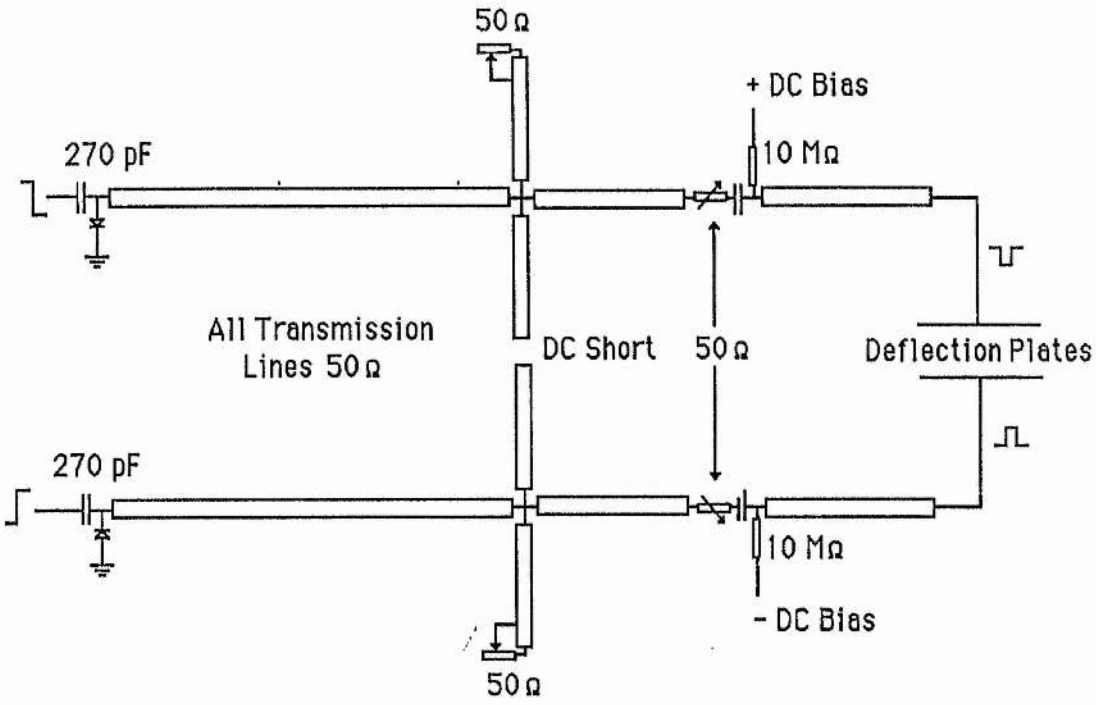

Figure 2.9. Diagram of the full PFN employed.

2.10.3 Computer Simulation of the PFN

By simulating the performance of the PFN to a step input of 1.5ns rise-time it was possible to predict the theoretical dynamic performance of the system. Figure 2.10 shows the effect of increasing the value of the resistance of one of the terminations.

This analysis was conducted on a single PFN with a 50Ω output termination and a 1 Volt step input. The stubs employed had a round-trip time of 1.5ns (15cm long) and the reflection (4ns after the initial pulse) was due to the short transmission line length between the input and stubs of the simulated PFN due to simulation requirements. In practice 10ns (1m) round trip time cables are employed thus ensuring that any reflections occur after the luminous event.

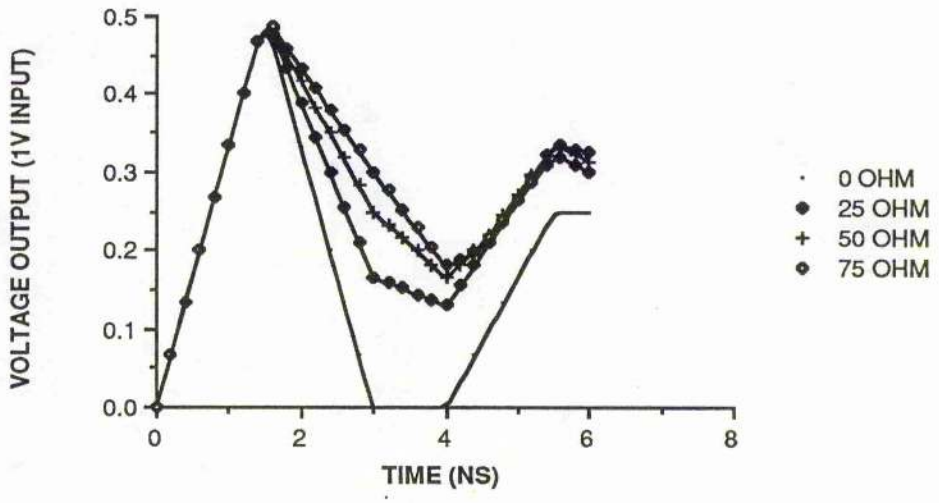

Figure 2.10. The simulated response of the PFN to different terminations.

It can be seen that by increasing the resistance R the triangular pulse is effected in two ways viz: the FWHM is increased as R is increased, and dV/dt is decreased as R is increased. Experimental verification of this was achieved using a high speed oscilloscope in conjunction with an avalanche transistor circuit and PFN whose output was suitably attenuated. The multi-exposure oscillogram shown as figure 2.11 shows the effect of increasing the termination resistance between 0 and 100Ω on successive triggering of the circuit. It is seen that the voltage rate of change is unchanged at the leading edge of the triangular waveform (although temporal displacement between shots is evident which is due to oscilloscope trigger jitter) while the trailing edge shows wide control of the effective dV/dt.

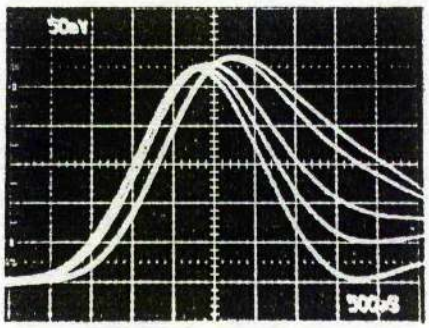

Figure 2.11. Multi-exposure oscillogram of the effect of varying the termination resistance of the PFN.The oscilloscope was a Tektronix 7104 (~400ps rise-time).

A complete simulation of the circuits and deflectors incorporating symmetrical deflection waveforms was undertaken with both PFN stubs being short circuited to produce a 'symmetrical' triangular waveform.The results of this simulation are presented graphically as figure 2.12, which shows the voltage of one of the deflection plates with respect to time with no external dc bias applied.

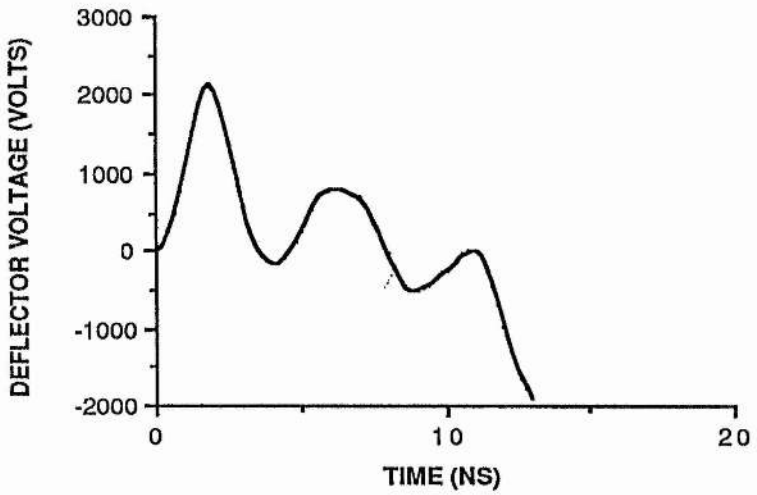

Figure 2.12. Computer simulation of the voltage appearing at the deflection plates of a symmetrically driven deflection system. The reflections after the main pulse are due to simulation requirements and would not in practice appear so soon after the pulse.

It should also be noted that the computer simulation shows that the voltage appearing on the deflection plates is greater then half of the 3kV input ramp. This is due to the impedance mismatch between the transmission line feeder and the deflection plate itself. This effect is fortuitous but its usefulness requires that no other impedance mismatches occur near the intersection, which is often not the case. This voltage magnification was ensured when care was taken over the capacitor mounting and when all wire lengths were kept to a minimum. The theoretical predictions were found to be in good agreement with the deflection observed on the phosphor screen of the framing camera. The peak deflection voltage amplitude appearing at the deflection plates was estimated by applying a suitable dc to the framing deflectors (while maintaining the compensation deflectors at anode potential) such that the streaked image appeared at the centre of the phosphor screen. The bias potential then represented the peak voltage amplitude

appearing and was measured to be ~1.9kV.

2.10.4 Deflection Waveform Timing

The spatial (ie. temporal) separation of the resulting two frame may be accomplished in two ways. Either a suitable dc bias may be applied to the compensation plates at the correct instant or the phase between the framing and compensation waveforms may be adjusted [7] to provide a net dc bias as shown in figure 2.13. The latter technique was a more practical solution and was adopted due to its ease of operation.

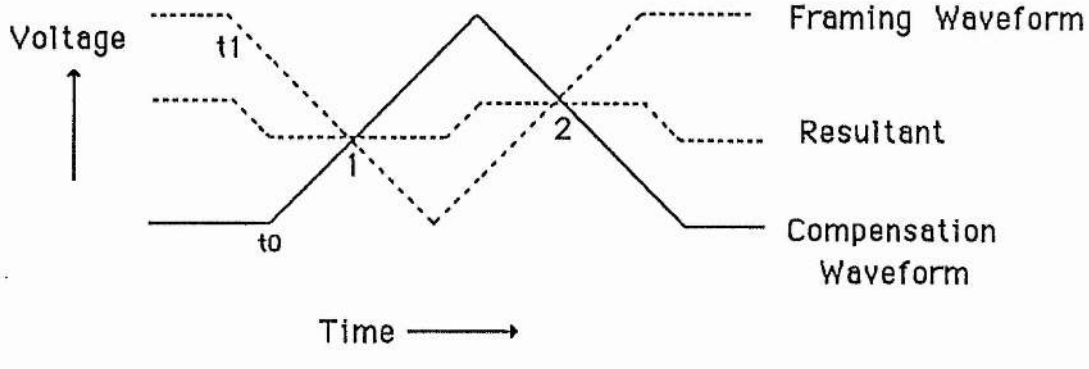

Figure 2.13. Deflection waveform timing for the double frame operation of the Picoframe I.

2.10.5 The Experimental Set Up

Two optical pulses are achieved with the use of a Michelson type optical delay, in which one of the two 100% mirrors was mounted on a translation stage. This was required as the adjustment of the external dc bias moved the region of operation on the triangular voltage pulse either nearer to the apex or the base. This then defined the inter-frame time and the system was operated at the highest dc bias possible (± 850V) in order to reduce the inter-frame time without causing image degradation due to the non linearity of the apex of the generated deflection waveforms. A complete schematic for the experimental set up is shown in figure 2.14.

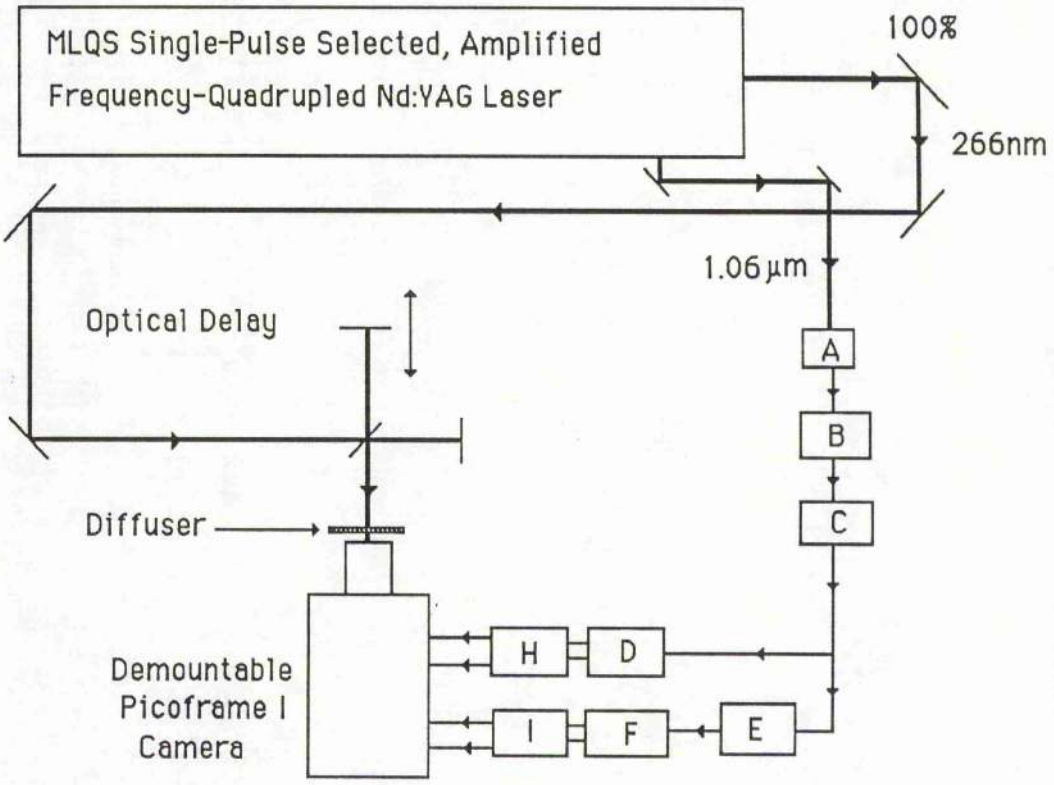

Figure 2.14. Key to diagram :- A trigger photodiode, B,E transmission line delay (continuously variable from 0 to 1ns), C transmission line delay (adjustable in 250ps steps from 0 to 64ns), D, F avalanche transistor circuits, H, I, pulse forming networks plus associated electronics.

A reproduction of a typical frame doublet is presented in figure 2.15.

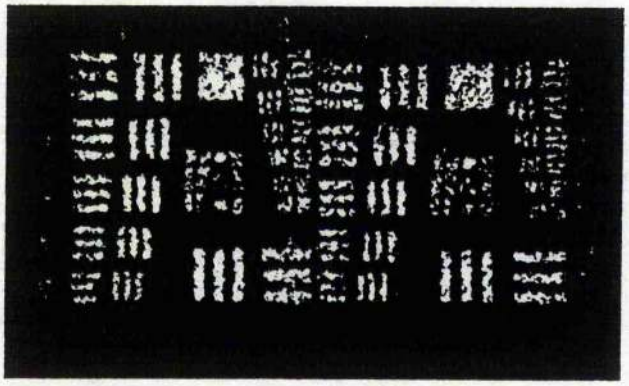

Figure 2.15. Reproduction of a double frame result from the Picoframe I in double frame mode of operation, first image right, second left.

Inspection of the original negative reveals the spatial resolution of both frames exceeded 8 lp/mm. The inter-frame time was deduced from the optical delay introduced between the two laser pulses which was easily measured from the mirror separation and was found to be 2ns. The frame time was deduced as previously described with the single-frame Picoframe I system and was estimated to be 250ps FWHM for each frame, temporal transmission curves are given as figure 2.16 (a) and (b).

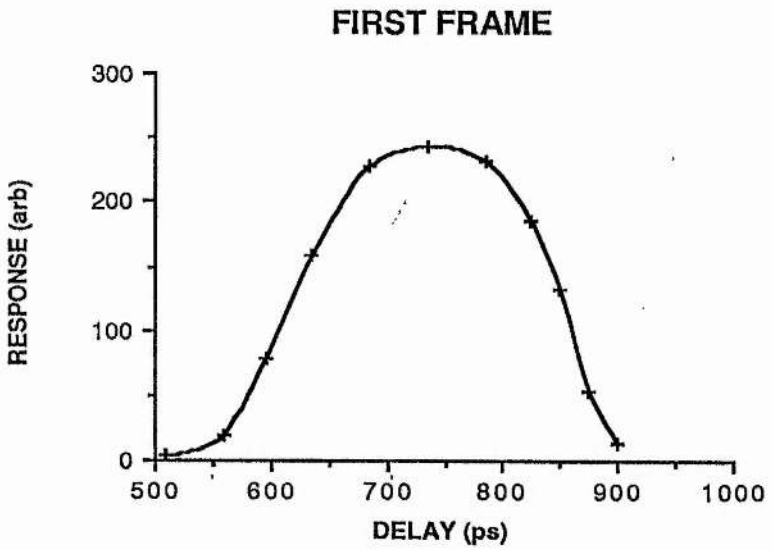

Figure 2.16 (a) showing the temporal transmission response to the first frame.

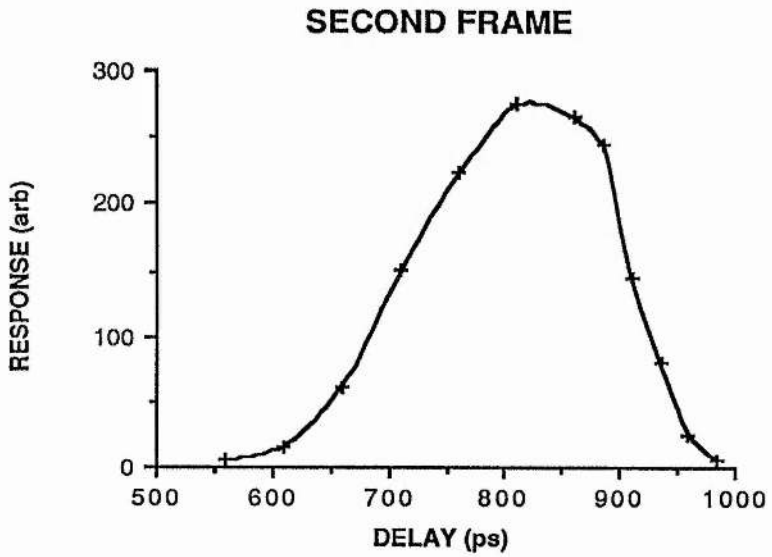

Figure 2.16 (b). The temporal response curve for the second frame.

2.11 Discussion

It is of interest to note that that the usable cathode area of the demountable camera is reasonably large (6mmx6mm). Previous work with the sealed-off visible-sensitivity camera showed that the image format on the cathode should be kept small to maintain spatial resolution. The demountable camera on the other hand makes use of a large area, high conductivity gold photocathode which may reduce undesired cathode edge distortion effects.

It has been found that the best images are attained when only moderate MCP gains are employed which means that relatively high photon fluxes are required to provide the correct film exposure. This has been attributed to the statistical probability of an electron being emitted from a point on the cathode, due to photon excitation. The USAF test chart has the unfortunate property that the higher resolution elements occupy a very small area, thus the photon density must be reasonably high to ensure an adequate number to statistically define the resolution element as detailed further in section 2.11.1.

2.11.1 Dynamic Range of the Picoframe Camera

The dynamic range of a UV/X-ray-sensitive framing camera is of prime importance when the system is required to resolve weak luminous events in close proximity to intense ones, as in the case of a laser produced plasma. Typical X-ray photon liberation from a laser produced plasma may be of the order of 10^{12} photons per joule of incident laser radiation for a solid target. This photon flux may be liberated (in a temporal period roughly equal to the duration of the laser pulse) from a region similar in size to the focal spot, while weak 'coronal' X-ray emission from the plasma edge may yield detailed information on the plasma evolution. It is therefore essential that the dynamic range of the camera be known before being used as a diagnostic under these conditions.

The electron-optical image framing camera operating in conjunction with a high gain intensifier such as the Mullard type XX1330A (50/40) with a maximum gain of ~2000 and Ilford HP5 photographic film combination ensures the ability to record single photoelectrons emitted from the photocathode. Under these conditions the

minimum photon flux density arriving at the photocathode must be sufficient to liberate sufficient photoelectrons within the frame exposure time in order to define the required resolution element. The number of photoelectrons required is independent of the type and sensitivity of the photocathode. Providing there is no loss of photoelectrons liberated from the photocathode (not entirely true as the mesh alone intercepts some 30%) as a first approximation, we may evaluate the required photoelectron density at the cathode.

The signal-to-noise ratio (SNR) of the system may be defined as

$$SNR = \frac{S}{N_t} \qquad (2.5)$$

where S is the average signal (photoelectrons emitted from the photocathode) per pixel or resolution element and N_t is the total root-mean-square noise appearing at the phosphor screen of the image intensifier. If we assume that the intensifier is noise free (reasonable if operated at usual moderate gains) and the complete system is capable of single photon detection, then the only noise within the system is statistical noise of the photons arriving at the photocathode. Thus

$$SNR = \sqrt{S} \qquad (2.6)$$

If the SNR is arbitrarily (but usually) chosen as 10 then we must have at least 100 photoelectrons emitted per resolution element from the photocathode. Given that a gold X-ray-sensitive photocathode has a typical quantum efficiency of 5% (ie.1 electron emitted per 20 incident photons) [13] for a photon energy of ~1.5keV, the total photon flux density required is ~4000 per resolution element.

The maximum current density has been found empirically to be ~7×10^{-2} A/cm^2 at the photocathode [14], limited by the space charge effects within the image tube which cause electron packet spatial and temporal distortions. This evaluation was undertaken on a standard electron-optical geometry of a Photochron II type streak camera but it is believed that the results are generally applicable to the electron-optical design of the

Picoframe type geometry. Thus the dynamic range (or more precisely the contrast ratio) of the camera may be estimated from

$$\text{Dynamic Range} = \frac{I_{max}}{I_{min}} \qquad (2.7)$$

where I_{max} and I_{min} are the maximum and minimum current densities at the photocathode. I_{min} may be calculated knowing the cathode area (6mmx6mm), the frame exposure time (100ps FWHM) and the desired spatial resolution (10 lp/mm in both directions) to be ~6.5×10^{-3} A/cm^2 yielding a dynamic range of ~10. This dynamic range can increase to ~40 if the resolution restriction is relaxed to 5 lp/mm. This calculation defines the dynamic range of the image tube if the entire cathode area is illuminated (it is assumed that little degradation in resolution occurs due to finite photocathode resistance due to this being negligible when using UV and X-ray-sensitive gold photocathodes) which is not the case if a USAF resolution test chart is employed. With this chart only some 25% of the cathode area is actually illuminated which would infer an increase in dynamic range to about 40 at a spatial resolution of 10 lp/mm in both directions.

The effect of image definition due to photon statistics was demonstrated practically by operating the framing camera in 'static' mode under pulsed illumination conditions. The illumination was derived from a Q-switched and mode-locked frequency-quadrupled Nd:YAG laser employed during the dynamic testing of the UV-sensitive system (chapter 2). This system delivered up to 2mJ of radiation at 266nm in 60ps FWHM. Figures 1, (a) to (e) show the static, pulsed images recorded when successively decreasing the laser radiation intensity and increasing the intensifier gain to maintain the film exposure at a (roughly) constant level.

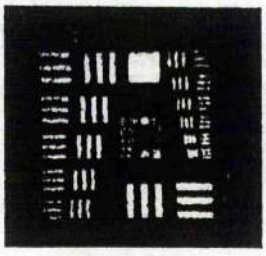

(a)

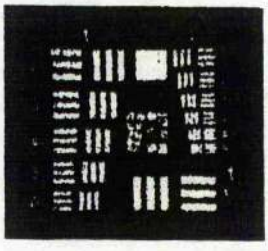

(b)

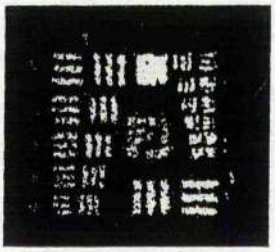

(c)

(d)

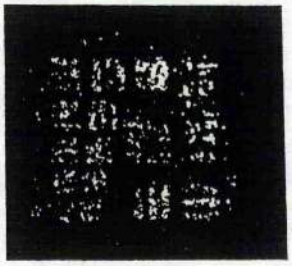

(e)

Figure 1, (a) to (e) Loss of spatial contrast due to progressive reduction in optical input intensity to the Picoframe camera. Intensifier gains were 50, 100, 200, 400, and 1000 for (a) to (e) respectively.

The corresponding intensifier gains employed were approximately 50, 100, 200, 400 and 1000 for images a to e respectively. Assuming that in dynamic operation, the electron packet axial dispersion due to Coulomb repulsion may be ignored due to the compensation deflectors operation, the pulsed static dynamic range should be comparable to the operational dynamic range. Analysis of these images yields that at an intensifier gain of 100 the 10 lp/mm resolution elements are not quite resolvable by eye (although the 8 lp/mm elements definitely are). The 10 lp/mm elements are easily resolvable by eye at an intensifier gain of 50 however. Further increase in the photon flux density arriving at the photocathode lead to the 10 lp/mm resolution elements becoming unresolvable and image distortion became noticeable,but it was not possible to record this effect due to the photographic film becoming overexposed even when operating the image intensifier at minimum gain (50). This then allowed an experimental value of the dynamic range to be deduced to have an upper limit of 50 for a resolution of 10 lp/mm. This figure represents the experimental dynamic range with a signal to noise ratio of ~10 due to the ability to resolve ~5% modulation by eye [15].

The 'corrected' theoretical dynamic range to be expected when measuring the dynamic spatial resolution of the Picoframe camera with the USAF resolution test chart agrees most favourably with the experimentally arrived at value.

It may be concluded from the above analysis that the camera should be operated in conjunction with an intensifier with a gain no greater then 100 in order that the dynamic range and spatial resolution be optimised.

Calculations based upon this idea have led to a predicted minimum photon density of $3x10^9$ photons per $36mm^2$ (cathode area). This figure implies a pulse energy of ~200pJ at 266nm in 100ps (the frametime). While the laser employed is quite readily able to provide this energy level, it must be realised that the cathode should be evenly illuminated, requiring the use of a diffuser and so much of the energy is lost. Photoelectrons 'lost' within the image tube itself due to mesh absorption, intersection with apertures due to high initial emission energies and angles will exacerbate the problem, but sufficient electron densities are quite easily achievable at the phosphor within the frame-times achieved. Shorter frame-times may prove problematical for this very reason although at present the parallel plate deflectors will limit the maximum usable sweep speed due to fringing fields (see chapter 3.7.1).

2.12 Conclusions

The Picoframe I camera which has been constructed in a demountable form for use with UV and x-ray excitation has been tested under UV illumination conditions. The static spatial resolution of the camera itself has been measured at 20 lp/mm and the camera with intensifier was 14 lp/mm. The dynamic performance of the camera in single frame mode has been evaluated, and frames having spatial resolutions ~ 8 lp/mm with 100ps FWHM have been demonstrated. The performance of the camera system in double-frame mode has also been tested. The pulse-forming networks used have been modified to allow greater flexibility in operation and precise control of the voltage waveforms has been achieved. The system has a demonstrated dynamic spatial resolution of 8 lp/mm for both frames and exposure times of 250 ps FWHM. The longer frame exposure time is due to the halving of the voltages switched by the pulse-forming network configuration used.

The dynamic range of the framing camera system has been evaluated and has been found to be ~50 at (10 lp/mm) with the intensifier employed. This dynamic range is limited by the maximum photocurrent that may be used due to the space charge effects within the electron-optical system, and the requirement that a minimum photon density is required to define the required resolution.

References for Chapter 2

1 M R Baggs, R T Eagles, W Margulis, W Sibbett, W E Sleat

Advances in Electronics and Electron Physics; 64B, 627, 1985

2 A E Huston

Applied Optics; 3 (11), 1231, 1964

3 H G Ahlstrom; 'Diagnostic of Eperiments on Laser Fusion'

Vol II Lawrence Livermore National Laboratory, Livermore

Ca UCRL 53106, 1982

4 R T Eagles

PhD Thesis, University of London, chapter 5, 1986

5 eg. H Kuroda, N Nakano, E Inuzuka, Y Takiguchi, M Sugiyama, Y Tsuchiya, Y Suzuki

Proc. 16 ICHSPP (Strasbourg), SPIE 491, 108, 1984.

6 P A Jaanimagi, D K Bradley, J Duff, G G Gregory, M C Richardson

Rev. Sci. Instrum., 59 (8), 1854, 1988

7 R T Eagles, W Sibbett, W E Sleat

Optics Comm., 57 (6), 423, 1986

8 M C Jackson, R D Long, D Lee, N J Freeman

Laser and Particle Beams, 4 (1), 125, 1986

9 M J Eckart, R L Hanks, J D Kilkenny, R Pasha, J D Wiedwald, J D Hares

Rev. Sci. Instrum., 57 (8), 2046, 1986

10 G F Ross

IEEE Trans. Microwave Theory Techn.

MTT-13 704, 1064

11 W Margulis, R Persson

Rev. Sci. Instrum., 56 (8), 1586, 1985

12 R T Eagles

PhD Thesis, University of London, chapter 4, 119, 1986

13 B L Henke, J Liesegang, S D Smith

Physical Review B, 19 (6), 3004, 1979

14 B R Thomas

AWE, SPE (N8/78) Internal Report, 1978

15 A Rose

'Vision, Human and Electronic', Plenum Press, New York, 1974

Chapter 3

Picoframe I X-Ray-Sensitive Camera in Single And Double Frame Modes of Operation

3.1 Introduction

In order to evaluate the dynamic spatial resolution of the X-ray sensitive Picoframe camera design under soft x-ray illumination, an intense, pulsed source (in order that the sweep circuit recovery does not cause 'fly-back' and over-write the desired image) must be used. The generation of soft x-rays may be achieved with the electron bombardment of suitable anode materials [1], thus causing characteristic K line and Bremsstrahlung emission [2]. While these units are able to produce considerable x-ray flux densities [2,3] from a small 'point' source, are small and relatively cheap, they do suffer from trigger jitter due to the use of laser activated spark gap switches [3]. This trigger jitter may not prove to be a problem as the x-ray emission from these devices is typically quite long (a few tens of nano seconds) thus considerably alleviating the synchronisation requirements between the camera and x-ray pulse. Unfortunately such a device was not available and so it was decided that a laser produced plasma should be used to provide a point x-ray source. The major disadvantage of this scheme is the low repetition rate presently available from the solid state (eg. Nd:YAG or Nd:phosphate glass) high power pulsed laser systems. In order to generate sufficient x-ray flux densities, laser power densities in excess of 10^{12} W/cm^2 are required to impinge upon a target with a high atomic number (see chapter 1). While this can be achieved with ~1J of laser radiation delivered in ~100ps focussed to a ~30μm diameter spot, lasers capable of delivering these peak powers are usually still restricted to a few shots per hour due to the thermal effects caused by the flashlamp pumping of solid-state rod or disc laser amplifiers.

There is a distinct advantage in using a laser produced plasma x-ray emission system for evaluation of the framing camera, and that is the operating conditions and environment closely simulate the conditions in which the camera will ultimately be used when observing laser induced compression of microspheres [4]. It is also reasonably easy to evaluate the imaging (x-ray pinhole camera or grazing incidence microscopes

[5,6,7]) apparatus which may ultimately be used in conjunction with the framing camera.

3.2 The Merlin Laser Facility

The laser system available (MERLIN, at AWE Aldermaston) consisted of a mode-locked and Q-switched Nd:glass oscillator. Active mode-locking is achieved using an acousto-optic modulator and an intracavity dye cell is used to reduce the amplified spontaneous emission. The pulse width achievable with this system ranges from ~100ps to 1ns (with intracavity etalons). A single-pulse selector achieves the switch out of a single mode-locked pulse from the middle of the Q-switched train. The pulse is then amplified using a chain comprising four phosphate glass amplifiers to an energy of ~10 Joules. Amplifier isolation is achieved using Faraday rotators between the main amplifier stages. Spatial filtering of the beam is undertaken before and after the last amplifier in order to maintain beam quality. A schematic diagram of the laser is reproduced in figure 3.1.

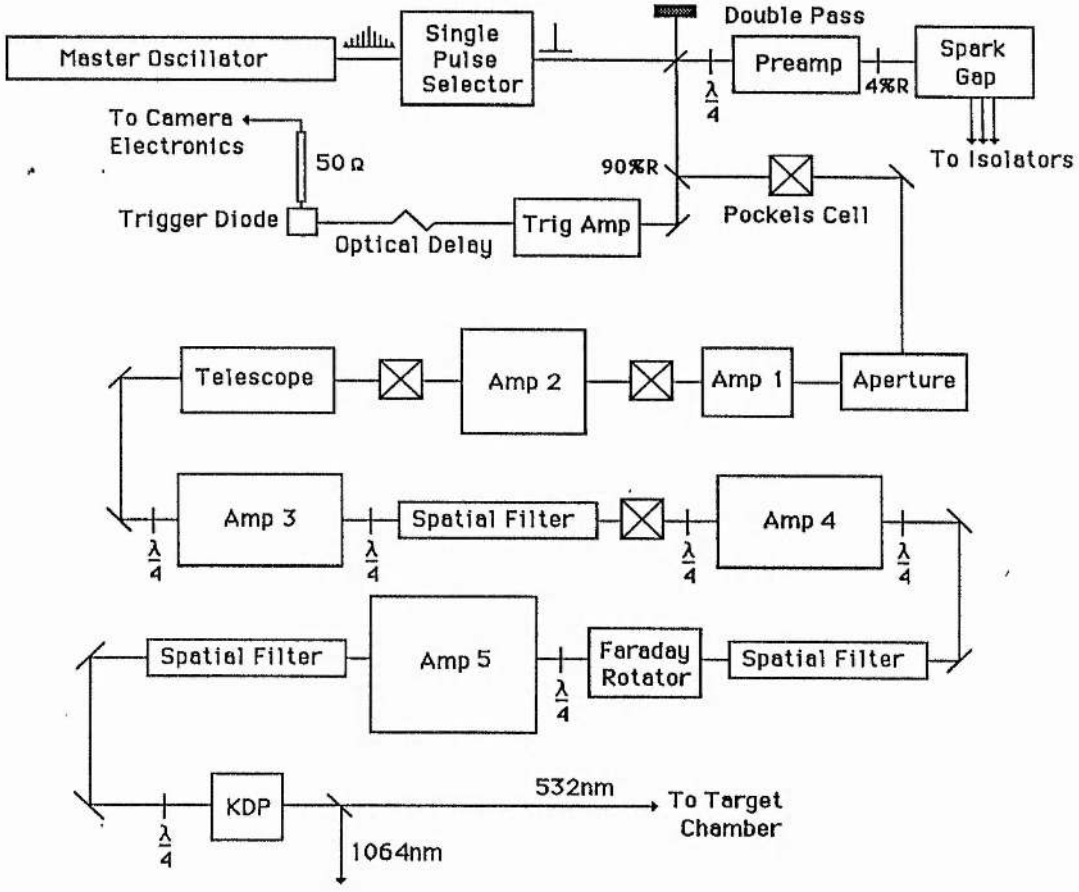

Figure 3.1. Schematic diagram of the Merlin laser facility.

Frequency-doubling of the 1.06μm radiation is achieved (to improve coupling efficiency of the laser radiation to the plasma [18]) using an angle tuned (type II phase matching) KDP crystal with a conversion efficiency of up to 50%. The resultant radiation (532nm) was focussed to a 30μm spot onto a foil target which is positioned at the centre of a target chamber which was a 1m diameter cylindrical drum with ports positioned around the circumference and evacuated to $4x10^{-5}$ Torr or better. Target positioning was achieved by motorised micro-positioners and tele-microscopes. The targets used were gold foil 25μm thick, which provided a fairly broad-band x-ray emission spectrum from ~1keV to ~3keV which is reproduced in figure 3.2.

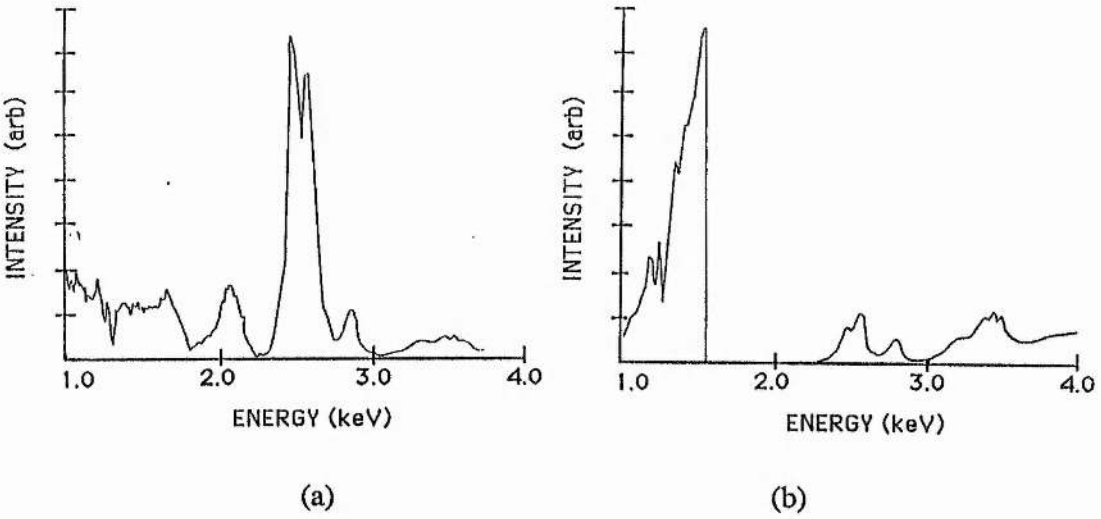

Figure 3.2 showing the time integrated X-ray emission spectra of a gold foil (a) , and (b) the effect of a 15 μm aluminium foil transmission filter.

These photon energies are sufficiently high to penetrate the cathode substrates (beryllium and aluminium as shown in figure 3.2,b) with only moderate attenuation for foil thickness of ~20μm. The targets were mounted on a carousel to allow up to twelve foils to be mounted within the vacuum chamber at any time, and approximately six shots at a single target could be achieved before complete annihilation occurred. It was then not necessary to let the chamber up to atmospheric pressure until around seventy laser shots were accumulated.

3.3 The X-Ray Sensitive Picoframe I Framing Camera

After optimising the dynamic spatial resolution of the UV sensitive system on the frequency-quadrupled YAG laser facility, the gold photocathode on fused silica substrate was replaced with an x-ray sensitive cathode on various substrates.

3.3.1 The Experimental Set Up

Initially a 24mm diameter beryllium (112 eV K absorption edge [8]) substrate 20μm [9] thick was used with a 9mm diameter active 10nm thick gold layer evaporated on it. The camera was bolted to an access port such that use could be made of the high photon flux backscatter, illustrated in figure 3.3. With the camera mounted normally to the port, direct x-ray stimulation of the phosphor was possible. Although this is easily removed by using a small wedge mount between the port and camera, this x-ray stimulation is not a problem, and it is often useful in determining if x-ray emission had indeed occurred.

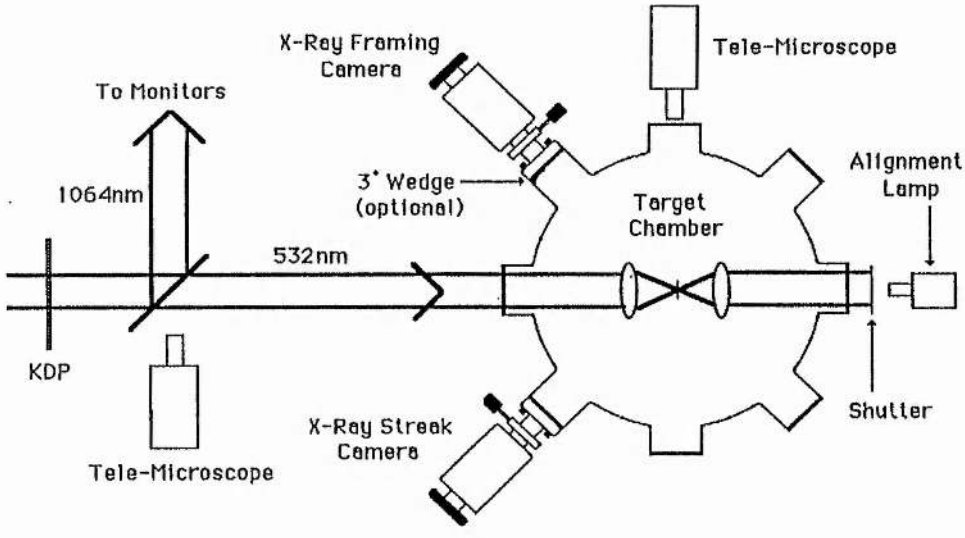

Figure 3.3. Merlin laser target chamber and camera diagnostics.

3.4 Evaluation of The X-ray Picoframe I Framing Camera

Approximately 4 J of 532nm laser energy delivered in ~100ps focussed to a 30μm diameter spot on the target (resulting in irradiances of ~7×10^{14} W/cm^2) [10] was used to irradiate the target in initial experiments. It was not possible to observe the phosphor of the image intensifier by eye due to the intense laser radiation and so all

images had to be recorded on either Polaroid or HP5 film placed in intimate contact with the fibre-optic faceplate output of the image intensifier. With both sets of deflectors earthed the camera was operated in 'static' mode. It became apparent that the x-ray photon flux density was too high and so a 20μm thick aluminium foil filter (K edge absorption at 1.56 keV [8]) was used so that correctly exposed images were obtained at moderate intensifier gains.

3.4.1 Static Spatial Resolution Evaluation

In order to evaluate the dynamic spatial resolution of the system a copper mesh (consisting of 150μm diameter wires in a square grid with a period of 450μm) was positioned in front of the photocathode. 'Static' operation of the camera (all the deflectors maintained at anode potential) revealed that the copper mesh was easily resolvable, indicating a static spatial resolution >10 lp/mm

3.4.2 System Timing

With a repetition rate of ~4 shots per hour, timing of the system becomes more difficult. Previously, the UV camera was timed by operating the camera in 'streak' mode, which meant that the framing deflectors were maintained at anode potential while the compensation plates were driven as in framing mode. The main electronic delays were then adjusted systematically until the streak was positioned centrally on the phosphor screen. The framing deflectors were then reconnected and small adjustments to the timing made to optimise the dynamic spatial resolution of the frames, remembering that the transit time of the electrons from the framing to compensation plates is ~1ns with an anode potential of 15kV. It is clear that such a technique requires many laser shots and so was not adopted when timing the x-ray system. Initial timing was achieved by measuring the relative temporal delay between the electronic trigger pulse (derived from a laser irradiated photodiode) and the incident light upon the target chamber with a Tektronix 7104 oscilloscope. Knowing that the diameter of the target chamber was 1m it was possible to estimate the camera timing to within ~2ns. With the framing deflectors earthed the compensation deflectors were operated via decoupling capacitors to remove the dc bias the avalanche transistor circuits provide [11]. It is then

possible to adjust the electronic delays until the image is just streaking. In this way the timing may be achieved with relatively few laser shots. The framing and compensation deflectors were then operated in framing mode and the delays adjusted to obtain an even image exposure on the photographic film. It must be stressed that at no time was the relative timing between the avalanche transistor circuits altered when the camera is operated on the Merlin laser facility as mistiming would almost certainly result due to the difficulty in adjusting the camera at such low repetition rates. Once timed, a roll of HP5 was used to record the images obtained, and a typical shot is reproduced in figure 3.4, with moderate intensifier gains of ~200.

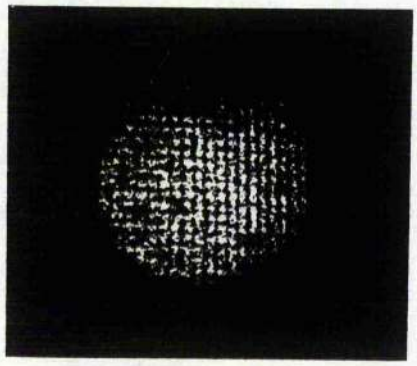

Figure 3.4. Reproduction of a typical X-Ray frame result from the Picoframe I.

3.4.4 Analysis of Single X-ray Frame

Analysis of the image was required as direct comparison with the USAF test chart was not possible due to the unequal bar-space widths of the mesh. Due to the non-linear response of the photographic film, a density step wedge was recorded on all film used before processing. This enabled the film response to be characterised so that the density axis of the line scan could be related to intensity. A curve showing intensity against position of a horizontal line across the image is shown in figure 3.5. The intensity baseline was set to the intensity equivalent fog level of the film.

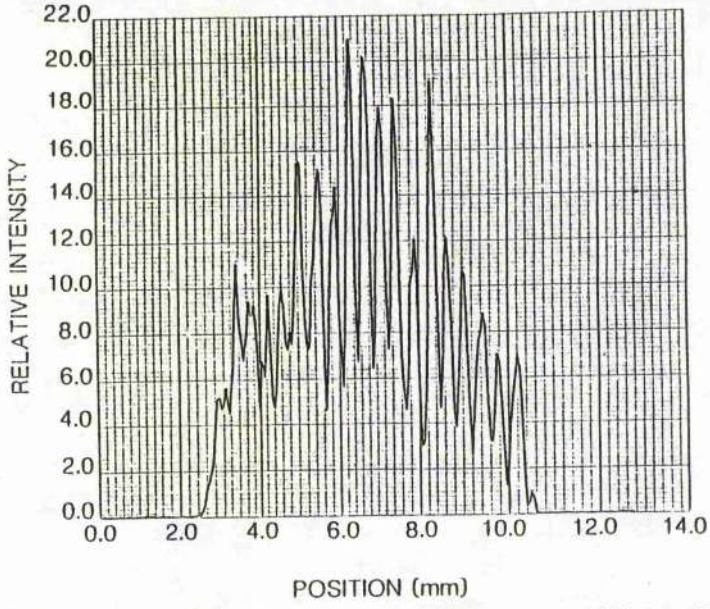

Figure 3.5. Microdensitometer trace along the centre of figure 3.3

The modulation depth is then deduced using equation 3.1

$$\text{Contrast (of modulation)} = \frac{I_{max} - I_{min}}{I_{max} + I_{min}} \qquad (3.1)$$

It was then possible to deduce that the intensity modulation depth corresponding to the scan is between 40% and 85%. A computer programme developed at AWE [12] was used to evaluate the limiting spatial resolution of the image, which indicated that the dynamic spatial resolution of the x-ray-sensitive device was between 300μm and 120μm at the photocathode, depending on the position inspected. The frame time was evaluated using the quadrupled Nd:YAG laser facility and was found to be 120ps FWHM.

For comparison purposes, the single frame UV image was scanned and analysed in the same way. An intensity plot of group 3 element 1 of the image (corresponding to a resolution of 8 lp/mm at the photocathode) is represented as figure 3.6.

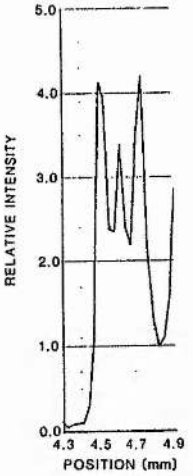

Figure 3.6. Microdensitometer trace along the 8 lp/mm resolution elements of the single frame result obtained from the UV-sensitive Picoframe I.

This curve shows a modulation depth of ~20% and so, using the computer programme, the dynamic limiting spatial resolution was calculated to be 90μm at the photocathode. The usable photocathode area for the X-ray framing camera was deduced to be 6mm x 6mm from Figure 3.5.

3.5 Re-evaluation Of The Dynamic Spatial Resolution Of the X-Ray Picoframe I

Due to the ambiguity of the spatial resolution obtained with the mesh test pattern (indicating a dynamic spatial resolution of between 2.4 lp/mm and 6 lp/mm) it was felt that the camera should be retested under similar conditions but using a more appropriate test chart. A free standing copper USAF test chart was obtained with group zero removed. This replaced the copper mesh previously employed. The cathode substrate was a 24 mm diameter, 15μm thick, aluminium foil with a 9mm active 10nm thick gold cathode. This substrate was adopted in order that the aluminium filter may be removed. Correct film exposure was obtained with only 1.5 J of 532nm laser energy irradiating the gold target, and reduced intensifier gains of ~100. A reproduction of the best image obtained under these conditions is shown in figure 3.7 and group 2, element 5 is resolvable by eye indicating that the limiting spatial resolution with reference to the photocathode is 6.35 lp/mm. The frame exposure time was evaluated with the use of the frequency-quadrupled Nd:YAG laser facility to be 95ps FWHM in this case.

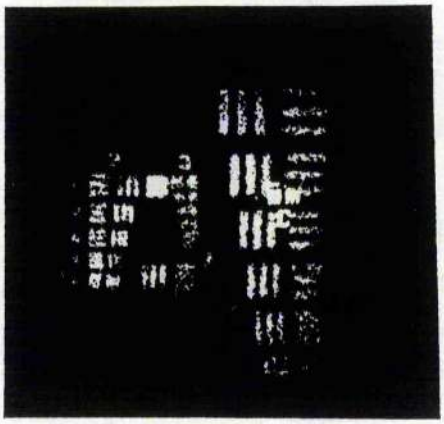

Figure 3.7. Single frame of a USAF resolution test chart with the X-ray-sensitive Picoframe I camera.

3.5.1 Image Evaluation

It is evident that, by direct comparison with the single frame UV results (chapter 2.9.3) that the spatial resolution under x-ray illumination is inferior to that attained under UV illumination, and reasons for this will be discussed in section 3.7.

3.6 Double Frame X-Ray Evaluation

In order to evaluate the performance of the Picoframe I in double-frame operating mode with soft x-ray illumination, double pulse excitation of the gold foil target was required, with a temporal separation of the pulses ~2ns. This was required as the inter-frame time of the double-frame Picoframe I system is approximately 2ns and the x-ray emission resulting from the excitation by 100ps pulses is approximately 100ps [13].

3.6.1 Double Pulse Laser Operation

Double pulse x-ray emission was achieved by introducing an optical delay into the laser system [10] after the first preamplifier as in figure 3.8. The polariser and quarter-wave plate are introduced to maintain isolation from the high gain laser preamplifier.

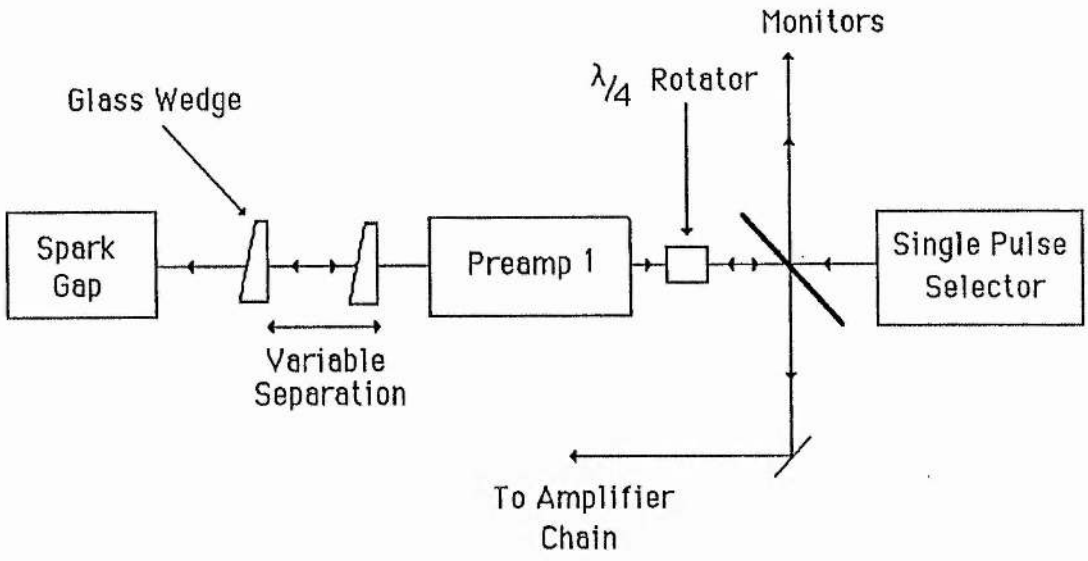

Figure 3.8. Arrangement employed for double pulse generation on the Merlin laser.

This technique resulted in the second optical pulse being lower in intensity due to the reflectivity of the optical glass wedges used. The two pulses were then propagated through the amplifier chain as usual. The optical pulses were monitored using a visible sensitivity (Hadland Photonics, type S20 Imacon 675) streak camera having a Reticon direct read-out device [14] and a typical streak showing the two main optical pulses propagated through a 200ps round-trip time interferometer type delay line for calibration purposes is shown as figure 3.9.

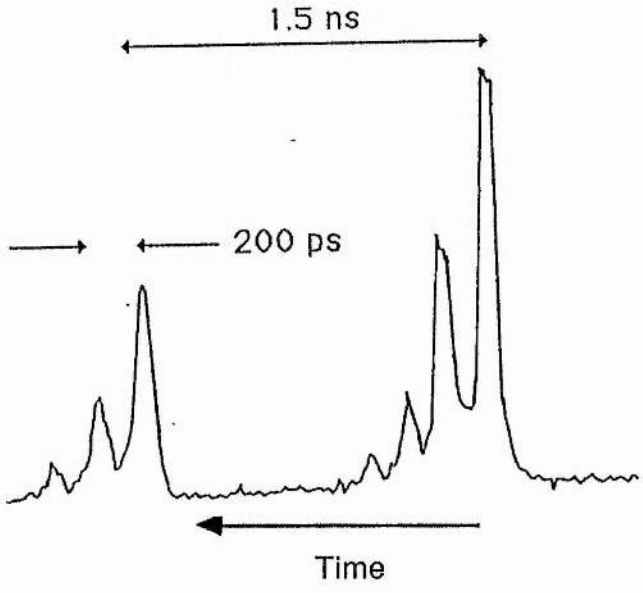

Figure 3.9. Double optical pulses generated by Merlin. The calibration delay used was 200ps and the streak speed was 6×10^8 cm/s.

Inspection of the x-ray emission was undertaken with an x-ray-sensitive streak camera developed at AWE based upon the Photochron II streak camera with a gold x-ray-sensitive cathode. This confirmed that two x-ray pulses were indeed being generated with a pulse duration of ~100ps and a variable separation with an incident laser energy of typically 2 J per pulse.

3.6.2 Camera Timing and Dynamic Spatial Resolution Evaluation

Timing of the camera in the double-frame mode was achieved by timing the first image with only one laser pulse being propagated through the amplifier chain.The second image was timed by suitably adjusting the optical delay. This was a non-trivial excersise because the adjustment of the optical delay necessitated the realignment of the laser system due to the long optical path length followed by the laser beam (estimated to be ~100m). The photocathode employed and intensifier gains were identical to that used in section 3.5 and a reproduction of the frames achieved is shown in figure 3.10.

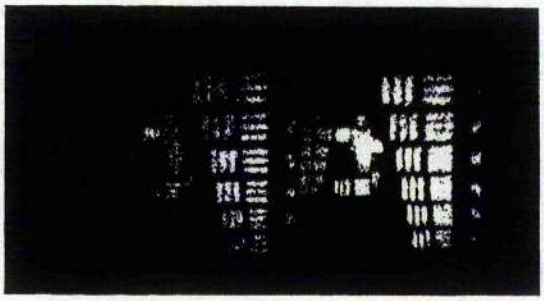

Figure 3.10. Reproduction of a typical double frame X-Ray result using the Picoframe I camera in double frame mode, first frame right, second left.

It is clear that the resolution of the double frame result is inferior to that achieved for the single frame case. The limiting dynamic spatial resolution attained (by visual inspection of the original negative) was 5 lp/mm (when referred to the photocathode) for both frames, but this was not maintained over the whole frame format. The frame and inter-frame times were measured to be 250 ps (FWHM) and 1.5 ns respectively using the frequency-quadrupled Nd:YAG laser. It can be seen that both images have comparable exposure despite the small amplitude difference in the two laser pulses. The

energy delivered by the laser was of the order of 2 Joules per pulse.

3.7 Discussion

The degradation in dynamic spatial resolution for the X-ray-sensitive camera arise through a number of factors. These include, (i) the inability to adjust the camera operating electronics due to the low repetition rate, it may be necessary to re-optimise the camera system due to change in environment, (ii) the secondary electron energy spread associated with x-ray illumination of gold photocathodes, (iii) contamination of the photocathode due to processing inadequacies and (iv) longer x-ray pulse (~100ps) than the UV test pulses used. Of these four reasons it is felt that (ii) is of the primary significance although (i) and (iii) will undoubtedly have considerable influence. It was possible to check for (iv) by increasing the pulse width of the UV laser using etalons and no degradation of the spatial resolution of the UV system was observed. Computer simulations [21] of the camera with secondary electron energies of 0.6eV and 4eV (representing UV and soft x-ray excitation of a gold photocathode [15, 16]) were undertaken for the Picoframe I camera design operating in single frame mode. It was clear that the higher energy electrons strike the anode electrode, resulting in the reduced number of photoelectrons arriving at the phosphor. It was also found that the crossover diameter of the photoelectrons was sufficiently large to be adversely affected by the deflection plates. Fringing fields and propagation close to the deflection plate structure (principally the framing plates) appear to be the main reasons for the degradation of spatial resolution in the x-ray framing system as detailed in section 3.7.1.

3.7.1 Dynamic Fringing Fields

The effect of dynamic electrostatic fringing fields at the entrance and exit of the deflectors is believed to be a major cause of dynamic image degradation in both streak and framing camera systems. This effect is separate from the loss of spatial resolution which occurs due to the curved image plane of the electron-optical lens [19] and while computer simulations have determined their effect [19,20] the physical mechanisms involved will be discussed within this section.

In order to explain one possible mechanism certain parameters will be simplified.

Firstly the electron beam will be considered to be of a finite and constant diameter within the deflection region. This is only reasonable for short deflection plates or long extended electron beam crossover regions such as that associated with the framing camera. Most systems employ deflection plates which are positioned in such a way as to maximise the deflection sensitivity, and so electron beam entrance and exit diameters are often comparable to the deflection plate separation, thus validating the first assumption. Secondly, the electron beam will be considered to be only slightly deflected with respect to other spatial parameters (such as when an image is formed at the centre of the output phosphor screen) and thirdly, the electron transit time is assumed to be sufficiently long so that the deflection electrode potentials will be different at the entrance and exit of deflection region for an electron 'packet' due to the time varying deflection potential. This latter consideration is very realistic at high streak speeds where the electrode potential may change by ~400V during the transit time of an electron through the deflection region due to the rapidly changing deflection waveform employed. The deflection signal is assumed to appear at all parts of the deflector electrode simultaneously.

Consider the situation where two electrons on the outer region (perimeter) of the electron beam approach the electrostatic deflection structure having a potential of $\pm V_0$ as shown in figure 3.11 (a). The solid lines represent the potential distribution of idealised parallel plate deflectors while the arrows indicate the electric field strength and direction. As electron 'A' enters the fringing field region at time T_0 it will experience a force component in the same direction as the drift velocity, thereby increasing its axial speed. Electron 'B' experiences an equal but opposite force and is therefore retarded.

The magnitude of this effect is determined by the position and potential and is therefore a complicated parameter, but a simplified analysis will be attempted. As the axial drift velocity of the electrons at the edges of the electron beam are different, there will be a transit time difference between them through the electrodes. This results in electron 'A' leaving the region at time T_1 and 'B' exiting at time T_2 (figure 3.11 (b) and (c)). Both T_1 and T_2 are substantially greater then T_0 hence the deflection potential will have changed to V_1 and V_2 respectively. The net result is that electron 'B' is deflected

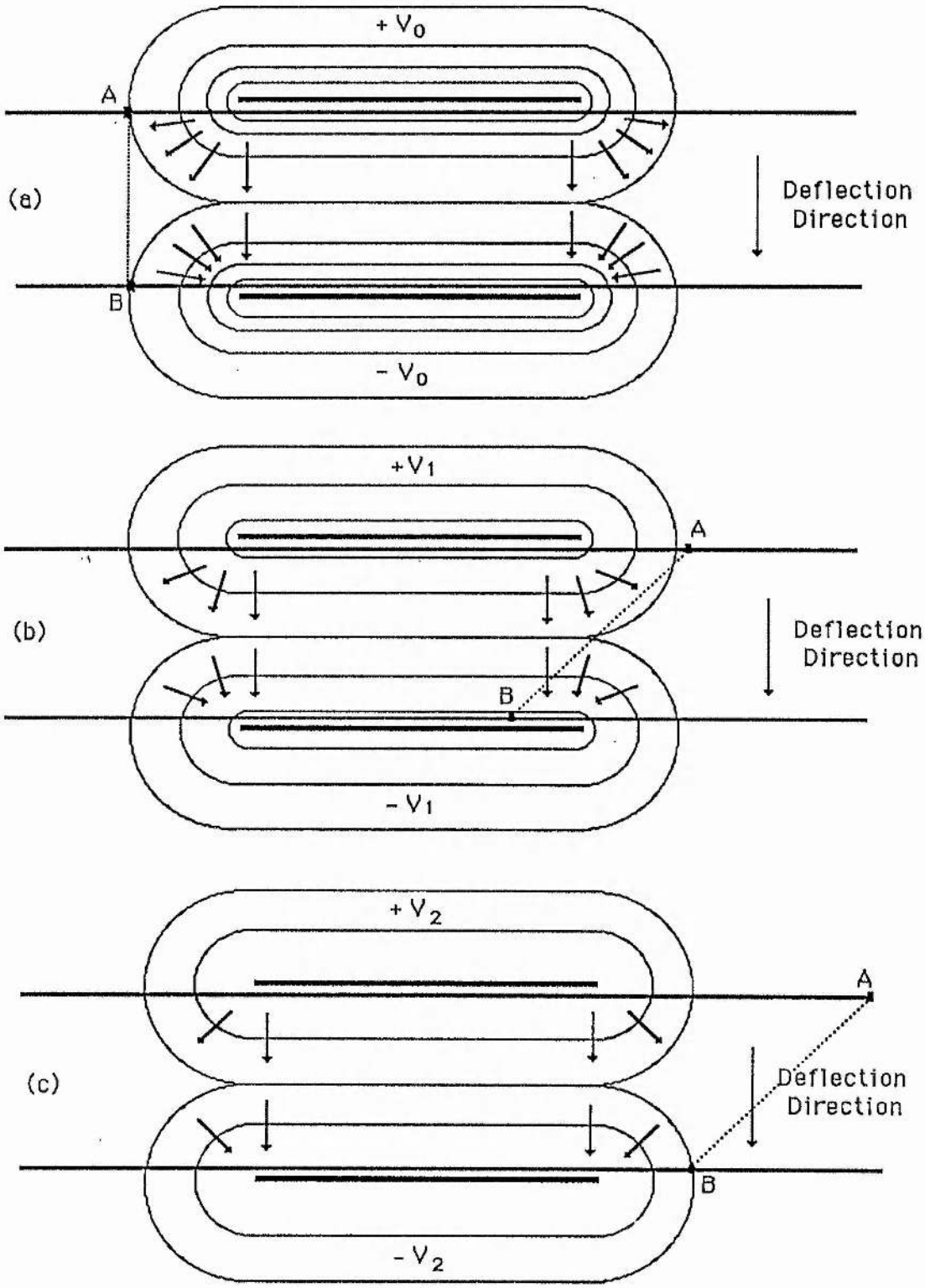

Figure 3.11. Dynamic fringing field effects. The electron beam axial drift velocity is from left to right. Arrows indicate the electric field direction and strength.

to a greater extent to that of 'A' hence causing a shift in the dynamic focal length of the system in the deflection direction, and the axial drift velocities of the two chosen electrons will be different even if they possessed the same velocity before deflection.

The framing camera system is yet further complicated by the additional compensation electrodes which are operated to provide an equal and opposite dynamic deflection to that of the initial framing deflectors. Due to the electron beam crossover between the deflectors electrons 'A' and 'B' experience similar effects to those outlined and hence causing the dynamic astigmatism to be further exasperated. Clearly the dynamic fringing field effects are dependent upon the deflection direction as this determines the whether the fields will be strongest at the entrance or exit of the deflectors and similar arguments may be used in both cases. In fact it appears that the focal length of the electron beam in the deflection direction may change at different deflection angles and thus making dynamic spatial resolution optimisation difficult.

The following represents a simplified analysis to determine the maximum dynamic effect of fringing fields due to the deflection electrodes. The transit time (τ) of the electrons with axial velocity v_e through the deflectors of length L is given by

$$\tau = \frac{L}{v_e} \qquad (3.2)$$

Given the deflection voltage gradient of K (volts / second) and assuming that the voltage on exit of a particular electron 'packet' is zero then the entrance voltage must be V_0 given by

$$V_0 = \tau K = \frac{K L}{v_e} \qquad (3.3)$$

As a first approximation, if the electron beam diameter is equal to the deflection plate separation then the electrons at the beam edge will experience an axial electrostatic acceleration due to V_0 to provide a resultant axial velocity v_r given by

$$v_r = \sqrt{\frac{(V_e \pm V_0)\, 2\, e}{m}} \qquad (3.4)$$

where V_e is the axial electron acceleration potential of the electron beam, e is the electrostatic charge and m is the electron rest mass. The deflector transit time difference ΔT may then be calculated as

$$\Delta T = \frac{L}{\sqrt{\frac{2\, e\, (V_e \pm V_0)}{m}}} - \frac{L}{\sqrt{\frac{2\, e\, V_e}{m}}} \qquad (3.5)$$

Given the typical values of K=2kV/ns, V_e=15kV and L=15mm we arrive at values of $V_0 = 413$ V from the above equation and so $\Delta T = 5.8$ ps, which represents the time difference between the exit of the two electrons on opposite sides of the electron beam due to the dynamic fringing fields. This represents a potential difference of 23V (using the indicated value of K) between the two deflection electrodes between the exit of the two electrons. This is analogous to supplying a dc voltage of ~23 V to both deflectors with respect to the anode potential, which will generate a cylindrical electrostatic lens orientated in the deflection direction and hence causing dynamic astigmatism.

It is of interest to note that in chapter 7 section 5 the extra electrodes were employed to compensate for the induced astigmatism. These have a theoretical dc deflection sensitivity of 0.9cm/kV to the phosphor screen while the framing deflectors have a sensitivity of 2.5cm/kV. It would thus be reasonable to calculate the required dc voltage to be applied to the extra electrodes as

$$\frac{2.5}{0.9} \times 23 = 64 \text{ V} \qquad (3.6)$$

assuming that only the framing deflection was to be compensated. This calculated value is some 10V higher then that found from experimental optimisation, which shows good agreement with theoretical predictions considering the simplistic model adopted.

The assumption that the compensation deflectors in the Picoframe framing camera play a smaller role in the dynamic defocussing than the framing deflectors is reasonable due to the electron beam diameter and deflection plate separation employed in the two regions. This is only true in the Picoframe I variant operating in the single-frame mode due to the axial image position on the phosphor screen. The double frame modes of operation all require the images to be displaced from the axial position and so decreasing the deflector to electron beam separation while increasing the deflector potential at the electron 'packet' entrance and exit and so increasing the dynamic fringing field effects. In this case increased dynamic defocussing will become evident at the same deflection rates, especially when high secondary electron emission energy spread photocathodes are employed such as the present X-ray-sensitive devices.

It is felt that increasing the separation of both sets of deflectors would improve the dynamic spatial resolution of the camera but would of course have the disadvantage of increasing the frame time. It was therefore concluded that that the reduction of the secondary electron emission energy spread would be a preferred route towards alleviating these problems.

During the evaluation of the single frame x-ray system a caesium iodide photocathode deposited onto an aluminium substrate was tried. It has been reported that the secondary electron emission energy spread for caesium iodide is 1.6eV [17] whereas that of the gold counterpart is ~4eV. It was therefore felt that some improvement in dynamic spatial resolution might be obtained, but unfortunately this was not the case. The ceasium iodide cathode was however more sensitive [16, 17] and further attenuation of the x-ray flux was required (using a 25μm aluminium foil filter) to produce well exposed images at moderate intensifier gains. It is believed that the secondary electron energy spread must be reduced to ~1eV before any noticeable improvement in spatial resolution is noted. Other alkali-halide materials have been reported to possess very low secondary electron energy spreads, most notably potassium iodide [17] has only ~0.6eV spread. It is believed that these low secondary electron emission energy spread materials will result in a higher dynamic spatial resolution of the Picoframe type x-ray-sensitive demountable camera but these were not available during the course of this work.

3.7.2 Frame Exposure Time

It should be realised that the frame exposure times were evaluated with a UV-sensitive photocathode and the high repetition rate (4 Hz) Nd:YAG laser after recording frames on the X-ray system. While no alterations were made to the camera system other than the replacement of the photocathode, the measured frame time is likely to represent a value somewhat shorter then that actually achieved with the X-ray-sensitive system. The reason for this is that the photoelectron beam diameter at the framing aperture will be larger in the X-ray-sensitive device then the UV-sensitive system due to the greater secondary electron energy spreads associated with gold X-ray photocathodes. As the frame exposure time is defined by the convolution of the photoelectron beam diameter at the framing aperture and the framing aperture diameter, then an increased beam diameter will yield a longer frame exposure time. Unfortunately there is no accurate direct experimental method available for deducing the frame exposure time of the X-ray-sensitive framing camera due to the long (100 ps) X-ray pulses available and the low repetition rate available. It is theoretically possible to measure the frame time as achieved with the UV-sensitive system, but optical pulse-to-pulse duration variations and system jitter necessitates the averaging of typically five laser shots per temporal delay setting, and so about 100 laser shots are required to define the required transmission function. This would require approximately one week to accumulate and so was not considered practicable.

The electron-optical simulation programmes developed at St Andrews University [21] have recently allowed the complete dynamic simulation of the framing camera under various conditions. The programmes allow the electron trajectories to be traced through the entire camera electrode system and so it was possible to attain some theoretical evaluation of the expected increase in frame exposure time under X-ray illumination as opposed to UV. The cathode secondary electron emission energy spread was set to 4 eV to represent a typical gold photocathode under soft X-ray excitation and the active photocathode area was 5mm x 5mm. Although the simulation clearly indicated some photoelectron intersection with the 4mm diameter anode electrode, the principle region of interest was the framing aperture plane. Under the conditions indicated 70% of the photoelectrons reaching the framing aperture plane fell within a

beam diameter of 2.5 mm. Similar simulations undertaken with a 6mm x 6mm active photocathode area and 0.6 eV electron emission energy spread (simulating a UV-sensitive photocathode) indicated that 70% of the electrons reaching the framing aperture plane were transmitted through the 1.8 mm diameter aperture. Thus the theoretical beam 'diameter' has been increased by 30% when utilising the X-ray-sensitive photocathode as opposed to the UV cathode. Therefore when employing a 1.8 mm diameter framing aperture it is expected that the X-ray frame exposure times will exceed those measured with the UV-sensitive device by 20%. The actual experimental X-ray frame exposure time will also be a function of the photocathode area illuminated but the diameter of the anode aperture restricts the usable cathode area 6 mm x 6 mm and so the computer simulations indicate that the X-ray frames presented within this thesis have up to 25% longer frame exposure times then those measured with the UV-sensitive system. For the reasons previously mentioned we have been unable to experimentally verify this figure with the X-ray source employed and so the frame exposure times have been quoted to be equal to those of the UV-sensitive device.

3.8 Conclusions

The Picoframe I camera system has been shown to operate under x-ray excitation of a simple gold photocathode. Single and double framing has been achieved with the soft x-ray emission of a laser-produced plasma (generated from a medium-power laser ~4 J of 532nm radiation in 100ps FWHM irradiating gold foil targets). The best single frame result indicates a dynamic spatial resolution of 6.4 lp/mm with a frame time of 95ps FWHM. The double frame system provided two frames, each of 5 lp/mm at best with frame and inter-frame times of 250ps (FWHM) and 1.5ns respectively. It has thus been shown that the Picoframe camera may be used in either mode for preliminary plasma studies.

References for Chapter 3

1 R S Shankland

'Atomic and Nuclear Physics' (second edition)

The Macmillan Company, 1960

2 Q Johnson and A C Mitchel

Rev. Sci. Instrum.,51(6), 741, 1980

3 Y Carmel and S Eylon

Rev. Sci. Instrum., 50(1), 17, 1979

4 M S Hill, Cyrus D Cantrell III

Physics of Quantum Electronics 3

Addison Wesley Publishing Company Inc.

5 G H McCall

'X-ray Imaging', SPIE 106, 1977

6 H Wolter

Ann Physik Vol 10 94 (1952) 'ibid 10 ' 286, 1952

7 M J Boyle, H G Ashlstrom

Rev. Sci. Instrum., 46 (6), 746, 1978

8 'Handbook of Chemistry and Physics' (63rd edition)

Editor R C Weast, Published by CRC Press Inc.,1982

9 C F Mc Conachy, L W Coleman

Applied Physics Letters, 25 (5), 268, 1974

10 G L Stradling, D T Attwood, R L Kauffman

Proc. 15th ICHSP (San Diego), SPIE 348, 777, 1982

11 M C Jackson, R D Long, D Lee, N J Freeman

Laser and Particle Beams 4 (1), 145, 1986

12 R T Eagles, N J Freeman, J M Allison, W Sibbett, W E Sleat, D R Walker

Advances in Electronics and Electron Physics, 74, 215, 1987

13 J E Balmer, W Lampert, E Roschger, J D Hares, J D Killkenny

Rev. Sci. Instrum., 56 (5), 860, 1985

14 Hadland Photonics Ltd., Bovingdon, Hemel Hempstead, Herts.

14 Hadland Photonics Ltd., Bovingdon, Hemel Hempstead, Herts.

15 B L Henke, J A Smith

Journal of Applied Physics 48 (5), 539, 1977

16 V K Chevokin, A M Prokhorov, V N Schemelev, M Ya Schelev

Proc. 15 ICHSP (San Diego), SPIE 348 , 741, 1982

17 B L Henke, J Liesegang, S D Smith

Physical Reviews B 19 (6), 3004, 1979

18 H C Gerritsen, H Van Brug, F Bijkerk, M J Van der Wiel

Journal of Applied Physics 49 (7), 2337, 1986

19 K Kinoshita, T Kato, Y Suzuki

Proc. 14th ICHSPP (Moscow), 199, 1980

20 W Sibbett, Y Lui, D R Walker

Proc. VII Ultrahigh Speed Photography, Photonics and Videography, (to be published), San Diego, August 1989.

21 L Yueping

Private Comunication, St Andrews University.

Chapter 4

Double Frame Operation of the Ultra-Violet / X-Ray - Sensitive Picoframe II

4.1 Introduction

While the operation of the Picoframe I camera in double frame mode using pulse forming networks has been achieved (chapter 2), the system is both complicated to operate and is restricted by the available drive electronics. The generation of multiple frames with this image tube is limited by the number of rising and falling voltage edges which may be generated with sufficient amplitude and rate of change which is at present restricted to two. Also the frame and inter-frame times are relatively long due to the reduced waveform gradient produced by the PFN's and associated dc decoupling capacitors etc.

4.2 The Picoframe II Camera

To overcome the shortcomings associated with the Picoframe I single-aperture design, the Picoframe II camera was devised. This camera is basically identical to the Picoframe I except that it has an additional framing aperture and set of compensation deflectors. A schematic is given as figure 4.1.

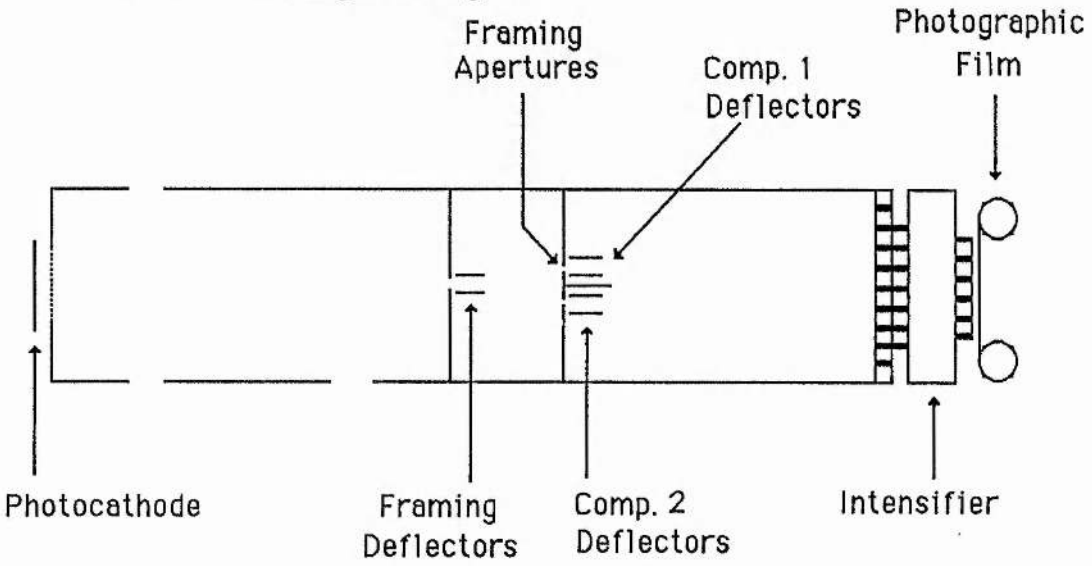

Figure 4.1 Schematic diagram of the Picoframe II electrostatic lens and deflection geometry.

Two aspects are of prime importance in the design of this image tube deflection region. Firstly, capacitive cross-coupling of the compensation deflectors and the capacitive coupling of the deflectors to earth must be kept to a minimum, and secondly the separation of the framing apertures must be kept to a minimum to reduce the inter-frame time (which is defined by the scan speed and the inter-aperture spacing only)

4.3 The Proposed Triple-Aperture Design

The initial design proposal was for a three aperture / compensation deflector construction [1] which would provide three frames from the application of linear voltage waveforms to the deflectors. Unfortunately this design is virtually impossible to implement due to the space available and amplitude of voltage waveforms easily generated. In a recent report [2] a similar three aperture design has been discussed, but multiple dc biased shift plates were used to avoid the capacitive cross-coupling problems mentioned. Only moderate dynamic spatial resolution was reported, probably due to the accumulated fringing field effects associated with the complex multi-deflector structure.

4.4 Initial Evaluation of the Picoframe II Design

The double aperture Picoframe II configuration designed initially by Eagles enabled the generation of two frames directly. This design was realised in a sealed-off visible-sensitivity camera image tube, but some misalignment of the electrodes either during construction or bake-out resulted in severe astigmatism. The 'undeflected' electron beam was non-axial and in fact was able to go through one of the apertures positioned some 5mm off the axis. By using electromagnets positioned around the glass envelope the electron beam could be brought into line with the tube axis and preliminary studies were undertaken to evaluate the feasibility of the design. Frame doublets were achieved, but these had low dynamic spatial resolution (< 4 lp/mm per frame) and frame and inter-frame times of ~150 ps (FWHM) and ~800 ps were indicated. More importantly it was confirmed that the compensation deflector cross-talk could be eliminated and independent compensation of the streaked images achieved. It

was therefore decided to construct suitable components to convert the Picoframe I demountable image tube into a Picoframe II camera.

4.5 The Vacuum Demountable Picoframe II

The aperture plate consisted of two framing slots, 1.8mm wide and separated by 9mm which was the minimum that could be achieved due to the compensation plate positioning. These were 14mm long and separated by 4mm. Compensation plate isolation was achieved by introducing an earth screen between the two sets of deflectors. Machinable glass ceramic was used for mounting the plates and copper braid used for the electrical connections as shown in figure 4.2

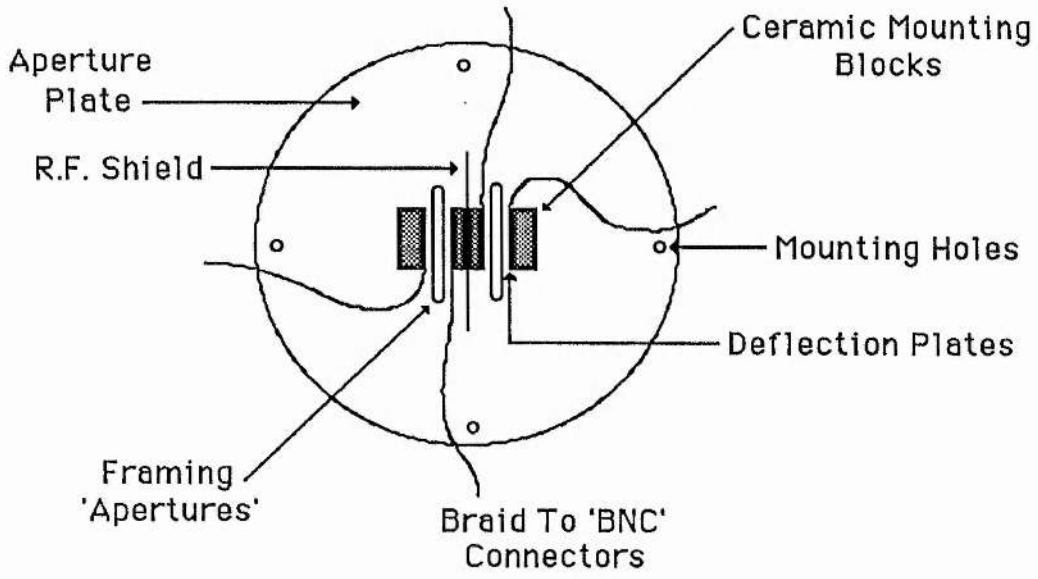

Figure 4.2. Construction of the compensation deflector arrangement.

4.5.1 The Static Spatial Resolution of the Picoframe II

To measure the limiting static spatial resolution of the Picoframe II camera design a dc bias deflection voltage must be applied to the framing deflectors. The two images resulting from the two framing apertures were inspected by illuminating the USAF test chart masked UV-sensitive photocathode with a mercury arc lamp. The framing and compensation deflectors were connected in inverse polarity and a suitable symmetrical

dc deflection bias voltage applied. The image intensifier was operated at a gain of ~100 in order that the resultant images were sufficiently intense to be inspected by eye. The resultant spatial resolution is shown graphically as figure 4.3 (a), (b) corresponding to the two images. The deflection voltages indicated refer to the positive component of the deflection potential and so it may be seen that a deflection voltage of approximately ±750 V is required to sweep the photoelectron beam from the centre of one aperture to the other. With this deflector geometry it is clear that only moderate static spatial resolution was attained, although one image was of a higher quality then the other due to the asymmetry of the apertures about the undeflected photoelectron trajectories.

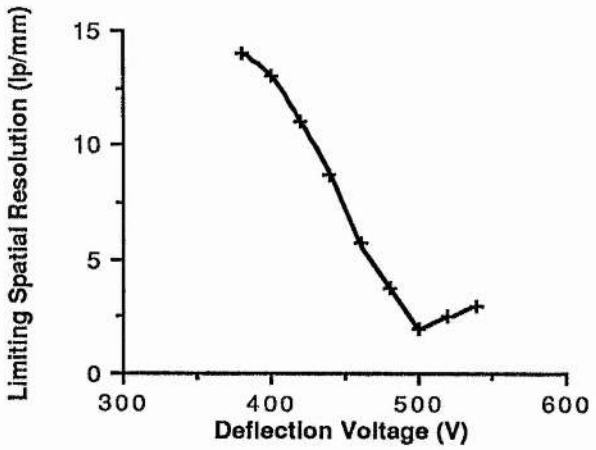

(a)

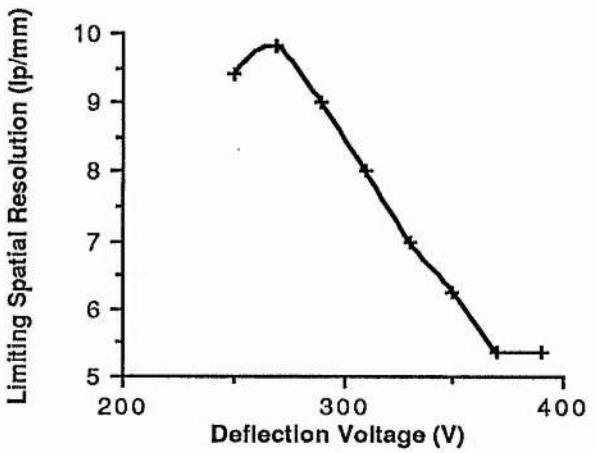

(b)

Figure 4.3 (a), (b) showing the limiting static spatial resolution of the two photoelectron images resulting from the two framing apertures with respect to the

symmetrical deflection voltage applied to the framing and compensation deflection plates. Non symmetry of the two framing apertures about the undeflected photoelectron beam is evident by the different deflection voltages required.

Careful analysis of the electron trajectories (achieved by electron 'ray tracing') revealed that the photoelectrons approached the outer of the two compensation plates near their exit. It was felt that electrostatic fringing fields (which are non uniform electrostatic fields at the entrance and exit of the deflection plates) were the main reason of the degradation of the spatial resolution.

4.6 Dynamic Evaluation of the Picoframe II

The camera was tested in dynamic operation using the frequency-quadrupled Nd:YAG laser. Two optical pulses were generated using a Michelson delay line as previously described in chapter 3. The additional set of compensation deflection plates in this image tube require another avalanche transistor sweep circuit, as it has been found that deflection voltage waveform linearity and rise-time are degraded if more than one set of deflectors are driven by one circuit. This was attributed to current 'saturation' of the avalanche transistors when driving the increased capacitive load presented by the additional deflectors and associated cables. This resulted in current limiting within the transistors causing reduced lifetime and deflection speed / linearity.

4.6.1 Deflection Voltage Timing

Spatial separation of the two images is achieved by suitably timing the triggering of the avalanche circuits to provide dephasing of the waveforms as shown in figure 4.4. In this way the two frames are symmetrically deflected by a displacement (corresponding to half the image size on the phosphor screen) off the camera axis. In order to achieve this, the two compensation deflection circuits must be triggered independently with a temporal separation corresponding to the time required to scan the photoelectron beam from one aperture to the other by the framing deflectors. Due to the aperture separation and streak speeds usually attained at the framing aperture plane, this

temporal separation was expected to be ~600ps, ie. t_2-t_1 ~700ps, which was experimentally verified from the calibrated transmission line delay unit employed.The rate of change of voltage applied to the deflection plates was adjustable using the trimmer resistive dividers described in chapter 2.8.1 and so any differences in the sensitivity of the framing and compensation plates could be compensated.

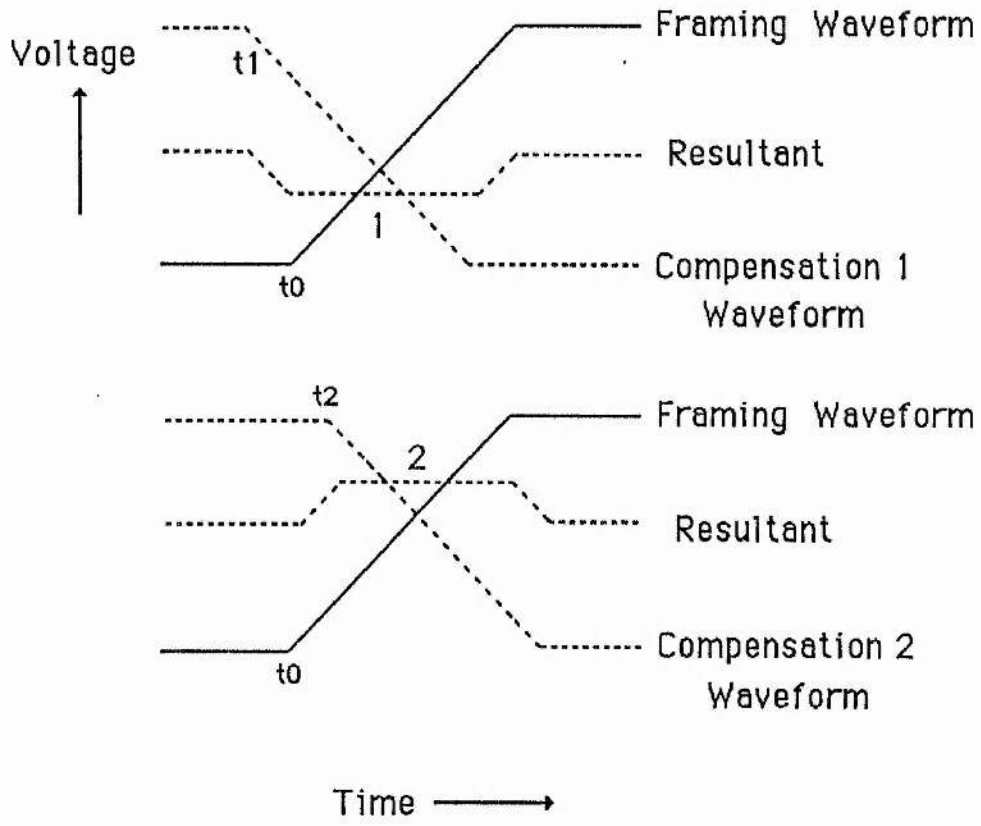

Figure 4.4. Relative timing of the deflection waveforms to produce spatial separation of the images at the phosphor screen.

4.6.2 The Experimental Set Up

A full electrical and optical outline of the experimental equipment is shown in figure 4.5.

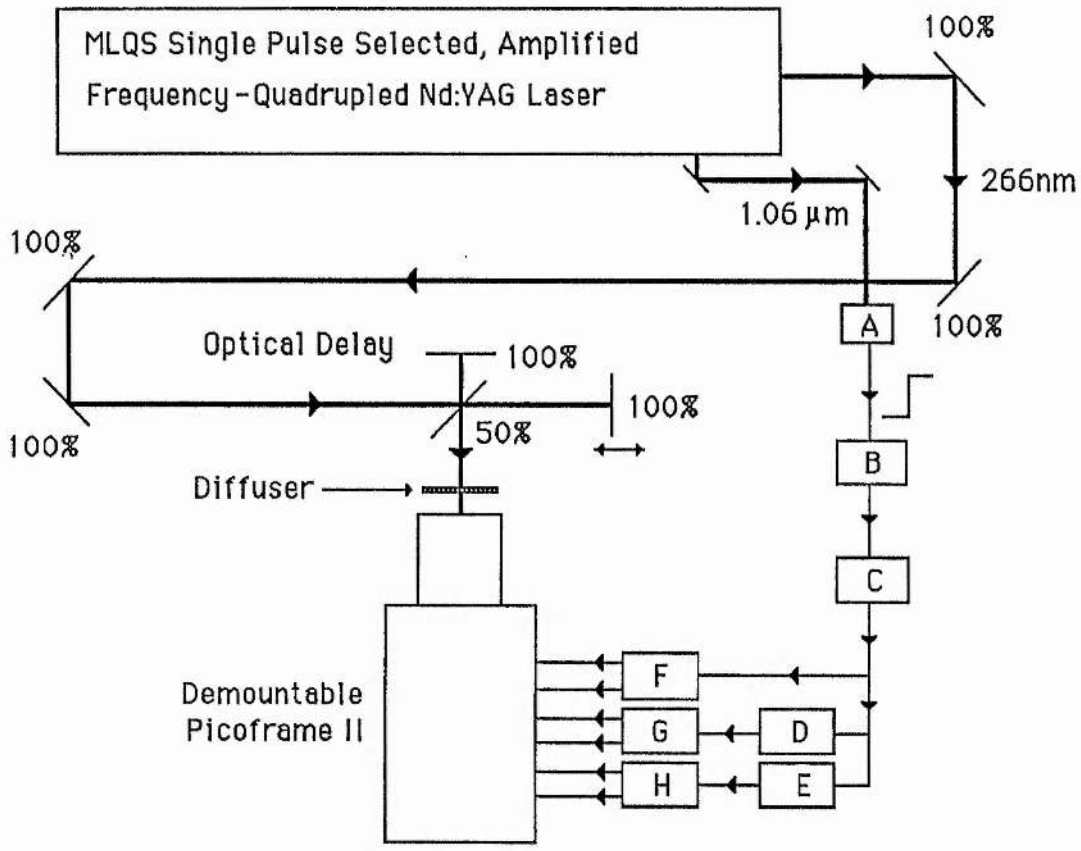

Figure 4.5 showing the experimental arrangement for the dynamic testing of the Picoframe II framing camera design. Key to figure, A; photodiode, B; electrical transmission line delay unit (0 to 64ns switchable in 250 ps intervals),C, D, E; continuously variable (0 to 1ns) electrical transmission line delay, F, G, H; avalanche transistor sweep circuits.

A reproduction of a frame doublet appears as figure 4.6. The limiting dynamic spatial resolution (by eye) for both frames is ~5 lp/mm with frame and inter-frame times measured as 100ps (FWHM) and 600ps respectively, deduced from the sampling scheme described (chapter 2.9.4) and the optical delay introduced respectively.

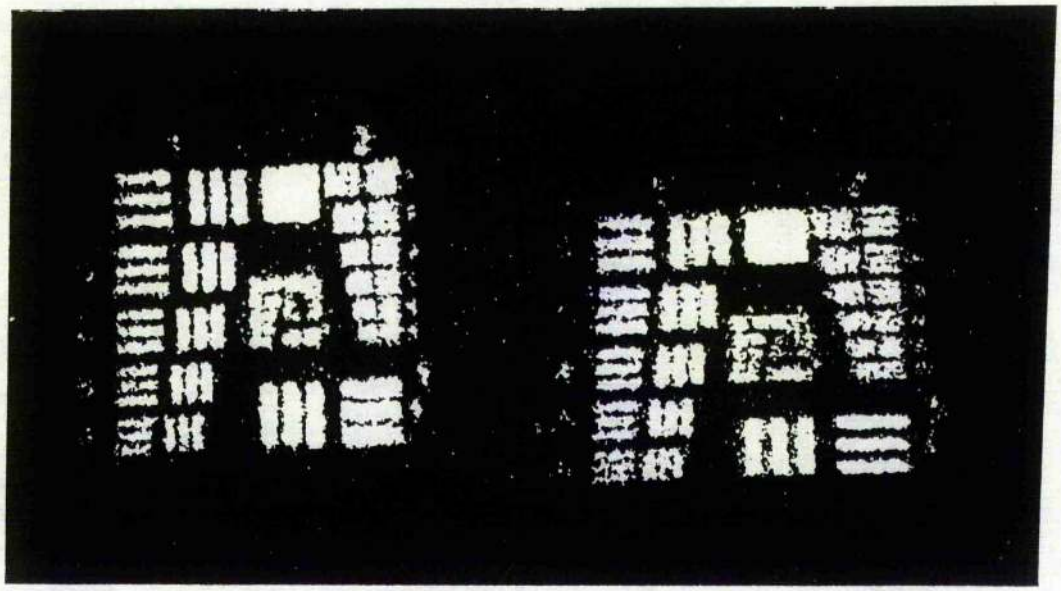

Figure 4.6. Reproduction of a double frame UV result employing the Picoframe II framing camera, first frame right, second left.

4.7 Modifications To The Picoframe II

As previously mentioned it was realised that the spatial resolution was being degraded due mainly to the fringing fields associated with the compensation plates. It was found that the compensation deflectors could be moved closer together by thinning down the ceramic glass spacers between the earthing screen and the inner deflection plate. After careful analysis of the photoelectron trajectories within the deflectors it was realised that the situation could easily be further improved by moving the two framing apertures together so that the framing apertures did not lie on the deflector centre line, but were in fact offset by 0.7mm as indicated in figure 4.7.

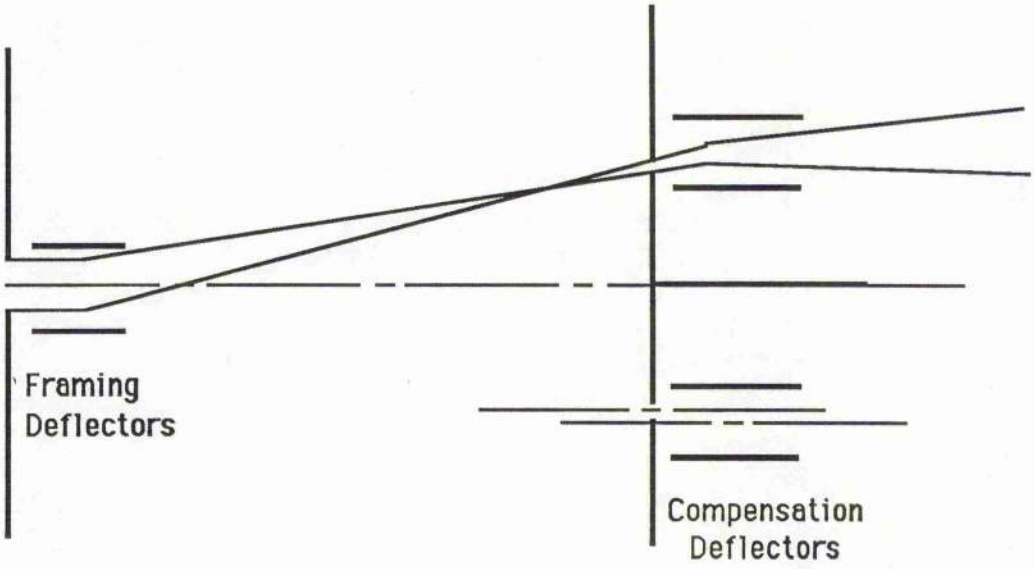

Figure 4.7 Framing and compensation deflector geometry of the modified Picoframe II camera design (not to scale). The effect of positioning the compensation deflectors off the framing aperture centreline is clearly indicated.

With the combination of these two techniques it was possible to reduce the inter-aperture separation to 7mm. The system was reevaluated in static mode, showing an almost uniform spatial resolution of >10 lp/mm for all applied dc bias voltages. Dynamic testing was carried out as before and the limiting dynamic spatial resolution was determined to be (by eye) at least 8 lp/mm for both frames when referred to the photocathode. A reproduction of an image doublet is shown as figure 4.8

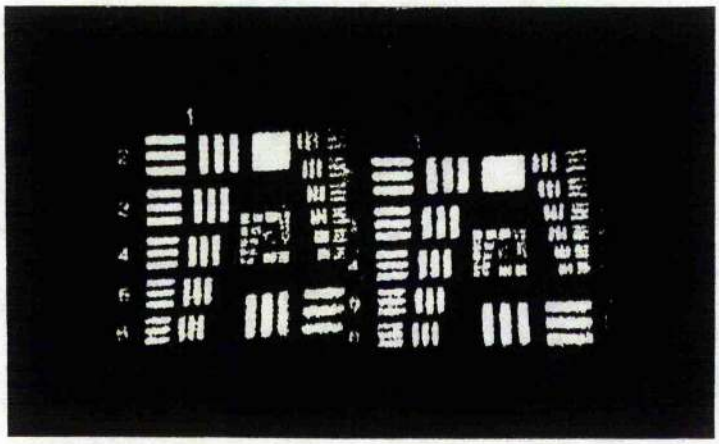

Figure 4.8. Double frame result obtained with the UV-sensitive Picoframe II camera, first frame right, second left.

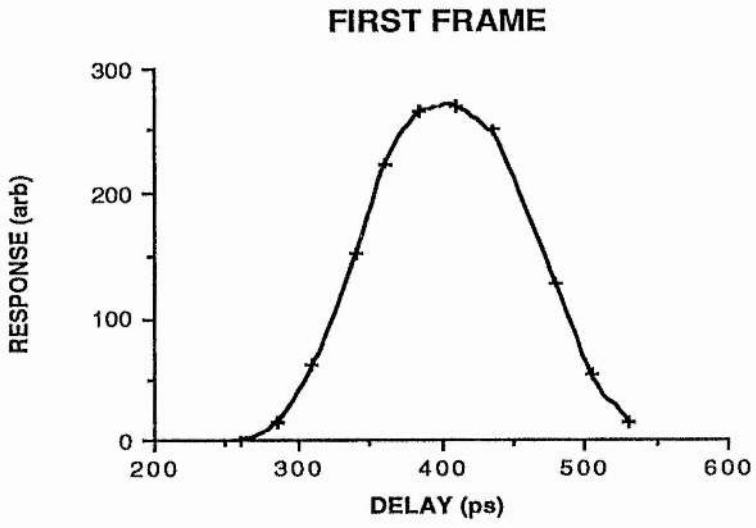

(a)

Figure 4.9 (a) showing the temporal transmission function of the first frame.

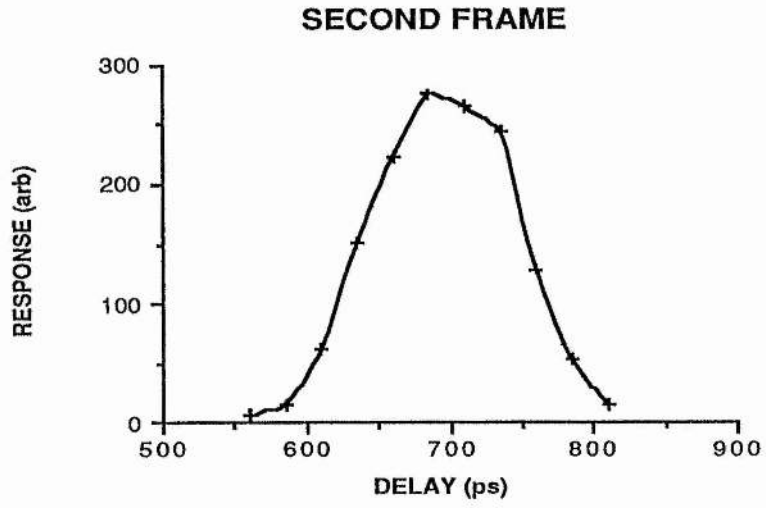

(b)

Figure 4.9 (b) showing the temporal transmission function of the second frame.

The frame and inter-frame times of the system were evaluated (chapter 2.9.4) as 120 ps (FWHM) (transmission functions shown as figure 4.9 (a) and (b)) and 400ps, allowing for the first time the generation of two high quality frames to be generated in under 1ns. These frame and inter-frame times correspond to a frame rate of almost 2.5 x 10^9 frames per second. It has therefore been shown that the Picoframe II design can produce high quality frames at very high framing rates with UV illumination.

4.8 Analysis of Image Features

From inspection of the frame doublet reproduced it may be seen that the two images are of slightly different magnification in the streak (horizontal) and non streak directions. Initially it was believed that this was due to the loss of symmetry of the framing apertures about the undeflected photoelectron trajectories [3]. However, when the framing and compensation deflectors were operated so that the photoelectron beam was swept across the framing apertures in the opposite direction, the magnification difference was noted to change between the two images. In fact it was found that the first of the two images displayed was effected in the same way, regardless of the scan direction, and likewise for the second image. From this it was apparent that the effect was directly related to the order in which the frames were generated. In figure 4.8 the right hand image is the first generated and this shows spatial 'stretching' in the scan direction, while the later frame has been 'squashed' in the scan direction.

This effect may be explained when consideration is given to the electron deflector transit time and the electrostatic fringing fields associated with the entrance and exit of a plane parallel plate electrostatic deflection geometry. Due to the finite photoelectron transit time through the deflector structure and the rapidly changing deflection voltage, the electron will experience different fringing fields at the entry and exit of the deflectors. The effect of this is to cause image defocussing (due to the induced dynamic electrostatic cylindrical lens) in the streak direction, which becomes more severe at higher streak speeds and deflection angles. This effect is detailed by Kinoshita et. al. [3] for the case of a streak camera showing the different asymmetric change in focal length of the electron optical system with respect to electron beam deflection, however the framing camera poses a more complex problem. A full computer simulation of the Picoframe I and II camera variants has now been undertaken, and results show that the image magnification difference is indeed indicated by the combination of the transit time / fringing field effects of the framing and compensation deflectors after optimising the dynamic focusing of the electron-optical lens. The details of simulation are the subject of a colleague's PhD [4] and indicate that this effect is a function of aperture separation, deflection plate length, separation, electron velocity, and the applied dynamic deflection voltage gradient.

As usual, a compromise between the frame / inter-frame times required and the degree of spatial distortion acceptable must be accepted because these two aspects are interconnected when the double aperture geometry and plane plate deflection electrodes are employed. The use of distributed or travelling-wave type deflectors (chapter 7) will reduce the unwanted dynamic fringing field defocussing effects, but this considerably increases the deflection structure complexity. In practice the magnification difference is small for the ~100ps frames obtained and this may be readily taken into account during image analysis. It should be noted that the Picoframe I camera does not suffer as much from the above effects due to the axial position of the framing aperture, and so reduced dynamic fringing fields associated with the framing and compensation deflectors when the photoelectrons strike the phosphor screen. Thus when the camera is operated in double-frame mode a compromise of the electron-optical focussing may be easily found.

4.9 X-Ray Evaluation of the Picoframe II Camera

Further evaluation of the picoframe II camera was undertaken with x-ray illumination by using the Merlin laser facility at AWE Aldermaston (chapter 3.2) in a double-pulse mode. Figure 4.10 shows a streak camera recording of the 532nm laser excitation beam propagated through a 200ps round-trip time delay line for calibration purposes. The streak speed employed was 1.5×10^9 cm/s.

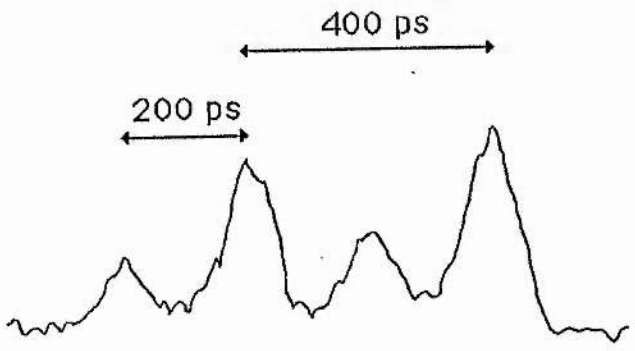

Figure 4.10. Temporal characteristics of the 532nm green double-pulse excitation beam showing 400ps separation. calibration sub-pulses are 200ps from main pulse.

As before, the camera was initially optimised on the UV system before the cathode was replaced with an X-ray-sensitive version (15μm aluminium substrate and 10nm gold, chapter 3.5) and the system transported to the laser facility. Timing was achieved as per the double frame operation of the x-ray-sensitive Picoframe I camera (chapter 3.6.1). Frame doublets were achieved, and a reproduction is shown in figure 4.11

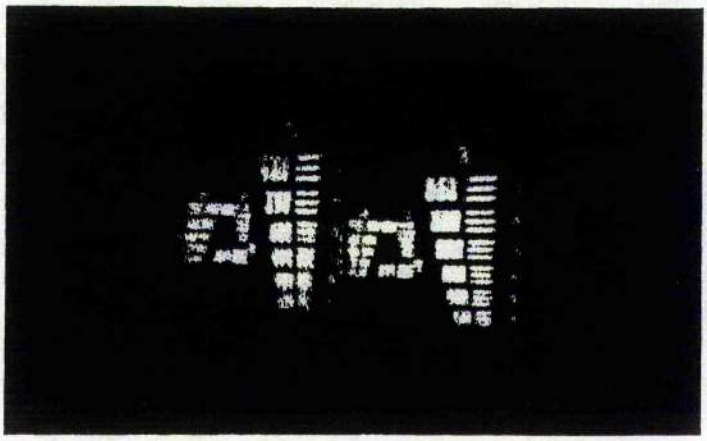

Figure 4.11.X-ray double frame result using the Picoframe II camera, first frame right, second left.

The limiting spatial resolution of both frame was deduced to be 4.5 lp/mm at the photocathode while the frame and inter-frame times were 110 ps (FWHM) and 400 ps respectively, measured on the frequency-quadrupled Nd:YAG laser as previously described (chapter 2.9.4).

4.10 Discussion

Excellent dynamic spatial resolution has been attained with the modified compensation deflection geometry when used in the UV-sensitive Picoframe II framing camera. It is noteworthy that the modified design relies on the triggering of the two compensation circuits to be temporally separated by ~500 ps. While this temporal separation is substantially larger then the avalanche transistor circuit trigger jitter (± 20 ps) it may be expected that the accumulated trigger jitter between all three circuits would have a considerable effect upon the camera performance. However this did not seem to be major problem as the operation of this camera system was highly reproducible.

The relatively poor dynamic spatial resolution of the x-ray-sensitive Picoframe II camera system was attributed the high secondary electron energies emitted from the photocathode interacting with the fringing fields associated with the framing and compensation plates. The fact that images are obtained only when the electron beam is deflected off the tube axis means that the transit voltages of ~400 V are required on the deflection plates during framing. With the increased crossover diameter resulting from the higher secondary electron energy spread of the x-ray excitation of the gold photocathode, the fringing field problem is further exacerbated. Jitter between the avalanche transistor circuits may be a further cause of dynamic spatial resolution reduction, but as previously pointed out, this was not apparent during the evaluation of the UV-sensitive Picoframe II camera.

4.11 Conclusions

With the Picoframe II camera both UV and x-ray double frame formats have been demonstrated. In both cases the frame and inter-frame times are shorter than the Picoframe I double frame system. The frame time of just over 100 ps is better then half of the single aperture double frame system, while the inter-frame time of 400ps is some 4 times shorter. The UV-sensitive system offers good dynamic spatial resolution at 8 lp/mm (when referred to the photocathode) for both frames, while the x-ray-sensitive version has demonstrated 4.5 lp/mm at the photocathode. The degradation of the resolution for the x-ray system is principally due to the higher electron energy spread which causes the photoelectron trajectories to approach both the framing and compensation plates. An increase in the separation of both sets of deflection plates would undoubtedly increase the dynamic spatial resolution but would drastically increase the frame and inter-frame times.

References for Chapter 4

1 W Sibbett, M R Baggs, H Niu

Proc.15th ICHSP (San Diego), SPIE 349, 267, 1982

2 G G Feldman, G I Bruikhnevich, V M Zhilkina, T A Ilina, V B Lebedev, V Simonov, V I Syrtsev

Proc.High Speed Photography, Videography and Photonics IV (San Diego), SPIE 693, 147, 1986

3 K Kinoshita, T Kato, Y Suzuki

Proc. 14th ICHSPP (Moscow), 199, 1980

4 Y Liu

Private Communication, St Andrews University

Chapter 5

Four-Frame Operation of The UV-Sensitive Picoframe II Framing Camera

5.1 Introduction

The ability for the Picoframe range of framing cameras to produce multiple exposures with good resolution, fast frame and inter-frame times and no parallax is very attractive as a diagnostic in the studies of laser-induced plasmas. Double frame formats have been demonstrated with the Picoframe I (with visible radiation [1]) and Picoframe II type cameras in the UV and soft X-ray spectral regions (chapters 2 to 4), while the capability to exceed two frames has not been experimentally demonstrated. In order to produce more than two frames with the Picoframe I camera, multiple triangular voltage waveforms must be generated with suitable voltage amplitude, which is difficult to achieve with the pulse forming networks (PFN's) and avalanche transistor circuits presently employed. On the other hand, the use of the Picoframe II design in conjunction with the PFN's (to generate triangular pulses) and circuits could potentially meet the requirements for a four frame system. In this system, two frames are generated on the leading edge of the triangular waveform and two on the trailing edge. Spatial separation of the two frames in each 'doublet' may be achieved by suitably dephasing the framing and compensation deflection waveforms as previously described (chapter 4, section 6.1) while the frame doublets are separated using dedicated shift electrodes mounted within the image tube. These shift deflectors are located between the compensation deflectors and phosphor screen and are mounted orthogonally to the streak direction as shown in figure 5.1. The application of a step input allows the spatial separation of the frame doublets to be achieved as described later in this chapter.

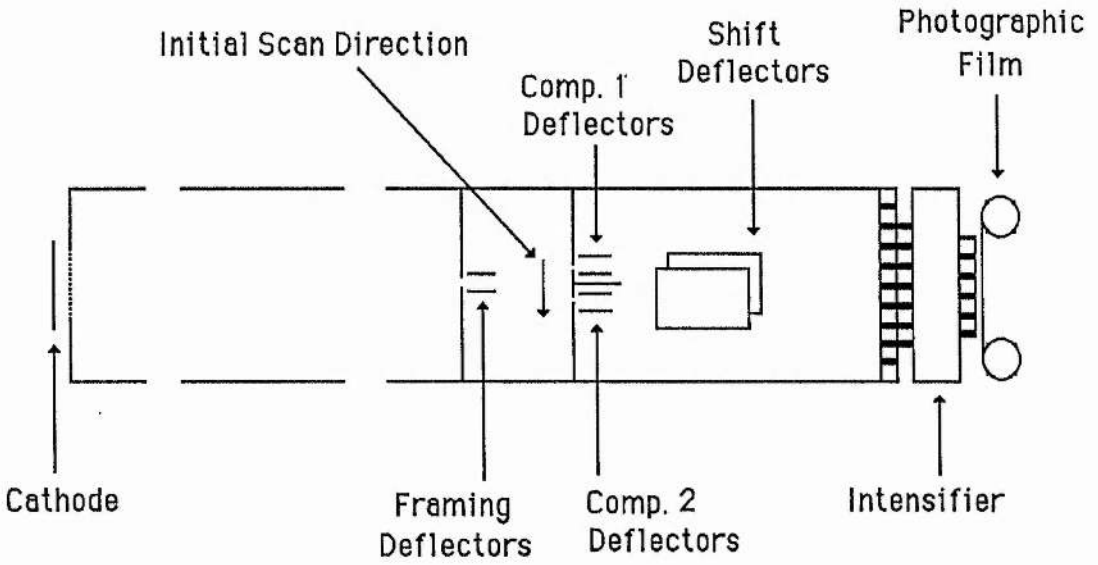

Figure 5.1. Schematic diagram of the Picoframe II with shift deflectors

5.2 The Shift Deflectors

The shift deflectors were constructed using 0.5mm thick copper sheet, which was bent to the required shape and polished. These plates were then mounted directly onto the 'BNC' bulkhead sockets using specially fabricated collets. The parallel plates were mounted 20mm from the compensation plates and were 25mm long, 20mm wide with a separation of 20mm to provide a dc deflection sensitivity of 10mm/kV at the phosphor screen with the usual anode operating voltage of 15kV. In operation, the dc bias applied to the shift plates is altered between the generation of the second and third frames, while remaining constant at all other times. This ensures that spatial separation of the two frame doublets is achieved while not degrading the dynamic spatial resolution, but practical difficulties arise in generating sufficiently fast voltage ramps with suitably flat plateau.

5.3 Framing and Compensation Waveform Requirements

As with the operation of the Picoframe II in two frame mode (chapter 4), spatial separation of the two frames within a doublet may be achieved by voltage waveform dephasing, when careful consideration must be given to the requirements placed upon the PFN's when using them in a four frame system. In order to explain the relative phasing required it is necessary to consider the direction in which the photoelectrons are

being swept across the two apertures. For clarity the compensation deflectors and associated apertures are defined as in figure 5.2

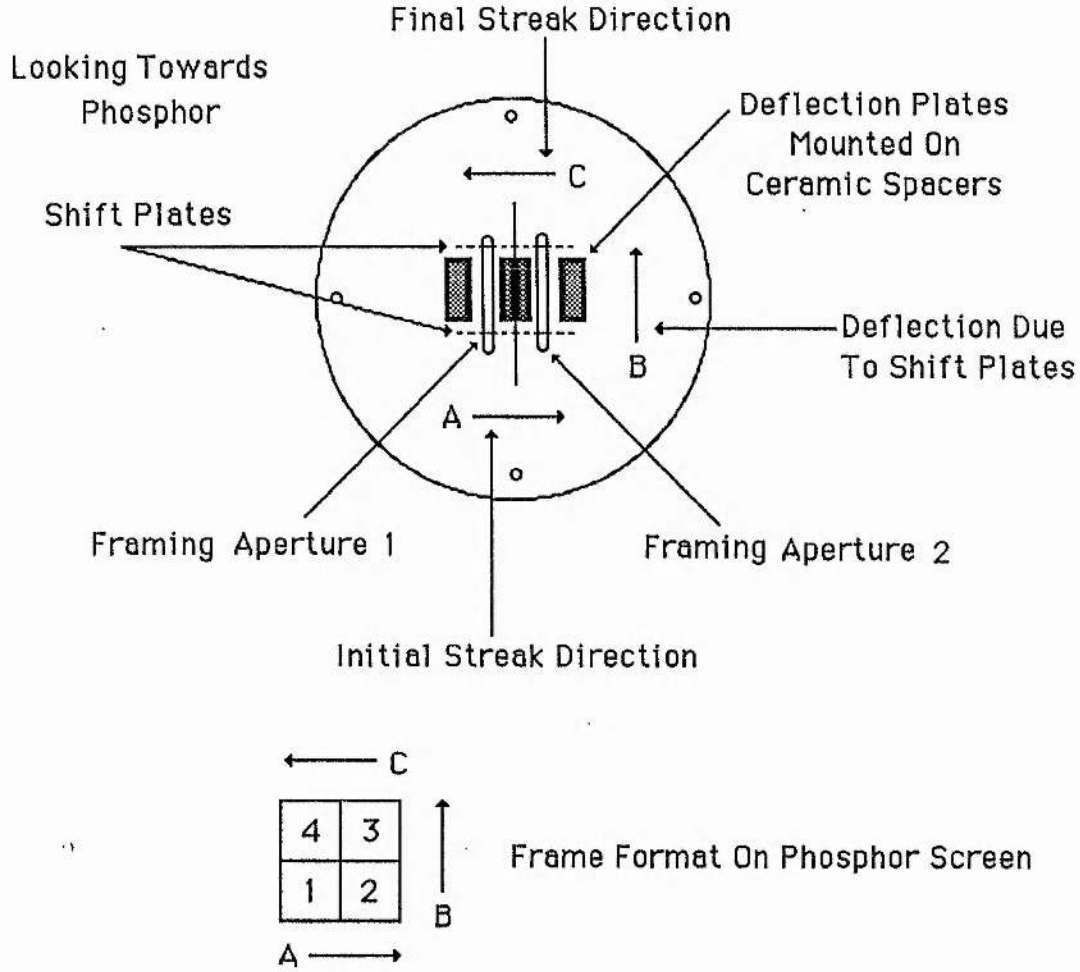

Figure 5.2. View of the framing aperture construction of the Picoframe II showing the deflection directions and resultant frame format on the phosphor screen.

The aperture which provides the first image in the sequence is defined as 'aperture 1' and the associated compensation deflectors, 'compensation 1'. This is the aperture that also defines frame four (on the trailing edge of the triangular deflection waveform). Likewise 'aperture 2' defines frames two and three. The streak direction produced by the leading edge of the triangular waveform applied to the framing plates is defined as 'A' while 'C' is the direction produced by the trailing edge. Deflection 'B' is due to the deflection produced by the shift plates. The voltages appearing at any time on the two sets of compensation plates are assumed to be independent due to the r.f. screen

employed, so the waveforms required will be considered separately. Firstly the waveforms required for 'compensation 1' will be considered. If a triangular voltage waveform is applied to the framing plates, and an identical but inverted and dephased waveform applied to the 'compensation 1' plates as in the Picoframe I double frame mode, horizontal displacement between images 1 and 4 will result as in figure 5.3.

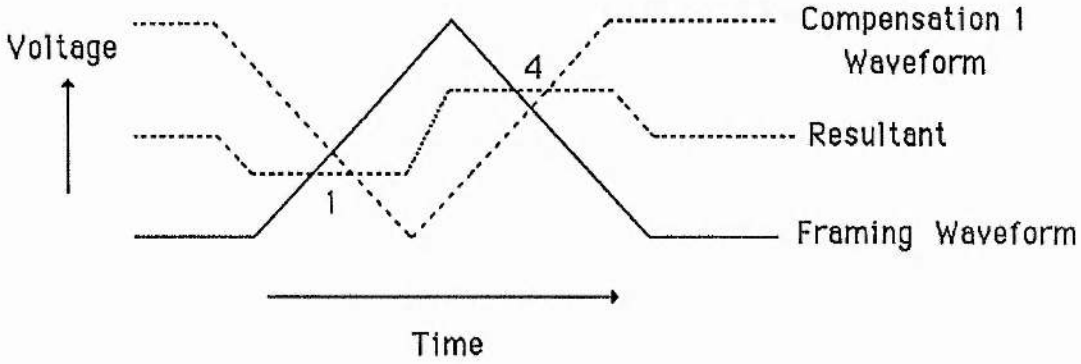

Figure 5.3 . Voltage waveform profiles achievable with the standard PFN's, taking into account of the photoelectron transit time from the framing to compensation deflectors.

Dephasing of the leading edge of the voltage profile is required in order that spatial separation of frames 1,2 may be realised, as in the double frame operation of the Picoframe II (chapter 2 section 10.4). Spatial separation of frames 1,4 is achieved using the shift plates and so displacement between these two frames due to the voltage phasing is not required. The only solution to this problem is to arrange for the leading edges to be phased correctly and then change the waveform pulse width in order to achieve the required trailing edge phasing. This technique is displayed schematically in figure 5.4.

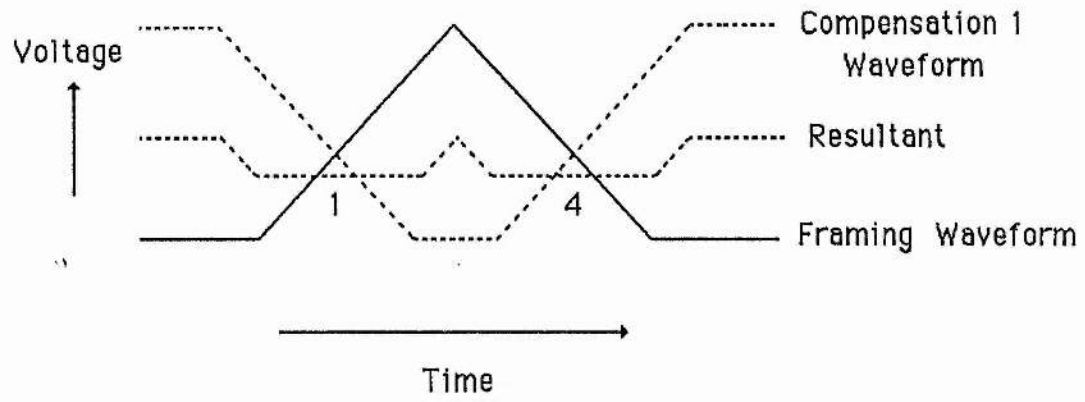

Figure 5.4. The desired voltage waveform profiles for the framing and compensation 1 deflectors to ensure correct image positioning on the phosphor screen, taking into account of the photoelectron transit time from the framing to compensation deflectors.

It can be seen that the 'compensation 1' waveform pulse width requires increasing to allow for the time required to scan the electron beam past 'aperture 2', to the apex, back past 'aperture 2' and back to 'aperture 1', thus images 1,4 are subjected to the same amount of horizontal displacement. Similarly it can be shown (figure 5.5) that the 'compensation 2' waveform pulse width requires shortening with respect to the framing waveform.

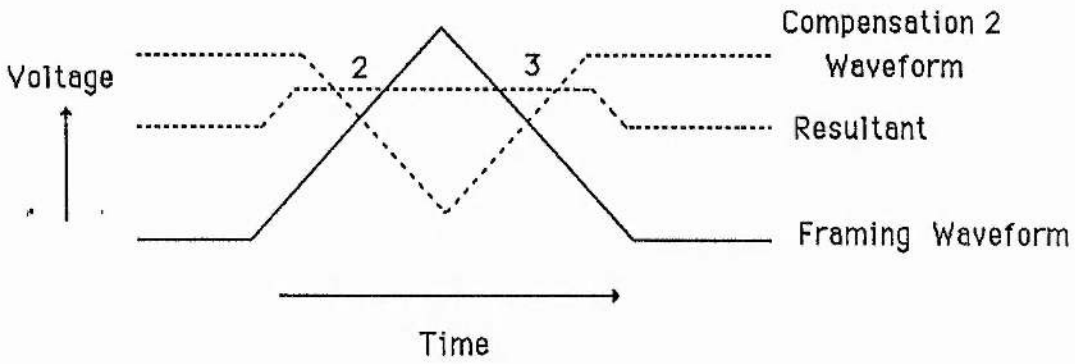

Figure 5.5. The desired voltage waveforms for the framing and compensation 2 deflectors, taking into account of the photoelectron transit time from the framing to compensation deflectors.

The amount by which the compensation 1 and 2 waveforms pulse width require increasing and reducing respectively is a function of the streak speed at the framing

apertures, the framing aperture separation, and the pulse width of the framing deflection waveform. The streak speed may be estimated to be ~7.2×10^8 from the experimental performance of the Picoframe II in the double-frame mode and the Picoframe I in single and double-frame modes. Therefore the frame time between images 1 and 2 (7mm aperture separation) was estimated to be approximately 1ns.

Given that the framing deflector waveform has FWHM duration of 2ns and the dc bias applied was half of the amplitude of the voltage pulse, then the camera timing may be deduced, as in figure 5.6.

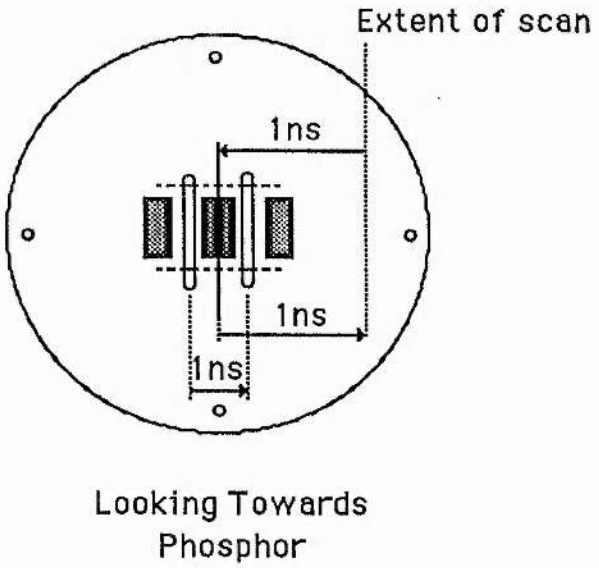

Figure 5.6. Timing of the inter-frame times expected from the Picoframe II in the four-frame operation.

Thus the waveform applied to the 'compensation 1' deflectors should be of 3ns FWHM while that applied to the 'compensation 2' deflectors be 1ns FWHM in order for the correct phasing to be achieved. A diagram showing the relative phasing of all the deflection waveforms appears as figure 5.7.

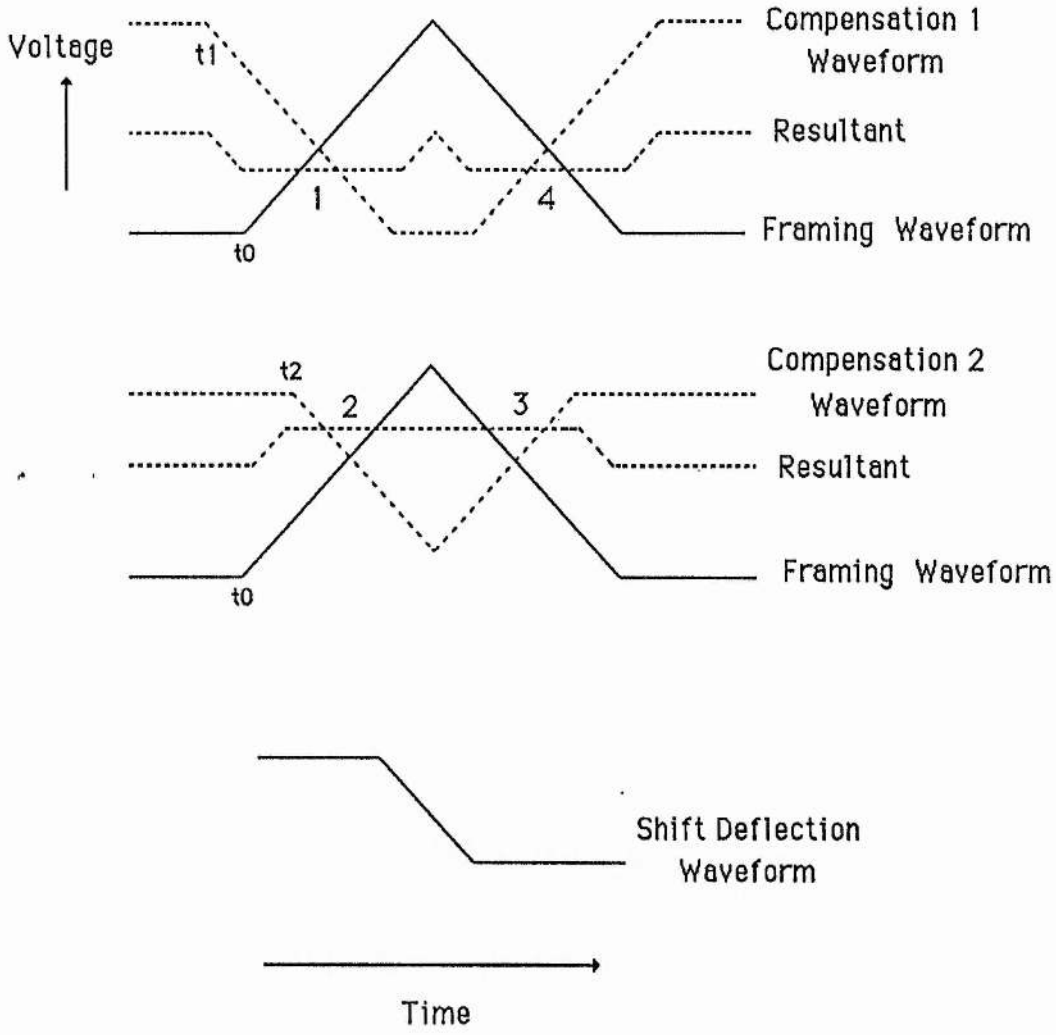

Figure 5.7. Complete voltage deflection waveform profiles for all of the deflectors of the Picoframe II in four frame operation. The trigger timing requirements are indicated by t_0, t_1, and t_2 for the deflection waveforms as shown.

The pulse widths of the waveforms generated by the PFN's are determined by the stub lengths used (chapter 2.10.1), and so the requirement for specially fabricated PFN's becomes evident. Due to the avalanche transistor circuit rise-time of 1.5ns it was not possible to produce triangular voltage pulses with a FWHM of less then this without loss of amplitude and so this was taken as the minimum pulse duration usable.

Standard 50Ω impedance co-axial cable and 'BNC' connectors were used to construct the networks, such that it was relatively easy to change the stub lengths as required. The increased losses at high frequencies associated with these connectors and cables

was not a problem for the 1.5ns rise-time waveforms employed. Care was taken over the construction of the home-made four way 'BNC' cross-pieces used, which were constructed out of four 'pcb' mounting 'BNC' sockets soldered directly to each other to ensure low losses. The three different sets of pulse forming stubs were fitted with 'BNC' plugs at either end to allow resistive, capacitive or short circuit terminations to be used. To allow correct phasing of the trailing edge of the pulses a 50Ω adjustable resistor was used to terminate one of the stubs in each of the PFN's (chapter 2.10.2). These allowed small changes to be made to the pulse width and the voltage rate of change at the trailing edge of the waveform. As dicussed within chapter 2 section 8.1, in-line 50Ω resistors were employed to control the dV/dt of the leading edge of the waveform and capacitors employed at either end of the PFN structure to remove and apply (chapter 2, section 10.1) the required dc bias (typically ±800V)

5.4 Shift Deflection Waveform Requirements

Due to the expected inter-doublet time of less than or equal to 2ns it was essential that the voltage waveform risetime applied to the shift plates be much less then this and so the standard avalanche circuits normally employed could not be used. An avalanche circuit switching -3kV in 400ps into a 50Ω load [2] was available although this unit was not ideal as only one avalanche transistor chain was employed thus producing only one negative going output which is shown as figure 5.8.

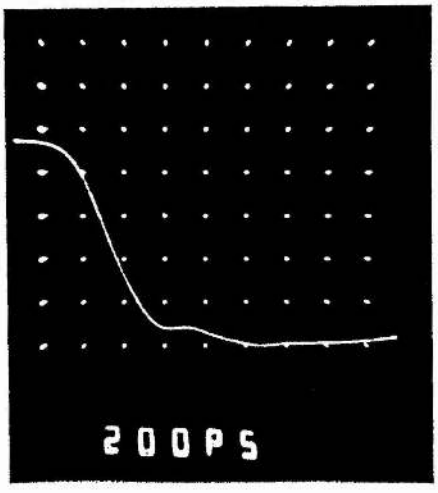

Figure 5.8. Oscillogram of the suitably attenuated output of the fast 'shift' avalanche circuit. The oscilloscope was a Thompson CSF TSN 660 with <100ps rise-time.

This meant that non-symmetrical deflection had to be employed at the shift plates, and the results of this will be discussed later (section 5.6). Due to the transit time of the electron beam through the shift deflection plates, the system possessed a finite risetime determined from the electron drift velocity and length of the shift plates which was determined to be ~500ps. Thus the deflection circuit and shift plate combination possessed a risetime of ~650ps, which limited the minimum inter-doublet time achievable with this system.

5.5 The Experimental Set Up and Results

A full diagrammatical layout of the electronics employed for the four-frame system is shown in figure 5.9

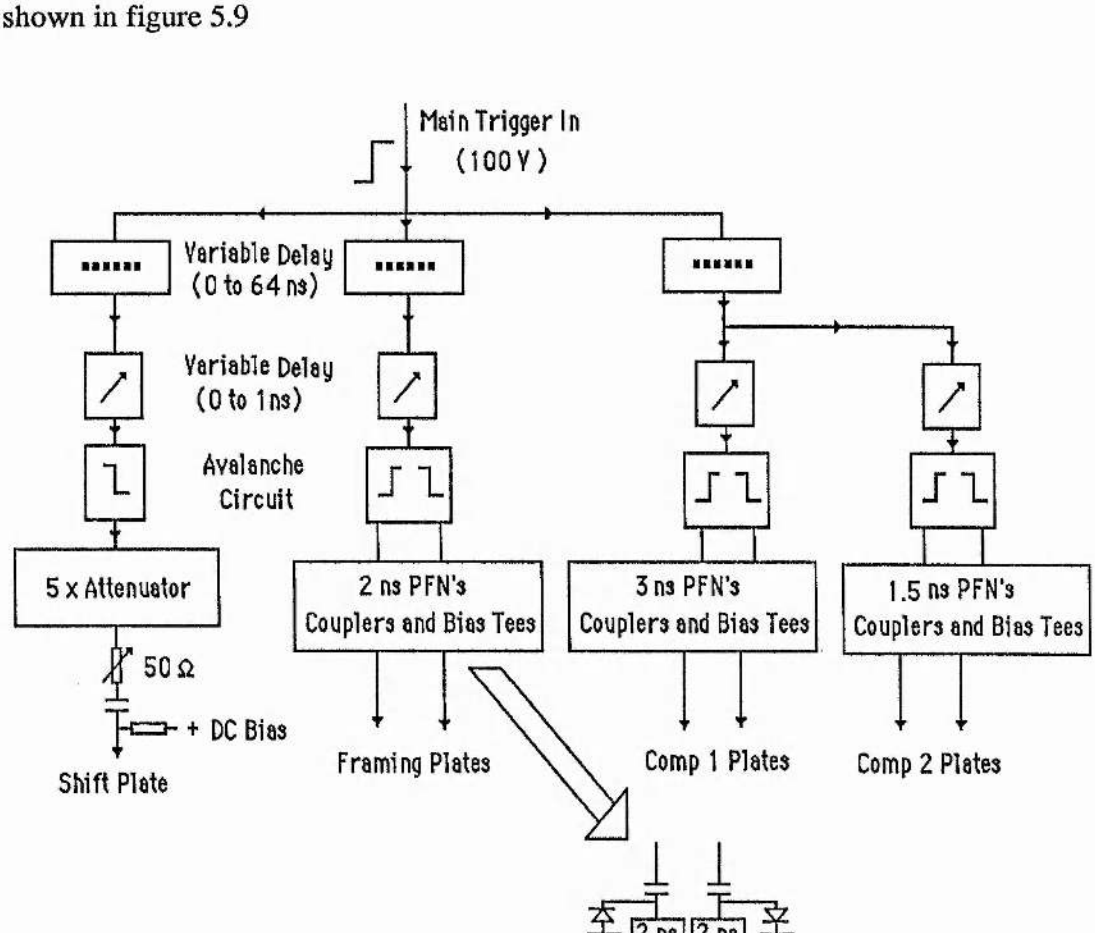

Figure 5.9. Electronic arrangement employed in the dynamic evaluation of the Picoframe II in four-frame mode.

Four optical pulses were generated from the single 60ps (FWHM) 266nm (frequency-quadrupled Q-switched and mode-locked Nd:YAG) laser pulse using a combination of a Michelson delay line and a beam-splitter delay as in figure 5.10.

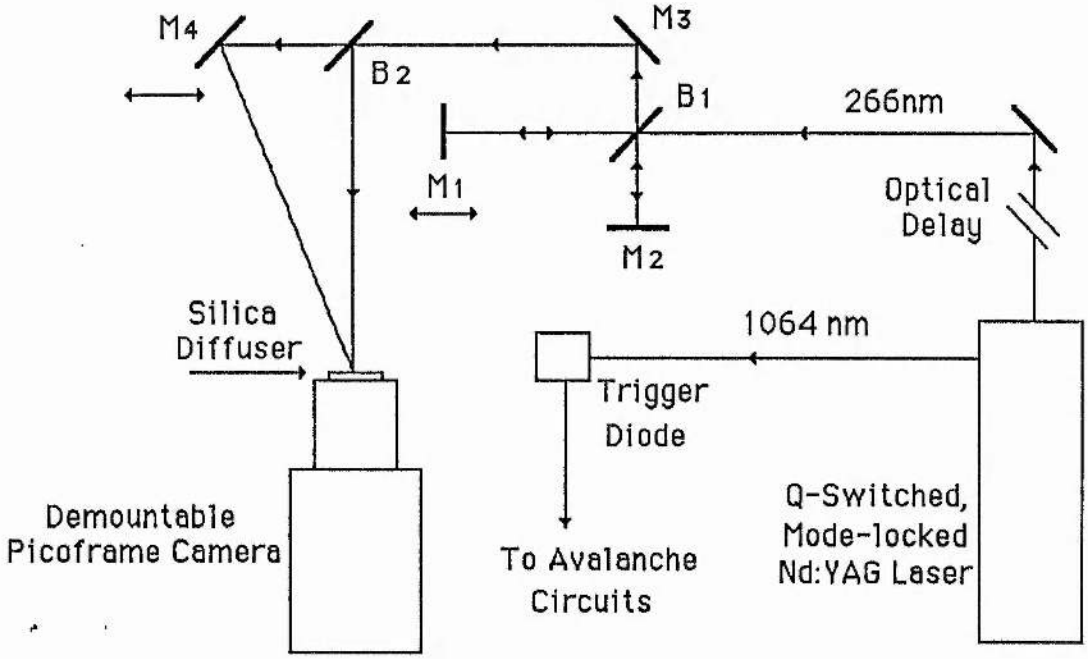

Figure 5.10. Optical set up for the evaluation of the Picoframe II in four frame mode showing the technique employed for generating four temporally separated UV pulses.

With this system it was possible to alter the temporal separation of the first and second (via M1), second and third (via B2) optical pulses independently, but the separation of the third and fourth had to be the same as the first and second. This was not a major problem as careful adjustment of the relative circuit trigger timing, deflection waveform pulse width and gradient allowed all four frames to be suitably timed. The resultant frames achieved with this technique were of a high quality and a typical four frame result is reproduced in figure 5.11. Recording of the images was achieved using Ilford HP5 film as previously described (chapter 2.7) at an intensifier gain of ~100.

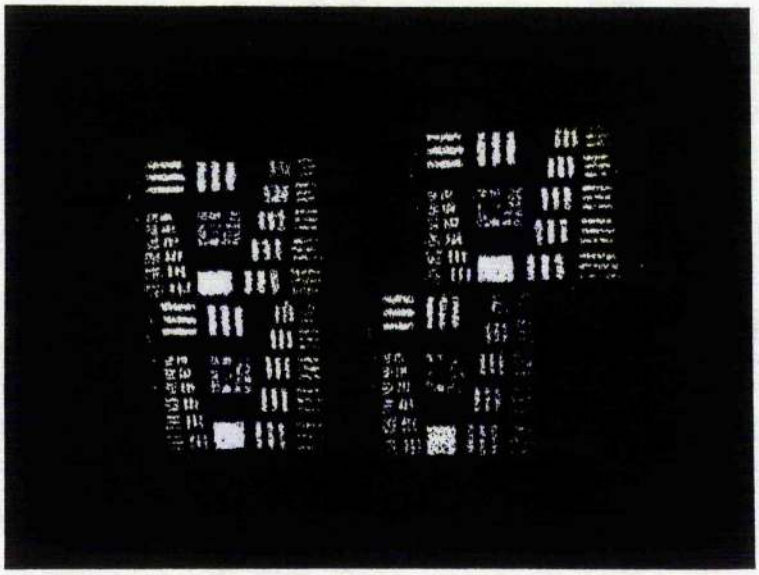

Figure 5.11. Reproduction of a typical four frame result.

The measured limiting dynamic spatial resolution for all four images is better then 7 lp/mm in the streak direction (ie. the 'vertical' resolution elements) and 6 lp/mm in the other when referred to the input photocathode. Displacement of image 3 is due to the waveform applied to the 'compensation 2' deflection plates which was non-ideal (some 500ps too wide). This did not lead to image degradation (which could be checked by altering the avalanche circuit trigger timing). The dc bias employed for the frame sequence reproduced was ± 850V to the framing and compensation deflectors. The frame time, measured as previously described (chapter 2, section 9.4) using the modified sampling scheme was determined to be 230ps FWHM. The temporal separation of frames 1 to 2 and 3 to 4 was determined from the optical delays to be 900ps while the temporal separation of frames 2 and 3 was found to be 1.2ns.

After optimisation of the system, the output of the PFN's was studied with a Tektronix (7104, <400ps rise-time oscilloscope) and suitable attenuators. The positive-going voltage pulse for the three sets of deflectors is shown as figure 5.12. Some discrepancy between the idealised waveforms is noted but this attributed to the practical operation conditions employed. The difference between the theoretically predicted waveforms required for four-frame operation, and those found after experimental optimisation are relatively small and may be attributed to the non-idealised waveforms employed. The general trend of the required voltage deflection is clear from

figure 5.12 which shows that the framing waveform has a pulse FWHM between that of the two compensation deflection waveforms as predicted.

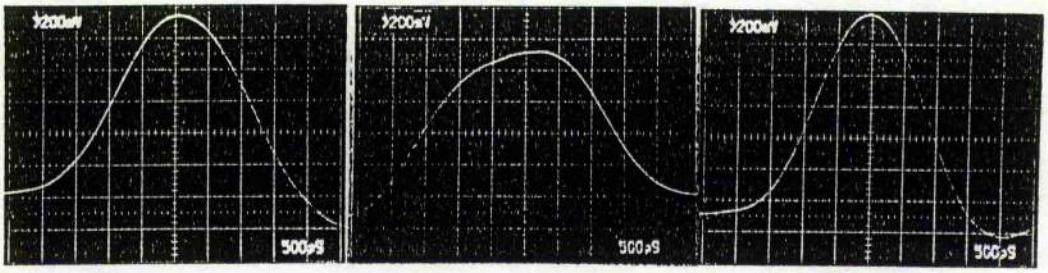

(a) (b) (c)

Figure 5.12, (a) framing, (b) compensation 1, and (c) compensation 2 positive-going deflection waveforms applied to the respective deflection plates.

The negative-going waveforms were found to be identical (but of inverse polarity) to their positive-going counterparts and so are not presented here.

5.6 Conclusions

The introduction of the shift plates and the associated deflection waveform has enabled four high quality frames to be generated with the Picoframe II demountable camera. Dynamic spatial resolution of ~7 lp/mm (when referred to the photocathode) has been achieved for all four frames with frame and inter-frame times of 230ps FWHM and ~1ns respectively. Some slight image magnification differences between frames 1,2 and 3,4 are apparent and it is also interesting to note the slight loss of dynamic spatial resolution orthogonal to the streak direction in images 3 and 4. The inter-doublet magnification difference is attributed to dynamic fringing fields as described in chapter 4, section 8, while the magnification difference between frames 1, 2 and 3, 4 is attributed to the fringing fields associated with the non-symetrical deflection employed at the shift plates. This was confirmed by blocking the optical pulses for frames 1 and 2 while maintaining the shift deflectors at anode potential. In this way it was also confirmed that the loss of 'vertical' dynamic spatial resolution was

due to voltage perturbations on the plateau of the shift deflector avalanche circuit as shown in figure 5.8. When these problems are rectified it is confidently expected that 4 frames with a dynamic spatial resolution of 8 lp/mm in both directions could be generated with UV illumination.

The operation of the camera system under soft X-ray illumination conditions is expected to give reduced dynamic spatial resolution for the reasons outlined in chapter 3, section 7. Although insufficient time was available to evaluate the camera under X-ray illumination conditions, from previous work (chapters 3 and 4) the resolution may be expected to be ~4 lp/mm to 5 lp/mm (referred to the photocathode) when employing a simple gold photocathode.

References for Chapter 5

1 R T Eagles, W Sibbett, W E Sleat

Optics Comm., 57 (6), 423, 1986

2 Kentech Instruments Ltd., Blackett Labs., Prince Consourt Rd., London, SW7 2BZ

Chapter 6

Repetitive Operation Of The Picoframe I Framing Camera

6.1 Introduction

In order to produce multiple frames with the Picoframe I camera, the generation of periodic, kilovolt voltage waveforms is required. As previously described (section 2.10) a triangular voltage waveform may be generated using pulse forming networks and a voltage step input. This technique has the disadvantage that the amplitude of the voltage pulse generated is reduced to one half or less of the total voltage switched by the electronic circuit employed, and is thus not suitable for the generation of multiple waveforms. Other pulse forming networks have been tried in conjunction with the framing camera (eg. Blumlein networks and various shorted stub configurations) but have proved unsuitable for one reason or another, or offer little advantage in performance. At present then, the practical limit to the number of frames achievable with the Picoframe camera design is 2 with the Picoframe I (chapter 2.10), or 4 with the Picoframe II variant (chapter 4) due to the difficulties encountered in producing suitable voltage waveforms.

Another approach to the generation of multiple frames may be to operate the framing camera in a 'continuous scanning mode' in which the electron beam is continuously scanned across the framing aperture, and to shutter the image tube itself when framing is not desired. In this way, resonant deflection techniques may be employed (as in the synchroscan streak camera, section 1.10), generating high deflection voltages for only moderate input power. Either the cathode or the mesh of the image tube could be suitably pulse biased to prevent any photoelectrons reaching the phosphor screen when not desired and so preventing the overwriting of images.

6.2 Repetitive Framing Technique

If a suitable sinusoidal waveform is applied to the framing deflectors and an inverted waveform of equal magnitude is applied to the compensation deflectors, then framing may be achieved [1], as shown schematically in figure 6.1 and as demonstrated by the Imacon 790 framing camera [2]. With this technique the frame exposure time (T)

is defined by the time required to scan the electron beam across the aperture, corresponding to a framing deflection voltage of $2xV_{aperture}$. The Imacon 790 type of framing camera suffers from poor dynamic spatial resolution (~5 lp/mm) at the maximum framing rate and because of the modest deflection frequencies employed (25 MHz) its frame exposure and inter-frame times are long (4ns and 20ns respectively).

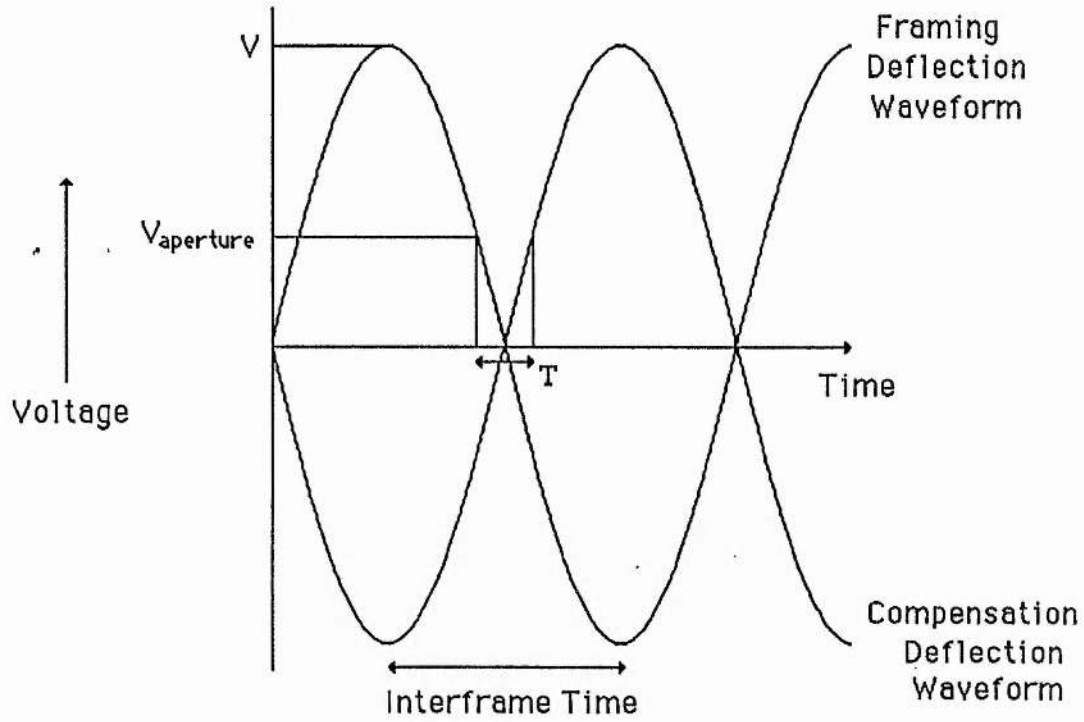

Figure 6.1 Deflection waveforms for the single frame operation of the framing camera with sinusoidal deflection voltages. $V_{aperture}$ is the deflection voltage applied to the framing deflectors in order to scan the photoelectron beam from the aperture centre to the edge. The resultant frame duration is T.

6.2.1 Single Frame Operation

For framing to be achieved it is only required for the voltage waveform to have sufficient amplitude so that the imaging photoelectrons are swept completely across the framing aperture by the framing deflectors. The waveform linearity is not of concern if the waveform applied to the framing and compensation deflectors is exactly π out of phase with each other, as the summation of the deflections experienced by the electron beam will always be zero, hence the image will remain fully compensated if the

deflection sensitivities of both sets of deflectors is equal. It may be seen that the frame-time is defined by the streak speed of the photoelectron beam at the framing aperture and the aperture diameter, while the inter-frame time is dependent upon the frequency of the applied waveform only.

6.2.2 Double Frame Operation

If the phase relationship between the two applied waveforms is not exactly π then frame doublets may be generated as in figure 6.2 which shows how a frame can be generated on each rising and falling edge.

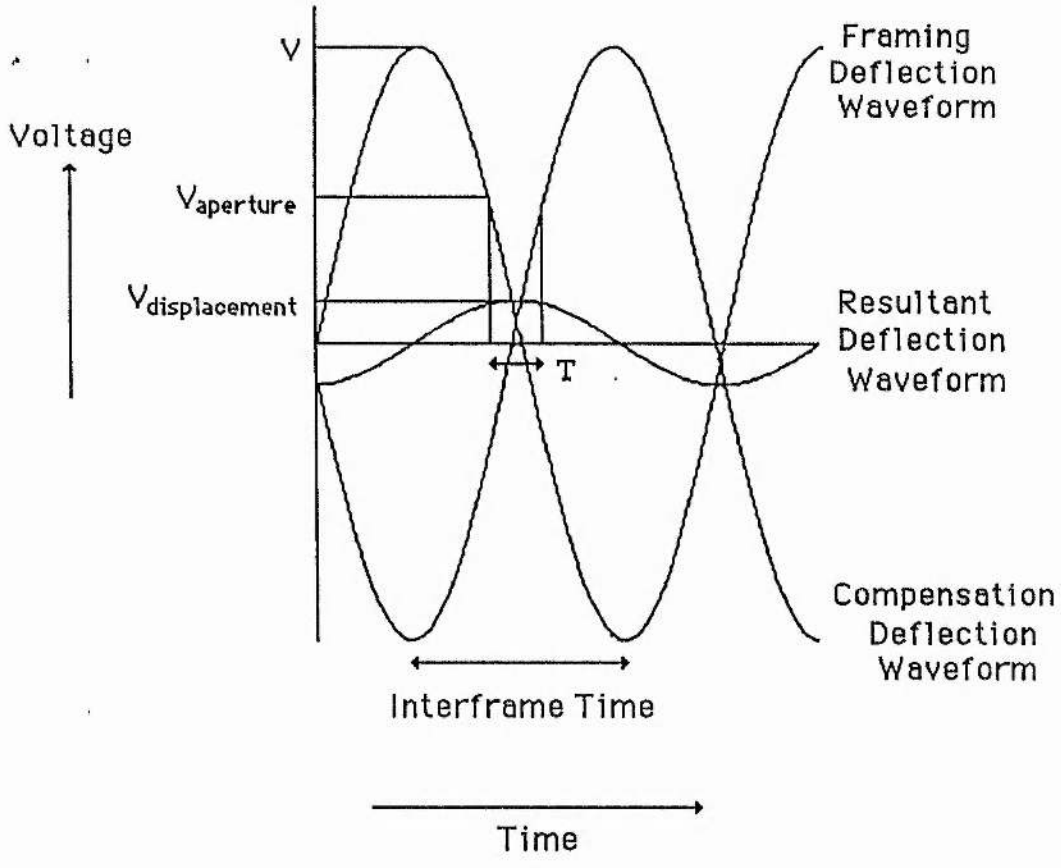

Figure 6.2 Phase relationship required between the framing and compensation deflection waveforms and the resultant deflection voltage experienced by the electron beam. $V_{displacement}$ corresponds to the effective dc deflection voltage amplitude the photoelectron beam experiences at the phosphor screen.

Spatial separation of the frames occurs due to the phase relationship between the two

waveforms and hence a separate frame is generated every half period of the applied deflection waveform. However, for this system to operate successfully, the amplitude of the waveforms (V) must be such that the region of interest (where the voltage waveform crosses 0V) should be linear. If this is ensured then the plateau of the resultant deflection experienced by the photoelectron beam will be pseudo- 'flat', hence compensation of the image smear will be achieved.

6.2.3 Requirements for the Deflection Waveforms

Given that the image size on the phosphor screen of the framing camera is s mm x s mm, the maximum relative displacement of the images must be s mm to prevent overlapping. Thus the resultant deflection due to the framing and compensation deflectors is sinusoidal with time (neglecting electron transit time effects) with an amplitude s/2 and frequency f_0 defined by the operating frequency as shown in figure 6.3 in order that spatial separation of the two images occurs.

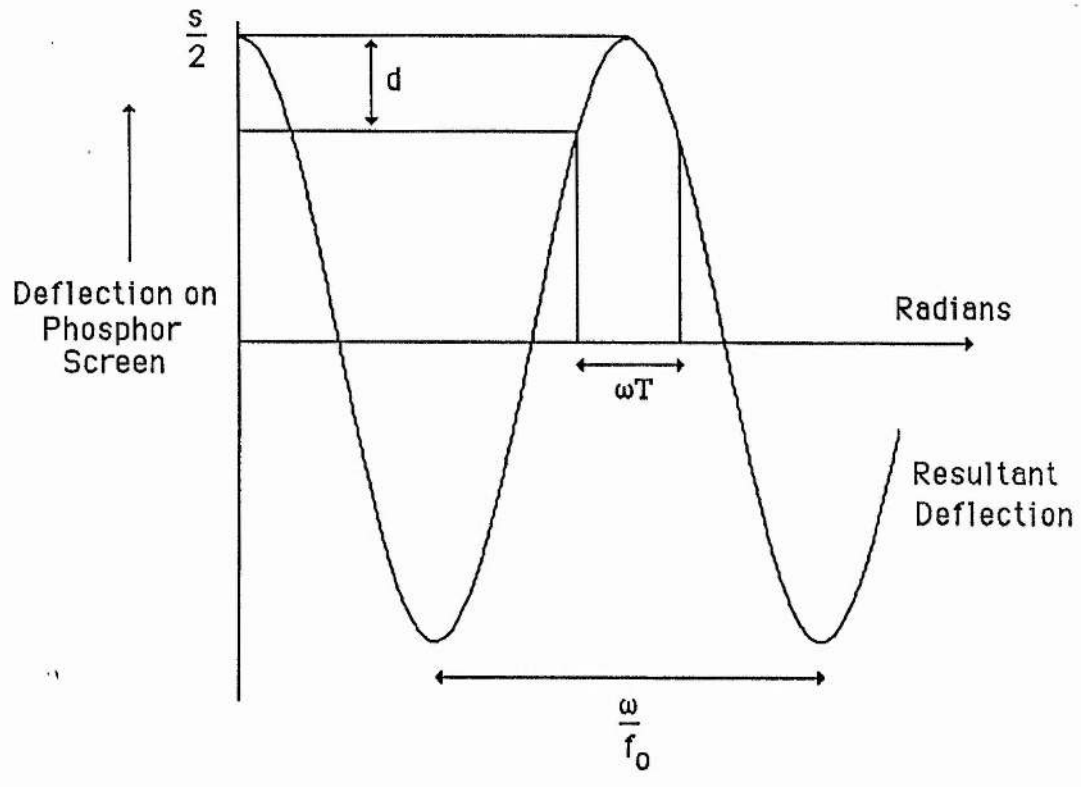

Figure 6.3 Resultant deflection of the photoelectron beam due to the framing and compensation deflection waveforms. T is the frame exposure duration, s is the image centre separation at the phosphor screen.

The displacement experienced by the image (at the phosphor screen) during exposure (defined as d) must be sufficiently small in order that the required resolution is maintained otherwise image blur will result and hence loss of dynamic spatial resolution. In order for 10 lp/mm to be resolved at the photocathode we require a resolution of 6.67 lp/mm at the phosphor screen of the framing image tube (given that the electron-optical magnification of the framing image tube is -1.5), ie. a point resolution of 75μm or less. Thus the resultant image on the phosphor screen must not move by more then 75μm during the exposure time, thus $d < 75\mu m$.
For a required resolution then, equation 6.1 may be deduced.

$$T = \frac{2}{\omega} \cos^{-1} \left(1 - \frac{2d}{s} \right) \qquad (6.1)$$

where T is the frame exposure time and ω is the angular frequency of operation. Given the deflection sensitivity of the framing deflectors to the framing aperture, S and the framing aperture diameter F it is possible to derive the deflection voltage amplitude required (V) in order to provide the required resolution, as given in equation 6.2.

$$V = \frac{F}{2 S \sin \left(\frac{\omega T}{2} \right)} \qquad (6.2)$$

Hence on substituting for T from equation 6.2 the deflection voltage amplitude required is defined in equation 6.3.

$$V = \frac{F}{2 S \sin \left[\cos^{-1} \left(1 - \frac{2 d}{s} \right) \right]} \qquad (6.3)$$

Substituting the relevant values for the Picoframe I type framing camera (F = 1.8 mm, d = 75μm, s = 6mm and S = 0.432 cm/kV) we arrive at the result in equation 6.4.

$$V = 937 \text{ Volts} \qquad (6.4)$$

Hence when using symmetrical deflection, the voltage amplitude required to maintain 10 lp/mm spatial resolution at the photocathode is ±468 Volts. These calculations neglect electron transit time effects within the deflectors, deflector fringing fields and finite electron beam diameter at the framing aperture which are all assumed to be negligible, but nevertheless the results indicate the feasibility of the technique. In fact these voltage amplitudes may easily be achieved when incorporating the deflection plates within an r.f. resonant circuit as employed in synchroscan streak cameras. Using this repetitive waveform technique in conjunction with the framing camera it is possible at least in principle to generate multiple frames whose frame-time is governed by the voltage waveform amplitude and frequency for a given image tube geometry, and whose inter-frame time is governed by the frequency alone. In order to generate frames with a minimum inter-frame time it is necessary to use the highest deflection frequency possible, where an upper limit is set by two main factors which are (i) the ability to incorporate the deflection plates into a suitably high frequency resonant circuit and (ii) the frequency response of the deflection plates themselves due to the electron transit time of the photoelectrons through the deflection region.

6.3 The resonant Circuit

A resonant circuit is easily constructed using a capacitor / inductor network as shown schematically in figure 6.4

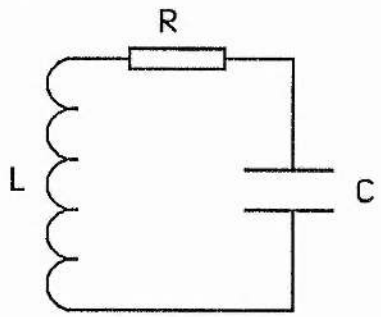

Figure 6.4. A simple parallel tuned circuit.

The resonant frequency of such a circuit with inductance L and capacitance C may be approximated to equation 6.5.

$$F_0 = \frac{1}{2\pi\sqrt{LC}} \qquad (6.5)$$

Given that the capacitance of the deflectors may be calculated as ~1pF then it it necessary to chose an inductance which will bring the circuit into resonance at the required frequency using equation 6.5. At frequencies >500MHz the required inductance becomes too small to handle conveniently (<100nF) and parasitic reactances become comparable in magnitude, hence the operation of a simple resonant circuit above this frequency becomes difficult.

6.3.1 The 'Quality' Factor

Another factor to be considered is the Q (or 'quality factor') of the circuit which is defined as

$$Q = \frac{2\,\pi \text{ x Average Energy Stored}}{\text{Average Energy Absorbed Per Cycle}} = \frac{1}{R}\sqrt{\frac{L}{C}} \qquad (6.6)$$

and

$$Q = \frac{F_0}{F_2 - F_1} \qquad (6.7)$$

where F_2, F_1 are the frequencies at which the deflection voltage has reached 0.707 of the resonant voltage developed at F_0 for the same input power and R is the effective circuit resistance. Energy is lost from the system in two main ways; (i) at high frequencies the resistance of all conductors is increased due to the 'skin effect' [3] and (ii) radio frequency discharges called multipacting may occur which will be discussed in section 6.6.1.

Relating Q to the voltage amplitude developed across the capacitor (deflectors), it may be seen that V is proportional to the square root of the circuit Q, and so as the circuit resonance bandwidth decreases the deflection voltage increases for a given power input. It may be seen that a high Q is desirable from the viewpoint of maximum deflection, but high Q circuits are difficult to keep in resonance (principally due to the effects of resistive heating), are easily effected by external influences and are very susceptible to alterations in the excitation frequency although the circuit Q is usually

limited by practical constraints to less than 100.

6.3.1.1 The Deflection Plate Bandwidth

The simple parallel plate deflection plates employed in most streak cameras have a deflection frequency response which is defined by their length and the electron drift velocity. This response is due to the fact that as the deflection frequency is increased, the transit time of the electron through the deflection plates becomes comparable to the radio frequency (r.f.) period of oscillation and thus the electron beam experiences a varying deflection field with time. The dynamic deflection sensitivity may be calculated analytically (neglecting the effects of fringing fields [4]) and their bandwidth is defined as the frequency at which the electron beam deflection amplitude is reduced to 0.707 of the maximum. A full explanation of this phenomena may be found elsewhere [5] and it is of interest to note that the deflection geometry employed in streak and framing cameras is usually >300MHz, although the dynamic spatial resolution may be adversely effected by fringing field effects before this value is reached.

It has been found that the operation of synchroscan streak cameras may be achieved at repetition frequencies of up to 300MHz before the system losses become too high and it was therefore chosen as an operating frequency to demonstrate the synchroscan framing technique. At this frequency the inter-frame time would be 1.7ns which is comparable to the double frame operation of the Picoframe I camera when using the avalanche transistor / pulse forming network combination (section 2.10). For convenience the sealed off visible-sensitive (S20 cathode) Picoframe I camera [6,7] was used to evaluate the performance of the synchroscan framing technique.

6.4 Construction of the Resonant Circuit

The circuit was formed by connecting an r.f. inductive loop across the terminals of the deflection plates. The loop length was chosen so that the radiation wavelength was $\lambda_0/8$ as shown in figure 6.5 where λ_0 is the radiation wavelength in free space.

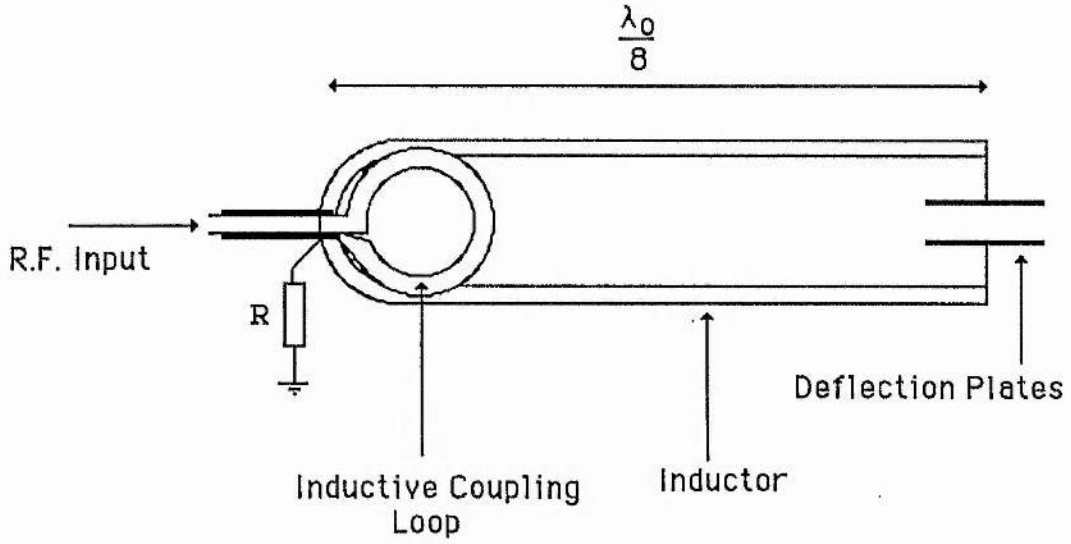

Figure 6.5. The experimental resonant circuit.

Although the intended loop length was 12.5 cm at 300MHz, consideration of the feed-through wires from the tube envelope to the deflection plates resulted in a loop length of ~9cm. A loop width of ~1cm brought the system into resonance at ~300MHz tuning was achieved by altering the loop inductance (ie separation of the parallel wires [8]). The loop was constructed out of tinned copper wire (16 SWG) and connections to the image tube were achieved with Selectro sockets [9]. Power was fed into the circuit by inductive coupling of the r.f signal via a single loop of wire intimately positioned near the resonant loop. The resistor R (typically 1MΩ) connected to the centre of the resonant circuit inductor was included to provide a dc path to ground for the deflection plates, which may become electrostatically charged due to photoelectrons impinging upon them. The resistor has little effect on the resonant circuit if the inductor loop length is correct, as this centre point will remain at 0 Volts when the circuit is in resonance. The measured Q of the resonant circuit was ~60 (using equation 6.7) and the deflection voltage amplitude was measured to be ±550V applied to each deflection plate at an input power of ~15W.

6.5 Experimental Evaluation

Two such resonant circuits were required, one for each of the compensation and framing deflectors in order that the phase between them could be adjusted independently. Cross-coupling of the two resonant circuits was prevented by the use of

a r.f. screen. A schematic diagram of the circuits and camera and r.f feed-in is shown in figure 6.6.

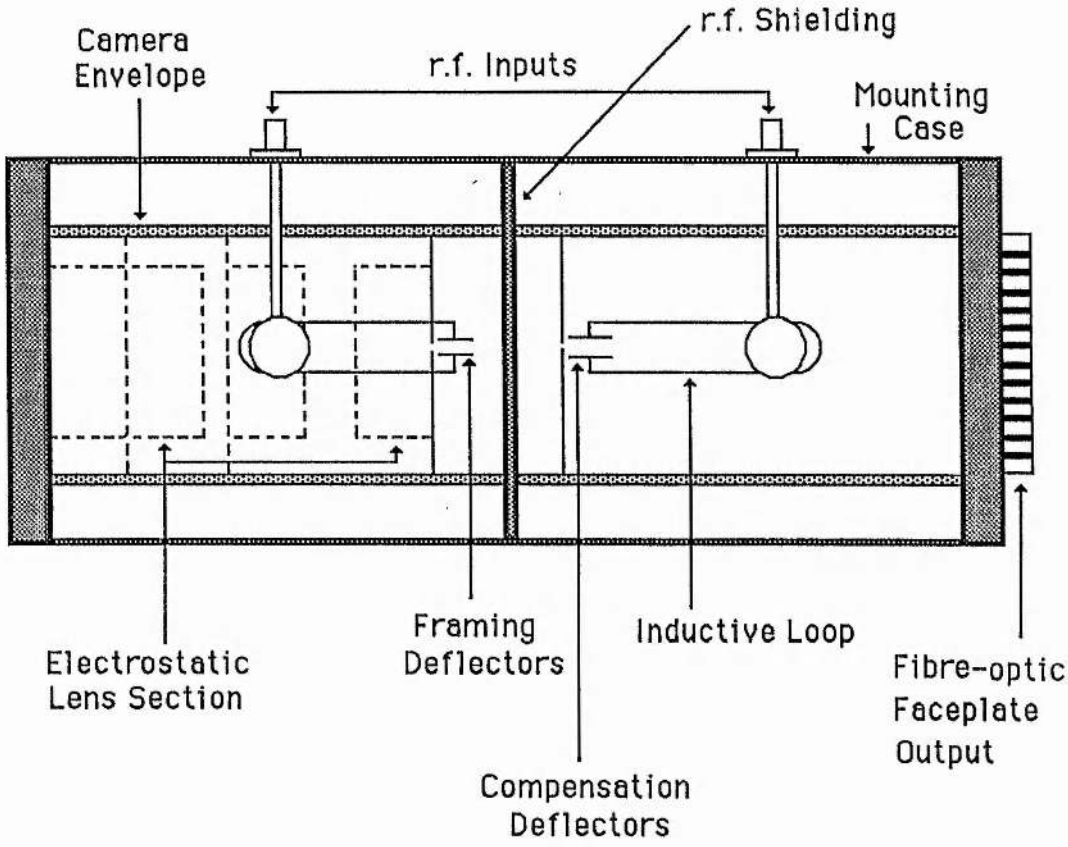

Figure 6.6 showing the Picoframe camera mounting and r.f. details.

6.5.1 The Laser System

In order to evaluate the frame exposure time an actively mode-locked c.w frequency-doubled (using an angle tuned KTP crystal), Nd:YAG laser (Control Laser series 500 with Spectra Physics 342A acousto-optic mode-locker) was employed to provide optical pulses of ~70ps FWHM at 532nm. The laser had a cavity round-trip time of 12ns resulting in a pulse train repetition rate of 83.33MHz. If a fast PIN photodetector is used to monitor such a pulse train then the output consists of Fourier components separated by 83.33MHz. Electronic filtration and subsequent amplification of the third-harmonic (333MHz) may then be used as the deflection reference frequency for the camera as this will ensure phase-locking between the laser pulses and camera (providing the pulse-to-pulse jitter of the laser output and phase noise introduced by the

electronic components may be neglected [10]). Small adjustments to the inductive loop length and inductance readily allowed the resonant circuit to be brought into resonance at this frequency.

6.5.2 Experimental Arrangement

In order to realise an independently variable phase between the framing and compensation waveforms, the 333MHz signal was split and amplified up to 20W by two independent power amplifiers. The incorporation of a variable transmission line delay in the input to one of the amplifiers allows the relative phasing to be altered and figure 6.7 shows a schematic diagram of the electronic arrangement employed. The photodetector was a PIN diode (Telefunken BPW 28) with a ~1.5GHz bandwidth. The interdigital [11] and Cam filter [12] combination provided good harmonic rejection while the amplitude limiter (based on the 560C broadband r.f. amplifier) has been described in detail elsewhere [13]. The variable delays (Tektronix part number 119-0321-02) employed were of the transmission line type and the preamplifiers were TRW [14] CA2820 wide band hybrid amplifiers providing a gain of 30dB and bandwidth of 1MHz to 520 MHz. The power amplifiers were retuned 432MHz tuned amplifiers (Microwave Modules Ltd, type MML 432/100) capable of providing 30W at 333MHz.

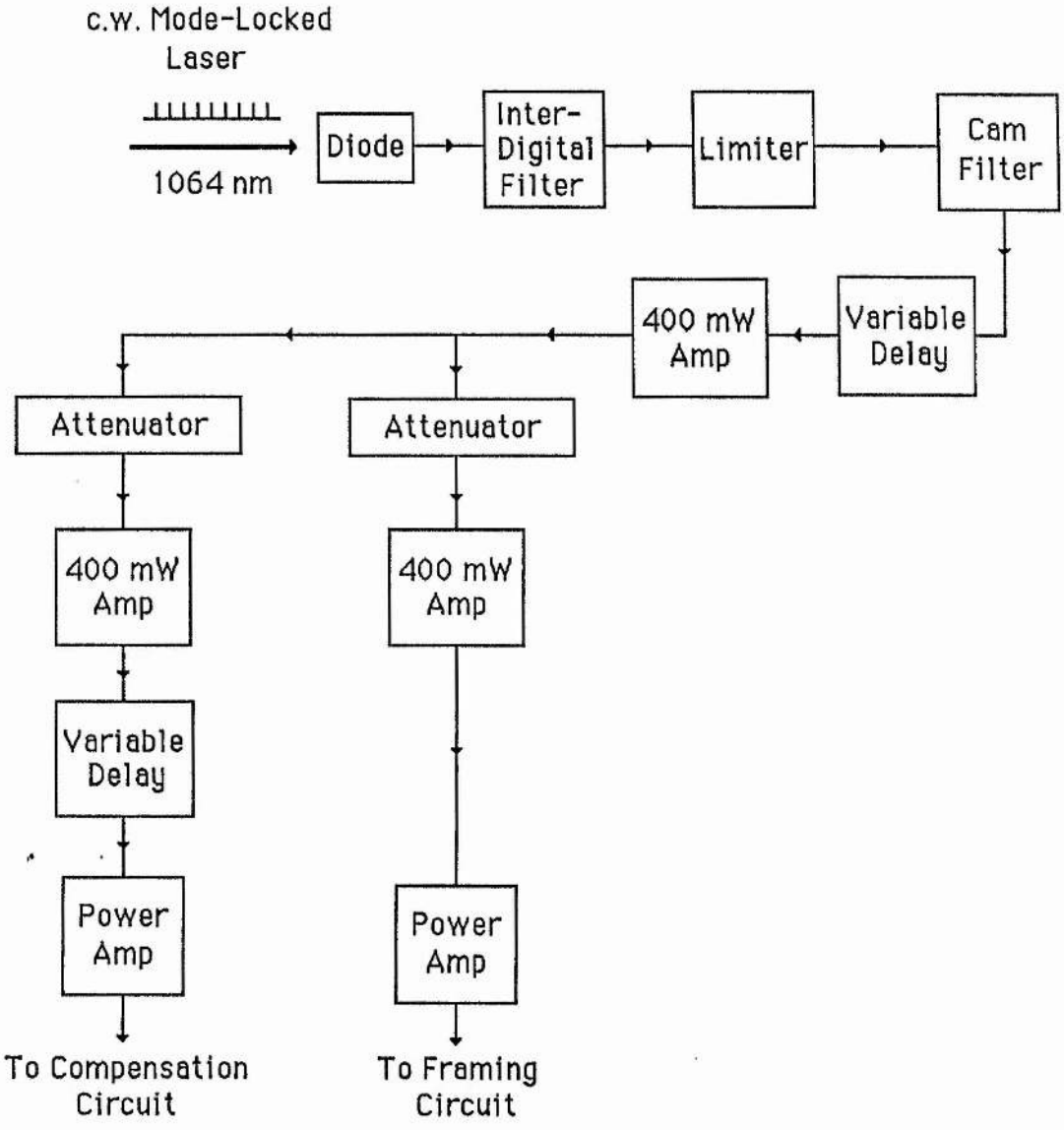

Figure 6.7 detailing the electronic components employed for the 'synchroscan' framing technique.

Each optical pulse from the laser was split into two with the use of a Michelson type delay line (giving a temporal separation of 1.5ns corresponding to the inter-frame time at the operation frequency of 333MHz) and directed onto the camera photocathode via a diffuser, USAF test chart and imaging lens (-2/3 magnification). Although it was not essential to use an image intensifier due to the large number of frames that were integrated in the camera phosphor screen it did allow convenient 'shuttering' of the system. A Mullard XX1330A image intensifier was employed which was fibre-optically coupled to the output screen of the framing image tube. Ilford HP5 film was placed in intimate contact with the output fibre-optic faceplate of the MCP image

intensifier which was gated on for 200μs to allow an image to be recorded. Figure 6.8 shows the experimental arrangement employed.

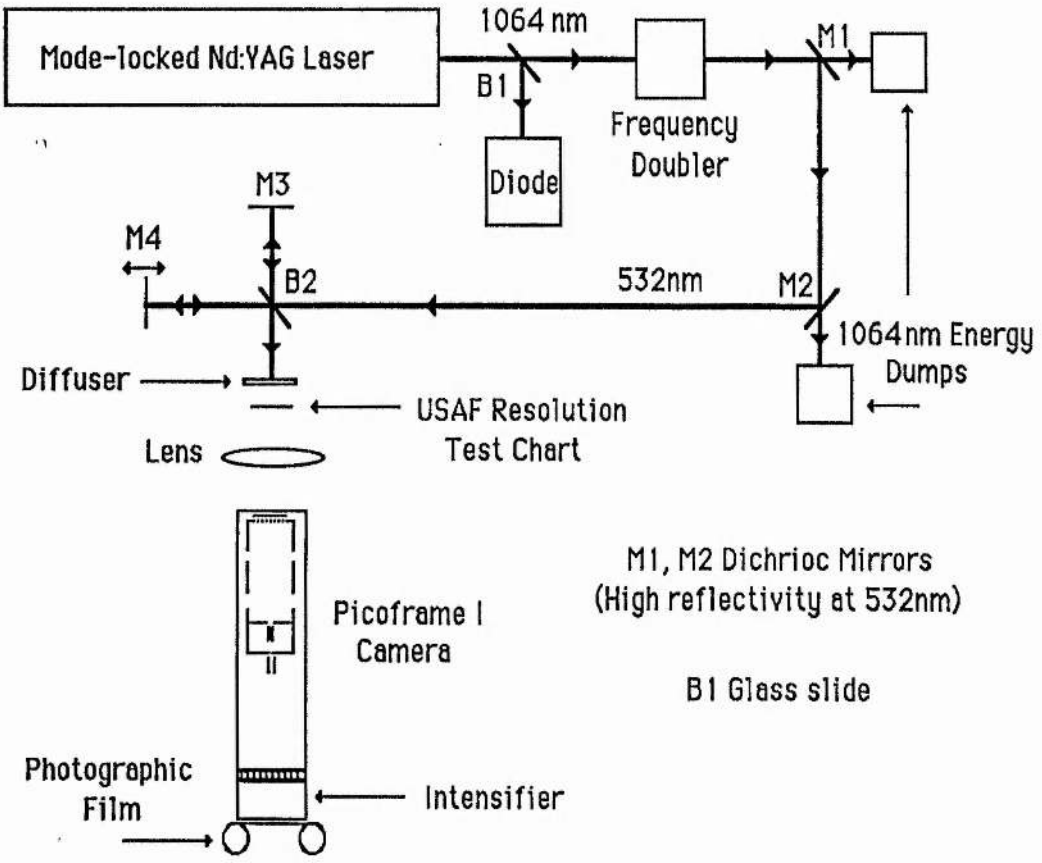

Figure 6.8 Experimental arrangement.

The camera input intensity was attenuated until correctly exposed images were obtained when the film was processed for a rating of 800ASA and image intensifier gains of ~50 were used. Single and doublet images were easily achieved and a reproduction of a double frame result is shown as figure 6.9.

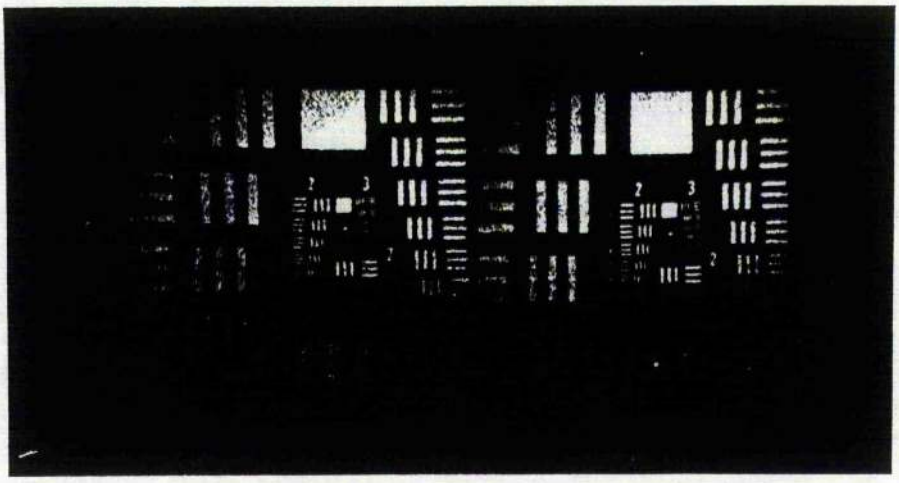

Figure 6.9. Reproduction of a typical double frame recording using the 'synchroscan' technique. The dynamic spatial resolution for both frames is better then 12 lp/mm when referred to the photocathode.

The dynamic spatial resolution of the recorded frames was >12 lp/mm for images in single or double frame mode of operation. The exposure time of the frames was evaluated using the sampling scheme previously described (section 2.9.4) and confirmed using a calibrated optical delay technique similar to that employed by Eagles [15]. This technique involved a two stage process. Firstly the USAF resolution test chart and input optics were removed and the photocathode illuminated while maintaining all deflection plates at anode potential. The corresponding circular image (which was imaged onto an OMA) then defines the spatial extent the photoelectrons may deviate from the camera axis while still going through both apertures. The second stage was to replace the input optics but image a narrow slit onto the cathode instead of the USAF chart. The compensation deflectors were maintained at anode potential and the framing deflectors resonantly driven under the same conditions as when framing. This then streaked the slit image which was illuminated by the 532nm pulse train via a calibrated 200ps Michelson type optical delay line and the corresponding image was recorded using an OMA. Comparison of the two images then provides the frame exposure time of the camera under these conditions. A reproduction of the streak and static intensity profiles is included as figure 6.10. Identical frame exposure times for both images in the double frame mode of operation was evident and only one streak

image is reproduced.

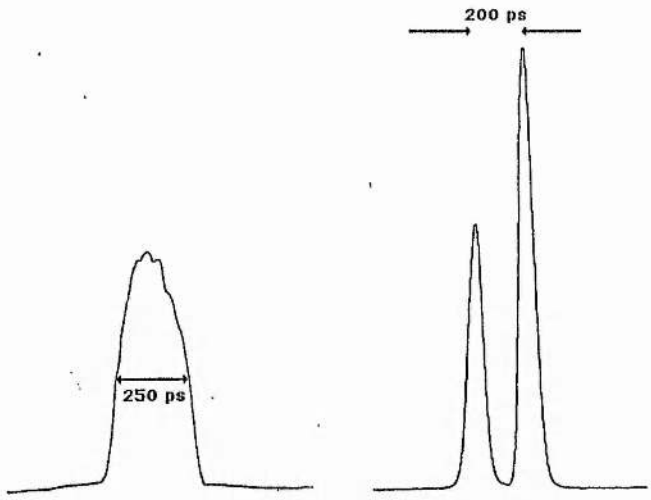

Figure 6.10 Static (left) and streak intensity profiles (right) for one of the frames.

Frame exposure times of 250ps FWHM were obtained with both techniques while the inter-frame time of 1.5ns was confirmed by measuring the optical delay introduced by the Michelson delay system. The calculated frame exposure time from equation 6.1 under the indicated conditions was 237ps, showing good agreement with the experimental results.

6.6 Discussion

The 'synchroscan' framing technique has demonstrated the ability to provide good image quality and more importantly, reproducibility. The stability of the system was such that good quality frames were generated when the system was switched on even after several days when it was unused. The resultant images have a good signal-to-noise ratio, due to the overlaying of many frames (~$6x10^4$ for a 200 μs gating period) which both improves the signal-to-noise ratio and reduces the space-charge effects within the image tube (section 1.2.1), it is to be acknowledged of course that when operated in true framing mode (by progressively deflecting the electron beam orthogonally to the streak direction using shift plates {section 5.1}) this would not be the case. It was not possible to operate the camera in this mode due to the absence of shift plates within the sealed off image tube. The system as described suffers from three major problems when operating with a single-shot pulsed laser (eg. in laser-produced

plasma experiments) viz. (i) the difficulty in phase-locking the sinusoidal waveforms to a single shot-event, (ii) the inability to reduce the inter-frame time significantly due to the difficulty in constructing a high Q, high frequency deflector / resonant circuit and (iii) multipacting within the camera envelope (see section 6.6.1).

The ability to phase-lock the r.f. signal to a single event is a problem of available electronics and is believed to be surmountable given sufficient attention. In the case of actively mode-locked [16] laser oscillator, the reference may be derived from the r.f applied to the mode-locker. The deflection geometry used at present does not easily lend itself to the incorporation within a high frequency resonator due to the parasitic effects. A solution to this problem may be to use a microwave cavity deflection device, which will be discussed in more detail in section 6.6.2.

6.6.1 Multipacting

At moderate r.f. fields, a discharge may be set up within a high vacuum system. This discharge is called multipacting. Although little damage appears to be done to the camera tube itself, the multipacting absorbs energy from the r.f resonator and so reduces the Q, hence reducing the deflection voltage attainable for a given input power. It usually appears as a glow discharge in the deflection region, and it is believed that this is due to impact ionisation of trace elements within camera envelope by the energetic electrons. This phenomena has been studied in some detail [17, 18] and so only a brief outline of its origin will be given here. If an ion or electron appears within a high electrostatic field region it will be accelerated, and will impinge upon one of the electrodes as shown in figure 6.11 (a).

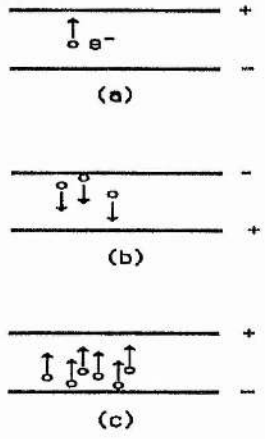

Figure 6.11 Development of multipacting effects.

Upon impact, if conditions are favourable (ie the impact energy is higher then the secondary emission number of the material), further electrons may be emitted due to the impact ionisation. If by this time the electric field polarity has reversed (b) then the emitted electrons may be accelerated and strike the other electrode, causing the release of further electrons (c). These oscillations may build up given that the frequency and plate separation are favourable as well as the electron energies and the secondary electron emission coefficients of the electrodes. Due to the geometry, frequency and the power levels employed in streak cameras this problem can be severe, resulting in direct excitation of the photocathode or phosphor screen in extreme cases. During the course of this work it was in fact confirmed that multipacting can only occur between the deflection plates at low power (<1 W of drive r.f.) [17] and is usually predominant between the back of the deflection plates and other surrounding structures. Application of a D.C. bias to the deflectors (~-200V with respect to the anode) was employed in the evaluation of the Picoframe I to remove any excited electrons from the deflection region but this results in image degradation, and so either careful mechanical design (electrodes positioned so that multipacting is not possible at the desired frequency of operation and the voltages employed) or special processing techniques [18] are preferred solutions to this problem.

6.7 The Microwave Cavity

In order to improve resonant isolation from outside effects, increase frequency of operation without loss of Q and hence improve the streak speed of a synchronously operating streak or framing camera, microwave cavity deflectors may be considered. At frequencies >1GHz it becomes attractive to change the resonant circuit construction from a discrete component design to a distributed network construction. In order to increase the resonant frequency of a fixed capacitance circuit it can be seen from equation 6.5 that the inductive element must be reduced in magnitude. This may be achieved by adding equal value inductors in parallel and the resultant inductance may be calculated from equation 6.7.

$$L_{res} = \frac{L_1 L_2 L_3 \ldots\ldots}{L_1 + L_2 + L_3 + \ldots\ldots} \qquad (6.7)$$

If multiple inductive elements are constructed around an air-spaced capacitor then the circuit evolves into a 'cavity' type resonator whose oscillation frequency my be calculated from equation 6.5 provided all the capacitive and inductive elements are considered. This geometry lends itself well to a high frequency resonant deflection unit due to the distribution of the electric and magnetic fields within the cavity [19]. Such systems are useful at frequencies above 1GHz (below this their size becomes too large to be easily constructed and implemented) and if constructed correctly can attain Q's in excess of 500 which leads to large voltages being developed across the 'capacitive' region for moderate input powers. Figure 6.12 shows the field line arrangement and inductive input coupling for a typical cylindrical resonator cavity design excited at its fundamental resonant frequency.

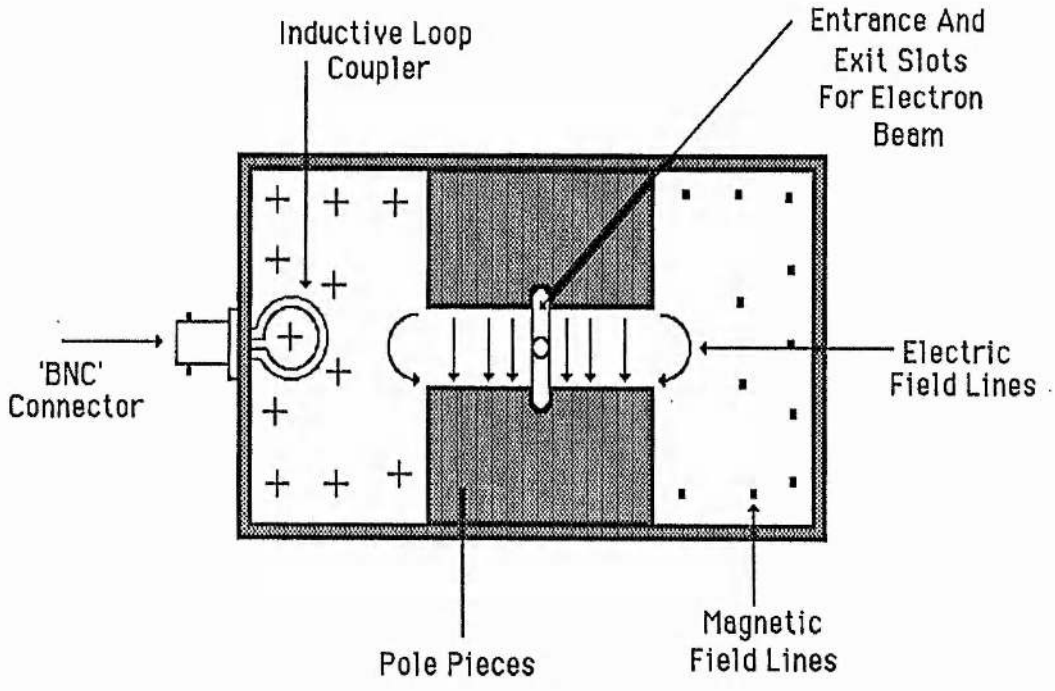

Figure 6.12. A cross-sectional view of a reentrant cavity design showing the distribution of the electric and magnetic field lines within the structure.

6.7.1 Design Considerations

Design equations and curves are readily available for this cylindrical [20,21] and square [22] cavity and so preliminary investigation of this structure as an electron deflection system was undertaken. Unlike a Klystron [20] where the electron beam

enters the cavity coaxially so that velocity modulation occurs, the requirement is for electron beam deflection and so the electron beam is introduced through the side wall as shown in figure 6.10.

6.7.1.1 Dynamic Fringing Fields

Assuming peak voltage amplitudes of ± 500 V may be generated within the deflection region at resonance then it is essential that the length of the deflection elements be such that dynamic fringing field effects are maintained within acceptable limits. It is difficult to theoretically estimate a meaningful 'value' for this parameter although from experimental data, it would appear that for the Picoframe camera ~100ps frame time is the minimum attainable before image distortion effects become severe, corresponding to a deflection voltage of 3kV/ns applied symmetrically to the 11mm long (framing) deflector plates. This corresponds to a parameter defined as D (the product of the voltage temporal gradient and the deflector plate length) as 3.3 kV cm / ns, and this is taken as the upper limit to be employed if resolution is to be maintained. Calculations and experiments indicate that ~1kV amplitude voltages must be developed between the deflection plates in order to achieve double framing and good spatial resolution when using sinusoidal deflection waveforms.

If the cavity were to operate at 1GHz then the approximate voltage rise-time (10% to 90%) is 350ps in which time the voltage has changed by 800V indicating an average voltage temporal gradient of 2.3 kV/ns. However the instantaneous gradient about 0V is ~6 kV/ns, which may be a more meaningful figure as this is the principal temporal region of interest. It may be concluded then that dynamic fringing field effects may be apparent if a resonant cavity at 1GHz with 11mm long deflection elements and ~1kV peak-to-peak deflection voltage was used to deflect 15keV electrons. Under these conditions, and employing the Picoframe design parameters ~100ps (full exposure) frames should be generated with an inter-frame time of 500ps.

Reducing the deflection plate length will reduce the parameter D, although this also has the undesirable effect of reducing the deflection sensitivity and so larger deflection voltages are required. As such there is no merit to be gained in such a procedure unless a multi-deflection element resonant cavity is designed in which the

electron transit time of each element is short compared to the deflection voltage risetime.

6.7.2 Experimental Evaluation

In order to confirm that electron beam deflection may indeed be achieved, square and cylindrical geometry 1GHz resonant cavities were designed and constructed from brass and copper. The deflection element lengths and separation were maintained at 1cm and 4.5mm respectively while the other cavity dimensions were designed in order to bring the system into resonance at the desired frequency. In both cases Q values were measured by inserting a small loop probe into the cavity and tuning the exciting r.f. through resonance. The probe output was examined using a spectrum analyser and Q's of ~500 were achieved for both cavity designs. A vacuum demountable system was employed to evaluate the performance of the cavities, and a vacuum of 10^{-5} Torr was achieved after prolonged pumping. Electron beam deflection was measured by placing a phosphor screen and electron beam source at either side of the cavity. At low r.f. input powers of less than 800 mW (generating deflection voltages of ~300V (peak-to-peak) at each deflection element) electron beam deflection was achieved, but multipacting was observed (from the presence of a red glow discharge) at input powers around 1W. All attempts to suppress this discharge were unsuccessful although it may be that at higher r.f. powers (not achievable with the equipment available) the discharge conditions would become unfavourable.

6.7.3 Discussion

Although microwave deflection structures appear to be ideally suited for either streak or framing camera applications it appears that both dynamic fringing fields and r.f. discharges may restrict their useflness. While the former may be tolerated to some extent, it is essential that the discharge should be suppressed in order that full advantage be taken of the high unloaded Q values of a microwave cavity.

6.8 Conclusions

Resonant deflection has been employed on the Picoframe I camera to provide repetitive operation in the framing mode. Frame doublets of exposure <250ps FWHM

have been achieved with a spatial resolution exceeding 12 lp/mm when referred to the photocathode using the sealed off visible-sensitive Picoframe I camera. It seems ironic that the temporal performance of the camera is similar in both modes of operation although the dynamic spatial resolution is appreciably better when resonant deflection techniques were employed. It must be acknowledged, however, that the signal-to-noise ratio will be increased due to the overwriting of many images and dynamic space charge effects will be reduced due to the lower incident optical energy employed.

At present the frame exposure and inter-frame times are limited by the frequency of the applied sinusoid and the practical power that may be applied before thermal effects become excessive or discharges become evident. Increasing the frequency of the resonant circuit is problematical for the deflectors in their present form, primarily due to parasitic reactances but eventually by the deflection plate bandwidth. In order to combat the former difficulty, preliminary studies on microwave resonant cavities have been undertaken as a possible use for electron deflection. The results of this analysis show that although microwave cavities may indeed be used, dynamic fringing fields will probably reduce the dynamic spatial resolution available due to fringing fields at high streak speeds, and multipacting may prove to be a major problem. Until at least the latter defect has been solved then these systems are unsuitable in their present form for inclusion within a streak or framing camera.

References for Chapter 6

1 K Kinoshita, Y Inagaki, T Nakamura

Proc. Int. Nat. Conf. on High Speed Photography Vidiography and Photonics IV, (San Diego), SPIE 693, 2, 1986

2 Imacon 790 series Technical Manual, Hadland Photonics Ltd., Newhouse Labs., Newhouse Rd., Bovingdon, Hemel Hempstead, Herts, England.

3 D S Jones

'The Theory of Electromagnetism', Published by Pergamon Press, 323, 1964

4 K Kinoshita, T Kato, Y Suzuki

Proc. 14th ICHSPP, (Moscow), 199, 1980

5 K R Spangenberg

'Electron and Electronic Engineering Series', Published by McGraw-Hill Inc., 467, 1948

6 M R Baggs, R T Eagles, W Margulis, W Sibbett, W E Sleat

Advances in Electronics and Electron Optics, 64B, 627, 1985

7 W Sibbett, M R Baggs, H Nui

Proc. 15th ICHSPP (San Diego), SPIE 348, 267, 1982

8 W T Scott

'The Physics Of Electricity and Magnatism', 2nd Edition

John Wiley and Sons, New York, 1966

9 Selectro Ltd, Walton Rd., Farlington, Portsmouth, Hants., England

10 A Finch, Y Liu, W E Sleat, W Sibbett, G Chen

Proc. 18th ICHSPP (Xian), SPIE 1032, 97, 1988

11 I White

Radio Communications, 120, Feb 1984

12 eg. S Evans, G R Jessop

'VHF/UHF Manual', Radio Soc. of Great Britain

13 A Finch, W Sibbett, W E Sleat

Rev. Sci. Instrum., 60, (5), 839, 1988

14 TRW RF Semiconductors, 14520 Aviation Blvd., Lawndale CA902, USA

15 R T Eagles, W Sibbett, W E Sleat

Optics Comm., 57 (6), 423, 1986

16 eg. P Kean, K Smith, W Sibbett

Optics Comm., 61 (2), 129, 1987

17 J Rodney, M Vaughan

IEE Transactions on Electron Devices, 35 (7), 1172, July 1988

18 K Kinoshita, K Shinoda, Y Suzuki

Proc.15 ICHSP (San Diego), SPIE 348, 227,1982

19 M R Brown, T E Sheridan, M A Hayes

Rev. Sci. Instrum., 57 (12), 2597, 1986

20 D R Hamilton, J K Knipp, J B H Kruper

'Klystrons and Microwave Triodes', published by Mc Graw-Hill, 1948

21 M Migliuolo, T G Castner

Rev. Sci. Instrum., 59 (2), 388, 1988

22 M Giordano, F Momo, A Sotgiu

J. Physics E, Sci. Instrum. 16, 774, 1983

Chapter 7

Travelling-Wave Deflection Systems

7.1 Introduction

In order to scan an electron beam in a streak or framing camera an electrostatic or magnetic deflection system must be employed. Usually electrostatic deflection is achieved with a pair of parallel or flared deflection plates. The length and separation of the plates defines the deflection sensitivity for a given electron velocity while the width of plate is chosen to minimise the capacitance while still maintaining good image quality. The image quality is adversely affected due to the undesired fringing fields which appear on all the edges of the deflection plates.The static deflection sensitivity for a set of parallel plate deflectors acting on an electron initially accelerated through a voltage V is given by equation 7.1.

$$S = \frac{l\left(\frac{1}{2}l + L\right)}{(2Vd)} \qquad (7.1)$$

The derivation of equation 7.1 may be found in [1]. The relevant symbols are defined in figure 7.1.

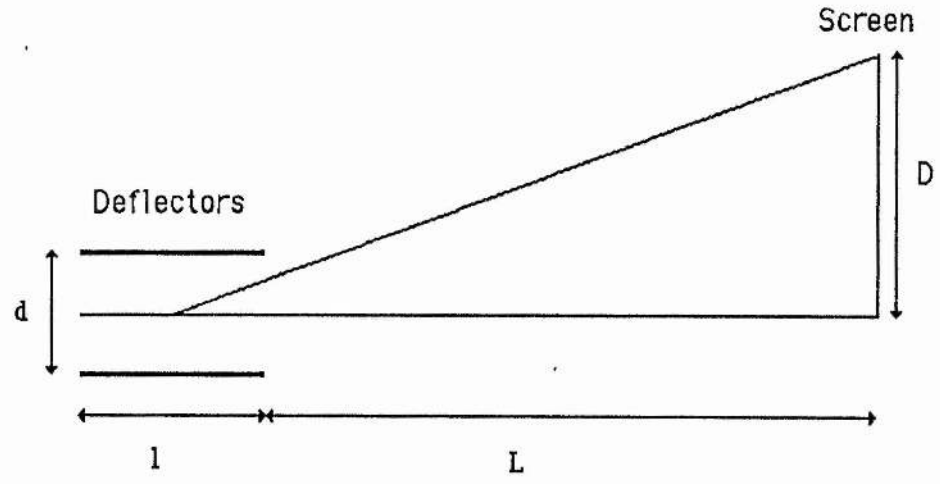

Figure 7.1

While this deflection scheme is straightforward to implement and provides good static image quality it possesses an inherent bandwidth limitation due to the transit time of the electrons within the deflection region [2]. The bandwidth limitation may be easily understood if we consider the effect of driving the deflection plates with a sinusoidal waveform with a period equal to the transit time of an electron through the deflection region. In this case the resultant deflection imparted to an electron will be zero after passing through the deflection region, although some lateral displacement will be apparent. The amount of lateral displacement which the electron will experience will be a function of the relative phasing between the deflection waveform and the electron. It is thus intuitive that as the deflection frequency is reduced towards dc the deflection amplitude achieved will tend to the dc deflection.The equation of motion of an electron between a pair of parallel deflectors is readily derived [2] when neglecting fringing fields and is given as equation 7.2, where the relevant symbols are; e, electronic charge; V, peak deflection voltage amplitude; d, deflector plate separation; m, electron rest mass; ω, angular frequency of oscillation; t_0 time of electron entrry into deflection system.

$$y = \frac{e V}{m d \omega^2} [\cos \omega t_0 - \cos \omega t - \omega (t - t_0) \sin \omega t_0] \qquad (7.2)$$

A typical example of the bandwidth achieved with a standard pair of deflectors 2cm long deflecting 15 keV electrons is 600MHz, whereupon the dynamic deflection sensitivity has dropped to ~90% of the static deflection sensitivity due to electron transit effects alone.

It can also be shown that if the period of the deflection waveform used to drive the deflection plates is fast compared to the electron transit time then the fringing fields at the entry and exit can cause severe image degradation due to the difference in deflection potential at the entry and exit of the deflection structure [3] (see chapter 3, section 7.1). A full computer simulation of the Picoframe camera design has been completed although the details are outside the scope of this thesis. The simulations of the electron trajectories when the camera is operated in dynamic mode, clearly indicate a

shift of the electron-optical focal plane towards the photocathode as shown in figure 7.2 (the static focal plane is indicated by the vertical line at the 'phosphor' position).

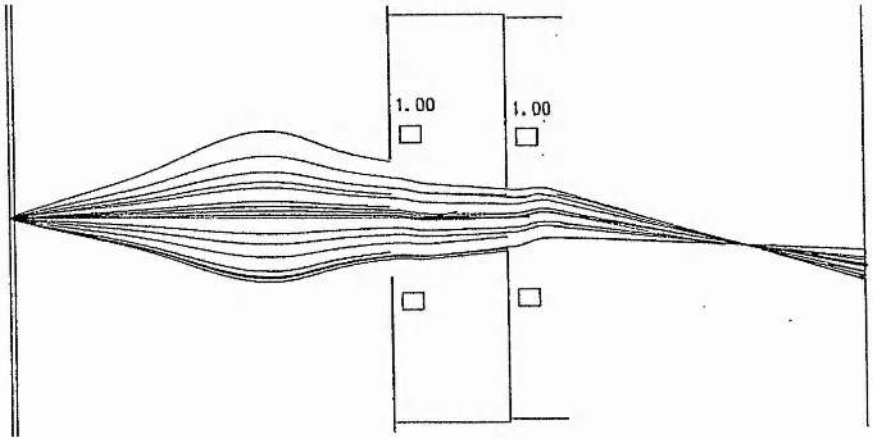

Figure 7.2. Computer simulation of the electron trajectories emitted from a single point on the photocathode within the Picoframe camera. The static focal plane (indicated by the solid vertical line) is clearly further from the photocathode than the dynamic one.

The other main problem found with this simple deflection structure is that it possesses no defined characteristic impedance thus it proves difficult to drive them as fast as desired due to the parasitic inductive leads and the capacitive load presented by the deflection plates. The calculated risetime of a typical streak camera deflection structure using the equation 7.3

$$T_r \sim \pi \sqrt{L C} \qquad (7.3)$$

may be calculated to be ~2ns where L is the inductance of the feed-through connections and C is the plate capacitance. These limiting factors have led to the search of new deflection systems which possess the required characteristics.

7.2 The Travelling-Wave Deflector

One form of deflector that should prove most satisfactory is the so-called Travelling-Wave Deflector (TWD). This system comprises of a transmission line which is periodically brought into close proximity to the electron beam to be deflected, in such a way that the electron beam is deflected by the same voltage each time it traverses the

line. In this way the problems associated with the simple plate deflectors are circumvented. Unfortunately other problems are introduced with this system such as axial electron beam velocity modulation [6], loss of dc voltage deflection sensitivity per unit length of deflector and constructional constraints.

There are two basic forms of TWD at present, viz (i) the meander line and (ii) the helical deflector [5].

Crude travelling-Wave deflection schemes have been used for a number of years and have been employed in many systems including an oscilloscope [6] (Tektronix type 519, tube type T519C which used co-axial deflection geometry), thus the basic problems can be overcome in practice. Unlike all other previous applications, streak and framing cameras alike require good spatial resolution, high streak speeds and low temporal dispersion within the deflection structure itself. An associated problem with the above three criteria is that the electron velocity is relatively high and thus the deflection sensitivity is reduced correspondingly. The oscilloscope tube mentioned (and indeed most tubes) employs a technique called post deflection acceleration but it was previously thought that this technique would prove unsuitable for streak and framing cameras due to loss of resolution in the system due to space-charge effects. Interestingly recently a streak camera design involving post-deflection focusing has been proposed [7] although its performance has not yet been established.

7.3 The Meander-Line Deflector

Of the two deflection systems the meander type [8] is the easier to design and construct with little difference in predicted performance over the helical geometry. A variation on the meander line deflector is the trough type deflector [9] which has shielding between lines to prevent inter-line coupling. This structure is theoretically only marginally better then the simple meander line [10] but is much more difficult to construct and is restricted to low power applications. It was therefore decided to consider only simple meander line structures (figure 7.3 shows the schematic of a meander type TWD) for the remainder of this work. Figure 7.4 shows the relevant dimensional parameters for the TWD.

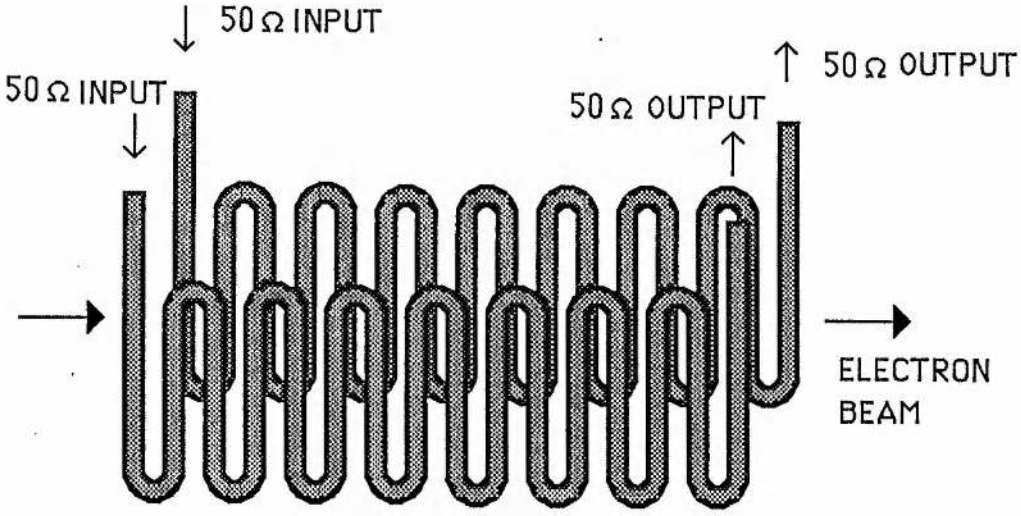

Figure 7.3. Schematic diagram of a travelling-wave deflection geometry.

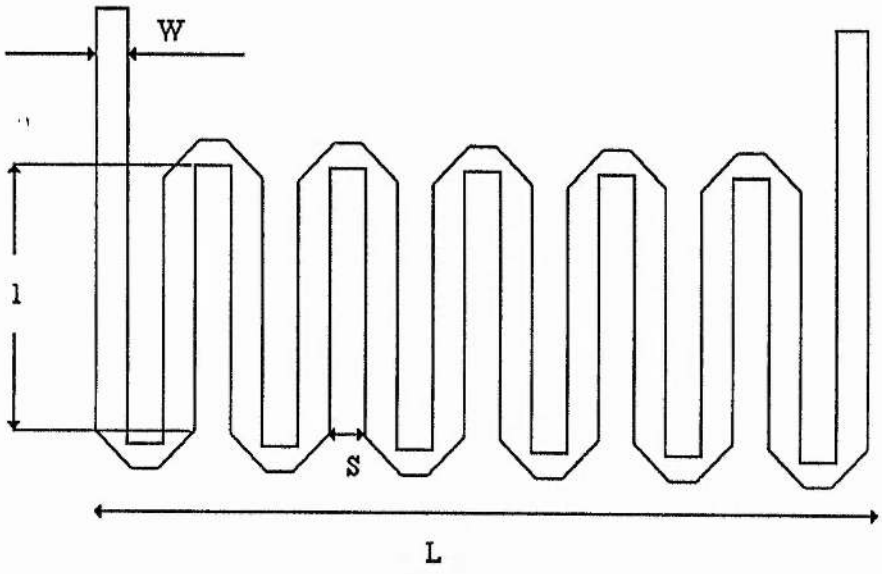

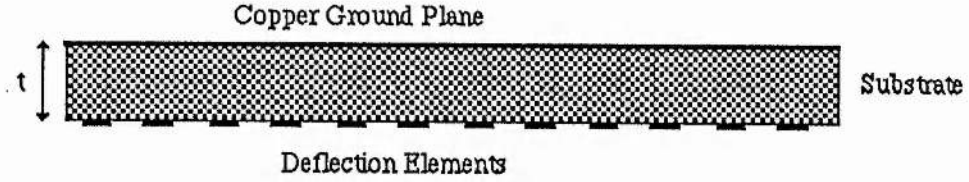

Figure 7.4 Relevant dimensions of the TWD.

7.3.1 Design Considerations

The characteristic impedance of a single ground plane micro-strip line [11] with a dielectric constant of E may be calculated using equation 7.4 where E_r is the dielectric constant of the substrate, w and t are as shown in figure 7.4.

$$Z_o = \frac{120\,\pi\,\sqrt{E_{eff}}}{\frac{w}{t} + 1.393 + 0.667\,\ln\left(\frac{w}{t} + 1.444\right)} \qquad (7.4)$$

where

$$E_{eff} = \frac{E_r + 1}{2} + \frac{E_r - 1}{2}\sqrt{1 + 12\,\frac{t}{w}} \qquad (7.5)$$

Given that the electron velocity and the axial signal velocity within the TWD must be the same and the characteristic impedance of the deflector is defined, the other dimensions of the TWD are readily derived. Theory for a standard microstrip line is well detailed [12, 13, 14] and may be used to calculate the characteristic impedance of the line to good approximation. Thus for a given dielectric constant and line ground plane spacing the line width is defined for a given impedance. The signal group velocity in the line defined as Vg may be calculated using equation 7.6 where c is the velocity of light in a vacuum. While other more elaborate and accurate equations may be found the one below proved to be in very good agreement with others tried.

$$V_g = \frac{c}{\sqrt{0.47\,E_r + 0.67}} \qquad (7.6)$$

Thus the width of the deflector may be calculated if it is assumed that no inter-track coupling arises. The inter-track coupling is due to the fringing fields around the line which are not easily calculated analytically. However it can be shown [12, 13] that the coupling is principally a function of the line thickness, inter-line separation and the line/ground plane separation . If the geometry of the deflector is then carefully chosen the inter-track coupling may be maintained at a reasonably low value, but the meander

line TWD does suffer from this defect. Inter-line coupling may occur in both directions in the neighbouring track. The operation of the TWD dictates that neighbouring tracks are approximately at the same voltage (this depends on the deflection voltage risetime but for most practical purposes of ~1ns rise-ime waveforms is true) but in opposite directions. The effect of this is that mutual backward coupling (in a direction opposite to the signal propagation) will 'enhance' neighbouring track signals, while forward coupling (which is usually negligible) will tend to 'reduce' the propagating signal. Analysis of this effect is complicated further by the structure of the TWD which requires sharp directional changes in the micro-strip line.

The effect of this inter-line coupling is deleterious to the performance of the deflector as it alters the characteristic impedance of the structure and thereby causes reduced bandwidth, but little can be done to prevent this. In order to reduce the cross-coupling problem, the microstrip lines should be of a high characteristic impedance and large separation. Ironically this is opposite to the desired deflector characteristics of low impedance (50 Ω) and small separation (to maintain deflection sensitivity) and since little can be done about this in practice, it was decided to neglect such effects during the design of the deflection structure. It must be conceded nevertheless, that optimisation of frequency response will only be achieved when full consideration is given to such effects. Also, due to the backward coupling effects the deflection signal will tend to 'skip' from one track to another, thus increasing the effective signal group velocity along the electron beam axis. Such effects will only become predominant when fast rise-time (~100ps) deflection waveforms are employed and so again this was neglectedin the preliminary assessment, but should be considered during a full optimisation of the system.

The sharp bend at the top and bottom of the TWD if not designed correctly will lead to impedance mismatch conditions [12, 13] because the propagating signal will 'see' a sharp discontinuity thus causing reflections back down the line. This will manifest itself as an undesired reduction in bandwidth of the structure. It is a rule of thumb that the transmission line should not have a curve with a radius less then three times the line width for correct impedance matching and this would cause the inter-line separation to be too large. Thus mitre corners may be adopted [13] to allow sharp

changes of line direction. Although these structures are to some extent bandwidth limited themselves they have not been found to be strongly so.

7.3.2 Construction Techniques

The main decision to be made in the initial design of the TWD is that of construction technique. Ideally the dielectric constant occupying the volume between the ground plane and the line itself should be as low as possible, preferably unity, to maintain a high signal group velocity so that large deflectors may be constructed. Most commonly used materials used for microstrip line have a dielectric constant of around 3 to 5 which would cause a prohibitively low signal velocity although the line width is easily chosen to achieve a wide range of characteristic impedances. A streak tube achieving 300fs resolution [15] used a 'free wound' line in close proximity to a ground plane to overcome these problems, but a difficulty in this method is to maintain the correct separation without introducing dielectric discontinuities in the line. In this case the characteristic impedance was chosen to be 100Ω as great difficulty was experienced with the much higher tolerances required to fabricate a 50Ω line. It was then necessary to use broadband impedance matching networks in order that standard 50Ω cable could be used. This system (chapter 8) worked well allowing high streak speeds to be achieved ($2x10^{10}$ cm/s) with only moderate voltage waveforms (total of 6kV switched in 1.5ns) [21] although the insertion loss of the deflectors and connectors was found to be ~2dB. Another problem of this construction technique was its fragility and the difficulty in mounting such a structure in a demountable image tube.

7.3.3 'PCB' Type of Travelling-Wave Deflector

For the above reasons it was therefore decided to employ a substrate of some form in order to maintain the ground plane and line separation to high accuracy so that a 50Ω transmission line might be constructed. The most appropriate substance found was a PTFE based circuit board substrate (Trade name RT Duroid) which could be ordered in various thicknesses and coated with different copper sheet densities. The main attractions of this material was its very low dielectric constant (2.2) and low loss and

dispersion at up to 10 GHz. With a dielectric thickness of 250μm the track width required for a 50Ω transmission line is 0.7071 mm and the signal group velocity is 2.3×10^8 cm/s.

The inter-line separation was chosen to be 0.5 mm as this would allow a reasonable number of passes to be made per unit length while not causing sufficiently large cross-coupling between the neighbouring lines (typically <10% for the backward cross-talk). With these parameters defined the electrical properties of the TWD system are defined but in order for correct phase matching of signal and photoelectron beam (15keV) the length l may be calculated as 3.53mm. The use of lower camera anode voltages (ie. reducing the axial photoelectron velocity) means that the TWD width may be increased to maintain synchronisation. It is also not essential in practice that the phases of the signal and electron beam be matched exactly and some leeway is available, so that a TWD system designed for the Framing camera with anode voltage of 13kV has a width defined by dimension l = 5.5mm.

The TWD's constructed in this way possessed a bandwidth of up to 2GHz (measured using Marconi Synthesizer and HP Spectrum Analyser) when mounted on a copper plane using silver loaded epoxy and 'BNC' feed in / out connectors. A very slight ripple was noticed (1/2 dB modulation) throughout the pass-band but this was probably due to the feed-in connections. In any case the modulation depth was too small to be of any major concern.

Although these deflectors provided all the correct radio frequency parameters, difficulties were experienced in their implementation within an electron-optical camera. The thin substrate was able to hold off a static dc potential in excess of 3kV (120kV/cm) when mounted correctly, but under the influence of these large electrostatic fields the substrate itself became electrostatically charged or 'stressed'. This meant that the deflectors behaved well if low deflection voltages were employed (<500 V with respect to the ground plane) but at the more usual voltages employed of ±1.5kV substrate charging was evident. The result of this was that after applying a dc voltage of ~1kV for a few seconds, disconnecting the supply and earthing the deflectors resulted in image displacement which could only be removed if an equal amplitude but inverted polarity was applied for a few seconds. In dynamic testing, when applying a ±1.5kV

deflection voltage the resultant 'scan' was badly distorted in both spatial directions, and this was felt to be due to the same problem.

Combating this problem proved to be extremely difficult. One solution attempted was to etch 'grounded fingers' between the signal carrying and so forming a trough type deflector previously mentioned. Although this technique proved successful in defeating the substrate 'charging' effect it also reduced the allowable usable voltage to ~700V due to surface tracking across the substrate between the earthing screen and the copper track which were only 100μm apart.

It was concluded that although this construction technique offers many advantages over the 'free space' separation technique, it is not suitable for deflection schemes that employ voltages in excess of ±500V unless a more suitable substrate material can be found.

7.3.4 Vacuum Mounted Travelling-Wave Deflectors

From the considerations discussed in the previous section it was concluded that the TWD's should be 'vacuum mounted' in order to overcome the problems encountered. The design procedure adopted was the same as before with the only difference being that the dielectric constant of the material between the signal carrying micro-stripline and the ground plane being unity. The major difficulty encountered when implementing this construction technique was that of mounting the microstrip-line at an accurate distance from the ground plane. Using a 2mm wide line (chosen to allow a reasonable number of passes per unit length of the deflector) a characteristic impedance of ~100Ω is achieved with a separation of 1.2mm while a 50Ω impedance line requires a separation of ~400μm. While the 100Ω line is easier to construct it requires the use of impedance matching devices if standard 50Ω cables and connectors are to be used, while the redesign of the available avalanche transistor circuits would be required if other cables and connectors were employed. It was therefore decided that the deflectors should be constructed to provide a characteristic impedance of 50Ω provided that a suitable mounting technique was developed and electrical breakdown avoided between the micro-stripline and ground plane.

The free standing micro-strip tracks were etched from 20μm thick copper foil

which was pretreated with photoresist (Radio Spares aerosol positive resist) and both sides masked, exposed and developed in the usual way. It was found that the foil thickness was critical as thicker foil did not etch accurately due to the copper being dissolved underneath the photoresist. To assist in the handling of the copper foil it was stuck to a glass slide (using double sided adhesive) before etching, and was later removed using acetone. The resultant copper line was mounted above aluminium mounting blocks which acted as the ground plane (which could be mounted directly onto the demountable camera aperture plates) using 'instant' adhesive (Superglue) and glass rod spacers which were drawn to a diameter of 400μm (± 20μm) to provide the correct separation as shown in figure 7.5.

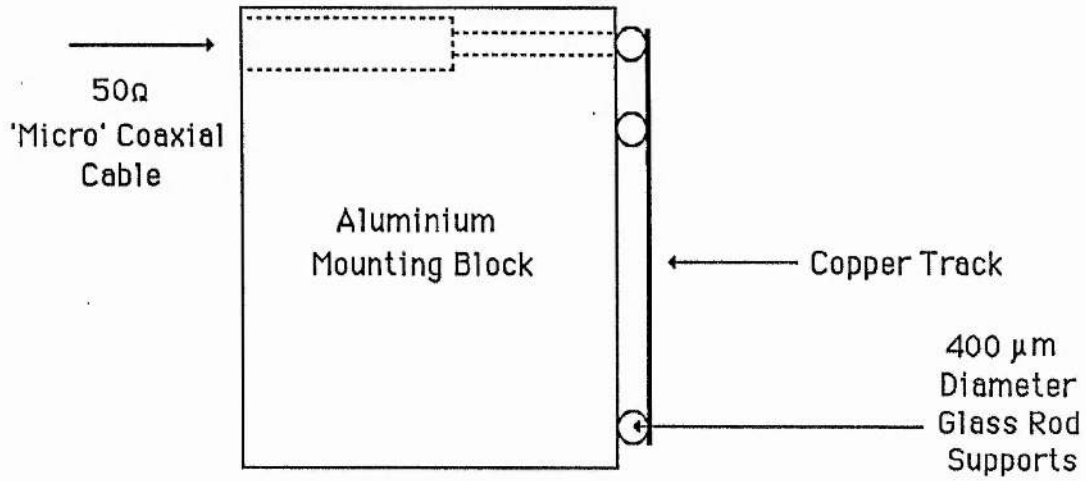

Figure 7.5. Mounting of the 'free standing' micro-strip onto the deflection mounting block

Every effort was made to keep the foil micro-strip flat while mounting as small variations in the ground plane/line separation lead to variations in the characteristic impedance of the line and increased electric field. The deflectors were tested for electrical breakdown (while under vacuum) which did not occur until the potential difference exceeded 3kV, representing a field above 75kV/cm with line-to-ground plane separation of 400μm. The interline spacing selected was 0.8mm resulting in < 5% backward coupling coefficient for the tracks. For the dielectric constant of unity the signal phase velocity was equal to light speed and so the length of the line had to be

increased to 15mm to ensure that the axial phase velocity was equal to the electron drift velocity. Mitre impedance matching at the sharp corners were not adopted due to the mechanical weakness that such techniques induce. Impedance discontinuities at the bends caused impedance mismatching, but this was difficult to avoid using the simple construction techniques employed and improvements in this area should be possible by using improved techniques. Signal dispersion through this deflector should be low and should be limited to the interline cross coupling effects (see section 7.4.1).

7.4 Experimental Evaluation of the TWD in the Picoframe I camera

Suitable meander line travelling-wave deflectors for the demountable UV-sensitive Picoframe framing camera were constructed. Due to the restrictions on deflector length (imposed by the electron-optical configuration) the framing deflectors were 13.3 mm long (having 5 passes of the tube axis) and the compensation deflectors were 16 mm long (6 passes of the tube axis).

The designed separation of the TWD's for the framing and compensation deflectors was identical to that of the parallel plate counterparts, achievable by mounting the new structures 1mm away from their respective aperture electrodes as opposed to the nominal 3mm normally used for the plane plate deflectors.

7.4.1 Bandwidth of the TWD

The frequency bandpass characteristics were evaluated by monitoring the output of a fast PIN photodetector (BPW28) illuminated by the pulses from a mode-locked laser, using a spectrum analyser. The TWD was then inserted between the photodetector and the spectrum analyser (HP 8559A, 0 to 22GHz) and the difference between the two was attributed to the deflector and connections. This technique resulted in an easy way of deriving the frequency pass characteristics of any assembly and a response curve for a single TWD is shown as figure 7.6. The bandwidth was ~1.5GHz, inferring a corresponding risetime of ~280ps.

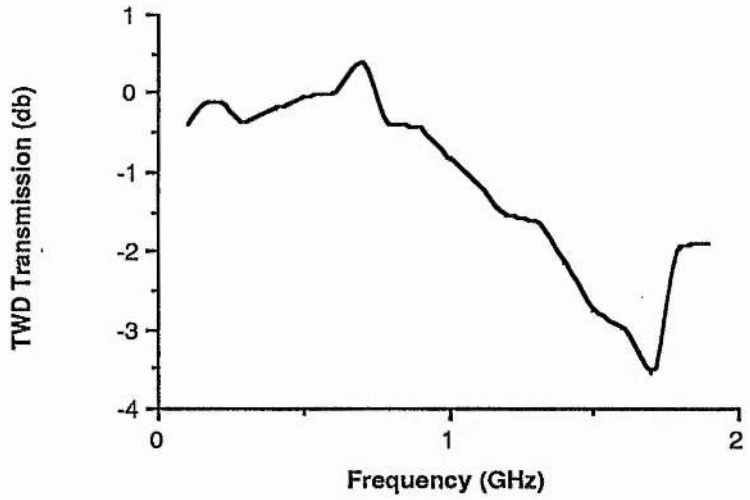

Figure 7.6. Frequency pass characteristics of the unmounted TWD.

7.4.2 Rise-time of Deflectors and all Connectors

When mounted within the demountable Picoframe framing camera the risetime of the cables, connectors and deflectors was measured directly, using a fast oscilloscope (100ps rise-time). A fast <100ps risetime (scope limited) voltage pulse was propagated through the feed cabled in to the oscilloscope directly and then via the TWD structure. A double exposure oscillogram of the 'probe' waveform and resultant slower risetime waveform due to the insertion of the TWD is shown as figure 7.7.

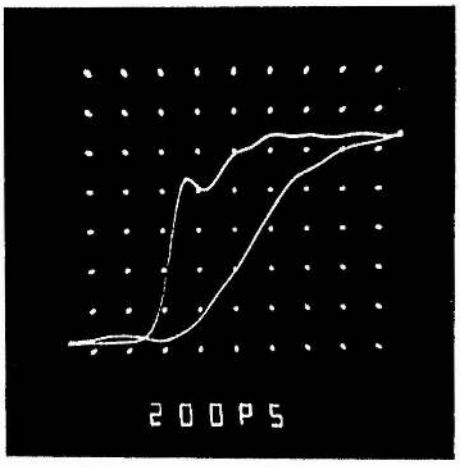

Figure 7.7. Probe <100ps rise-time pulse and resultant TWD output. The oscilloscope used was a Thomson CSF TSN 660 with a 100ps rise-time.

The resultant risetime may be seen directly as ~500ps, indicating a system (cables, connectors and deflector) bandwidth of just less then 1GHz. While this bandwidth is somewhat lower then previously measured , it should be pointed out that standard 'BNC' connectors, the micro-coaxial cable employed within the vacuum envelope and the introduced interfaces between connector, cable and deflectors will all degrade the system bandwidth. It is then expected that the losses could be reduced with the use of improved mounting and connector designs. Because the AWE avalanche transistor circuits used in most of the evaluation experiments of the Picoframe framing camera have a minimum rise-time of 1.5ns into a 50Ω load, the deflector risetime is not too significant. No degradation in risetime of the avalanche circuit was noted when the TWD's were inserted and the response inspected with a 100ps rise-time oscilloscope as before.

7.4.3 Static Image Deflection Evaluation

When incorporated within the demountable Picoframe camera system the dc deflection sensitivity of the framing and compensation deflectors to the phosphor screen of the framing camera was measured to be ~2.8cm/kV with an operating cathode potential of -15kV (anode at 0V). No degradation in spatial resolution was observed when the image was symmetrically deflected by ±200V by either deflection structure.

7.4.4 Dynamic Operation of The Picoframe I with Travelling-Wave Deflectors

Dynamic testing of the camera with TWD's was performed as described in chapter 2. The only difference was the necessity to provide terminations for the output of the TWD. An ac termination was employed to avoid decoupling the dc bias that the avalanche transistor circuits provide. The terminations were constructed from a 110pF capacitor in series with a 50Ω carbon resistor, the other end of which was held at anode potential. The terminations were mounted on the end of coaxial cables (characteristic impedance 50Ω) having a round trip-time >2ns (>20cm long) so that any reflections resulting from the non-perfect impedance match would arrive at the deflectors after the electron beam was swept clear of the framing aperture. The measured frame time (as previously described) was 180ps FWHM when the terminations were employed and

120ps FWHM when the output of the TWD's were left unterminated. The different frame-times result from voltage multiplication and reflection back through the deflector (in the opposite direction to the electron axial velocity) causing enhanced (but not doubled) sweep speeds when the deflector output was unterminated. Frame quality was adversely effected by these counter-propagating reflections as might be expected, and severe defocussing of the image resulted when not using terminations on each of the four TWD outputs. The limiting dynamic spatial resolution attained with the terminated deflectors was however higher than that achieved with parallel plate deflectors and was measured to be (by eye) 10 lp/mm in both directions. Slight loss of resolution was noted at one edge of the image and this was attributed to the framing aperture which was noted to be slightly off axis. A reproduction of a typical frame is included as figure 7.8.

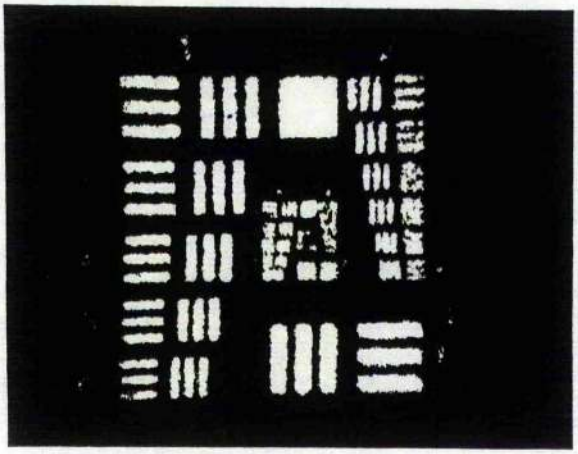

Figure 7.8. Reproduction of a typical frame when using the TWD, demonstrating a limiting dynamic spatial resolution of 10 lp/mm in both directions.

7.5 Plane Plate Deflector Compensation

While the use of TWD's has been demonstrated to reduce the fringing field effects associated with the framing and compensation deflectors of the Picoframe framing camera, increased frame exposure time resulted. Another solution to the problem may be to retain the standard plane plate deflectors employed but to introduce another cylindrical electrostatic lens orthogonal to that created by the deflectors. In this way it is reasonable to assume that the focal length in the scan and non-scan directions may be equalised, ie. remove the astigmatism introduced, although magnification differences between these scan and non-scan directions may still arise.

In order to test this idea a set of parallel plate 'deflectors' were introduced after the

framing deflectors as shown in figure 7.9. The additional electrode dimensions employed were 25mm long, 20mm wide with a separation of 20mm and they were located 5mm from the framing deflectors as indicated (see figure 7.9).

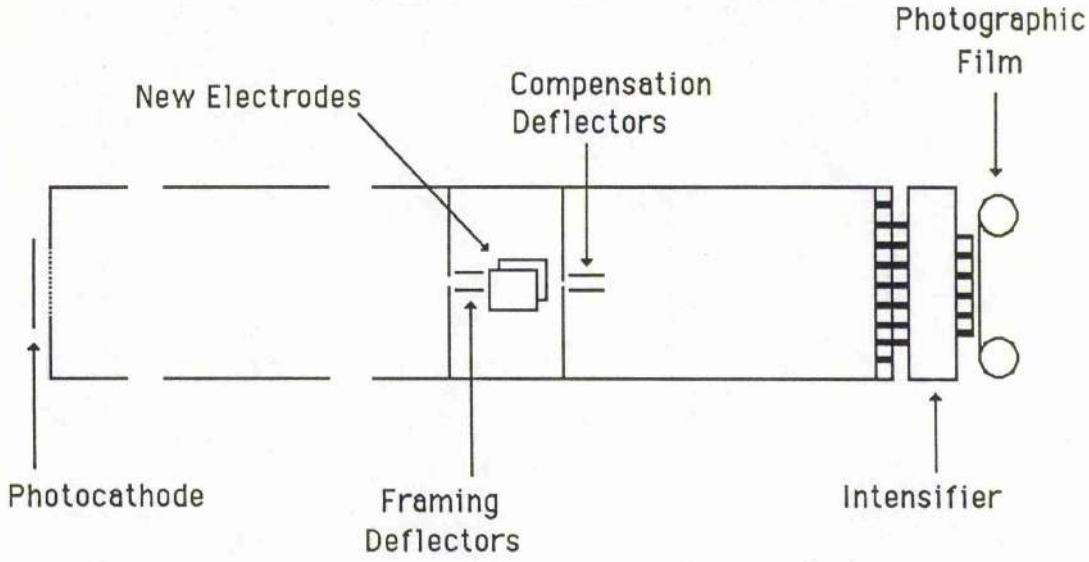

Figure 7.9. Additional lens electrodes, introduced between the framing and compensation deflectors.

The UV-sensitive Picoframe camera was dynamically tested as before (chapter 2.9) but a dc voltage was applied to the electrodes. Dynamic refocussing of the electrostatic lens and optimisation of the applied dc voltage to the 'astigmatic compensator' electrodes resulted in single frames of high dynamic spatial resolution which was ~10 lp/mm when referred to the photocathode. The dc voltage applied was -55V to both of the electrodes in the configuration employed. A reproduction of a frame obtained with this technique is shown as figure 7.10.

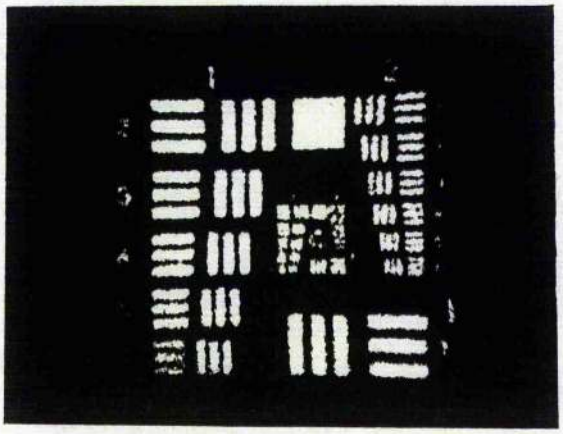

Figure 7.10. Showing a single frame image obtained using the UV-sensitive Picoframe I camera employing plane deflection plates and 'astigmatic compensation' electrodes.

Only slight magnification differences in the scan and non-scan directions are observed.The frame exposure time was measured to be 105ps FWHM (chapter 2.9.4). It has thus been shown that compensation for fringing field defects of the deflectors may be achieved using an additional cylindrical electrostatic lens and such techniques may play an important role in future developments in this camera design.

7.6 Discussion

It should be noted that no dynamic refocussing (as required when employing plane deflection plates) was required to optimise the dynamic spatial resolution when travelling-wave deflectors were employed. Previously, the potential applied to the focus electrode of the electrostatic lens was adjusted by up to ±200V between optimal static and dynamic spatial resolution. The dynamic refocussing was required due to the effective cylindrical lens the deflectors present to the electrons when their deflector transit time is not negligible with respect to the rate of change (dV/dt) of the deflection voltage. This unwanted lensing action caused by the resultant fringing fields will move the position of the effective image plane in the scan direction closer to the photocathode when the combined effects of the framing and compensation deflectors of the Picoframe camera are considered, and so refocussing is required in order that the optimisation of the spatial resolution in the scan, and non-scan directions can be achieved. Travelling-wave deflectors should not suffer from this defect due to the 'constant' deflection voltage experienced by the electron beam when the deflection signal and photoelectron axial velocities are matched and also the transit-time across each of the deflecting elements is very short (~40 ps). These theoretical predictions have therefore been confirmed experimentally for the parameters described. The experimentally measured (and theoretically predicted) frame time (with is inversely proportional to the scan speed at the framing aperture) was found to be greater for the travelling-wave deflectors then for the plane plate deflectors. Although the travelling-wave deflectors exhibit a slightly higher dc deflection sensitivity, this is easily explained by the lack of voltage multiplication at the deflector-feed cable interface for the terminated travelling-wave deflectors. Reduction in frame time is possible by the use of faster avalanche transistor circuits (circuits switching 3kV in 400ps are now becoming available, chapter 5.4) or photoconductive switches [16] with little or no loss expected

in the dynamic spatial resolution. Such techniques should provide, in conjunction with improved bandwidth deflectors, frame exposure times of 50ps FWHM.

Another technique which may be adopted is the 'impedance mismatch' structure, in which the impedance of the feeder cable is lower then that of the deflector. The output of the deflector must be matched to a suitable high impedance cable or termination however, which necessitates the use of special connectors and cable or 'in tube' terminations where the termination components are mounted directly on the TWD within the vacuum envelope. These techniques may be considered for future developments of the deflector geometry.

Another interesting possibility arises from the fact that the output of the framing travelling-wave deflectors may be used to drive the compensation travelling-wave deflectors via a suitable transmission line delay. Unfortunately the present vacuum demountable design is not directly compatible with this technique due to the moderately large separation of the two sets of 'BNC' connectors employed for the two sets of deflectors. This problem is easily resolved by redesign of the sections. This technique should allow the generation of frames from a single symmetrical avalanche transistor circuit or photoconductive switch and thereby negating any problems associated with trigger jitter and shot-to-shot amplitude fluctuations between the two (or more) circuits currently employed. It is believed that this would further improve the camera performance reproducibility and hence its use as a diagnostic tool.

7.7 Conclusions

The Picoframe I framing camera design has been operated in the single frame mode with specially designed travelling-wave deflectors. It has been found that for all practical purposes, the travelling-wave deflectors should be of the 'free standing' type where no substrate is employed between the substrate and deflector elements. The deflectors ware designed and constructed to have a characteristic impedance of 50Ω and had a measured bandwidth of 1.5GHz (~280ps rise-time). When mounted and tested within the UV-sensitive vacuum demountable Picoframe I, the connectors, cables and deflectors had an experimentally measured risetime of ~500ps (<1GHz). The measured dc static sensitivity was 2.8 cm/kV for both the framing and compensation deflectors.

The limiting dynamic spatial resolution attained was 10 lp/mm (when referred to the photocathode) while the frame time was measured to be 180ps FWHM. The dynamic and static electrostatic lens focussing conditions were found to be identical when using the travelling-wave deflectors unlike the plane plate deflectors, so confirming the theoretical predictions.

A technique has also been introduced to compensate for astigmatism caused by the plane plate deflection electrodes, which has yielded dynamic spatial resolutions comparable to that obtained with the TWD's while maintaining ~100ps FWHM frame exposure times.

References for Chapter 7

1 O Klemperer, M E Barnett

'Electron Optics', 3rd Edition, Cambridge University Press, 1971

2 K R Spangenberg

'Vacuum Tubes', 'Electrical and Electronic Engineering' seriese, Published by Mcgraw-Hill, 1948

3 K Kinoshita, M Ito, M Suyama

Proc. 14th ICHSPP (Moscow), 199, 1980

4 J Goldberg

Rev. Sci. Instrum., 13 (12), 1320, 1960

5 N Finn, T A Hall, E Mc Goldrick

Applied Physics Letters, 46 (8), 731, 1985

6 'Coaxial Deflection CRT has 3GHz bandwidth', Microwaves, Feb 1963

7 K Kinoshita, M Ito, M Suyama

Proc. 18th ICHSPP (Xian),SPIE 1032, 441, 1988

8 A Silzars

Proc. of the Society of Information Display, 19 (1), 9, First Quarter 1978

9 I Yamada, T Takagi

IEEE Trans. on Electron Devices, 19 (2), 204, Feb 1972

10 H Niu, Y Liu, Q Yang

'Theoretical analysis of TWD', (unpublished), Xian Institute of Optics and Precision Mechanics.

11 I J Bahl, D K Trivedi

Microwaves, 174, 1977

12 A Tam

Radio Engineers Design, 29, 1988

13 H Howe Jr

'Stripline circuit Design ', Publisher Artech House Inc, 1974

14 D S Evans, G R Jessop

' VHF-UHF Manual ', Radio Society of Great Britain, Publication 3rd edition.

15 A Finch, Y Liu, H Niu, W Sibbett, W E Sleat, D R Walker, Q L Yang, H Zhang

Proc. 18th ICHSPP (Xian),SPIE 1032, 622, 1988

16 G Mourou, W H Knox, S Williamson

'Picosecond Optoelectronic Devices', Editor Chi H Lee, Academic Press, 219, 1984

Chapter 8

Experimental Evaluation Of A Single-Shot Streak Camera Employing Travelling-Wave Deflection

8.1 Introduction

While the generation of ultrashort optical pulses has now become routine in laser physics, duration measurement of these pulses is restricted to nonlinear techniques (second-order autocorrelation, two-photon fluorescence etc.) which do not directly provide the pulseshape, although methods are now being devised which can provide indications of the pulseshape under certain conditions using interferometric autocorrelations and spectral measurements as previously discussed (section 1.1). The only ultrafast linear optical pulse measurement technique presently available is the streak camera which is at present is usually limited to a resolution of ~1ps in the synchroscan mode of operation to 0.5ps in the single-shot mode [1]. Recently, subpicosecond synchroscan results have been reported using a Photochron IV streak camera and colliding pulse mode-loked ring dye laser [2], but this technique is limited by the system jitter and electronic phase noise [3]. Single-shot streak camera resolution is not related to the system jitter and so these cameras are more useful in determining the true camera instrumental performance, although in theory if the system possesses no signal jitter, the synchroscan technique should provide better resolution and dynamic range as mentioned in chapter 1. The general effects of intense illumination and loss of dynamic temporal resolution have been discussed in chapter 1 and so will not be repeated here.

One major area of loss of temporal resolution and dynamic image degradation is the electrostatic deflectors themselves. In order to achieve high streak speeds at the phosphor screen, it is desirable to include high deflection sensitivity systems within the image tube. For this reason, the deflection electrodes are positioned as close together as possible, and are made as long as possible so that the electron beam experiences a high transverse electric field for the maximum period. This explanation is simplistic but accurate if only dc or slowly varying ac potentials are applied to the deflection system. However, as high electron sweep speeds are desired, high voltage, fast risetime

deflection waveforms are usually employed when optimum camera temporal resolution is required, and this causes image degradation due to electrostatic fringing fields [4] and loss of deflector sensitivity due to electron transit time within the deflection region. The effect of the dynamic fringing fields is to cause dynamic image defocussing which is a function of the deflection angle, deflector length and deflection voltage risetime.These problems have been discussed in more detail in chapter 7 and for single-shot streak cameras it has been shown that travelling-wave deflection techniques may offer significant advantages over the standard parallel or flared plates.

8.2 The Experimental Image Tube

With these points in mind a single-shot streak camera was designed and constructed to provide a high temporal resolution when modest deflection waveforms were employed. A schematic diagram of the image tube appears as figure 8.1 and although of 'classical' design, offers some significant advantages over the standard single-shot streak camera.

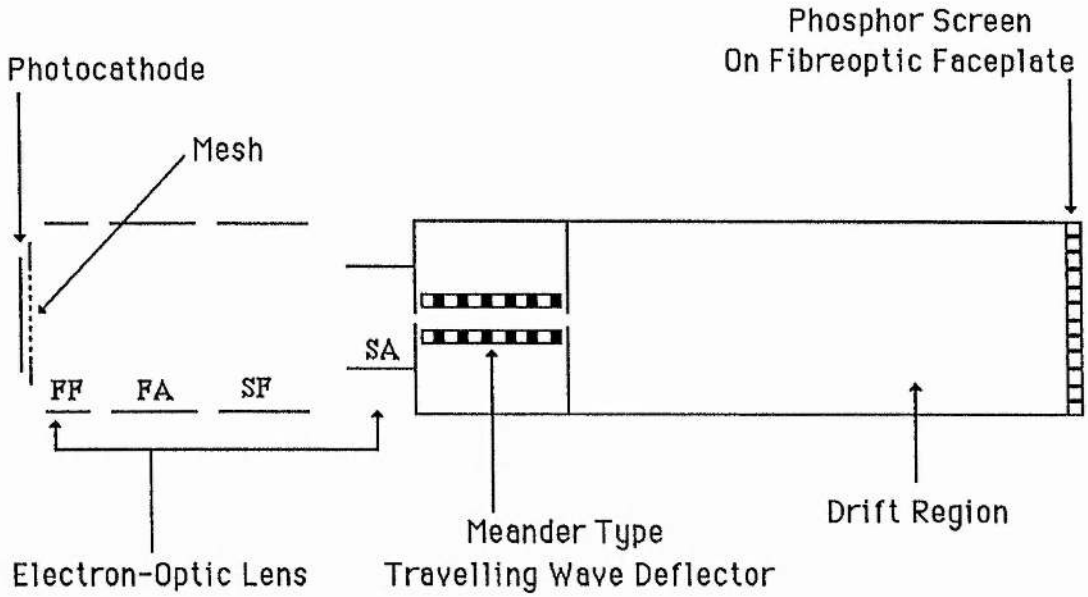

Figure 8.1. Schematic diagram of the new travelling wave deflection streak tube.

8.2.1 Photocathode

A specially thin photocathode was deposited onto a high conductivity layer on a quartz substrate. The cathode was specially designed and band-gap engineered so that

the calculated secondary electron energy spread resulting from ~620nm radiation was reduced from ~0.3 eV for a standard S20 photocathode near the long wavelength cut-off to ~0.1eV. It operated in transmission mode and was ~80% transparent to the 600nm radiation and operated at an estimated quantum efficiency of ~0.01% at this wavelength. A spectral response curve taken for the cathode some months after manufacture is shown in figure 8.2. The integrated sensitivity under white light illumination was measured as 5.6μA/l, typically ~20 times lower then a standard S20.

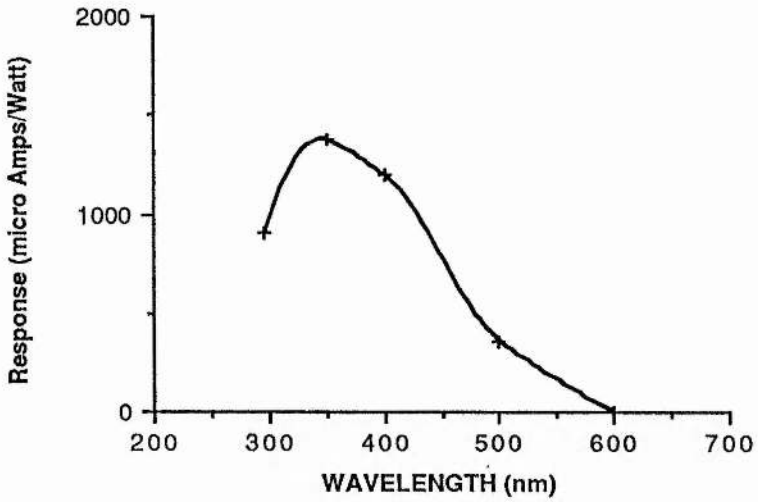

Figure 8.2. Spectral response of the photocathode of the single-shot streak camera.

The resistance of the cathode was reduced to <100Ω per square and the active area was ~10mm diameter. The cathode was fabricated in a special vacuum system and then vacuum transfer technology employed for location within the image tube.

8.2.2 Electron-Optical Lens

The mesh electrode was positioned 1.2 mm away from the photocathode and was designed to be operated at up to +6.25kV with respect to the photocathode, resulting in an electric field strength of 52kV/mm. The electrostatic lens consisted of four cylindrical electrodes and was designed around the Photochron IVM [5] type geometry using digital computer simulation programmes. The temporal dispersion characteristics of the electrostatic lens were estimated using the usual computational techniques by evaluating the electron trajectories within the lens under suitable conditions, and was calculated to be < 100fs at an operating potential of 10kV. The second cylindrical anode

electrode was of slightly smaller diameter then the other three to allow focusing to be achieved with a high mesh-cathode field and modest cathode-anode potential diference. The electron-optical magnification of the camera image tube was calculated to be -2.

8.2.3 Travelling-Wave Deflectors

The deflection system employed was a meander line travelling-wave deflection structure (chapter 7) with a dc deflection sensitivity of 8cm/kV with a camera cathode potential of -10kV. Its structure was based upon microwave transmission line techniques and constructed of a 2mm wide track positioned 1mm away from the ground plane by the use of small glass spherical beads positioned between the line and the ground plane. The characteristic impedance of such a structure was 100Ω and so impedance matching units were incorporated within the tube vacuum envelope. The impedance matching technique employed was of the tapered line type to help maintain frequency response when standard 50Ω coaxial cable was used to feed the deflection in and out of the deflectors while high frequency 50Ω connectors were used to transfer the signal through the image tube envelope. The measured bandwidth of a single travelling-wave deflection structure alone was ~2.5 GHz using time domain reflectometry while the measured frequency bandpass characteristics of the mounted deflectors, connectors and cables indicated a 1.3GHz bandwidth as shown in figure 8.3 (using frequency domain analysis as described in chapter 7), inferring ~300ps rise-time.

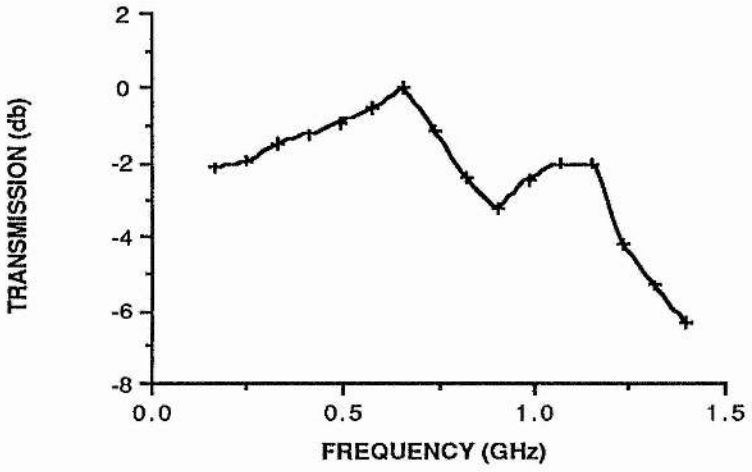

Figure 8.3 Frequency transmission characteristics of a single TWD.

The signal-carrying track passed the tube axis 23 times, the deflectors were positioned 4mm apart and were 4cm long in order to provide the required deflection sensitivity. Resonant cross-coupling between the two deflectors was noticed at ~800MHz, although this was not considered to be a problem when using only moderate risetime deflection waveforms employed.

The (high efficiency) phosphor screen was deposited (using the brush coating method) on a 49 mm diameter fibre-optic faceplate and a thin aluminium layer was evaporated onto the phosphor to aid in electron conduction and phosphor output coupling efficiency.

The camera envelope was constructed out of ceramic and stainless steel to provide mechanical strength and good vacuum qualities.

8.2.4 Operating Conditions

Although the camera was designed to operate at the above mentioned potentials it was evident that cold cathode emission caused by mesh irregularities and cathode impurities resulted at cathode-mesh potentials exceeding 5kV. The operating potentials of the camera were then reduced to -8kV, -3kV, -6.24kV, 0V, -6kV and 0V for the photocathode, mesh, first focus (FF), first anode (FA), second focus (SF) and second anode (SA) electrodes respectively. High tension (HT) voltages were supplied by a Brandenburg 0 to 15kV power supply (Alpha series) via a resistive divider chain. With these potentials the electrostatic field strength near the photocathode was 41kV/cm and the calculated temporal resolution of the entire camera was ~250 fs. A time-spread function for a single axial photocathode position with the camera operating under the stated potentials and illuminated with 630nm radiation [6] is shown as figure 8.4.

The limiting spatial resolution of the camera image tube alone was measured (by projecting a resolution test chart onto the photocathode using a Baum [7] projector) as ~50 lp/mm (when referred to the photocathode) with an electron optical magnification of -2.

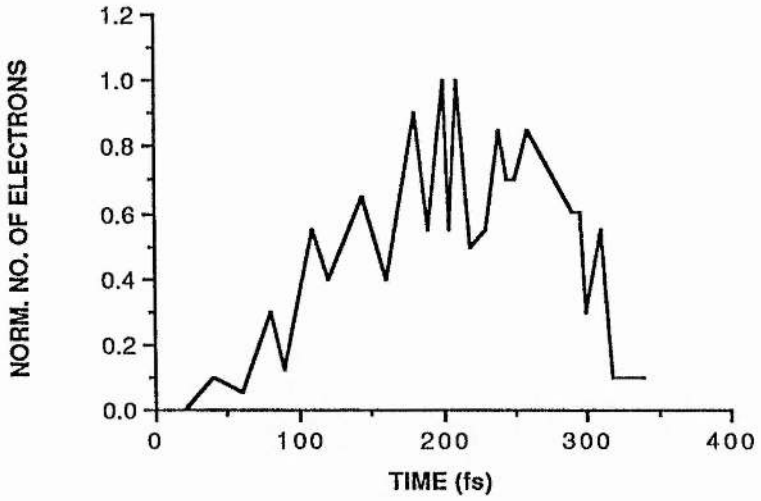

Figure 8.4. Time Spread Function of the single shot streak camera under the experimental conditions indicated (500 electrons traced) showing a theoretically predicted temporal resolution of 200fs.

8.3 Experimental Evaluation

In order to evaluate the temporal performance of the streak camera a test source of optical pulses is required. The source should be near the long wavelength response threshold of the photocathode in order so that the electron emission energy spread be minimised and the duration of the optical pulse should preferably be much less then the expected temporal resolution of the instrument in order that the true instrumental performance could be measured.

3.3.1 The CW Ring Dye Laser

Evaluation of the camera in dynamic operation was undertaken using a colliding pulse mode-locked (CPM) ring dye laser operating at 633nm and employing a rhodamine 6G / DODCI dye combination of saturable gain and absorber respectively [8]. Dye concentrations of $2x10^{-4}$ Moles per litre and $1.8x10^{-3}$ Moles per litre of ethylene glycol were used for the Rh. 6G and DODCI respectively during the course of this work. Intracavity dispersion compensation elements (required due to the dispersion which occurs within the dye jets and dielectric mirrors) was achieved using a four prism sequence [9] and pulses as short as 19 fs generated directly from this laser have been reported [10]. The mode-locked ring dye laser was optically pumped using a

(Spectra Physics 2030) argon ion laser operating at ~3W on the 514nm green laser line and the dye laser delivered ~2mW of radiation in each of the two output beams, with a 100MHz mode-locked pulse repetition rate, giving 20pJ per pulse. A schematic diagram of the CPM ring dye laser employed appears as figure 8.5.

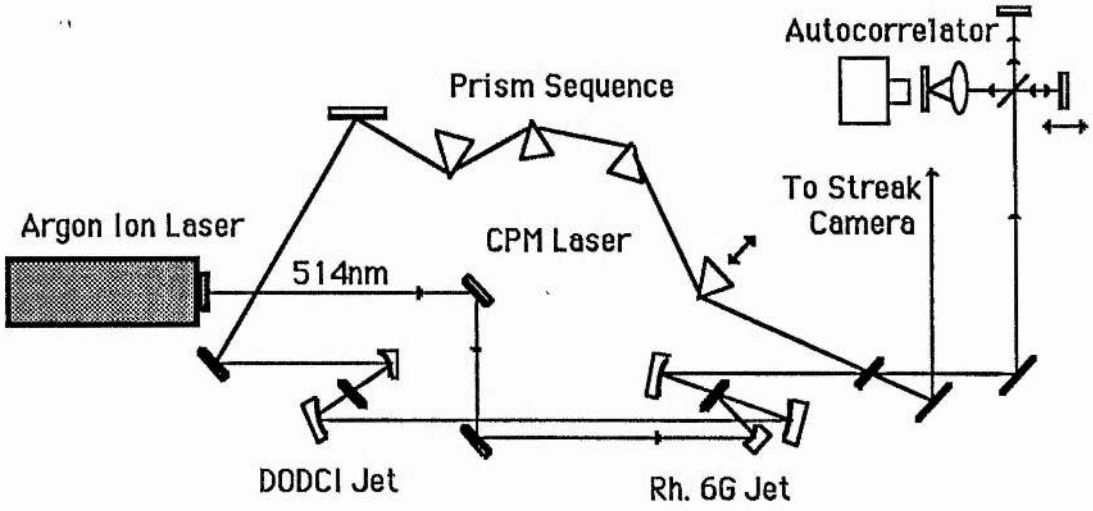

Figure 8.5. The colliding pulse mode-locked laser showing the prism sequence and autocorrelator.

8.3.2 Operating Conditions of The CPM Laser

The pulse durations available from this laser system can be increased up to several hundred femtoseconds by adjusting the dye concentration and intracavity dispersion, and so it was possible to reduce the pulse peak power while maintaining the average power. It was felt that the testing of the camera using ultrashort sub-50fs optical pulses may in fact induce gross space-charge effects [11, 12, 13] and associated intensity dependent effects due to the high peak powers illuminating the photocathode, and so the pulse durations (monitored using a real time autocorrelator) were set to ~150fs for camera evaluation, giving a peak pulse power of 133 Watts. A typical interferometric autocorrelation result for the laser operating with pulse widths of ~150fs is shown as figure 8.6. The optical pulse duration was determined from intensity autocorrelation techniques.

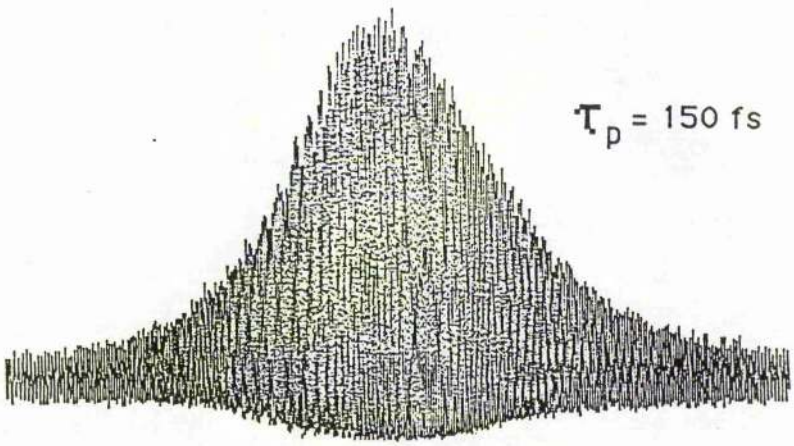

Figure 8.6. Typical interferrometric autocorrelation trace of the CPM operating at a pulse duration of 150fs.

Again, to reduce intensity-dependent effects no laser amplifier was employed as in previous single-shot streak camera evaluations [14] and a high gain image intensifier (Mullard 20/30) was fibre-optically coupled to the image tube faceplate via a 20mm diameter, 20mm long fibre-optic block.

8.3.3 Image Intensifier

To record single optical pulses the system photon gain must equal or exceed unity (to maintain dynamic range) if a single photon sensitive recording medium is employed and this may only be achieved if sufficient image intensification is available. It must be realised, however, that the system noise must also be taken into consideration when operating such intensifiers and so all units were pre-run for a number of days in an attempt to reduce the background level. The system gain was estimated by imaging a 30μm slit (illuminated with the CPM laser output) onto the photocathode using a suitable lens and monitoring the output of the camera+image intensifier combination using an optical multichannel analyser (OMA). With the deflection plates maintained at ground potential the intensifier gain was increased (by increasing the voltage applied across the MCP) and neutral density (ND) filters inserted in front of the camera until the slit image was just recordable on the OMA. In this way

the entire system gain was evaluated to be ~10^6. As the laser repetition rate was 10^8 Hz and the phosphor lifetime ~20ms, the system photon gain was estimated to be in excess of unity and so it was expected that single optical pulses would be recordable. The limiting static spatial resolution of the camera with intensifier was measured to be ~40 lp/mm with respect to the input photocathode using the Baum projector as previously described (8.2.4).

8.3.4 Deflection Circuit

To obtain high streak speeds, many workers have resorted to the use of laser illuminated photoconductive switches [eg. 14, 15] which have multi-kilovolt switching capability with a sub-nanosecond risetimes and picosecond jitter . These devices unfortunately require a high optical power (~200μJ to saturate a 3mm gap Ga:As switch [16]) short pulse (~100ps in order to achieve fast risetimes) laser system which is often inconvenient. It was felt that although these systems have been shown to work in the application of single-shot streak camera's, their reproducibility is often questionable due to surface damage, alignment, and laser output considerations and so their use was avoided. Due to the high deflection sensitivity of ~10cm/kV (when the camera was operated at the reduced potential of 8KV) offered by the travelling-wave deflectors, waveform requirements were somewhat relaxed and so use was made of avalanche transistor circuits developed at AWE [17]. These circuits (used throughout the framing camera evaluations chapters 2 to 5) provided complementary outputs of ± 3kV in 1.5ns into a 50Ω resistive load. The output of the TWD structure was terminated using a 100pF capacitor in series with a 50Ω carbon resistor to ground which provides an ac termination with a VSWR <1.5 for frequency components >70MHz [18]. The terminations were connected to the output of the deflectors via a short ~10cm length of 50Ω transmission line ensuring that any reflections resulting from the imperfect termination occurred ~1ns after the recorded event. Unfortunately the 'fly-back' of the avalanche transistor circuits occurs ~800μs (at the 1/e point) after triggering (see figure 8.7), and so unless some form of pulse selection or gating is employed then the streaked image would have been overwritten due to the circuit recovery [22].

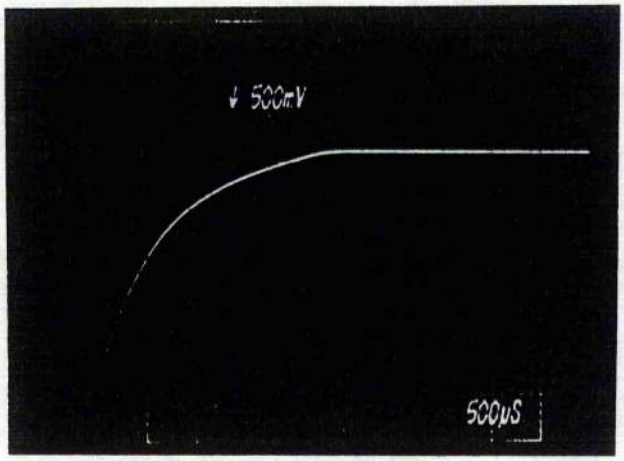

Figure 8.7 Oscillogram showing the recovery time of the avalanche transistor circuits. The oscilloscope used was a Tektronix 7904, and the output of the circuits was attenuated using a Tektronix high voltage probe (type P6105 ~2ns rise-time).

The use of electro-optic single pulse selectors was rejected due to their low extinction ratio (typically 500 to 1000) and insertion loss which, although low, could not be ignored. Initial experiments therefore relied on camera gating techniques.

8.3.5 Camera Gating

The technique employed relied on gating the camera off between the avalanche circuit voltage output rise and fall. Thus the streaked image was displayed and the camera was gated off when the circuit fly-back occurred, thus preventing overwriting. Camera gating was achieved by switching the cathode voltage from -8kV to 0V using a krytron (KN 22) based circuit which is shown in figure 8.8, thus preventing photoelectrons emitted from the cathode from reaching the phosphor screen due to the reverse potential.

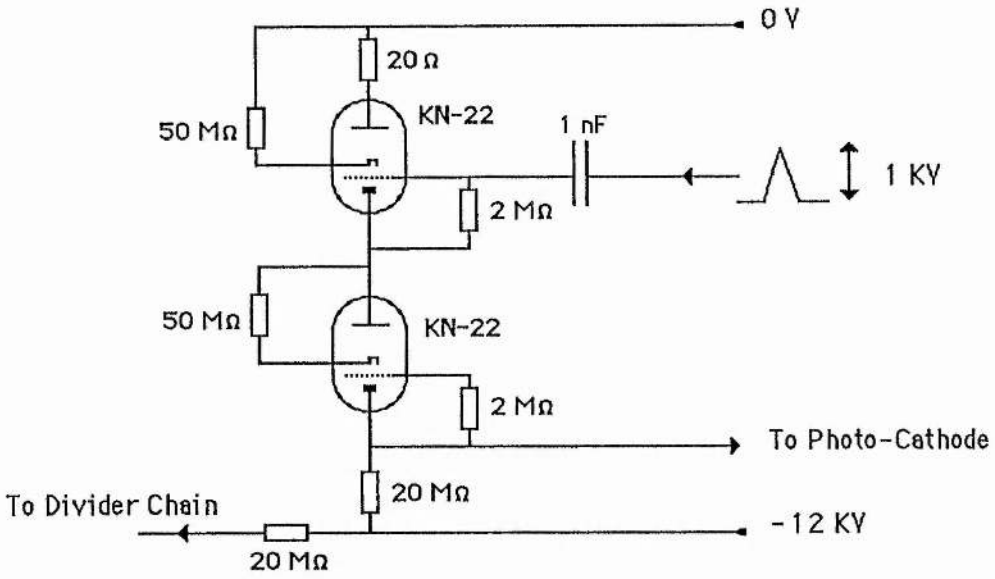

Figure 8.8. Circuit diagram of the krytron based gating.

The krytrons were triggered with a +1kV trigger pulse generated from an avalanche transistor circuit (based on the BSX 61 transistor), a circuit diagram is given in figure 8.9.

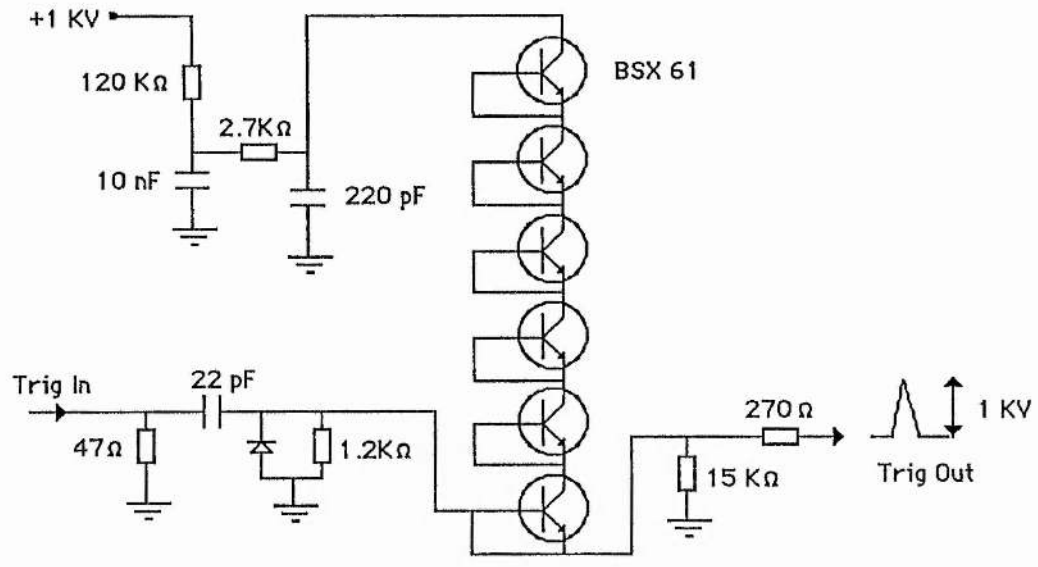

Figure 8.9. Circuit diagram of the avalanche transistor chain used to trigger the krytron gating circuit.

The avalanche transistor circuit used to activate the krytron circuit was itself activated from the transistor streak circuit which possessed supplementary trigger outputs.

8.3.6 Synchronisation

Synchronisation of the streak circuit trigger and the mode-locked laser output was achieved by using a high speed electronic gate (ECL MC10231) fed by a low frequency (4Hz) square wave gating signal and an r.f. signal which was phase-locked to the laser, as shown in figure 8.10.

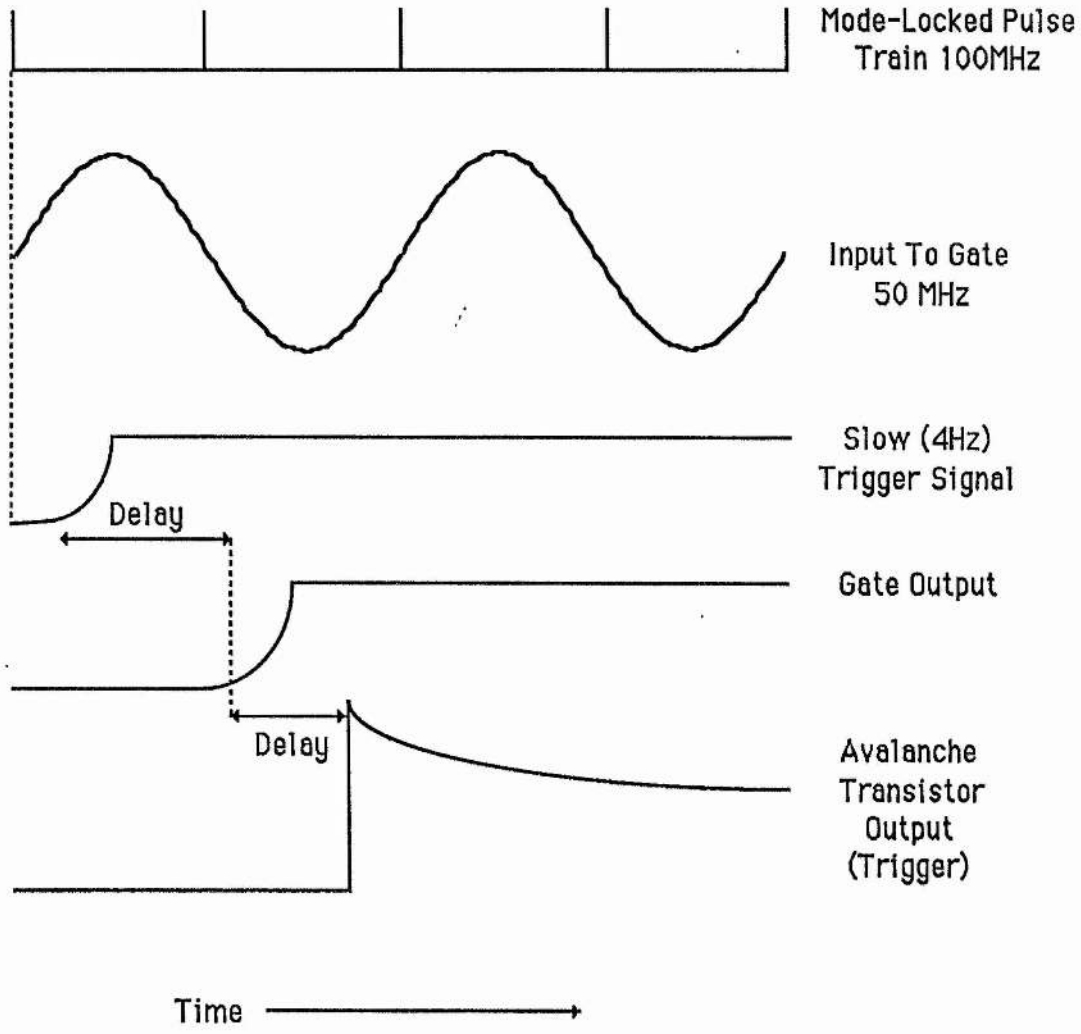

Figure 8.10. Timing diagram showing the relative triggering of the components within the synchronisation circuit.

The gate output was used to initiate avalanche breakdown within a transistor (type 2N 2369) which provided a suitable 65V trigger pulse for the avalanche transistor streak circuits. A block diagram of the full synchronisation system employed appears as figure 8.11.

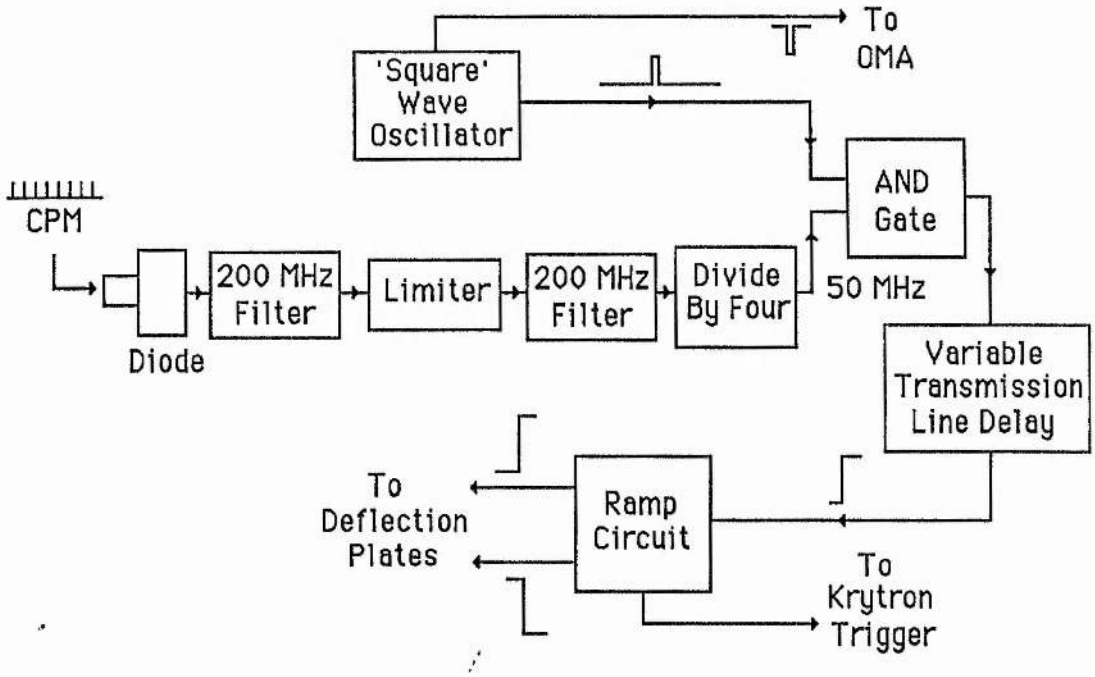

Figure 8.11. Block diagram of the electronic synchronisation system employed.

The filters were simple tuned circuit band-pass inductor / capacitor units while the amplitude limiter (chapter 6.5.2) was employed to remove any amplitude modulation due to the laser, and hence reduce the trigger jitter.

8.3.7 Modified Gating Technique

In standard streak camera image tubes this technique works satisfactorily, but because of the highly transmissive photocathode and thinly aluminised layer on the camera phosphor employed in this tube it became evident that laser light was transmitted along the camera tube axis and was either exciting the phosphor or the image intensifier photocathode directly. This resulted in a very large noise signal which dominated any streak recording. The solution adopted was to shutter the input light using a chopper whose reference output was electronically divided by 10 and used to trigger the synchronisation circuitry instead of the free running square wave trigger oscillator. This improved the signal background noise by an order of magnitude but did not completely remove the effect of the direct laser illumination. Some improvement was achieved by arranging for the input light to be non-coaxial with the camera, causing the light to be intersected by the internal camera apertures although this was not

completely successful.

Further improvements to the signal-to-noise ratio was achieved by reducing the optical shutter 'open' time by focussing the laser beam through a thin (~600μm) slit mounted on the spinning chopper wheel, which provided ~100μs shutter time with the chopper employed. Due to the rapid optical shuttering achieved with this technique it was found that the krytron gating circuit could be dispensed with, thus simplifying the electronic circuitry required although the alignment and synchronisation of the system became much more critical.

It was essential that the reference output from the chopper (generated from an internal LED / diode combination and activated once per revolution) and the maximum transmittance through the chopper slot occurred at the same moment . If this did not occur then the incident laser light would be highly attenuated when the avalanche streak circuit was triggered. This was checked by monitoring the light transmitted by the chopper (using a BPX 65 PIN photodiode reverse biased at 130V) and the chopper reference output simultaneously using an oscilloscope (Tektronix 7904), and moving the chopper as required. Figure 8.12 shows the unresolved mode-locked pulse train gated by the chopper and the chopper reference signal correctly timed.

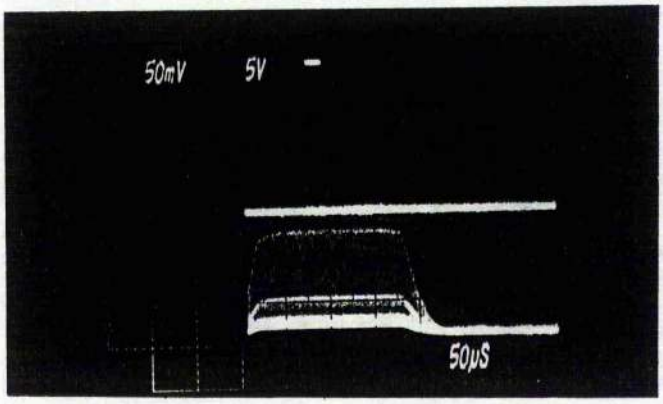

Figure 8.12. Oscillogram of the chopper transmission (lower trace) and reference output (upper). Horizontal scale 50μs per division showing ~200μs optical shutter in this case.

8.3.8 Optical Multichannel Analyser

To record the streak images an OMA (type B&M Spektronik OSA 500 Vidicon with WP1 and WP2 data processing and display units) was synchronously gated by the

deflection electronics to reduce the noise which would otherwise be integrated on the intensified silicon target. This technique proved easier then gating the image intensifier which would otherwise be required in order to reduce the integrated noise on the intensifier phosphor and detector. Because of this technique it was not possible to record the resultant streak images on photographic film, which in some ways may have been preferable as two-dimensional image analysis would then have been possible. However due to the complications associated with the nonlinearity of the photographic film response, the necessary microdensitometer equipment or video digitiser and time associated with these factors, the use of the OMA was decided upon. Ideally a two dimensional CCD camera could have been employed, but these systems were not available with sufficient sensitivity at the time the experiment was undertaken.

8.3.9 The Experimental Set-Up

The complete experimental set-up is shown schematically as figure 8.13.

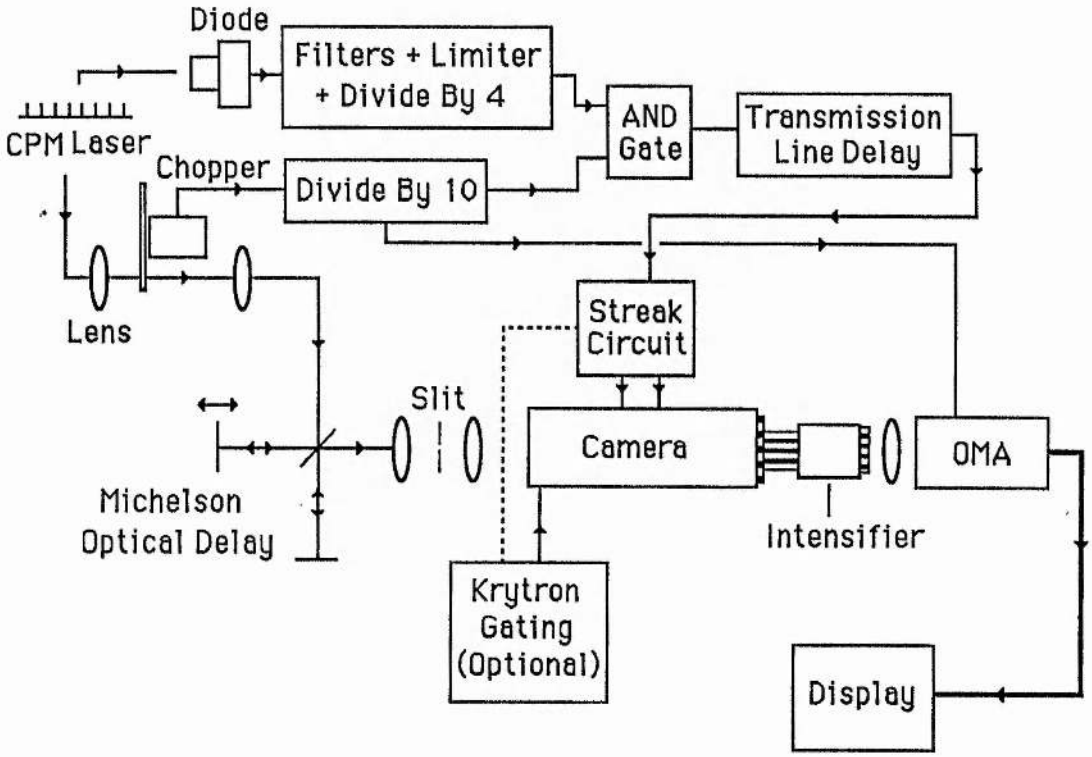

Figure 8.13 Complete camera set-up employed.

A 20μm wide 2mm long slit was imaged onto the camera photocathode with an optical relay lens (-2 magnification and f / 2.8) to form an illuminated slit image. The static

image on the OMA (which was used in combination with an optical lens of magnification -1.3) was 6 channels wide at the FWHM which represented the static spatial resolution (~ 40 lp/mm) of the streak camera.

The system timing proved to be quite easily arranged as only a 10ns period had to be inspected due to the multiple mode-locked pulses transmitted by the chopper. This was a achieved using the transmission line delay (Tektronix, 0 to 1ns). Temporal calibration of the streaked images was possible by using a Michelson-type optical delay to provide a precise temporal pulse separation. The delay introduced was evaluated from the differential spatial separation of the two mirrors from the beamsplitter.

8.4 Results

Initial results revealed that (i) the camera required adjustment of the focus potential when operated in dynamic mode to achieve the best dynamic resolution and (ii) gross modulation was observed on the streak images.

The first point is easily understood in that it results from the slight asynchronisation in triggering the two complementary avalanche transistor chains comprising each sweep circuit. This results in a dynamic 'electrostatic' lens being set up in the deflection region which causes defocussing in the streak direction. This effect was not a defect of the streak camera but of the deflection waveform generation which becomes critical at high streak speeds. It was found that some circuits were better than others in this respect although quantitative measurements were not possible due to the timescales involved, but it was ascertained that all circuits tested had a transistor synchronisation of better then 100ps measured using a Thomson CSF TSN 660 oscilloscope. The focus potential had to be altered by ~300V to obtain properly focussed dynamic images.

The second problem was not so easy to understand. Figure 8.14 shows a typical modulated but focussed streak record. The calibration pulse separation is 6.67ps.

In order for the image modulation to be 'real' (ie. result from the optical input pulse to the camera) a modulation frequency of 10^{13} Hz would be required, which would be apparent on the autocorrelator output if produced by the laser.

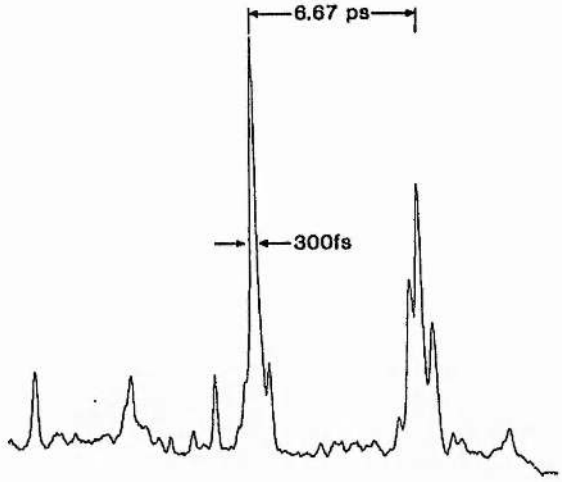

Figure 8.14. Streak record showing gross modulation on only one of the optical pulses.

As it was confirmed that no Fabry-Perot effects were the cause then it was evident that the problem was associated with the camera system rather then the input optical pulses. It was believed that the modulation was caused by spatial gain properties of the multichannel-plate image intensifier which will be discussed later. A more efficient intensifier was available of the same type, and this was substituted directly, which enabled sufficient gain to be achieved at a lower operating voltage. Re-testing of the system showed that the modulation had essentially disappeared and a reproduction of a typical streak record is shown in figure 8.15.

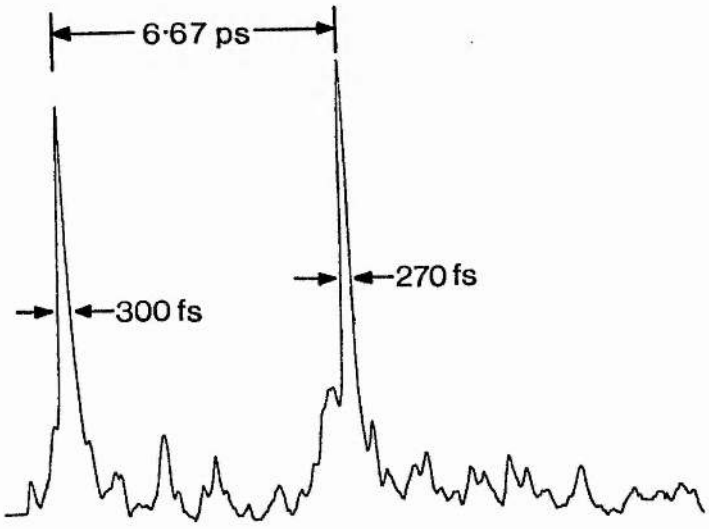

Figure 8.15. Streak record showing 300fs temporal resolution.

The recorded streak images have a measured duration of 300fs and 270fs FWHM which was represented by 8 and 7 channels respectively at the image FWHM on the OMA. The measured streak speed, determined from the streak image separation (169 channels and 6.67ps temporal separation) was $2x10^{10}$ cm/s. The measured signal-to-noise ratio was measured at ~6 for the record shown. The observed signal-to-noise ratio was low although much of the noise was attributed to laser-related light directly illuminating the intensifier even though extreme precautions were taken to avoid this effect. Analysis of the dynamic range of this camera was not possible due to the cathode sensitivity deterioration over a few weeks. The effect of this was that insufficient light from the laser was available to provide any noticeable dynamic image pulse broadening and in fact the cathode sensitivity deteriorated to such an extent that the camera became almost unusable at the illumination levels available from the unamplified laser system.

The system jitter was appreciably higher then that achieved with photo-conductive switches and was estimated to be ±20ps over short timescales (~20 shots). On the other hand the synchronisation system proved highly reliable.

8.5 Discussion

The modulation effects caused by the use of a MCP intensifier operated at high gains has proved to be a major problem when evaluating the dynamic performance of the single-shot camera at low light intensities. It is now believed that these effects are due to trace elements (eg. photocathode constituents)within the MCP intensifier, leading to channel cross-coupling. Similar effects have been noted [19] in the operation of a synchroscan camera when operated under similar conditions which infers that the problem is not associated with optically pulsed inputs (as occurs with a single-shot streak camera) as previously thought.

The trigger jitter of the system employed was attributed to both the synchronisation electronics and the avalanche sweep generator which has demonstrated a jitter of less then ±20ps [19] over many shots. It is conceded that the system jitter was considerably higher then that previously mentioned over long time intervals (tens of minutes) but the shot to shot reproducibility was acceptable. The problem of image

capture was further exacerbated by the small viewing 'window' provided by the OMA (~5mm at the image intensifier phosphor output screen) and the high streak speed which resulted in a temporal capture range of ~25ps. However the system proved easy to implement without the requirements associated with photoconductive switches while demonstrating good performance.

Although initial optical laser pulses employed were ~150fs FWHM to reduce the peak current density within the camera, theoretical and experimental evidence [21] indicated that this would not effect the observed result obtained. Pulse durations between 50fs and 200fs were employed during the course of this work and while 300fs represents the optimal temporal resolution attained, it did not seem to be increased when employing shorter optical pulses, thus no experimental evidence is suggested to contradict the results reported.

8.6 Conclusions

Although many workers claim subpicosecond resolution for their streak camera designs on the basis of computer simulations, such resolution is rarely demonstrated. Recently a magnetically focussed streak camera has had an experimentally demonstrated a temporal resolution of 500fs, but the streak camera we employed is the first electrostatically focussed design to achieve a temporal resolution of less then 500fs. At the time of writing, the resultant measurements presented in this chapter represent the shortest optical pulse yet recorded with a linear-response technique. The experimental results reveal that the temporal resolution of the camera employed was 300fs under the conditions indicated. The theoretical evaluations of the camera yield a predicted temporal resolution of 200fs (under the experimental conditions) which is acceptably close to that obtained experimentally. Further advances in the development of ultrahigh speed electron-optical streak cameras are required to attain the theoretically achievable temporal resolution of 10 fs, however the results presented indicate that sub 500 fs temporal resolution is now a reality.

References for Chapter 8

1 K Kinoshita, M Ito, Y Suzuki

Rev. Sci. Instrum., 56 (6), 932, 1987

2 A Finch, W Sibbett, W E Sleat

Rev. Sci. Instrum., 60 (5), 839, 1989

3 J P Willson, W Sibbett, W E Sleat

Opt. Comm., 42 (3), 208, 1982

4 K Kinoshita, T Kato, Y Suzuki

Proc. 14th ICHSPP. (Moscow), 199, 1980

5 M R Baggs

Ph.D Thesis, University of London, 1983

6 H Niu, H Zhang, X H Wang, Q L Yang, Y P Liu, Y C Weng, Y A Reng, J L Zhou

Proc. 18th ICHSPP (Xian), SPIE 1032, 468, 1988

7 W A Baum

Advances in Electronics and Electron Physics, 16, 391, 1962

8 R L Fork, B I Green, C V Shank

Appl. Phys. Lett., 38 , 671, 1981

9 J A Valdmanis, R L Kork, J P Gordon

Opt. Lett., 10, 131, 1985

10 A Finch, G Chen, W E Sleat, W Sibbett

J. Mod. Opt., 35, 345, 1988

11 S Majumdar

Proc. 12th ICHSP (Toronto), SPIE 97, 1976

12 H Nui, W Sibbett

Rev. Sci. Instrum., 52 (12), 1830, 1981

13 R Kalibjan, GG Paterson

Proc. 15th ICHSPP (San Diego), SPIE 348, 195, 1982

14 M R Baggs, R T Eagles, W Margulis, W Sibbett, W E Sleat

Advances in Electronics and Electron Physics, 64B, 617, 1985

15 W Knox, G Mourou, S Letzring

Proc. 15th ICHSPP (San Diego), SPIE 348, 308, 1982

16 G Mourou, W H Knox, S Williamson

'Picosecond Optoelectronic Devices', Chapter 7, 219, 1984

17 M C Jackson, R D Long, D Lee, N J Freeman

Laser and Particle Beams, 4, 145, 1986

18 H Howe Jnr.

'Stripline Circuit Design', Chapter 2, Published by Artech House Inc., 63, 1974

19 R T Eagles

Ph D Thesis, University of London, 1986

20 A Finch, Private Communication, St Andrews Univ., 1988

21 M Suyama, K Kinoshita

Proc. 18th ICHSPP (Xian), SPIE 1032, 448, 1988

22 A Finch, Y Lui, H Nui, W Sibbett, W E Sleat, D R Walker, Q L Yang, H Zhang

'Ultrafast Phenomena VI', Springer Series in Chemical Physics Vol. 48, 159, 1988

Chapter 9

General Conclusions and Proposed Camera Design Modifications

9.1 UV-Sensitive Picoframe Framing Camera

A vacuum demountable Picoframe type framing camera has been costructed and tested in static and dynamic modes of operation. The camera was designed such that UV and X-ray sources could be employed to test the imaging capability at these wavelengths. UV radiation from a frequency-quadrupled Nd:YAG laser (266nm) was initially employed for static and dynamic testing of the camera in different modes of operation using a simple UV-sensitive gold photocathode. The limiting static spatial resolution of the image tube was 20 lp/mm (under constant illumination) when referred to the photocathode and the usable cathode area exceeded 6mm x 6mm. The limiting spatial resolution of the Mullard XX1330A (50/40) image intensifier and camera combination was 14 lp/mm at the photocathode. Dynamic testing of the UV-sensitive Picoframe I employing one framing aperture was undertaken and a dynamic spatial resolution of ~8 lp/mm has been achieved in single and double frame modes (using pulse forming networks). The frame exposure times achieved with this camera were ~100ps and ~250ps FWHM respectively for the single and double frame modes, and the inter-frame time 1.5 to 2ns for the double frame mode.

The Picoframe II variant employing two framing apertures has enabled the generation of two frames with the application of single linear voltage ramps, and was thus easier to operate then the Picoframe I double frame system. Limiting dynamic spatial resolution of > 8 lp/mm (when referred to the photocathode) has been attained for both frames while demonstrating frame and inter-frame times of 120 ps FWHM and 400 ps respectively. This camera geometry has also been operated in four-frame mode (not possible with the Picoframe I design due to the difficulties in generating suitable deflection waveforms) by the inclusion of 'shift plates' within the drift region. Dynamic spatial resolution of 6 to 7 lp/mm (referred to the photocathode) has been achieved for all frames, demonstrating frame and inter-frame times of ~250ps and ~1ns respectively.

9.1.1 X-ray-Sensitive Picoframe Camera

Further evaluation of the Picoframe camera design under soft X-ray illumination conditions has been achieved using the self-emission of a laser produced plasma. Approximately 4 J in 100 ps FWHM of 532nm laser radiation was focused to a 30μm diameter spot onto a gold foil target. The resultant power density was ~10^{15} W/cm^2 and the X-ray emission was reasonably broad band within the range 1 to 3 keV. Gold photocathodes on both beryllium and aluminium substrates were usually employed but caesium iodide cathodes were also tried in an unsuccessful attempt at improving the dynamic spatial resolution. Beryllium substrates proved to be highly transparent to the X-rays, and the sensitivity of the gold photocathode was such that aluminium filters were required to produce well exposed images at moderate intensifier gains and so aluminium substrates were adopted.

The limiting dynamic spatial resolution of the Picoframe I camera under soft X-ray illumination conditions in single and double frame modes was 6.35 lp/mm and 5 lp/mm (for both frames) respectively when referred to the photocathode, while the usable cathode area was determined to be 6mm x 6mm. Direct evaluation of the exposure times under X-ray illumination was not possible and so temporal evaluation was undertaken on the frequency-quadrupled Nd:YAG laser. This yielded frame exposure times which were less then that actually expected on the X-ray-sensitive system due to the higher secondary electron emission energy spread (hence increased electron beam diameter at the framing aperture plane) from the X-ray-sensitive photocathodes employed. Similar frame exposure durations were measured to those already mentioned for the UV-sensitive camera. The Picoframe II X-ray-sensitive camera demonstrated a limiting dynamic spatial resolution of 4.5 lp/mm for both frames when referred to the photocathode, while the temporal characteristics have been outlined for this design.

The reason for the reduced dynamic spatial resolution of the Picoframe camera design under X-ray illumination was attributed to the higher secondary electron emission energy spread. This causes an increase in electron beam diameter in the crossover region, which is then deleteriously effected by the dynamic electrostatic deflector fringing fields when employing fast sweep speeds. Thus the dynamic spatial

resolution was degraded. Caesium iodide photocathodes showed no noticeable improvement in dynamic spatial resolution even though the secondary electron energy spread is ~2eV instead of ~4eV for the gold cathode, but a higher sensitivity was apparent.

9.1.2 Deflector Improvements

An attempt was made to reduce the dynamic fringing field effects associated with the deflectors by employing specially designed and constructed travelling-wave deflectors. Under UV illumination conditions the Picoframe I demonstrated ~10 lp/mm dynamic spatial resolution (when referred to the photocathode), but frame times of 180ps FWHM resulted because of impedance matching conditions. Increasing the characteristic impedance of the deflectors will increase the achievable scan speed (hence reduce the frame time), but terminations would have to be employed within the camera vacuum envelope which may prove difficult due to space restrictions.

When employing standard deflectors a new cylindrical electron-optical lens was introduced between the framing and compensation deflection plates. This enabled the defocussing effect of the deflectors to be compensated in the orthogonal direction, and under UV illumination conditions and single frame mode, frames of dynamic spatial resolution ~9 lp/mm were achieved with a frame exposure time of ~100ps FWHM.

The dynamic range of the UV/X-ray-sensitive Picoframe camera family has been evaluated both experimentally and theoretically. The indicated dynamic range is ~50 for a resolution of 10 lp/mm (referred to the photocathode) in both directions when the USAF resolution test chart is employed.

9.1.3 Repetitive Operation

Repetitive operation of the sealed-off visible-sensitivity Picoframe I camera version has been achieved by applying 333MHz deflection waveforms to the framing and compensation deflectors, resulting in frame exposure and inter-frame times of ~250ps FWHM and 1.5ns respectively. Multiple framing capability with the introduction of shift plates is ensured with this technique and the dynamic spatial resolution attained for the two frame was 12 lp/mm when referred to the photocathode.

It may be that such an operating scheme may be employed in future development of the UV / X-ray-sensitive vacuum demountable device as multiple image formats may be attained without recourse to ultra-fast high voltage switching devices.

9.1.4 Further Developments of the Picoframe Camera

Further optimisation of the electron-optical lens was attempted in order to increase the separation of the anode and framing apertures without increasing the framing aperture diameter or reducing the usable photocathode area.

$$T = \frac{(a + E_d)\, 2\, V_a\, d}{l\,(\frac{1}{2} l + L)\, V_d} \qquad (9.1)$$

Equation 9.1 shows the calculated frame-time T available from a given geometry where l is the framing deflector length, L is the distance between the end of the framing deflectors to the framing aperture, V_d is the deflection voltage gradient (V/s), d the framing deflector separation, V_a the axial electron accelerating voltage, E_d the electron beam diameter at the framing aperture and a, the framing aperture diameter. Decreasing T is possible by decreasing a, E_d, V_a or d or increasing l, L, or V_d. Simply increasing V_d , l and decreasing d is not sufficient to generate high spatial resolution images with low exposure times when using plane plate deflectors due to the resultant increase in the dynamic spatial distortion of the image due to electrostatic fringing field effects and finite electron deflector transit time. Thus L should be increased or a and E_d should be decreased while not reducing the usable cathode area. Unfortunately this is not possible to do arbitrarily [1] and compromise between the various factors is essential [2]. Optimisation was achieved with the use of computer simulations of the electron trajectories within the electrostatic image tube.

Due to the requirements of the electron-optical lens for the framing camera, ie. long thin 'crossover', large usable cathode and only moderate spatial resolution a purely graphical design approach was adopted. No attempt was made at evaluating the modulation transfer function [3] or the temporal spread function [4] as is usual during

the design of a streak camera. Evaluation of static spatial resolution was then left to experiment in which use was made of a vacuum demountable system.

9.1.4.1 Computer Aided Design

The computer simulation programme was standard in nature [5], determination of the potentials within the desired rotationally symmetrical region was achieved by the solution of the Laplace equation at discrete points on a mesh set up within the volume. The electric field is then evaluated using interpolation and differentiation routines [6]. The electric field at any point defined within the boundary conditions may then evaluated from numerical interpolation [7]. Electron trajectories were then analysed by solving the equations of motion for an electron in a electrostatic field, thus producing an electron 'ray -tracing' diagram. A more complete description of the computer simulation procedure may be found elsewhere [9]. From this, the magnification, focal plane location, usable photocathode area, and aperture diameters required may be determined and so rapid development of system may be achieved. The resultant output was via a high resolution video monitor, showing the electrode structure, the potential field lines set up by the electrodes and the electron trajectories through the system.

Under the conditions of the simulation the initial electron energy spread emitted from the photocathode was 0.6eV, as it is expected that suitable cathode materials may be found to cover the required usable range to yield this figure. Electrons were emitted at 0 and 45 degrees to the normal of the photocathode and at 45 degree intervals around the axis of the system, ie. 32 electrons from each cathode point chosen. Cathode points at up to ±3mm off the image tube axis were chosen to determine the maximum electron beam diameter at the anode and framing apertures when the full cathode was illuminated. The calculation mesh size adopted was 1mm as increased accuracy was not required and would increase the calculation time appreciably.

9.1.4.2 New Electrode Structure

Although the basic three electrode structure of the electron-optical lens was maintained it was felt that improvement of the electrostatic imaging properties may be achieved by the adoption of shaped electrodes. This yields a 'two lens' system which

weakly focuses the electrons to form an extended crossover. The overall potential of the electrostatic lens was reduced from 15kV to 12kV in order to increase the deflection sensitivity slightly, while the mesh cathode separation was 2mm and the potential difference 4.6kV. The simulated system focused at the following electrode voltages (from cathode to anode), -12kV, -7.4kV, -9.7kV, 0V yielding an electron-optical magnification of -1.8 with an optimum focal plane found to be 420mm distant from the photocathode. The electrostatic lens structure was shortened from 194mm for the Picoframe design to 134mm and so the electron drift region was extended by 20mm. The resultant electron crossover was situated 55mm (with an estimated diameter of 1mm) from the 3.5 mm diameter anode aperture. The electron beam diameter at a distance 72 mm from the anode aperture was <1.8mm and so a 1.6 mm framing aperture was chosen at this plane. This allowed compensation deflectors to be designed to have an equal deflection sensitivity to the framing deflectors. Figure 9.1 shows a reproduction of picture taken of the high resolution monitor output, showing the electrode structure and electron trajectories in the top section, and the electrode structure and regions of constant refractive index (analogous to optical refractive index) in the lower section. This effective index is calculated from the electrostatic potential distribution and is a result of the principle of least action. The two lenses are clearly seen in figure 9.1.

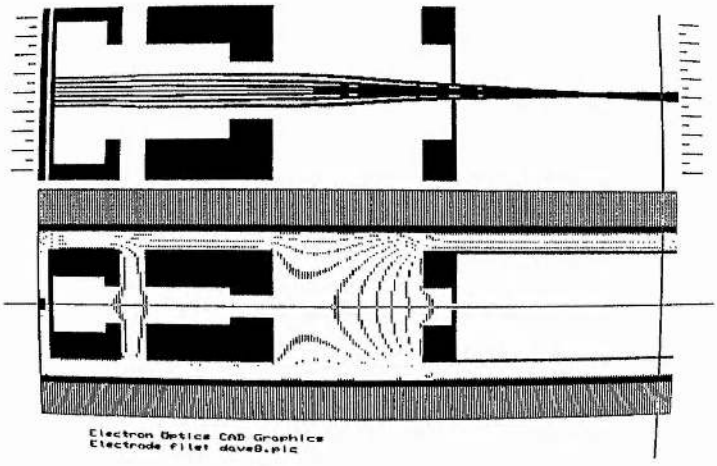

(a)

Figure 9.1(a) Computer simulation output of the optimised electron-optical framing camera lens section.

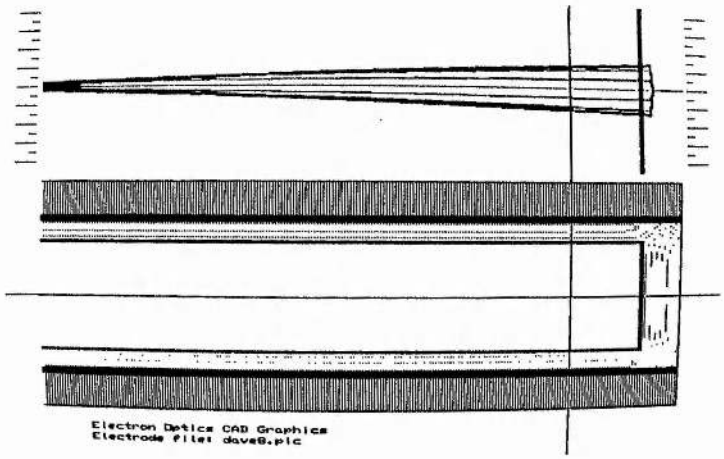

(b)

Figure 9.1. Computer simulation output of the optimised electron-optical framing camera drift region (b).

The electrode dimensions and relative position within the system are shown in figure 9.2.

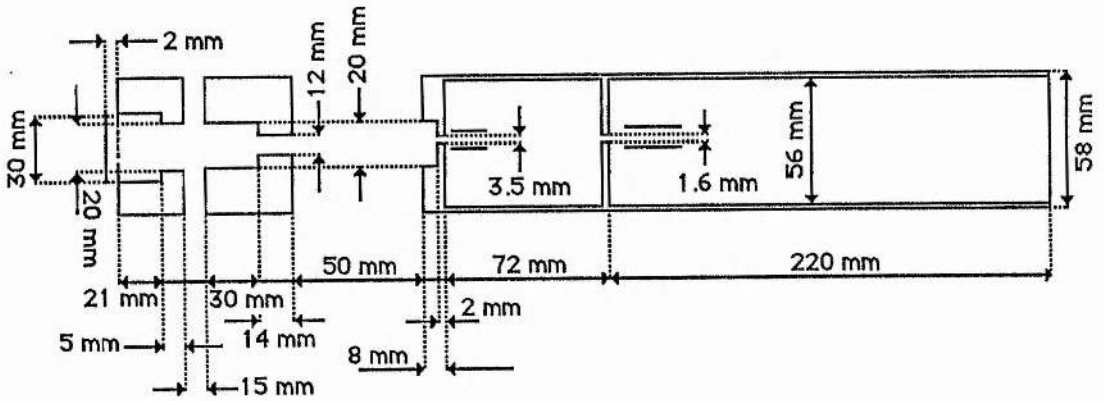

Figure 9.2. Dimensions of the elements within the new electron-optical lens design.

Framing deflectors 12mm long, separated by 4.5 mm and located 2mm from the anode aperture provide a dc deflection sensitivity of 0.69 cm/kV as opposed to the value of 0.49cm/kV for the Picoframe design to the framing aperture. Compensation deflectors 15.5mm long separated by 4.5 mm provide equal deflection sensitivity to the phosphor screen and so aid in compensation of the image. The calculated frame exposure time of this new design when employing deflection voltages identical to those used during the evaluation of the Picoframe camera is 65ps FWHM, a significant

improvement over the old design.

9.1.4.3 Demountable Camera

Static spatial resolution evaluation of the system was achieved with a vacuum demountable image tube and UV-sensitive cathode. The three machined aluminium lens electrodes were mounted on steel bearers and PTFE insulation bushes while the copper mesh (60 cells/mm) was located onto the first electrode with a 0.2mm thick machined stainless steel plate. The gold or aluminium coated fused silica (1/2 inch diameter) cathode (with a USAF resolution test chart mask) was located using nylon screws and PTFE separators to the first electrode, thus the required cathode mesh separation was easily achieved. The drift tube section was constructed from 1mm thick machined aluminium tubing with the required inside diameter, and the framing aperture was machined out of a 1.2mm thick steel plate. The relative positioning of all the electrodes, cathode and framing apertures were all easily altered to allow changes to be made if required.

The entire assembly was located within a vacuum system with windows located at either end to allow UV illumination of the photocathode and observation of the P20 phosphor screen mounted on the drift tube. The required voltages were applied via Brandenburg high voltage connectors and an Alpha series high voltage power supply and resistive divider network. The vacuum system employed (rotary and oil diffusion pump combination) was capable of attaining vacuums of better then 10^{-5} Torr. Illumination of the photocathode was achieved with a 200W mercury arc lamp providing high output in the UV spectral region.

The experimental image tube focussed at the voltages predicted (± 100V) and the limiting static spatial resolution was measured at 25 lp/mm referred to the photocathode at the centre of the photocathode (as opposed to 20 lp/mm measured for the Picoframe design). No image distortion was noted over the cathode test chart employed (6mm x 6mm) and it was indeed confirmed that a 1.6 mm diameter framing aperture could be located 72mm from the anode aperture without any detectable attenuation of electrons reaching the phosphor screen under UV illumination conditions. The electron-optical magnification was measured as -1.9 with the voltages indicated.

Insufficient time during the course of this project was available for dynamic evaluation of the new design, however indications are that the dynamic spatial resolution of the device should equal or exceed that of the present design employed. The frame exposure time of the system in single frame mode with a single framing aperture or double frame mode employing two framing apertures is expected to be significantly reduced from ~100ps FWHM to ~65ps FWHM when employing simple parallel plate deflectors and the currently employed avalanche transistor circuits. As such this design offers a distinct advantage over that of the one currently employed, but it must be conceded that further optimisation may be required before the all of the stringent requirements of the visible / UV / soft X-ray-sensitive framing camera have been met.

9.2 Streak Cameras

Development of streak cameras into the femtosecond temporal regime is being actively pursued by many workers due to their unique ability to record ultra-short optical phenomena using linear processes and maintain multichannel abilities where optical information is presented along the length of the slit. As such the experimental verification of the computer predicted temporal resolution of an ultra-high speed streak camera indicates that the modelling processes involved are accurate and the practical difficulties met during construction and evaluation may be overcome.

9.2.1 Single-Shot Streak Camera

A new streak camera designed for single-shot operation has been experimentally evaluated using a colliding pulse mode-locked ring dye laser, capable of directly generating optical pulses as short as ~20 fs. The streak camera electron-optics were designed to provide low temporal distortion of an electron 'packet' emitted from the photocathode and hence maintain temporal resolution. It's design was based upon the Photochron IVM type of electrostatically focussed streak camera but was modified to allow lower operating voltages to be employed. The cathode was designed to have a low secondary electron emission energy spread but proved to be insensitive and unstable. The deflection structure employed was of the travelling-wave type meander

line in order to reduce the undesired effect of dynamic fringing fields associated with standard deflectors. This enabled high streak speeds to be attained ($2x10^{10}$ cm/s) with only moderate deflection waveforms (±3kV in 1.5ns) at a total electron accelerating potential of 8kV. The cathode extraction field was 41 kV/cm (with a cathode mesh separation of 1.2mm), and given the expected electron energy spread from the photocathode of 0.1ev yields a minimum analytical temporal resolution of ~140 fs in the cathode-mesh region alone. The static spatial resolution of the electron-optical lens was evaluated at 50 lp/mm (referred to the photocathode) and the magnification determined to be -2. The temporal performance of the device was evaluated using computational techniques to be 250 fs under the operating conditions imposed, and an experimentally achieved resolution of 300 fs FWHM has been demonstrated. At time of writing this represented the fastest linear recording system reported to our knowledge and future developments are expected to improve this value.

Further developments to streak camera design are required to increase their temporal resolution and usable dynamic range. The camera tested was largely limited by the photocathode extraction field that could be employed due to cold cathode discharge. Pulse biasing of the photocathode or mesh is possible, and in this way the extraction field may be increased, however damage to the image tube and image defocussing often occurs due to voltage transients and reproducibility is adversely effected. For these reasons the technique is only adopted as a last resort and is not to be recommended. Preliminary evaluation of an image tube circumventing these problems has been achieved and forms the material for section 9.2.2.

9.2.2 New Design Concept

Previously the mesh electrode was introduced to increase the cathode extraction field, whereas recent design developments have revealed that this electrode may be disposed of and so reducing the image tubes susceptibility to mechanical damage. This is an important feature to be considered if the camera is to be used in an environment in which it may be subjected to harsh vibrational shocks which may easily rupture the mesh electrode. Other reasons for persuing the development of a meshless streak camera include (i) improved spatial resolution due to the lack of mesh electron-optical

microlensing and (ii) an improved camera efficiency as ~30% of the electrons emitted from the photocathode are intercepted by the mesh in a standard design. The criteria adopted in the design of the new image tube were (i) high extraction field, (ii) short electron-optical lens with no low field regions, (iii) low electron-optical magnification, and (iv) high deflection sensitivity. Using the simple graphical design approach previously outlined to evaluate the feasibility of a meshless design the following electrode structure shown as figure 4.3 was arrived at.

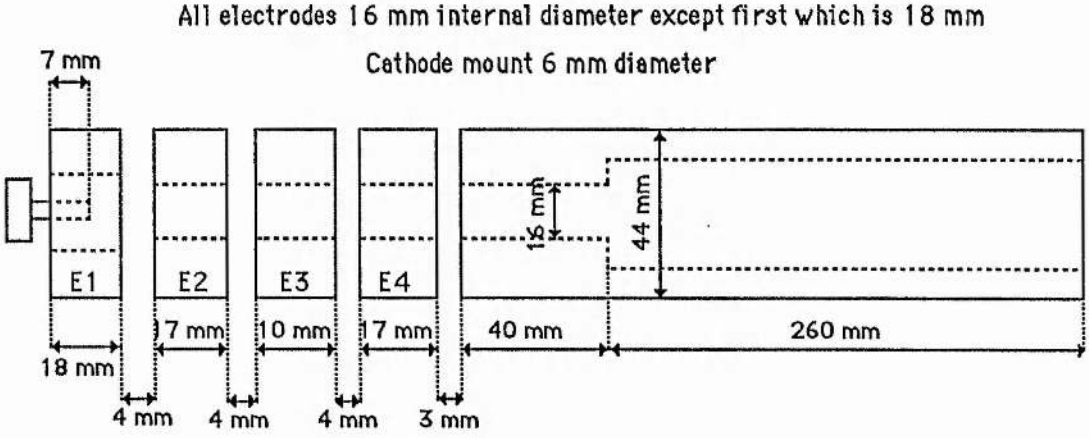

Figure 4.3 Electrode structure for a computer-aided design meshless streak tube.

The cathode was mounted in a reentrant fashion into the first electrode forming the electrostatic lens. Computational analysis indicated the voltages to be employed with this design to allow the focal plane to be 370 mm from the photocathode, cathode -18kV, E1 +6kV, E2 -8.75kV, E3 +6kV, E4 -10kV, anode 0V. The relevant dimensions are shown in figure 4.3.

The electron-optical magnification was determined to be -2.5 at the indicated potentials while the axial electric field perpendicular to the cathode was 12 kV/mm. Due to the non-uniform extraction field over the cathode surface it was clear that this design was only suitable for small usable cathode area applications such as circular scan (in which a point image is scanned circularly by two orthogonally orientated deflectors [10]) or restricted area single shot or synchroscan systems. However due to the high voltages, short lens section and moderate magnification, a good temporal performance can be expected.

9.2.3 Demountable Version

A vacuum demountable experimental image tube was constructed to evaluate the focal properties, spatial resolution and possibility of electrical breakdown between electrodes. It was experimentally verified that the system did focus at the indicated voltages and electrical breakdown was not a problem provided the steel electrodes were carefully polished after manufacture and vacua of better then 10^{-5} Torr were employed. The photocathode employed was a gold or aluminium (~10nm thick) photosensitive layer deposited on a a USAF resolution test chart masked fused quartz substrate. The magnification was measured at between -2.5 and -4 for small variations in applied voltage. The usable photocathode area was determined to be ~0.5 mm diameter at the cathode centre, while the static spatial resolution was determined to be >80 lp/mm when referred to the photocathode. Stray electromagnetic fields caused considerable image blur. Figure 9.4 shows a picture of the static image produced at the phosphor screen as observed through a x100 microscope. Shielding of the system was attempted but no satisfactory method was found.

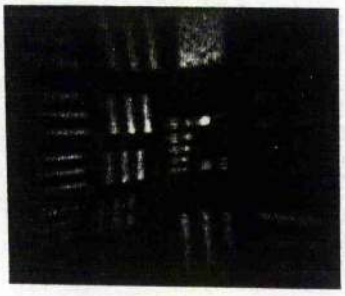

Figure 9.4. Reproduction of the photoelectron image appearing at the phosphor screen of the new camera design.

An extremely narrow electron beam crossover diameter has allowed 20 mm long deflection plates to be positioned 2mm apart to provide a dc deflection sensitivity of ~7cm/kV. This electron-optical design lends itself well to travelling-wave deflection techniques if single-shot operation were desired.

Although analysis of this design is far from complete it has been shown that good spatial resolution and very high photocathode extraction fields are possible if a reduced cathode area is acceptable. The camera proposed offers a new design concept for future streak camera development which may circumvent some of the practical problems

associated with the more 'standard' designs described earlier in this thesis.

9.3 Final Conclusions

The Picoframe camera design has demonstrated single and double frame formats in the visible, UV and soft X-ray spectral regions, and has shown its multiple framing capability in four frame mode with UV illumination. An alternative deflection scheme has been considered using sinusoidal deflection waveforms which has achieved good dynamic spatial resolution and moderate frame and inter-frame times, while ensuring that multiple framing is still possible. It is believed that the Picoframe camera system may now be used as a valuable diagnostic tool in laser produced plasma experiments although future developments are believed possible, such as re-optimised the electron-optical lens and reducing the secondary electron emission energy spread from the photocathode.

It is now firmly believed that the standard deflector arrangement impose serious restrictions upon the dynamic spatial resolution attainable at the high streak speeds required to produce short frame exposure times with this camera geometry. The effect is more pronounced when the electron beam is deflected off the axis (as in the multiframing modes), the beam diameter is comparable with the deflector separation (ie. in the X-ray-sensitive system) and high streak speeds are employed. This latter effect has been observed experimentally where standard deflectors and ultrafast deflection voltage waveforms employed. A single resultant UV frame showed a dynamic spatial resolution of <4 lp/mm and a frame time of ~60ps FWHM. The image was badly distorted and a large magnification difference of the image in the scan and non-scan directions was evident, thus making the system useless.

The secondary electron energy spread for the X-ray-sensitive system may be reduced by utilising different photocathode materials hence reducing the electron beam diameter. Such techniques should yield both shorter frame-times and increased dynamic spatial resolution. It has been reported that [11] potassium iodide may prove to be a suitable X-ray-sensitive photocathode material, but unfortunately insufficient time was available during this work to evaluate this type.

In order to combat the distortion imposed by the plane plate deflectors,

travelling-wave deflectors have been designed and dynamically tested in the UV-sensitive Picoframe design operated in single frame mode. While the dynamic spatial resolution was improved the exposure time was increased over the plane plate deflectors due to impedance matching considerations but it is believed that these may be circumvented in the future.

An alternative scheme has been provisionally inspected in which the distortion effects imposed by the standard deflection plates have been reduced. This system has been dynamically tested in the UV-sensitive Picoframe I design an single-frame mode and has demonstrated superior dynamic spatial resolution while maintaining the ~100 ps frame exposure time.

Design improvements to the electron-optical lensing section of the Picoframe type camera has been undertaken using computer simulation techniques, and the design proposed should provide frame exposure times of approximately one half of those of the present design without reducing the usable photocathode area. It is expected that the dynamic spatial resolution of the new design should equal or exceed the present device performance.

An ultrafast single-shot streak camera employing travelling-wave deflectors has been evaluated and a temporal resolution of 300 fs has been demonstrated. A dependable electronic trigger/shutter scheme has been developed in order that a cw mode-locked ring-dye laser could be employed as an ultrashort pulse test source for the single-shot streak camera. The camera streak deflection was achieved using avalanche transistor circuits for convenience and the total system jitter was found to be ~±20 ps over short timescales.

A new streak camera design has been proposed which does not employ a mesh electrode in close proximity to the photocathode as is usual in ultrahigh speed devices. Computer simulation techniques have allowed the rapid assessment and development of a new design in which high photocathode extraction fields are employed over a limited area, and short electron-optical lensing section.

Vacuum demountable evaluation techniques have allowed the new streak camera to be provisionally tested and the image tube has shown to focus at the simulated potentials. The limiting static spatial resolution of the electron-optical design has been

measured and found to be ~80 lp/mm when a UV-sensitive photocathode was employed. It is confidently expected that this design will demonstrate subpicosecond temporal resolution in the soft X-ray spectral region.

Although UV and soft X-ray-sensitive ultrafast streak and framing cameras have been primarily developed as laser-produced plasma diagnostics, an increasing amount of interest is being shown by other workers. Ultrafast one and two dimensional (temporally or spatially resolved) linear diagnostics are now becoming useful in photobiological investigations within the water 'window' spectral region around 2.3nm to 4.4 nm. At present, contact X-ray microscopy is used in conjunction with laser-produced plasmas emitting X-rays in the 280 eV to 530 eV spectral range [12, 13]. It is expected that the soft X-ray-sensitive framing camera, capable of taking multiple ultrafast pictures along the same line of sight will assist in the collection of data from these experiments. Interest is also being shown in temporally / spectrally and spatially resolving techniques in connection with work being undertaken into the feasibility of X-ray lasers [14]. When the active gain medium of these lasers is a laser-produced plasma, it is imperative that the temporal, spatial and spectral emissions are accurately known in order that lasing may be achieved and confirmed.

These are just two of the more topical areas of interest where UV and soft X-ray-sensitive streak and framing cameras are expected to make considerable contributions in the next few years.

References for Chapter 9

1 P Grivet

'Electron Optics', 2nd English Edition, Pargamon Press, 1972

2 M R Baggs

Ph.D Thesis, University of London, 1983

3 J C Richmond

Advances in Electronics and Electron Physics, 40B, 519, 1976

4 H Nui, W Sibbett, M R Baggs

Rev. Sci. Instrum., 53 (5), 563, 1982

5 B A Carre

Compt. J., 4, 73, 1961

6 W E Milne

'Numerical Calculus', Princeton University Press., 1948

7 C F Gerald

'Applied Numerical Analysis' 2nd Ed.

Addison-Wesley, 1978

8 eg. R T Eagles

Ph.D. Thesis, University of London, 1986

9 A Finch

PhD. Thesis, St. Andrews University, 1989.

10 W Sibbett, W E Sleat, W Krause, J R Taylor

Proc. 16th ICHSPP, SPIE 491, 76, 1984

11 B L Henke, J Liesegang, S D Smith

Physical Reviews B, 19 (6), 3004, 1979

12 J Rosser, K G Baldwin, R Feder, D Bassett, A Cole, R Eason

Annual Report to the Laser Faculty Committee

Rutherford Appleton Lab., A4.12, 1985

13 R W Eason

Annual Report to the Laser Faculty Committee

Rutherford Appleton Lab., A4.1, 1986

14 eg. Annual Report to the Laser Faculty Committee

Rutherford Appleton Lab., 1985, 1986, 1987

Acknowledgements

I would like to thank my supervisor Professor Willson Sibbett for his encouragement, support and optimism during the course of this work. Thanks also go to Dr. Sleat who has come up with some interesting ideas and N J Freeman for his help at AWE Aldermaston.

Special thanks must go to Dr. R Eagles who has helped me throughout the work involving the demountable framing camera which would have been impossible without his assistance. The staff at the MERLIN laser facility at AWE Aldermaston are also to be thanked for their efforts in keeping the laser operating (most of the time).

I am grateful to Dr.A Finch for his assistance in the evaluation of the single-shot streak camera, Miss Y Liu and Dr.R Killean for their assistance in the computational modelling and design of the cameras. I would also like to acknowledge the workshop staff at St. Andrews University who made some of the devices, and the boys in the rest of the laser group in St Andrews who maintained a jovial attitude when all else failed.

Finally, I am indebted to the Science and Engineering Research Council and AWE Aldermaston for their financial support during this work.

Publications

Multiple-Frame UV/X-Ray Picosecond Framing Camera
R T Eagles, W Sibbett, W E Sleat, D R Walker, J M Allison, N J Freeman
Advances in Electronics and Electron Physics, 74, 209, 1988

100 ps UV/X-Ray Framing Camera
R T Eagles, N J Freeman, J M Allison,W Sibbett, W E Sleat, D R Walker
Proc. 32nd International Symposium on Optical and Optoelectronic Applied Science and Engineering (San Diego), 1988

Recent Advances Towards a 100 fs Resolution Streak Camera
A Finch, Y Lui, H Niu, W Sibbett, W E Sleat, D R Walker, Q L Yamg, H Zhang
Ultrafast Phenomena VI, Springer Series in Chem. Phys., 48, 149, 1988

Development and Evaluation of a New Femtosecond streak camera
A Finch, Y Lui, H Niu, W Sibbett, W E Sleat, D R Walker, Q L Yamg, H Zhang
Proc. 18th ICHSPP (Xian), SPIE 1032, 622, 1988

Double Frame UV/X-Ray Picoframe framing camera systems
W Sibbett, D R Walker,W E Sleat, R T Eagles, N J Freeman, (In Press)

Four-Frame UV/X-ray Picoframe II Framing Camera
W Sibbett, D R Walker,W E Sleat, R T Eagles, N J Freeman
Proc. 33rd International Symposium on Optical and Optoelectronic Applied Science and Engineering (San Diego), 1989

Theoretical Analysis and Design Considerations of a Picosecond Framing Tube
W Sibbett, Y Liu, D R Walker
Proc. 33rd International Symposium on Optical and Optoelectronic Applied Science and Engineering (San Diego), 1988

Development and Evaluation of a New Femtosecond Streak Camera

A. Finch [1], Y. Liu [2], H. Niu [2], W. Sibbett [1], W.E. Sleat [1], D.R. Walker [1], Q.L. Yang [2] and H. Zhang [2]

[1] J.F. Allen Physics Research Laboratories, Department of Physics and Astronomy,
University of St Andrews, North Haugh, St Andrews, Fife KY16 9SS, Scotland, U.K.
[2] Xian Institute of Optics and Precision Mechanics, Xian, China.

ABSTRACT

The design and measured performance of new femtosecond streak camera are discussed. The experimental setup that has been employed in the assessment of the single-shot streak performance of the camera will be described and data will be presented to show that the present design of camera has a resolution of approximately 300fs. This is very close to its theoretically predicted temporal resolution of 250 fs for current operating conditions. Design modifications aimed to further improve camera performance to its limiting temporal resolution of ~100fs will also be outlined.

1. INTRODUCTION

During the past few years the refinement of mode-locked lasers has led to the direct generation of sub-30fs duration pulses in the visible spectral region[1,2] and pulse durations of ~200fs in the near-infrared range[3]. With additional extracavity amplification and temporal compression pulse durations as short as 6fs at 630nm[4] and 9fs at 800-840nm[5] have been produced. Whereas nonlinear techniques such as second harmonic generation autocorrelation have kept pace with the temporal resolution requirements in the femtosecond domain[4], this has not been the case for the linear-response electron-optical streak camera development. Although subpicosecond temporal resolution was reported for a Photochron II camera about a decade ago[6] the advance towards temporal resolution in the femtosecond regime has been rather slow and the best temporal resolution reported to date is ~0.5ps[7]. In this paper we therefore address the basic performance-limiting features in a streak image tube and describe a design procedure that is aimed at the ultimate achievement of instrumental functions of 100fs or less. Some preliminary experimental data have been included to illustrate that a new camera system in its present state of development has a temporal resolution of approximately 300fs.

2. DESIGN CONSIDERATIONS FOR A FEMTOSECOND STREAK TUBE

Within the general design concept of an image tube having improved temporal resolution in streak operation there are four primary requirements that must be satisfied. These are (i) a 'fast' photocathode from which the electrons are released with a narrow energy distribution, (ii) an electron-optical lens arrangement that provides optimised temporal and spatial characteristics, (iii) a high sensitivity travelling-wave deflector geometry, and (iv) a phosphor screen having an optimum quantum efficiency.

Traditionally no special processing considerations have been applied to the photocathode and so the temporal resolution of the streak tube has been limited by the electron velocity dispersion. However, with substantial improvements in the electron-optics over our earlier Photochron IV design[8] the photocathode performance has become more critical. A standard S20 photocathode has an initial electron energy spread of ~0.6eV whereas a specially tailored photocathode has now been processed with an increased bandgap for which the initial electron energy spread has been reduced to 100 meV at 620nm. The electron emission time has been minimised in an extremely thin cathode which has been introduced to the streak tube using vacuum transfer techniques.

The electrostatic lens configuration is based on the Photochron IV which has a demonstrated single-shot temporal resolution of 700fs[9]. The design has been further improved[10] to be compatible to lower anode voltages while maintaining a high cathode extraction field. Operating voltages of -8kV and -3kV for the photocathode and mesh respectively with regard to the grounded anode are typical. With a mesh-cathode separation of 1.2mm the axial electric field in the cathode vicinity is 40 kV/cm and under these conditions the electron-optical magnification is –2 and a static limiting resolution of 50 lp/mm can be observed on the phosphor screen. For the low energy photoelectrons this phosphor screen was designed to have an enhanced quantum efficiency in order to reduce space charge effects while still providing sufficient luminous gain. A schematic of this new femtosecond streak tube is included as Fig. 1.

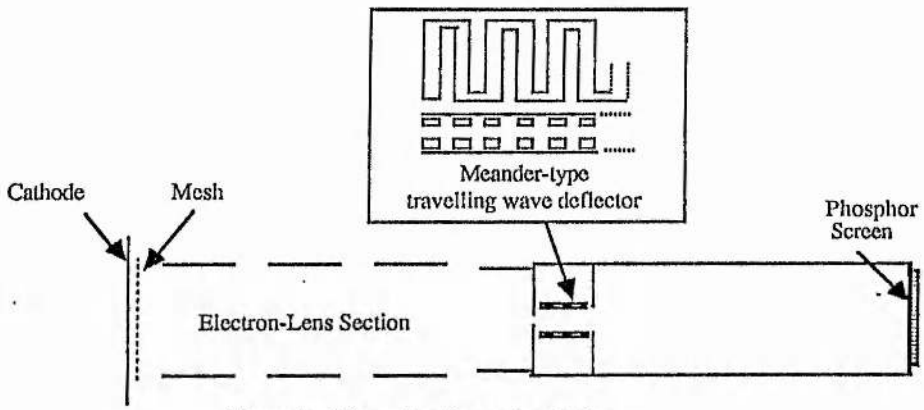

Figure 1. Schematic of new streak tube.

The travelling-wave deflectors[11] represent a major improvement over the more conventional parallel-plate deflectors because they offer both increased deflection sensitivity and frequency bandwidth. The bandwidth of a pair of plate deflectors is largely limited by the electron transit time through the deflector geometry but it is also limited by the impedance mismatch which is always present at a capacitive load. Typically the bandwidth of parallel plate deflectors is restricted to ~300MHz which means that high voltage drivers (+/- 5kV) are necessary in order to achieve the required streak speeds. The travelling-wave deflector system overcomes these problems because the electron transit time through each of the elements is very short and the network can be designed to have a specific characteristic impedance. The applied deflection waveform is propagated along the meander microstrip line which in the present tube crosses the electron beam path 23 times. The meander length and separation of individual lines has been designed to allow correct phase matching between the axial group velocity of the electromagnetic wave and the drift velocity of the signal photoelectrons so that the electron beam is subjected to the same deflection voltage each time it traverses the meander lines. Because of the very short deflector element width (~1mm) this arrangement has the added advantage of reducing the undesired fringing field effects. Unfortunately the fabrication of 50Ω microstrip line with suitable characteristics has proved to be problematical and so the deflection structure used was based on a 100Ω impedance line and the tube was fitted with integral tapered impedance matching systems on all inputs and outputs to the 100Ω travelling-wave structure (see Fig. 2). The insertion loss of all connectors, impedance matchers and deflectors was ~2dB at 200MHz and the frequency response of the deflectors was essentially flat up to 2.5GHz. With the long meander lines (4cm) having a small separation (4mm) it was possible to obtain a deflection sensitivity of 10cm/kV as a consequence of the exploitation of travelling-wave techniques.

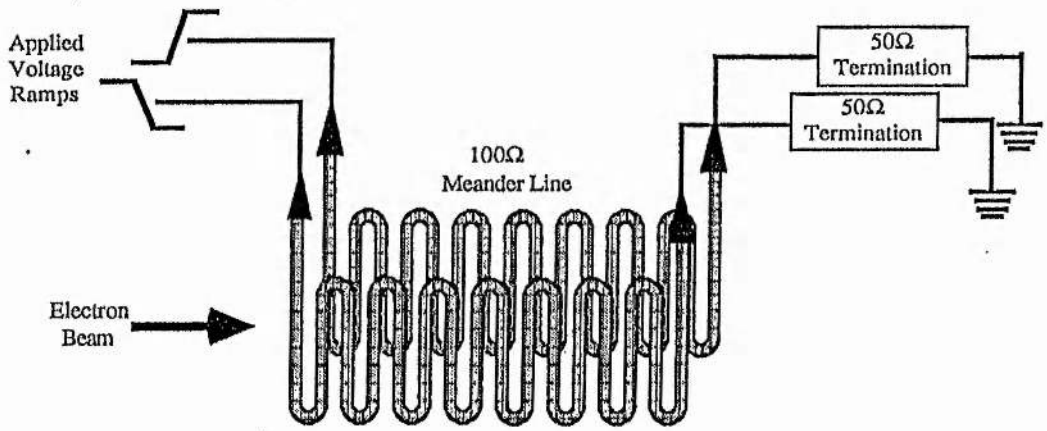

Figure 2. Schematic of deflectors

3. DYNAMIC OPERATION

The dynamic resolution of the streak camera was evaluated using ultrashort pulses from a colliding-pulse, passively modelocked ring dye laser[2]. This operates at a wavelength around 630nm and delivers 20pJ per pulse at a repetition rate o 100MHz at the camera input (see Fig. 3). Our laser was deliberately operated with excess negative group velocity dispersion in the cavity in order to broaden the pulse (150 fs) and thereby alleviate the peak current density within the tube. The purpose of this was to reduce the space charge effects associated with high current densities which leads to a degradation of tempora resolution[12].

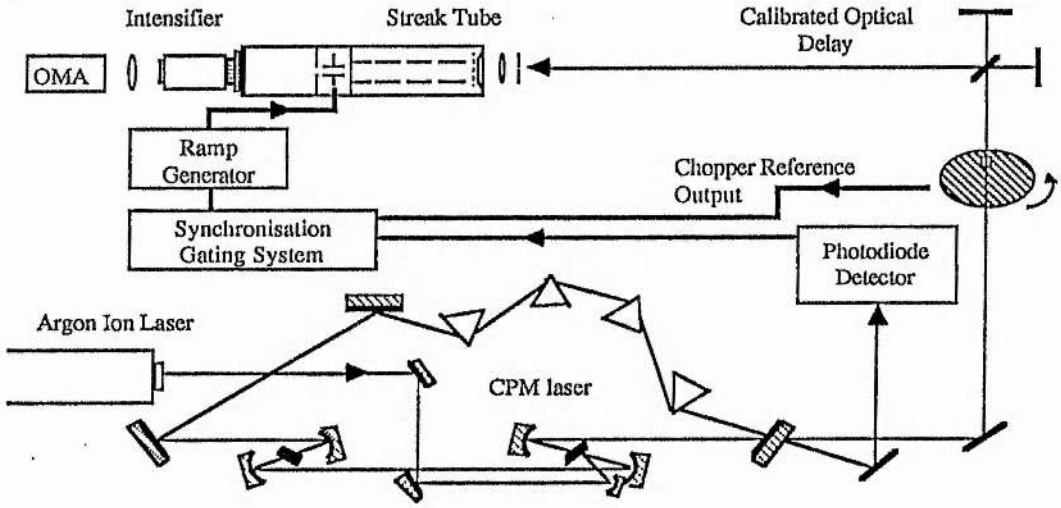

Figure 3. Experimental arrangement.

The microchannel plate intensifier employed was a Philips 21XX unit which was fibre-optically coupled to the output faceplate of the streak tube via a 2cm long fibre-optic block. The intensifier had a measured gain of 10^4 and a limiting spatial resolution of 50 lp/mm at its photocathode. The complete system (streak tube with intensifier) had a total luminous gain in excess of 10^6 which was sufficient to monitor the laser pulses directly without recourse to the multi-stage dye amplifier which was used previously [9]. An Optical Multichannel Analyser (OMA) was used to record and store the streak image data.

The travelling-wave deflectors were driven by a double avalanche transistor chain which produced differential voltage ramps of 3kV with risetimes of 1.5ns into a 50Ω resistive load[13]. The deflectors were terminated using a 100pF capacitor in series with a grounded 50Ω resistor and the resulting streak speed achieved was 2×10^{10} cm/s. These circuits had a measured 1/e recovery time of 800μs following the initial ramp, which caused the streak record to be overwritten. This problem was solved by using an optical shutter in the form of a rotating (20 revs./sec.) chopper wheel containing a 600μm slit. The laser beam was focused through this slit and recollimated before entering the calibrated optical delay line and thus 100 μs gating periods were obtained. The system timing was then arranged such that the chopper reference output was activated when the transmission of the laser beam through the slit was a maximum. An AND gate provided synchronisation between the incident laser pulses and the ramp circuit triggering. Total system jitter which was less than 50ps and was attributed to a combination of AND gate and ramp circuit jitter where the latter has been measured to be less then +/-20ps. Although jitter between the two avalanche transistor chains was not a serious problem it became evident during the experimental assessments that they were not in perfect synchronisation. A slight delay between the two chains (<250ps) caused defocusing of the undeflected electron beam as a result of the non-zero potential on both deflectors but this was readily rectified by refocusing the camera in dynamic mode.

The dynamic intensity resolution of the camera was observed initially to be quite low when a sub-standard Philips 20/30 intensifier having a rather inadequate luminous gain of 10^3 was being used. When this intensifier was operated at its maximum gain in order to achieve recordable image intensities the typical record reproduced in Fig. 4 was obtained.

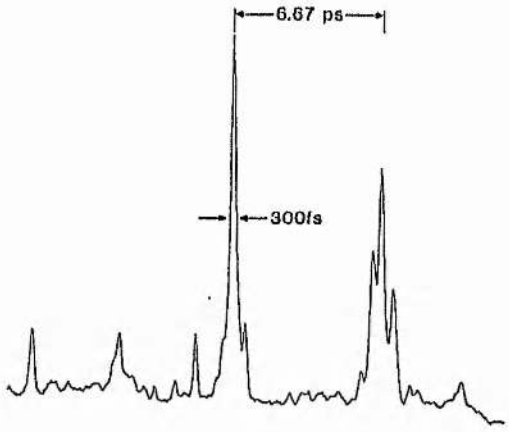

Figure 4. Intensity profile of recorded streak image showing intensity modulation

The source of an observed parasitic modulation in the streak intensity was not obvious, but one possible cause was tha the photoelectron signal was being scattered at the entry to the microchannels and thereby giving rise to cross-talk couplin in the intensifier. Replacing the intensifier with one that could be operated at an optimised gain that permitted the inpu intensity to the streak tube to be reduced by -0.5dB rectified the problem. As previously mentioned the dynamic intensit resolution was poor and this was further exacerbated by the thin photocathode, which transmitted light along the camera axi and illuminated the phosphor which was insufficiently aluminised. This proved to be an inconvenient problem because mos of the background noise was attributed to this origin. This effect was alleviated by directing the incident illumination ont the photocathode at a slight angle and thus reducing the optical signal intensity on the axis of the streak tube. Under thes optimised practical conditions the camera instrumental function was consistently measured to be less then 400 fs and th streak result shown in Fig. 5 shows intensity profiles corresponding to a temporal resolution of approximately 300fs. Thi compares very favourably with the theoretically predicted instrumental function of 250fs for this new streak tube when th above operating parameters are assumed (see Fig. 6).

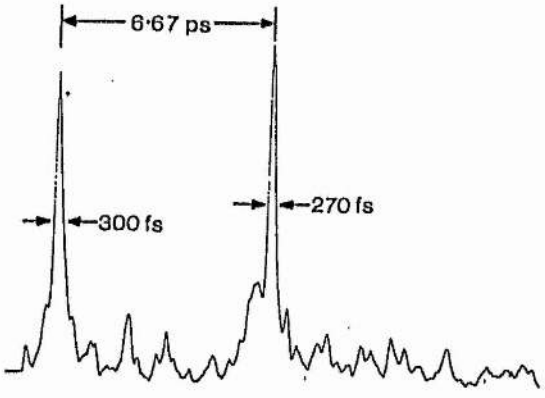

Figure 5. Streak intensity profiles illustrating a temporal a resolution of 300fs

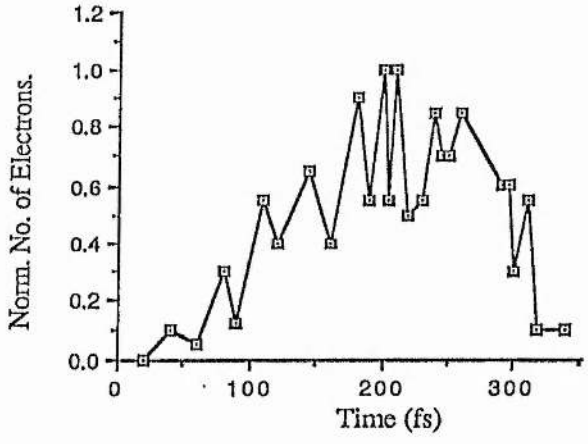

Figure 6. Theoretical Normalized Time Spread Function of tube showing the theoretical temporal resolution to be 250fs (500 electrons traced).

4. CONCLUSIONS

Despite the preliminary nature of these experimental data we are encouraged by the performance of this femtosecond str tube. The travelling-wave deflection system functioned very effectively and enabled high streak speeds to be obtained w moderate amplitude voltage waveforms. It is planned to investigate somewhat higher speed circuitry and laser-illumina photoconductive switches so that further improvement of the streak performance may be realised. Our expectation is tha resolution of better than 200fs could be achieved whenever the tube fabrication procedures permit the design parameters to fully implemented. For instance the mesh-photocathode electric fields must be increased using appropriately applied D.C. gated voltages. With these and other refinements an instrumental function in the region of 100fs is possible for this type camera which should have many applications. For example, direct quantitative measurements of the "solitonic" pulse shap effects that occur in the CPM dye laser system[14] could be made, and more generally, the possibility of electron-opti chronography in the hundred femtosecond regime becomes much more of a practical reality.

5. ACKNOWLEDGEMENTS

The support of this collaborative programme by The Royal Society and The Chinese Academy of Sciences is gratefu acknowledged. Acknowledgement is also made for personal support as a Chinese Royal Fellow (Y.L) and for visits St.Andrews (H.N,Q.L.Y) and Xian (A.F, W.S, W.E.S) by the Royal Society and The Chinese Academy of Sciences. Two us (A.F and D.W) also express our gratitude for CASE PhD Studentships from the Science and Engineering Resear Council.

6. REFERENCES

1. J.A. Valdmanis, R.L. Fork and J.P. Gordon, "Generation of optical pulses as short as 27 femtoseconds directly from laser balancing self-phase modulation, group velocity dispersion, saturable absorption, and saturable gain," Opt. Lett. 131-133 (1985).

2. A. Finch, G. Chen, W.E. Sleat and W. Sibbett, "Pulse asymmetry in the colliding-pulse mode-locked dye lase Journ. of Mod. Opt. 35, 345-354 (1988).

3. N. Langford, R.S. Grant, W. Sibbett and K. Smith, "Dispersion-compensated passively mode-locked colour cen laser", CLEO '88 Tech. Dig. 7, THJ2, 326, (1988).

4. R.L. Fork, C.H. Brito-Cruz, P.C. Becker and C.V. Shank, "Compression of optical pulses to six femtoseconds using cubic phase compensation," Opt. Lett. 12, 483-485 (1987).

5. P.C. Becker, H.L. Fragnito, R.L. Fork, F.A. Beisser and C.V. Shank, "Generation of tunable 9 femtosecond optic pulses in the near infrared," Proc. IQEC '88, Post-deadline paper PD-15, 36 (1988).

6. D.J. Bradley and W. Sibbett, "Subpicosecond Chronoscopy," Appl. Phys. Lett. 27, 382-384 (1975).

7. K. Kinoshita, M. Ito and Y. Suzuki, "Femtosecond streak tube," Rev. Sci. Instrum. 58, 932-938 (1987).

8. W. Sibbett, H. Niu and M.R. Baggs, "Photochron IV subpicosecond streak image tube," Rev. Sci. Instrum. 53, 75 761 (1982).

9. M.R. Baggs, R.T. Eagles, W. Margulis, W. Sibbett and W.E. Sleat, "Subpicosecond chronoscopy using a Photochr IV streak tube," Adv. in Electronics and Electron Phys. 64B, 617-625 (1985).

10. Y. Liu, H. Niu, Q.L. Yang and H. Zhang, "A new subpicosecond streak tube with travelling wave deflector," Pro 5th National Conf. on High Speed Photography and Photonics, China (1985).

11. A. Silzars, "Travelling wave deflectors for high-speed electron beam modulation," Proc. S.I.D 19, 9-16 (1978).

12. H. Niu and W. Sibbett, "Theoretical analysis of spacecharge effects in Photochron streak cameras," Rev. Sci. Instru 52, 1830-1836 (1981).

13. M.C. Jackson, R.D. Long, D. Lee and N.J. Freeman, "Development of X-ray streak camera electronics at AWRE Laser and Particle Beams 4, 145-156 (1986).

14. F. Salin, P. Grangier, G. Roger and A. Brun, "Observation of high-order solitons directly produced by a femtosecon ring laser," Phys. Rev. Lett. 56, 1132-1135 (1986).

Four-frame UV/X-ray Picoframe II framing camera

W Sibbett, D R Walker and W E Sleat

J F Allen Physics Research Laboratories
Department of Physics and Astronomy
University of St Andrews
North Haugh
St Andrews
Fife KY16 9SS
Scotland, UK.

R T Eagles and N J Freeman

AWE Aldermaston
Reading
Berkshire RG7 4PR
England, UK.

ABSTRACT

Electron-optical framing cameras having X-ray/XUV photosensitivities and which can provide a sequence of framed images in the subnanosecond regime are of major relevance and importance to the quantitative monitoring of the kinetics of laser-produced plasmas. Our *Picoframe* family of framing cameras which has been developed comprise specially designed image tubes that permit the recording of single or multiple frames in the picosecond domain. For instance, an experimental UV-sensitive Picoframe I camera system has been demonstrated to have temporal and spatial resolution of 100 ps, 8 lp/mm in single frame format and 250 ps, 8 lp/mm in a double-frame format having an interframe period between 1.5 ns and 2ns.

In this presentation we will describe a double-aperture *Picoframe II* version of this camera and details will be given in respect of the performance of a demountable, UV-sensitive system. Particular emphasis will be devoted to its operation in a four-frame image format where the generation and implementation of appropriate deflection voltage profiles are especially significant. Experimental data will be presented to show that four discrete frames can be recorded with a frame period of 230 ps, interframe time of ~1 ns and a dynamic spatial resolution (referred to the photocathode) of 7 lp/mm. This spatial resolution was retained over the entire area of the 6 mm x 6 mm image geometry at the photocathode. Such a UV-sensitive camera can be readily adapted for operation in the soft X-ray spectral region, as previously reported for the Picoframe I counterpart, and some of the projected performance characteristics will be discussed.

1. INTRODUCTION

With the development of ultra-high power, short pulse lasers significant interest has been shown in their potential use to initiate fusion reactions in microballoon type deuterium-tritium filled targets. In order for the reaction to be efficient it is essential that the target be illuminated evenly on all sides in order to provide uniform compression and hence maintain confinement time. It is therefore important to study the two-dimensional evolution of X-ray self emission of laser-produced plasmas with

various target structures. For this to be achieved an ultrafast framing camera diagnostic is required with a frame time of 100ps and spatial resolution of 10 lp/mm [1] over a usable cathode image format of 5mmx5mm [2]. The cathode should have UV or soft X-ray sensitivity to match the electromagnetic spectrum of the plasma self-emission. Such a camera should also have a multiple frame facility (two or more) with interframe periods of less than 1ns. It is highly desirable for these multiple frames to be temporally separated by as little as 200ps along the same viewing axis so that quantitative analysis of the recorded images can be readily undertaken

2. THE PICOFRAME FRAMING CAMERA

At present the gated Microchannel Plate (MCP) image intensifier with multiple cathodes is able to provide a single frame per cathode with an exposure time as short as 100ps FWHM and a spatial resolution of >10 lp/mm with X-ray radiation [3]. Multiple MCP schemes have been developed [4] but these at present do not allow multiple frames along the same viewing axis in the X-ray spectrum due to the geometrical problems associated with the use of suitable mirrors.

Among the other schemes being investigated [5,6,7] is the Picoframe camera systems which can potentially meet all of the requirements for image framing. Details of the operation of this type of camera have been reported elsewhere [8] so it is only necessary here to briefly review its operating principles. The imaged photons (visible through to X-ray) impinge upon a photocathode placed in close proximity to a fine mesh electrode. This mesh electrode enables the photo-electrons to be accelerated into the electrostatic focusing region after which they form an extended crossover. A ramp voltage applied to a set of framing deflectors sweeps the electrons across a small aperture allowing a short temporal transmission while the set of compensation deflectors has an equal and opposite deflection in order to remove the temporal smearing caused by the framing deflectors. Multiple frames may be obtained by using triangular deflection profiles with a single-aperture Picoframe I camera [9], or a multiple-aperture (Picoframe II) version of the image tube design [10] or a combination of both methods.

3. 4 FRAME UV-SENSITIVE CAMERA

The ability to provide four frames is a major advantage of the Picoframe type of camera and in this paper we present descriptions and performance data for the four-frame operation of an experimental UV-sensitive camera system. In order to generate four frames, two separate schemes may be adopted. Because of space considerations and capacitive cross-coupling effects it is difficult in practice to arrange for more than two apertures and associated compensation plates to be used in multi-aperture options of framing tube design. Therefore, either a single-aperture framing image tube (Picoframe I) may be employed with two triangular voltage waveforms to drive the deflection plates or a double aperture tube (Picoframe II) be chosen which requires only one triangular waveform to be generated for each deflector. With either system spatial separation of the doublet-frames is achieved by providing a suitable voltage ramp to a pair of shift plates oriented orthogonally to the framing and compensation deflectors. These deflectors are located between the compensation deflectors and the phosphor screen as illustrated in fig.1.

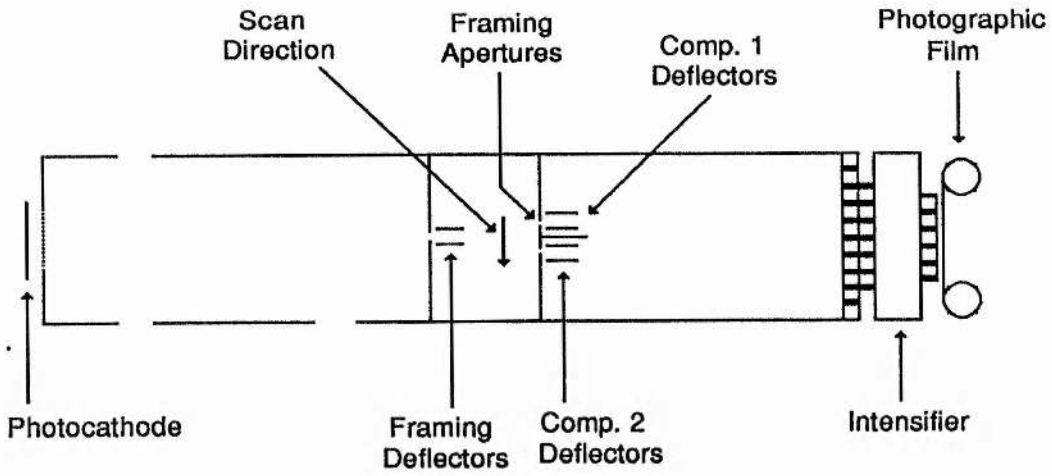

Figure 1. Configuration of Picoframe II camera

The electron-optical design used was based apon the Picoframe II camera system which has provided frame doublets (UV exposure) with a frame time of 100 ps FWHM, interframe time of 400 ps and a spatial resolution of 8 lp/mm [10]. The pulse-forming networks (PFN's), which have been described in detail elsewhere [11], when implemented in conjunction with the avalanche transistor sweep circuits developed at AWE [12] provide triangular voltage waveforms having a peak amplitude of 1200V into a 50Ω impedance load. Due to the DC short required at the end of the stubs used in the PFN, capacitive coupling between the network and the deflection plate was necessary for the application of DC bias, which was set to ± 850V.

In dynamic operation the image forming electron beam is swept over the two framing apertures on the rising edge of the waveform thus producing the first and second image exposures. On the falling edge of the deflection profile the electron beam is swept back across the apertures to provide exposures for images three and four. The first and fourth frames result from aperture one, and the second and third from aperture two. It should be noted that were it not for the shift deflection waveform the first and fourth frames would be superposed, as would the second and third. Consequently frames one and four must experience the same residual bias resulting from dephasing the framing and compensation waveforms. Similarly for the second and third frames, except in the opposite sense. Since the rising and falling edges of the triangular pulse must be suitably phased with respect to each other, this can only be achieved if the waveform width is altered. Idealised voltage waveforms that should be applied to the framing and compensation deflectors are illustrated in figure 2.

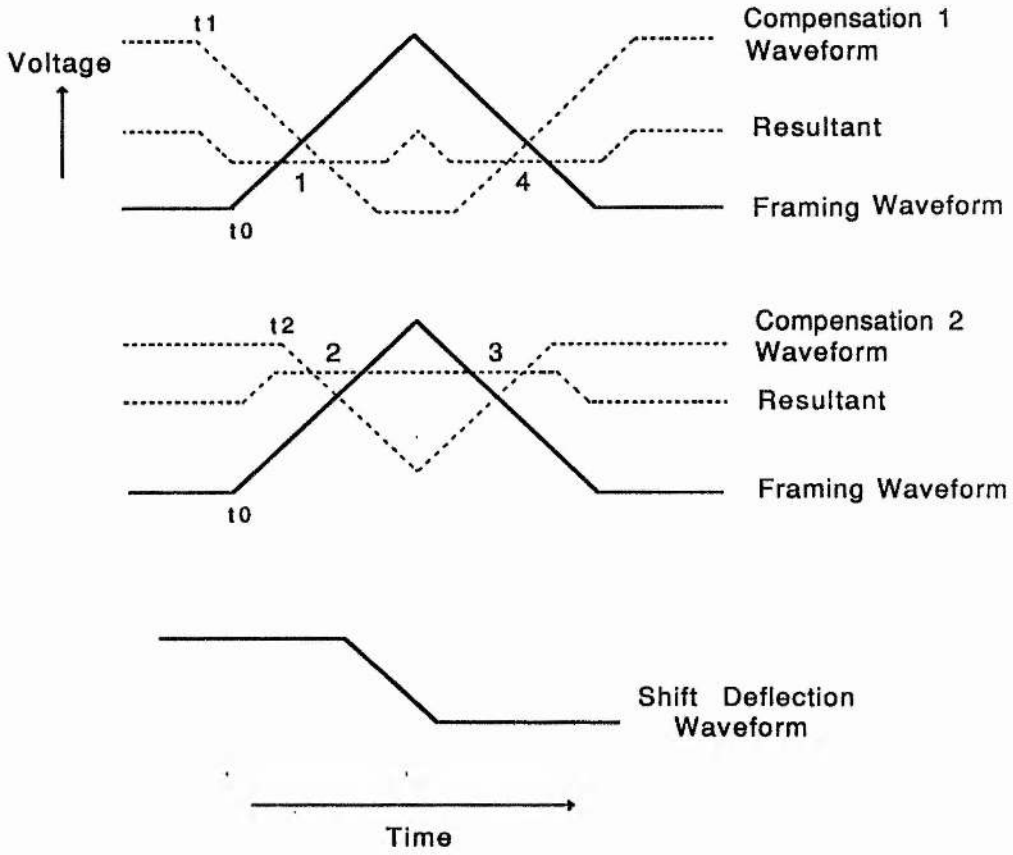

Figure 2. Voltage waveforms and relative timing schedule (allowing for the electron transit time between the framing and compensation plates) for all sets of deflection plates. Start of ramps denoted by t0, t1, t2 and t1< t0, t2>t1.

The performance of the PFN's is rather critical and it was found that conventional 50Ω coaxial cable offered greater design flexibility to the alternative semi-rigid coaxial construction. The 'BNC' connectors associated with the modified design proved to be quite acceptable and no deterioration of pulse shape due to parasitic inductance or capacitance was observed. Three different sets of PFN's were constructed to provide tailored voltage pulse profiles having 2ns FWHM (for the framing deflectors), 3ns FWHM (for the first set of compensation deflectors) and 1.5ns FWHM (for the second set of compensation deflectors). It was not possible to generate voltage profiles with less then 1.5ns FWHM without loss of amplitude due to the limited risetime of the avalanche transistor circuits (1.5ns) and so the DC bias used exceeded half the waveform amplitude so that the apex of the triangular pulse could be used. This non-ideal pulse width resulted in slight displacement of frame 3 but did not cause any noticeable image deterioration. The alternative solution to this problem would be to increase the triangular pulse width applied to the framing plates, but this was regarded as inappropriate in that the inter-doublet time would be proportionately increased.

Doublet separation was achieved by providing a step impulse to the shift deflectors as indicated previously. These deflectors comprised two parallel plates 25mm long, 20mm wide, with a separation of 20mm for which the DC deflection sensitivity was 10mm/kV at the applied anode potential of 15kV. A fast avalanche transistor circuit providing a 0V to -3kV voltage swing in 400ps into a 50Ω load [13] was employed to drive the shift deflectors in an asymmetric mode. The attenuated output was capacitively coupled to one shift plate with a DC bias supplied via a suitable high value resistor. The other shift plate was maintained at anode potential. The risetime of the deflection plates (limited by the electron transit time) was evaluated to be about 500ps and so the risetime of the deflection circuit and plates was ~700ps. This limited the temporal separation between the frame doublets. A general layout of our full electronic arrangement is shown in fig.3.

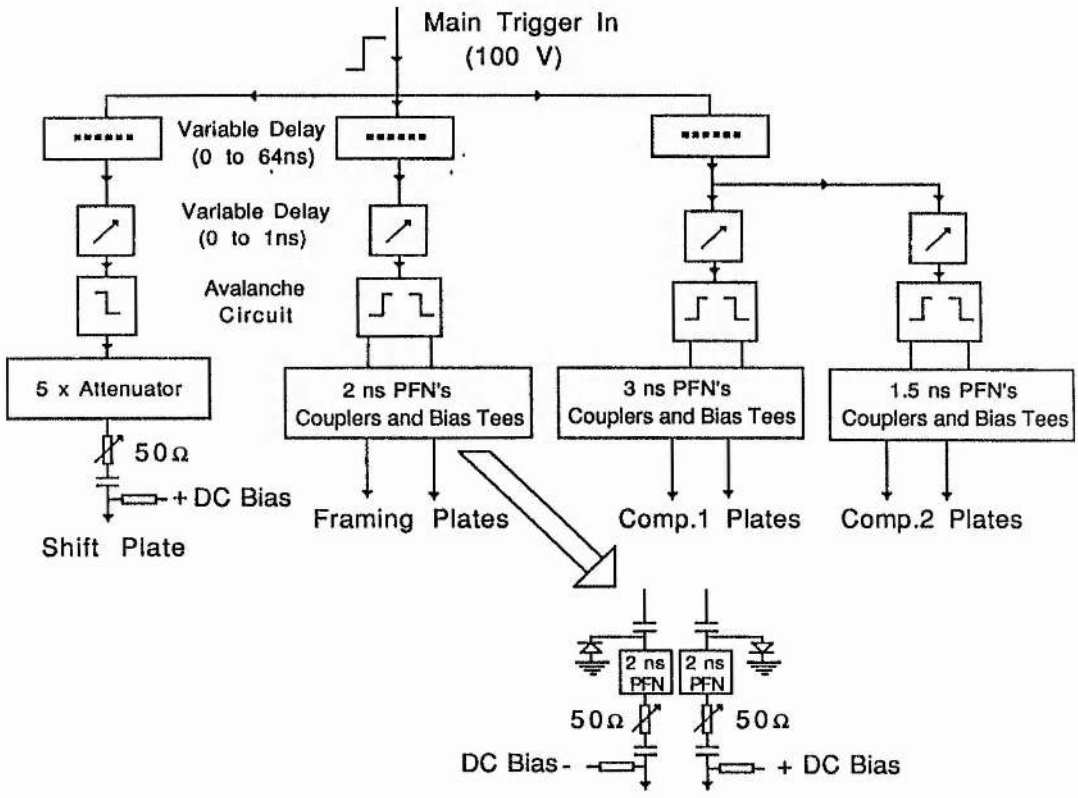

Figure 3. Drive electronics for 4-frame operation

To test this UV-sensitive, multiple-framing camera a Q-switched and mode-locked Nd:YAG laser was employed. A single mode-locked pulse was selected, amplified and frequency quadrupled to provide a 60 ps FWHM pulse at 266nm with an energy of 2mJ. In order to produce four pulses of variable temporal separation and of approximately equal amplitude a Michelson type optical delay and beam-splitter arrangement was adopted (fig.4).

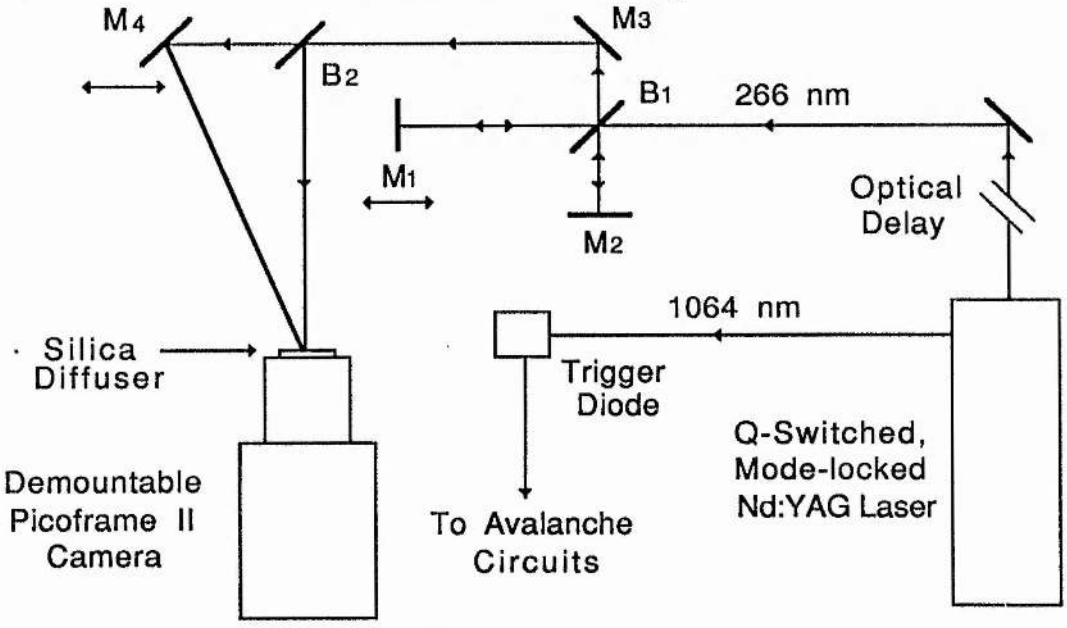

Figure 4. Arrangement of optical system

With mirrors M_1 and M_4 on translation stages it was possible to control the temporal separation between pulses 1 and 2 (via M_1) and 2 and 3 (via M_4) but it was not possible to alter the temporal separation of pulses 3 and 4 without altering that of 1 and 2. It was thus essential that the rate of change of voltage of the back edge of the triangular waveforms applied to all of the deflection plates could be altered. This was achieved by replacing the DC-short termination on one end of the two stubs used in each PFN with a small variable carbon resistor. Careful adjustment of these resistors allowed correct timing and compensation of the frames.

To evaluate the dynamic spatial resolution characteristics a UV-sensitive gold photocathode (10 nm thick) was evaporated onto a chromium negative USAF (1951) resolution test chart (6mm x 6mm), fabricated on a fused silica substrate [9]. Recording of the images was achieved by intimate contact of the photographic film (Ilford HP5) on the fibreoptic faceplate of the image intensifier (Mullard type XX1330A)which was gated on for 200μs. The film was processed for a speed rating of 1600 ASA.

Each of the four frames recorded (eg. fig. 5) possessed a spatial resolution exceeding 7lp/mm in the streak direction and 6lp/mm in the orthogonal direction (with reference to the photocathode). The frame exposure time was measured [14] to be 230 ps (± 10ps) FWHM. The interframe time between frames 1, 2 and 3, 4 as measured from the mirror separation was 900 ps (± 25ps) while the temporal separation between frame two and three was 1.2 ns (± 25ps).

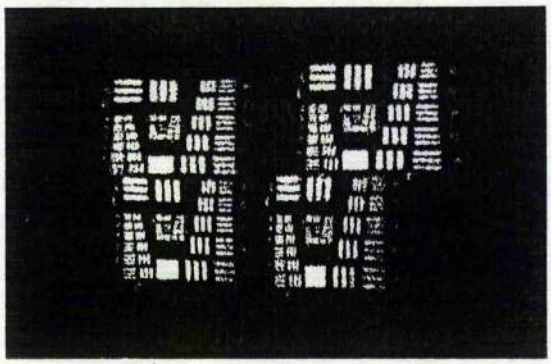

4	3
1	2

Frame Format

Figure 5. Reproduction of 4 frame recording.

It was evident that there was some degree of image degradation resulting from small voltage fluctuations on the plateau region of the deflection ramp used to drive the shift deflectors. This was investigated using a high bandwidth oscilloscope (Thomson CSF type TSN 660, risetime 80ps) and a typical oscillogram is included as Fig.6. It is also clear that there was a slight magnification difference between the first and second doublet pair. This is due to adverse fringing fields, resulting from asymmetric operation of the shift deflectors. When each doublet image was viewed independently, with the shift deflectors at anode potential and the appropriate mirrors blocked, a spatial resolution of not less then 7lp/mm was measured.

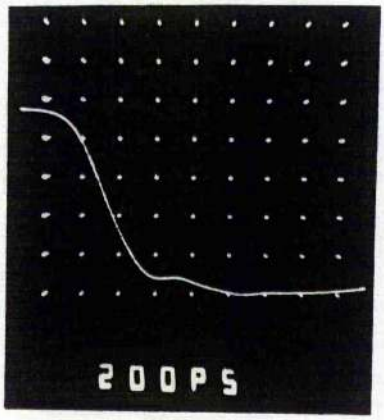

Figure 6 Oscillogram of shift plate voltage waveform. Vertical scale 100 V/div, horizontal scale 200ps/div.

4. CONCLUSIONS

The Picoframe II camera system which has been previously demonstrated in double frame generation for UV to soft X-ray spectral regions has now been shown to operate in the four-frame mode in the UV with frame exposure times of 230 ps, interframe times of around 1ns and spatial resolution of ~7 lp/mm.With refined circuit design (symmetrical deflection for the shift plates is considered essential) it should be possible to further improve the performance of the four-frame camera. In particular the frame exposure time may be reduced with the use of faster risetime avalanche circuits in conjunction with the existing PFN's but alternative methods are now being considered for the production of triangular voltage waveforms having a peak amplitude equal to that of the input ramp deflection voltage. Preliminary experiments indicate that the new PFN's will give a frametime of ~150 ps, interframe time of ~650ps and an inter-doublet time of ~1.5 ns, with a spatial resolution of ~7 lp/mm. The four frame UV Picoframe II camera is easily converted to an X-ray sensitive device, and this system will shortly be tested in such a configuration.

5. ACKNOWLEDGEMENTS

The financial support of the Paul Instrument Fund of the Royal Society and the Science and Engineering Research Council is gratefully acknowledged. One of us (DRW) is supported by an SERC CASE Studentship in collaboration with AWE. This work has been carried out with the support of the Procurement Executive, Ministry of Defence.

6. REFERENCES

1. M R Baggs, R T Eagles, W Margulis, W Sibbett, W E Sleat, 'A Picosecond Framing Camera For Single Or Multiple Frames', Advances in Electronics and Electron Physics, 64B, pp 627-636, (1985).
2. B K F Young, R E Stewart, J G Woodworth, J Bailey, 'Experiment Demonstration Of A 100-ps Microchannel Plate Framing Camera', Rev. Sci. Instrum. 57 (11), pp 2729-2732, (1986).
3. J D Kilkenny, P Bell, R Hanks, G Power, R E Turner, J Wiedwald, 'High-speed X-ray Imagers', Rev. Sci. Instrum. 59 (8), pp 1793-1796, (1988).
4. P E Young, J D Hares, J D Kilkenny, D W Phillion, E M Campbell, 'Four Frame Gated Optical Imager With 120-ps Resolution', Rev. Sci. Instrum. 59 (8), pp 1457-1460, (1988).
5. R Kalibjian, L W Coleman, 'Framing-Camera Tube Development For Sub-100ps Range', Proc. 13 th International Congress on High Speed Photography and Photonics. (Tokyo), pp 447-450, (1978).
6. S Majumdar, 'A Multiple Frame 100 Picosecond Framing Camera', Proc. 16 th International Congress on High Speed Photography and Photonics.(Strasbourg) SPIE 491, pp 913-916, (1984).
7. L L Shaw, L L Sleinmetz, W C Bohrendt, J B Sonderman, K Mikkelson, G R Beer, L G Sappala, E Romero, 'A High-Speed Eight Frame Electro-Optic Camera With Multipulsed Ruby Laser Illuminator', Proc. 16 th International Congress on High Speed Photography and Photonics. (Strasbourg), SPIE 491, pp 267-273, (1984).
8. W Sibbett, M R Baggs, H Niu, 'Picosecond Framing Image Tube', Proc. 13 th International Congress on High Speed Photography and Photonics. (San Diego) SPIE 348, pp 267-270, (1982).
9. R T Eagles, W Sibbett, W E Sleat, D R Walker, J M Allison, N J Freeman, 'Multiple Frame UV/X-ray Picosecond Framing Camera', Advances in Electronics and Electron Physics. 74, pp 209-217, (1988).
10. W Sibbett, D R Walker, W E Sleat, R T Eagles, N J Freeman, 'Double Frame UV/X-ray Picoframe Framing Camera Systems'. (In Press).
11. W Margulis, R Persson, 'Coaxial Electrical Pulse Shaper For Picosecond Electronics', Rev. Sci. Instrum. 56 (8), pp 1586-1588, (1985).
12. M C Jackson, R D Long, D Lee, N J Freeman, 'Development Of X-ray Streak Camera Electronics', Laser and Particle Beams. 4 (1), pp 145-156, (1986).
13. Kentech Instruments Ltd. Blackett Labs. Prince Consourt Rd, London, SW7 2BZ.
14. M J Eckart, R L Hanks, J D Kilkenny, R Pasha, J D Widwald and J D Hares, 'Large-Area 200-ps Gated Microchannel Plate Detector', Rev. Sci. Instrum. 57 (8), pp 2046-2048, (1986).

Theoretical analyses and design considerations of a picosecond framing tube

Y. Liu*, W.Sibbett, D.R.Walker

J.F.Allen Physics Research Lab.
Department of Phsics, University of St.Andrews,
St.Andrews, North Haugh, Fife KY16 9SS,
Scotland, UK.
* Permanent address: Xian Institute of Optics and Precision Mechanics,
Xian, China

ABSTRACT

To further improve the dynamic performances of picosecond-resolution framing cameras, a theoretical analysis has been accomplished which can simulate the dynamic trajectories of photoelectrons travelling through the entire image tube. It is shown that for the exsisting Picoframe-type camera design the spatial resolution is significantly degraded by the lensing effects of the deflectors during the dynamic framing operation. It is also shown that the minimum exposure 'frame' time for X-ray applications is limited by the reduction of the number of photoelectrons reaching the phosphor screen due to the high secondary electron energy spread.

A new design of framing tube incorporating either conventional deflectors or travelling-wave deflectors has been developed. In this design, the electrostatic focusing lens has been optimized for better beam quality and higher deflection sensitivity. The defocusing effect induced by conventional deflectors has been eliminated by (i). incorporating an extra cylindrical lens into the deflection section of the tube or alternatively (ii) by utilizing travelling-wave deflectors. The theoretically predicted frame time is about 60ps(FWHM) when using conventional deflectors and less than 50ps(FWHM) with the travelling wave deflectors. The implied spatial resolution referred to photocathode is 10 lp/mm for X-rays and exceeds 15 lp/mm for UV and visible radiations.

1. INTRODUCTION

Developments in research areas such as laser-induced fusion and laser plasma interaction have led to a demand for two-dimensional ultrafast diagnostic techniques with high spatial and temporal resolutions. Up to now a number of such approaches have been developed, among which electron-optical framing cameras exhibit unique advantages of short framing time, high sensitivity and broad spectral response (IR/visible/UV/X-ray). Several kinds of framing cameras have been reported[1 - 7], and exposure (or framing) times of 100ps have been achieved[1, 6, 7]. However, they suffer from rather limited spatial resolution, especially in the X-ray spectral region. The development of such a picosecond framing camera is important because of its applicability to plasma studies and to temporally/spatially-resolved photobiological investigations in the water window spectral region around 2.3-4.4 nm. It is therefore necessary to carry out theoretical analyses of the dynamic performance of the image tube with the aim of improving both the spatial resolution and temporal characteristics in the framing mode of operation.

A thorough theoretical evaluation of the dynamic performance of the Picoframe I tube[4] will be presented in this paper. It will be shown that the spatial resolution is limited mainly by the combined lensing effects of the two sets of 'framing' deflectors, which give rise to different optimum image

planes for the two orthogonal spatial directions. It will also be shown that the number of electrons reaching the phosphor screen is reduced for the case of X-ray illumination because of the large secondary electron energy spread of the photoelectrons. This thus implies that the minimum frame time will be restricted when space charge effects in the focusing region are taken into account. To overcome these problems, the following improvements have been made: (i) the focusing system has been redesigned and optimised to provide a better electron beam quality and a longer drift region, (ii) the exposure(or frame) time has been reduced by applying a lower anode voltage and increasing the distance between the two apertures A1, A2 (see fig.1) and (iii) the defocusing effect due to the deflections has been eliminated: either by introducing an extra cylindrical lens between the two deflectors or by employing travelling-wave deflectors.

A new framing tube design has thus been devised using either conventional or travelling-wave deflectors. The frame time has been predicted to be approximately 60ps when using conventional deflectors and less than 50ps if travelling-wave deflectors are chosen. The spatial resolution has been estimated to be10 lp/mm for X-ray and 15 lp/mm for UV illuminations.

2. THEORETICAL EVALUATION OF DYNAMIC PERFORMANCE

A typical Picoframe I-type framing tube configuration is shown schematically in Fig.1. It consists essentially of an electrostatic focusing lens and two pairs of deflectors, one set for the framing (or shuttering) operation, the other so-called compensating set to eliminate the image 'smear'. The operating principle of this camera has been described in detail elsewhere[4], but a brief review is also given here.

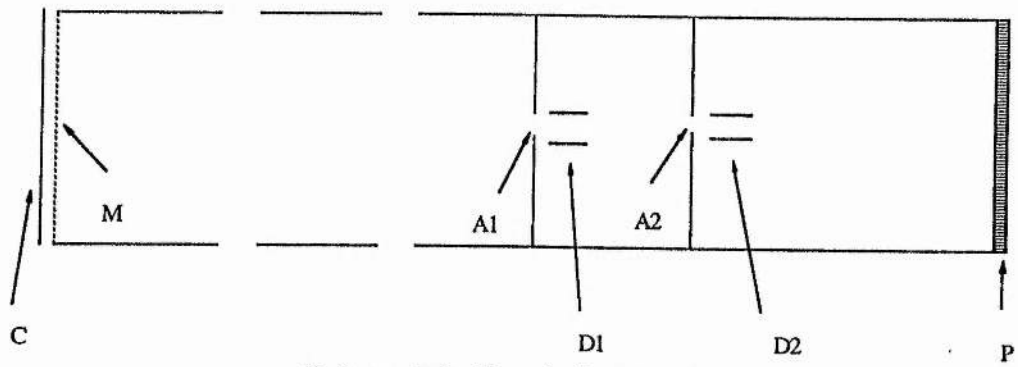

C: photocathode, M: mesh, A1: anode aperture
A2: framing aperture, D1: framing deflectors,
D2: compensating deflectors, P: phosphor screen

Fig.1 Schematic of Picoframe I image tube

A fast, linear, time-varying voltage ramp is applied to the framing deflectors, so that the electron beam is swept across the framing aperture and a single temporal transmission of photoelectrons is thus obtained. The imposed image 'smear' is then removed by applying a suitably phased reverse-polarity voltage ramp to the compensating deflectors. For multiple framing operation there are two techniques where in one case reverse-polarity symmetrical triangular waveforms are applied to the sweep and compensating deflectors and in the other approach a multiple framing aperture plate is used together with more than one set of compensating deflectors. In both options a pair of shift plates would be incorporated at an orthogonal orientation to these framing/compensation deflectors so that a sequence of multiple frames can be produced.

In most instances, the performance of Picoframe tubes has been generally theoretically predicted on the basis of the focus (or static) mode specification and the dynamic performance is deduced from experiments. It is found from experimental data that the spatial resolution is usually significantly lower in the dynamic mode than that in the static mode. To obtain a practical design for a framing tube with an optimized dynamic performance, it is necessary therefore to simulate and analyse the image tube in this framing operation. To do so, a suite of programmes has been developed which can indicate optimum image planes, magnification, crossover position and beam size, spatial and temporal modulation transfer functions(MTF), deflection velocity and photoelectron transmission through the apertures.

The electron trajectories in both focusing and deflection regions were calculated by the Runge-Kutta technique where potential distributions were determined by the finite difference solution of the Laplace equation. A Gaussian distribution was assumed for the intensity-temporal profile of the incident light signal. The initial energy spread distribution of emitted photoelectrons was modelled by a Beta function and the distributions of exit angles in the planes parallel and normal to the photocathode were modelled by uniform and cosine functions respectively.These parameters were assumed to be statistical variables which were generated using the Monte-Carlo technique. For the deflection region, a linear time-varying ramp voltage was taken, and the transit time of the deflection signal along the deflector was ignored. The trajectories of a group of electrons having specified initial conditions were traced through the entire tube in the framing mode.

Electron trajectories in the dynamic mode are shown in fig.2 for the original design of the Picoframe I tube. These theoretical data refer to the streak direction for both X-ray and UV illuminations. The phosphor screen has been located at the optimum plane for a static image. It is clear that in the dynamic mode, the best image position for the direction of streak is moved closer to the deflectors but remains unaltered for the orthogonal direction. The overall spatial characteristics are therefore seriously degraded in a framed image. By adjusting the focusing voltage, image quality can be slightly improved, but it is still considerably worse than that in the static mode.

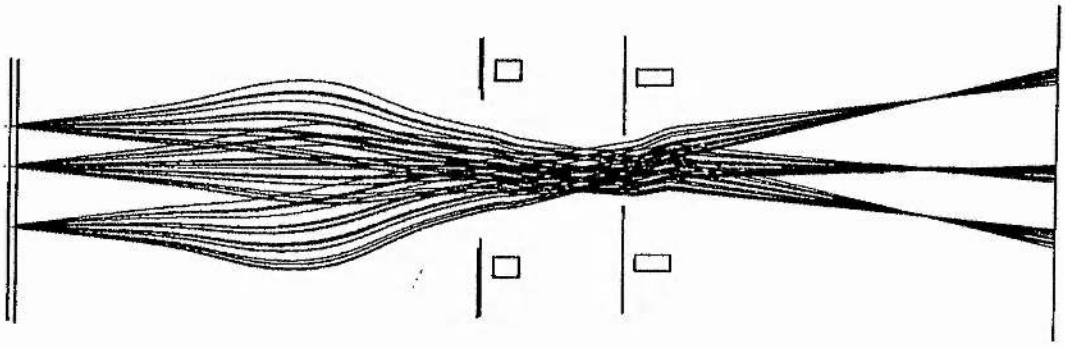

a). UV input illumination

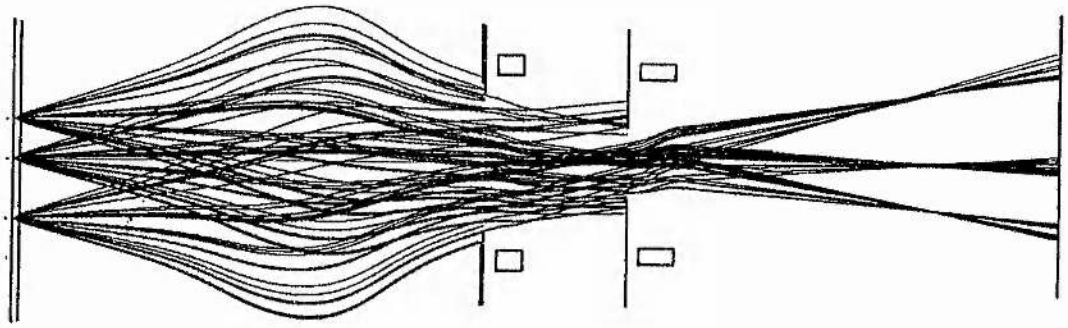

b). X-ray input illumunation

Fig. 2 Electron trajectories in Picoframe I tube
in framing operation

It is also indicated in Fig.2 that for the X-ray illumination, the photoelectron beam size is much larger than that for UV illumination due to its larger initial energy spread. This results in serious fringe-field effects in the deflectors, the reduction of electron transmission through the two apertures and the limitations to the frame time and the effective working area on the photocathode. On one hand, to ensure an adequate electron density at the phosphor screen, an appropriately high incident intensity must be provided and the diameters of the apertures must be large enough to allow a reasonable number of electrons to reach the output screen and enough image area. Also to minimize the deflection fringe-field effects and avoid electron beam impact on the deflection plates, the distances between the deflector plates and the lengths of the deflectors must be restricted. On the other hand, these requirements give rise to longer frame time and more significant space charge effects. A proposed solution to these problems is discussed in the following section.

3. DESIGN CONSIDERATIONS

The frame time and spatial resolution are the important characteristics of a framing tube and the consideration of them constitutes the subject matter of this section.

3.1. Frame time

In principle, the full exposure time of a Picoframe tube can be deduced to be:

$$t = \frac{2V_a Ad}{ka(a/2+L)}$$

where V_a is anode voltage, d is the separation of the framing deflectors, a is the length of the framing deflector, L is the distance from the exit of the framing deflectors to the aperture A2, K is the slope of linear voltage ramp and A is the sum of the diameter of the framing aperture and the electron beam diameter at the framing aperture A2. From this equation, it is seen that the shortening of the frame time requires a smaller electron beam size and framing aperture diameter, lower anode voltage V_a, faster deflection voltage gradient K, longer separation between apertures A1, A2 and optimum design of framing plates. In fact it is difficult to determine exactly the electron beam size due to the complex density distribution across its crosssection. Experimentally, specified exposure time is given by the full width of the half maximum exposure temporal transmission profile through the framing aperture and as a result it is shorter than that defined by the above formula.The electrostatic focusing lens has been redesigned and optimized in respect of the following considerations.

The electrode structure parameters and voltages have been rearranged so that the size of electron beam was minimized and the beam crossover position was located further from the anode aperture A1, and the anode voltage was reduced to 8 KV(from15KV) to provide a high deflection sensitivity. To minimize the space charge effects at shorter frame times, the length of the focusing region was decreased. The distance between the two apertures was increased to 80mm. The configuration of the framing plates was also modified to have optimum deflection sensitivity with the minimum fringe-field effects and to be fully compatible with the compensation deflectors.

3.2. Dynamic spatial resolution

The dynamic spatial resolution in a framing tube is primarily determined by the spatial aberrations of the focusing system, the construction of deflectors and the applied deflection signal parameters. Under framing conditions, the fringe-fields of the deflectors play a very important role in determining the image quality. In particular, with regard to the compensating deflectors, the spatial spread of the electron beam becomes significant during the temporal extent of the illuminating pulse. Thus the beam size becomes large and these fringe-field effects become especially serious. For the achievement of high spatial resolution, in addition to the appropriate design of the electrostatic lens, it is necessary to construct the two sets of deflectors so that the fringe-field effects are minimised and the image 'smear' caused by the framing deflectors can be eliminated completely by suitably-designed compensating plates.

To overcome the combined lensing effects of the two sets of deflectors, the focusing voltage must be adjusted so that the image in streak direction is focused at a prescribed plane. The induced defocusing effect in the non-streak direction is corrected by introducing an extra cylindrical focusing lens located immediately following the framing deflectors. From theoretical analyses, it has been found that the lensing effect of the two sets of deflectors is caused mainly by the finite transit time of photoelectrons travelling through the deflectors. In order to synchronise the photoelectrons with the deflection waveforms in such a way that the electrons pass through both apertures and reach the centre of the phosphor screen, account must be taken of the electron transit time within the deflectors. This results in a non-zero but different voltages appearing at the entrance and exit of the deflection electrodes. This is equivalent to an effective DC bias voltage being applied to the deflectors, which produces very strong fringe-fields. Because symmetrical ramp voltages(+/-) are applied to the two deflectors, their combined function essentially leads to a cylindrical lens effect. Although this lensing effect can be eliminated by incorporating an additional lensing section, it makes the manufacture of the tube more difficult and results in a difference of electron-optical magnification in the two image directions.

An alternative solution is to use travelling-wave deflectors instead of the more conventional deflectors where the finite transit time effect can be overcome. The configuration of the entire tube can thus be simplified and smaller beam size can be obtained. Moreover, it has the advantage of enhanced deflection sensitivity and frequency bandwidth. Faster linear ramp voltages can therefore be applied without giving rise to waveform distortions.

According to the above considerations, an improved design of a framing tube has been developed using either conventional or travelling-wave deflectors. In this modifed design, the deflection sensitivity is increased by three times for an image tube having conventional deflectors and by four times for a tube with travelling wave deflectors as compared to the origional Picoframe I tube but because of the shorter focusing system, the working area on the photocathode is reduced from 6 x 6 mm to 4 x 4 mm. To achieve complete compensation between the two deflections at shorter frame times, the voltage ramp gradients applied to them differ because of the different deflection sensitivities. The frame times are predicted to be approximately 60ps FWHM for the conventional deflector version and less than 50ps FWHM for the travelling-wave deflection design with a deflection ramp of +/- 1..6kV/ns and UV input illumination. The spatial modulation transfer functions are shown in fig.3 a, b for conventional and travelling-wave deflectors respectively. The dynamic spatial resolution referred to the photocathode is estimated to be 15 lp/mm for UV light source and 10 lp/mm for X-ray radiation source at a modulation depth ≈ 20%.

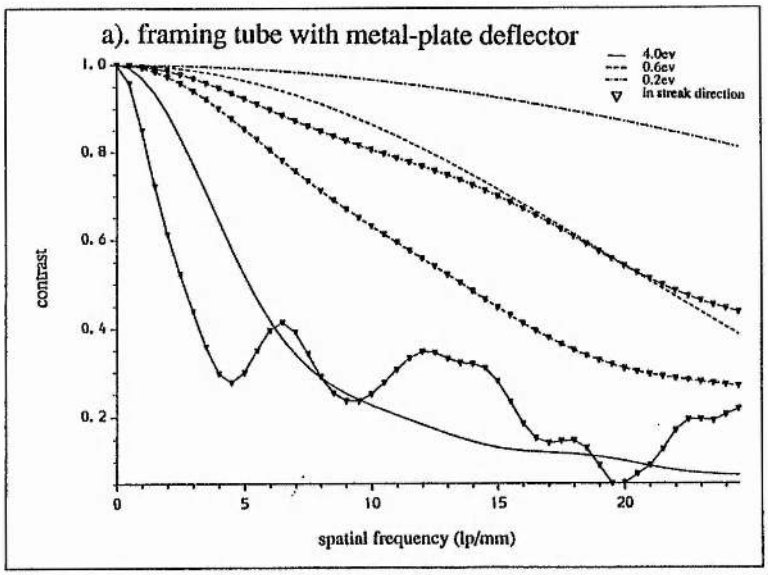

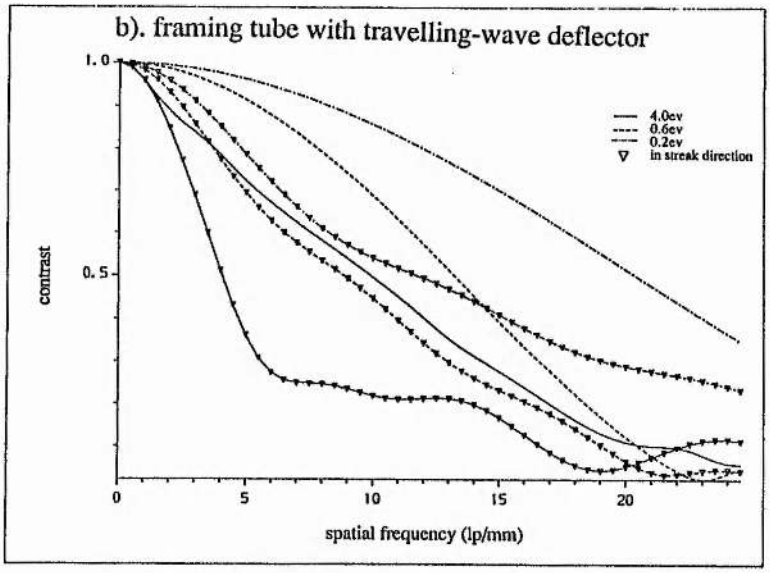

Fig. 3 Dynamic spatial MTFs in streak and orthogonal directions for improved framing tube

The magnifications of the tube with metal-plate deflectors in the streak and orthogonal directions are -1.8 and -1.4 respectively, while travelling-wave deflectors are employed the magnifications in both direction are -1.8. Further detailed analyses and improvements of the Picoframe I and Picoframe II cameras[8] are ongoing and comparisons with experimental data will be presented in the near future.

4. CONCLUSIONS

The theoretical analyses and evaluation of a Picoframe I camera have been undertaken. It is shown that the deflection sections have a major influence in determining the overall dynamic spatial resolution of the camera. The loss of dynamic spatial resolution can be minimized either by using an extra cylindrical lens or by replacing the conventional deflectors by the travelling-wave type. When incorporating an X-ray sensitive gold photocathode, the spatial resolution is lower as a result of the larger secondary electron energy spread. A preliminary design of a new framing tube has been achieved for which the frame times are predicted to be less than 100ps. Some of the theoretical analyses of the present Picoframe I camera system which have been described here have been related to experimental data that have been obtained for UV, X-ray sensitive image tubes[8].

5. ACKNOWLEDGMENTS

The financial support of the Paul Instrument Fund of the Royal Society and the science and Engineering Research Council is gratefully acknowledged. Acknowledgement is also made by Y.Liu for an University Studentship and ORS Scholarship from University of St.Andrews. One of us (DRW) is supported by a SERC CASE Studentship in collaboration with AWE.

6. REFERENCES

1. J.D.Kilkenny, P.Bell, R.Hanks, G.Power, R.E.Turner, J.Wiedwald, "High-speed gated X-ray imagers", Rev.Sci.Instrum. vol. 59 (8) pp.1793-1796, August 1988

2. P.E.Young, J.D.Hares, J.D.Kilkenny, D.W.Phillion and E.M.Campbell, "Four-frame gated optical imager with 120-ps resolution", Rev.Sci.Instrum. vol. 59 (8), pp.1457-1460, August 1988

3. R.Kalibjian, S.W.Thomas, " Framing camera tube for subnanosecond imaging applications", Rev.Sci.Instrum. vol. 54 (12), pp.1626-1628, December 1983

4. W.Sibbett, M.R.Baggs, H.Niu, " Picosecond framing image tube",SPIE vol. 348 High Speed Photography pp.267-270, San Diego 1982

5. N.Finn, T.A.Hall and E.McGoldrick, "Subnanosecond x-ray framing camera", Appl. Phys. Lett., vol. 46 (8), pp.731-733, April 1985

6. R.T.Eagles, W.Sibbett, W.E.Sleat, D.R.Walker, J.M.Allison, N.J.Freeman, "Multiple frame UV/X-ray picosecond framing camera", Advances in Electronics and Electron Physics, vol. 74, pp.209-217, 1988

7. D.G.Stearns, J.D.Wiedwald, B.M.Cook, R.L.Hanks, and O.L.Landen, "X-ray framing camera for picosecond imaging of laser-produced plasmas", Rev. Sci. Instrum., vol.60 (3), pp.363-367, March 1988

8. W.Sibbett, Y.Liu, D.Walker, "The theoretical and experimental evaluations of Picoframe I & II framing cameras", To be published in Rev.Sci.Instrum.